Optimization and Characterization of a New Microextraction Device for Determination of Phenols in Water Samples

By

Ghadeer Fouzi Abu-Alsoud

A thesis submitted to the
School of Graduate Studies
in partial fulfilment of the
requirements for the degree of
Doctor of Philosophy

Department of Chemistry
Memorial University of Newfoundland

February 21

St. John’s, Newfoundland

Abstract

Porous water-compatible molecularly imprinted polymer coatings with selective binding sites for extraction of phenols from environmental water samples were prepared on glass using an optimized mixture of water-soluble carboxylic acid functional monomers, ethylene glycol dimethacrylate crosslinker, catechol as a pseudo-template, and a porogen system of methanol/water with linear polymer polyethylene glycol. The MIP devices were combined with ultra high-performance liquid chromatography with a photodiode array detector suitable for the simultaneous determination of trace levels of phenol, alkylphenols and chlorophenols in seawater (SW) and produced water (PW). For effective imprinting, the MIP formulation was optimized through systematic optimization of critical factors like the nature and the amounts of functional monomer, crosslinker, template, and porogen. To improve the analytical method, the parameters that influence extraction, including salinity, pH, adsorbent mass, desorption solvent, and desorption time were optimized. Under the optimized conditions, the detection limits ranged from 0.1 to 2 μg L^{-1}, and enrichment factor between 12.8 and 133.5. The recoveries from spiked samples ranged from 85 to 100% with %RSDs of 0.2–14% for SW and 81–107% with %RSD of 0.1–11% for PW. The MIP device is simple, robust, inexpensive can be used in automation and high throughput sample processing.

To better understand the performance of MIPs, four different isotherm models were used to study molecular recognition of five phenols on catechol imprinted polymer and cross-reactivity for 11 phenolic compounds through individual and simultaneous adsorption

process, respectively. It was found that heterogeneity is a relative phenomenon depending on the chemistry of the adsorbates. The Langmiur-Freundlich isotherm model successfully explains the adsorption behaviour for small phenols and fails to explain the molecular recognition for the large phenols, while the BET isotherm successful in that and suggests formation of multilayer. It was observed that the competition of phenols for the binding sites of the catechol imprinted polymer depends on their hydrophobicity and solubility in water. In this work, we proved that a single isotherm model is not enough to explain the behaviour of the analytes toward adsorbent surface. Each model gives valuable quantitative data that help to explain the recognition mechanism for the adsorbates.

Acknowledgements

I would like to thank my supervisor, Prof. Christina Bottaro, for her support and guidance during my work on this project. She helped me a lot to analyze and explain the experimental data in a scientific way.

I would like to thank my supervisory committee, Dr. Karen Hattenhauer and Dr. Christopher Rowley, for the revision of my thesis. The Department of Chemistry and the School of Graduate Studies at the Memorial University of NL. Also, I would like to acknowledge Linda Winsor for training me on using some of the analytical instruments in the C-CART.

I would like to thank my dear husband Ibrahim Awad for his patience, support, and encouragement. Many thanks to my lovely kids Abdelrahman and Roa'a; thank you, my kids, for your understanding of my work and for giving me enough time to work without interruptions.

This work was supported by Atlantic Innovation Fund (AIF) Atlantic Canada Opportunities Agency (ACOA) [Grant number 781-18607-208053], Canada; Newfoundland and Labrador Department of Tourism, Culture, Industry and Innovation, Canada [Grant number 5404-12550-102]; the Natural Sciences and Engineering Research Council of Canada (NSERC) [Grant number 2015-06367] ; the Department of Chemistry and the School of Graduate Studies (SGS) Memorial University of Newfoundland (MUN), Canada.

Dedication

Praise and thanks to Allah Almighty for completing my Ph.D. journey.

To the Memory of my dear and lovely

father

I also would like to dedicate this thesis to:

My dear and lovely mother

My sisters Abeer and Ahlam

My brother Esam

My husband Ibrahim

My son and daughter Abdelrahman and Roa'a

My supervisor Prof. Christina Bottaro

Table of Contents

List of Tables

List of Figures

List of abbreviations and symbols

ΔG°	Gibbs Free energy
2-CP	2-chlorophenol
2-MP	2-methylphenol
3-MP	3-methylphenol
4-HBA	4-hydroxybenzoic acid
4-NP	4-nonylphenol
4-OP	4-teroctylphenol
4-VA	4-vinylanilline
4-VBA	4-vinylbenzoic acid
4-VP	4-vinylpyridine
a	pre-exponential constant
ACN	Acetonitrile
APs	Alkylphenols
B	The amount of bound analyte
BET	Brunauer, Emmett, and Teller adsorption model
c	The ratio between K_S relative to K_L
C_{cosol}	The concentration of cosolvent
CE	Capillary electrophoresis
C_e	The free analyte in the system at equilibrium
CEPA	Canadian Environmental Protection Act
CL	Crosslinker
CMP	4-chloro-3-methylphenol
CPs	Chlorophenols
DCP	2,4-dichlorophenol
DMP	2,4-dimethylphenol

DMPA	2,2- dimethoxy-2-phenylacetophenone
ECD	Electron-capture detector
EGDMA	Ethylene glycol dimethacrylate
FI	Freundlich adsorption isotherm model
FID	Flame ionization detector
GC	Gas chromatography
HAc	Acetic acid
HQ	1,4-dihydroxybenzene
IF	Imprinting factor
K	The adsorption constant
K_{ca}	Composite affinities
K_L	The equilibrium adsorption constant of the upper layers
K_S	The equilibrium adsorption constant for the first layer
K_{salt}	Setschenow constant
L-FI	Langmuir-Freundlich adsorption isotherm model
LI	Langmuir adsorption isotherm model
LLE	Liquid-liquid extraction
logP	Octanol/water partition coefficient
LPME	Liquid-phase microextraction
M	Functional monomers
MAA	Methylacrylic acid
MAC	Maximum acceptable concentration
MCL	Maximum contamination level
MeOH	Methanol
MIP	Molecularly imprinted polymer
MISBSE	MI-stir-bar sorptive extraction
MISPE	Molecularly imprinted micro-SPE
MMIP	Magnetic MIPs

MS	Mass spectrometry
N	The binding site density
n	The number of adsorbed layers
NAA	N-allylaniline
PAH	polycyclic aromatic hydrocarbon
PCP	Pentachlorophenol
PDA	Photodiode array detector
PEG	Polyethylene glycol
PETA	Pentacrythritol triacrylate
Ph	Phenol
PW	Produced water
Q	The amount (moles or mass) of analyte adsorbed relative to the mass of sorbent
q_m	The amount adsorbed corresponding to the formation of a complete monolayer
R^2	Correlation coefficient
RSD	Relative standard error
RSS	Sum of squares of the residual
S	Solubility
SD	Standard deviation
SEM	Scanning electron microscope
SF	Selectivity factor
SPE	Solid phase extraction
SPME	Solid phase micro-extraction
Sty	Styrene
SW	Seawater
T	Template
TCP	2,4,6-trichlorophenol
UHPLC	Ultra-performance liquid chromatography
US EPA	United States Environmental Protection Agency

x	The ratio of the partial pressure of the adsorbate to saturation vapour pressure of the system
γ	Activity coefficient
Σ	Solubilizing factor
α	Separation factor

Chapter 1

1 Introduction and Overview

Phenols are aromatic hydroxy organic compounds, which are common in the environment because of natural processes and from anthropogenic inputs. They are produced naturally in aquatic environments, usually from the decomposition of organic matter [1]. However, the main source of phenols in the environment comes from a range of human activities, predominantly industrial processes associated with petroleum extraction and refining, and chemical and pharmaceutical production.

Phenolic compounds may be nitrated, alkylated or halogenated [1]. The European Environmental Agency (EEA) and the United States Environmental Protection Agency (US EPA) have classified phenols as priority pollutants because of their toxic effects on humans and animals. The structures of main phenolic compounds considered priority pollutants by the US EPA are presented in Figure 1.1 [2]. EU Directive 2455/2001/EC sets a maximum concentration of 0.5 μg L^{-1} in drinking water, and their individual concentration should not exceed 0.1 μg L^{-1} [3]. So, it is crucial to determine the level of these compounds in environmental water samples. In this thesis, the focus is on phenol (Ph), chlorophenols (CPs) and alkylphenols (APs) because of their wide use in industry and, consequently, widespread occurrence in the environment [4].

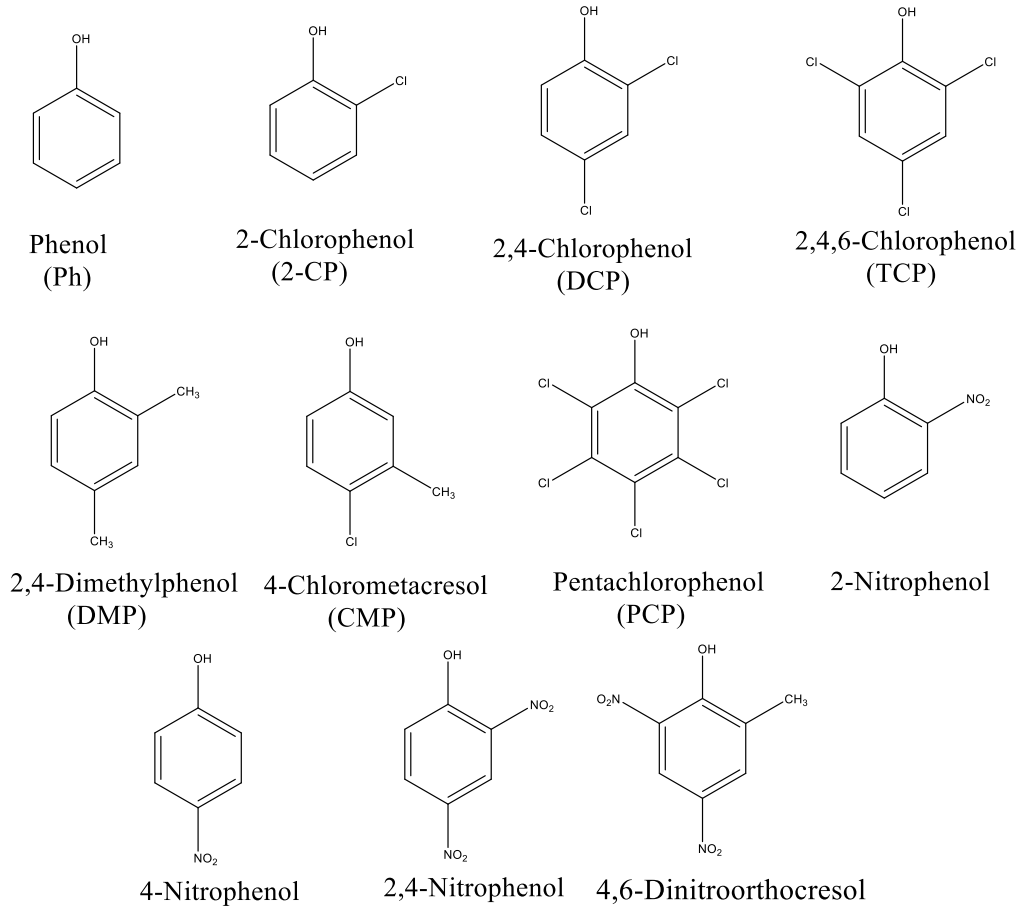

Figure 1.1. Structures of eleven phenolic compounds considered priority pollutants by US EPA. [2]

1.1 Common sources of target phenols in environmental water

1.1.1 Industrial and municipal wastewater treatment plant effluents in Canada

According to the Canadian Environmental Protection Act (CEPA), the concentrations of Ph or total phenols in surface water across Canada are below 2 µg L^{-1} [5]. About 58.5 tonnes of total phenols are released annually into Canadian surface water due to anthropogenic pollution like pulp, paper and wood products, steel and metal products, petroleum refining, and municipal wastewater treatment plants. So, it is expected that a

higher concentration of phenols are found in those areas exposed to industrial effluents. The degree of exposure to aquatic organisms was evaluated by measuring the highest annual industrial effluent concentrations of Ph/total phenols. The final concentration of Ph/total phenols at effluent for 26 pulp, paper and wood mills (1996 data), 8 outfalls of steel and metal products (1995–1997 data), 16 petroleum refiners (1993-1996 data), 31 municipal wastewater treatment plants (MWTPs) (1985-1997 data) were reported in the range of ND-0.4, 0.006–0.34, 0.0004–2.03, and 0.002–2.60 mg L^{-1}, respectively.

1.1.2 Produced water

Offshore produced water (PW) is formed during the production of oil and gas from offshore reservoirs [6]. PW is considered the primary waste effluent in offshore oil and gas production discharged at three times the volume of usable petroleum extracted from oil wells and at higher rates for gas wells [7]. PW contains oil (organic compounds) and inorganic substances (like salt and heavy metals) [8]. The dominant groups of organic compounds in PW are aliphatic hydrocarbons, slightly soluble aromatic hydrocarbons, organic acids and phenols [9]. Based on the partition and the solubility, most aliphatic and aromatic hydrocarbons are in the dispersed oil, while the water-soluble organic compounds, like some phenols and organic acid, are dissolved in the bulk water fraction. It is noteworthy however, that although most hydrocarbons are in the dispersed oil, the water fraction still contains some toxic organic hydrocarbons such as APs and polycyclic aromatic hydrocarbons (PAHs). The high molecular weight PAHs and APs tend to partition into the dispersed oil because of their low water solubility [10]. Several oil/water separation processes separate a significant amount of dispersed oil. Nevertheless, small oil droplets

remain in the water and are difficult to remove [11]. In 2012 [12], about 76,700 m^3 of PW were released daily to the Norwegian Continental Shelf from a single field. The total concentration of Ph and (C1-C9) of APs in PW which was discharged into the sea from an oil installation in the Norwegian Continental Shelf was between 0.1-0.23 mg L^{-1}. Ph and (C_1-C_3) are more dominant; C_4-C_6 and C_7-C_9 are available at low and very low concentration levels, respectively.

1.2 Classes of phenols as aquatic contaminants studied in this thesis

1.2.1 Phenol

Ph is a crystalline, colorless, pungent-smelling organic solid, and it was one of the first compounds listed by the US Environmental Protection Agency (US EPA) [2]. More than 9 x 10^6 tonnes of Ph is produced annually worldwide [13]. Ph can be obtained from toluene and cumene oxidation or extracted from coal tar and it is used as a feedstock in the production of plastics, pesticides, dyes, explosives and other chemical reagents [13]. Ph can cause chemical burns and have acute and chronic toxic effects. There are many routes of exposure, e.g., through food and water ingestion, inhalation of fumes, or transdermally. It is absorbed quickly through the skin and lungs [14]. Absorption of modest amounts of Ph can be detoxified by the formation of conjugates with glucuronic acid or sulfates and then excreted in the urine; however, with exposure to high concentrations of Ph, acute and chronic effects are observed in humans and animal models [15]. Acute effects include highly irritating skin and eyes, muscle weakness, coma, irregular breathing and

convulsions. The chronic effects include anorexia, salivation, gradual weight loss, diarrhea and gastrointestinal irritation [15].

1.2.2 Chlorophenols

CPs are a diverse group of molecules widely used in a wide range of applications [16]. The large production volume combined with their toxicity has garnered significant interest in their effects and distribution, both in human populations and most ecosystems [4,17]. CPs enter the environment via industrial effluents, by the degradation of other chemicals like phenoxyalkanoic acids, during the chlorination of drinking water or it can be formed in the environment through chlorination of polyaromatic compounds or humic matter. Naturally-occurring compounds featuring chlorophenol substituents, with a range of functional and bioactive properties, are also biosynthesized in numerous terrestrial and aquatic organisms. [18]. The main use of industrial chlorophenols are pesticides, preservatives, disinfectants, and feedstocks in the synthesis of chlorophenol-derived products like chlorophenoxyacetic acid herbicides and phenolic resins. Although chlorophenols are generally considered hydrophobic, many show relatively high solubility in water, with even PCP (the octanol/ water partition coefficient, logP 5.12) has a solubility ~14 mg L^{-1}) [16,19]. This can be attributed to the ionization of acidic chlorophenols, making water a significant route of exposure. The toxicity of CPs increases with hydrophobicity, which increases with increasing number of chlorine atoms substituents [16], although acute exposure to even mono- and dichlorophenols in humans cause muscular twitching, spasms, tremors, weakness, and collapse. PCP is regulated by most environmental protection agencies due to its extreme toxicity in humans and animals,

which is characterized by weakness, headache, anorexia, sweating, hyperpyrexia, nausea, vomiting, terminal spasms, and death [16].

1.2.3 Alkylphenols

APs have garnered attention because of their endocrine-disrupting effects on the biota, such as estrogen mimics.[20] For example, the growth of cultured human breast cancer cells is enhanced by octylphenol and nonylphenol with the toxicity of APs increasing with increasing length of the hydrophobic alkyl chain. The APs with long alkyl chain or even branched chains, like tertiary para substituent alkyl groups, are the most active as xenoestrogens. For example, accelerated growth in breast cancer cells resulted after exposure to 20 μg L^{-1} 4-tert-octylphenol (4-OP), considered the most estrogenic among APs, while similar effects only were seen at 220 μg L^{-1} nonylphenol. On the other hand, alkylation by short chains at the ortho-position results in phenols with no or very small xenoestrogenic effects. 4-OP and 4-nonylphenol (4-NP) are generally used as non-ionic surfactants in many industries to produce emulsifiers, detergents and other products [21].

Phenols with smaller alkyl groups are also of interest, such as methylphenols (MPs), commonly known as cresols, and di-alkyl phenols. These occur widely from both natural, petrogenic and anthropogenic sources. For example, they are found as natural components of oils from jasmine, peppermint and camphor plants, and they are produced through animal metabolism of aromatic molecules (e.g. tyrosine and toluene) [22–24]. Anthropogenically derived MPs enter the water through the use of cosmetics, explosives, disinfectants, and from a range of industrial processes, with the most concerning inputs associated with the processing of coal and other petroleum products [1,24]. Inhalation, oral,

and dermal exposure to MPs at high concentrations are harmful, irritating the lungs, eye, throat and nose, vomiting, and kidney failure, among other acute effects [22–24].

1.3 Physiochemical properties of phenols

The forms and fate of phenols in the environment are related to the physical and chemical properties (Table 1.1) of the individual compound [4]. As an example, as the number of chlorine atoms substituents in CPs increases, the melting, boiling point, and hydrophobicity (logP) increase, while water solubility and volatility decrease [19]. The phenols may occur in dissociated and non-dissociated forms in an aqueous medium with the proportions dependent on the pH of the aqueous solution. As an example, CPs are considered to be weak acids, so when the pH of the aqueous medium increases above the pKa, the solubility of these compounds are significantly increased as a result of the formation of the more soluble phenolate ion. Consequently, bioaccumulation and the affinity towards sediments decrease.

On the other hand, the hydrophobicity of the individual phenols influences the amount of these phenols present in the environmental aqueous medium in which the phenols with higher logP values can be adsorbed by the organic content of the sediments, as an example Ph, 2-MP, and 3-MP have a low affinity toward sorption compared to 4-OP, PCP, and 4-NP [19]. The main reason responsible for removing phenols from surface water is by microbial biodegradation and photooxidation, while volatilization does not play a significant role since most of the phenols have a low vapour pressure. In natural waters, microbial biodegradation is the main process for the removal of phenols from the water.

The degree of alkylation and chlorination increases the persistence of phenols in the environment. Consequently, the tendency to accumulate phenols in organism tissues increases as well. For example, phenol and C_1 -C_3 phenols do not accumulate in fish tissues to the same degree as phenols with bigger alkyl groups [25].

Table 1.1. Physical-chemical Properties of Phenols [26]

	Molecular weight (g/mol)	Melting point (C°)	Boiling point (C°)	Vapor pressure (Pa (C°))	Solubility (g L^{-1} (C°))	pKa	logP
Ph	94.11	40.9	181.8	46.66 (25)	84 (20)	9.99	1.46
2-MP	108.14	29.8	191.0	33 (25)	25.9 (25)	10.29	1.95
3-MP	108.14	11.8	202.2	14.66 (25)	24.0 (25)	10.1	1.96
CP	128.55	9.8	174.9	230 (20)	28.5 (20)	8.5	2.15
DMP	122.16	24.5	210.9	13.60 (25)	7.87 (25)	10.60	2.30
CMP	142.58	67.0	235.0	6.66 (20)	3.8 (20)	9.55	3.10
DCP	163.00	45.0	210.0	10 (20)	4.5 (20)	7.89	3.20
TCP	197.45	69.0	246.0	1.07 (25)	0.8 (20)	6.23	3.69
PCP	266.34	191.0	309-310	0.02 (20)	0.014 (20)	4.70	5.12
4-OP	206.32	84.5	279.0	0.064 (25)	0.007 (25)	10.33	5.25
4-NP	220.35	42.0	317.0	0.109 (25)	0.007 (25)	10.31	5.76

1.4 Recommended Guidelines for phenols

US EPA classifies CPs and APs as priority pollutants and reports that the maximum contamination level (MCL) of PCP in drinking water should not exceed 1 μg L^{-1} [27]. The EU has considered 4-OP, PCP, and 4-NP as priority pollutants, and they established the

maximum acceptable concentration (MAC) for PCP and 4-NP in surface water are 1 µg L^{-1} and 2 µg L^{-1}, respectively [28]. On the other hand, Health and Welfare Canada decided in 1979 that the MAC of phenols in drinking water should not exceed 2 µg L^{-1} [19]. Undesirable odour and taste are generated by chlorophenols when the concentration exceeds 5 µg L^{-1}. Corresponding to the Canadian guidelines for Freshwater Aquatic Life 1984, the MAC concentration in freshwater for monochlorophenols, dichlorophenols, trichlorophenols, tetrachlorophenols, and PCP should not exceed 7, 0.2, 18, 1, 0.5 µg L^{-1}, respectively. The level noted here for PCP is of particular importance since it is the most used chlorophenol in industry due to its usefulness as a wood preservative, as a bactericide and fungicide in the treating of paints and fabric, and that fact that it is the most persistent among the chlorophenols [19].

1.5 Methods of analysis of phenolic compounds from water samples

1.5.1 Extraction from aqueous samples

The detection limits required for environmental monitoring can only be obtained using suitable sample preparation techniques that give reasonable enrichment factors [29]. The current US EPA analytical methods, Methods 604, 625 and 8041, are based on the extraction of phenolic compounds using liquid-liquid extraction (LLE) for aqueous samples, followed by separation and detection using gas chromatography (GC) coupled with different detectors [30–32]. However, all these methods employ costly and hazardous organic solvents, which are undesirable for health and dumping reasons; moreover, it is time-consuming and needs derivatization of phenols to avoid broad and tailed peaks in GC

analysis [33–35]. Therefore, the traditional extraction methods have been replaced for other methods that are more sensitive, fast and eco-friendly, like solid-phase extraction (SPE). SPE emerged in the 1980s as an effective technique for chemical separation and purification. This methodology can be replaced by the LLE because of lower organic solvent consumption, fast analysis and its ability to be automated [33,34]. In this technique, the isolation of the analytes depends on their binding affinities toward the SPE adsorbent [36]. The undesirable impurities are eluted using different solvents, usually before elution of the adsorbed analytes. Although SPE is widely applied as a separation and clean-up method, its main drawbacks include low selectivity, the need for organic solvents during the elution step, the use of cartridges, which can be costly as they often are discarded after just one use and the fact that SPE cartridges are susceptible to plugging [37]. In 1990, Arthur and Pawliszyn introduced the method of solid-phase microextraction (SPME) [38], a technique which they demonstrated allowed for sampling, extraction, and enrichment in just one step. This technique relies on a fused-silica fibre coated with a polymeric stationary phase, all accommodated in the needle of a syringe for protection. SPME is based on the equilibrium of the analyte between the sample and the stationary phase [38–40]. Subsequently, the analytes can be thermally desorbed in the GC-injector or desorbed using an appropriate solvent prior to the chromatographic analysis. This technique is characterized by simplicity and short analysis time due to the cylindrical surface geometry of the coated fibres, which facilitate the extraction and desorption processes. It does not require using an organic solvent or complete removal of the analyte from the liquid sample like with SPE [38]. SPME suffers from poor selectivity during the extraction process, low

stability in organic solvents, fairly low maximum operating temperature during the thermal desorption process, and SPME devices are prone to delamination of the polymeric coatings and the glass fibres are prone to breakage [40,41]. Also emerging in the 1990s, liquid-phase microextraction (LPME) reduces the consumption of organic solvents through miniaturization. LPME, a variant of LLE, uses only a few µLs of solvent to preconcentrate analytes from samples instead of the hundreds µLs required in LLE [2,41,42]. Table 1.2 lists some methods for the determination of phenols in aqueous samples along with typical figures of merit.

Table 1.2. Selection of some analytical method that are used for the determination of phenols

Analytes	Method	LOD ($\mu g\ L^{-1}$)	RSD%	LR ($\mu g\ L^{-1}$)	Real sample	Ref.
Ph, 2-MP, 3-MP, 4-MP and DMP	LPME-HPLC-UV-vis	0.3-3.5	0.3-1.5	2.50-50 (Ph) 12.5-250 (others)	Tap water, river water, seawater and groundwater	[43]
Ph, 2-CP, 2-MP, DMP, DCP, TCP, CMP, PCP and nitrophenols	SPE-GC-MS (EPA method 528)	2.0×10^{4}-5.8×10^{5}	-	1.0×10^{5}-1.5×10^{7}	Groundwater and chlorinated surface water	[44]
CMP, 2-CP, DCP, DMP, PCP, Ph, TCP and nitrophenols	LLE-GC-MS (EPA method 625	1.5-42	-	5-1300	Drinking water, surface water, and industrial wastewaters	[32]
Ph, 2-CP, DMP, DCP, TCP, CMP, PCP and nitrophenols	LLE-GC-FID (EPA method 604)	0.14-6.0	-	12- 450	Surface water and industrial wastewater	[30]
Ph	DLLME-HPLC-UV-vis	29	2.1-13.1	0.1–100	Tap water, lake water, wastewater	[45]
4,6-DN-2-MP, 2-CP, DMP, CMP, DCP and TCP	RM-LLME-HPLC-UV-vis	0.29-0.63	1.0-8.1	5-500	Tap, river waters	[46]
4-cumylphenol, 4-tertbutylphenol, 4-OP, 4-NP	DLLME-HPLC-UV-vis	0.2-1.6	2.7-14	2-20	Seawater	[47]
Ph, nitrophenols and 4-CP	LPME-HPLC-UV-vis	0.3- 3.0	< 7.6	10-1000 (Ph) 5–500 (nitrophenols and 4-CP)	Tap water and lake water	[48]
Ph, 2-CP, 4-CP, DCP and TCP	SPE-HPLC-UV-vis	0.015–0.1 0.035–0.15	< 7	0.1-2.5	Tap water River water	[49]
Ph, 2-CP, DMP, CMP, DCP, TCP, PCP and nitrophenols	SPME-HPLC-UV-vis	1-10	0.7-17	10-1000	River water	[35]

All methods described here meet the sample preparation requirements, but, the SPME is one of the few microextraction techniques used in routine [50]. It is crucial to remember that the extraction process is based on the partitioning of analytes between the sample and

a stationary phase (liquid or solid). Unfortunately, no matter the chosen extraction technique, the use of different acceptor phases cover a relatively wide scale of polarity, extracting target analytes and undesired compounds together, which can pose problems associated with interferences in the analytical method. Therefore, in recent years, molecularly imprinted polymers (MIPs) have been used as a sorbent material to overcome many of the limitations previously reported with and lack of selectivity being a particular issue. These will be discussed in more detail in section 1.6.

1.5.2 Determination of phenols

Several analytical techniques have been used for the determination of phenolic compounds, including high performance liquid chromatography (HPLC) and capillary electrophoresis (CE) with ultraviolet detection (UV) or mass spectrometry (MS) detectors [43,48,51–57]. GC has also been used with various detectors, such as flame ionization detector (FID) [31], MS [58–60] or electron-capture detector (ECD) [61] but requires a derivatization of the phenol hydroxyl moiety [2]. The derivatization step for phenols to a less polar compound is crucial in the case of GC because the hydroxy group in phenols produces broad and tailed peaks. The derivatization for phenols could be applied either before or after extraction from water, and has been even carried out within the GC injector port [2]. HPLC is preferred for analysis of polar compounds like phenols because of the possibility of buffers or acids used in the mobile phase, the purpose of which is to suppress ionization of the phenols or residual silanol groups of the stationary phase [2]. However, HPLC tends to show much lower peak capacity than GC which has led to advances in the use of smaller particle sized packings. The use of smaller particles, increases in the

backpressure required better HPLC systems operating at higher pressures resulting in ultra high performance liquid chromatography (UHPLC). The separation mechanism depends on the van Deemter equation (Eq. 1) [62].

$$H = A + \frac{B}{v} + Cv \quad (1)$$

The van Deemter equation (Eq. 1) [62] describes the relationship between the height equivalent to the theoretical plate (*H* or HETP), which assesses the column efficiency, and the flow rate of the mobile phase (*v*). When HETP values are small, improvements in separations using UHPLC arise mainly from reductions in the A (multipath) and C (mass transfer) terms attributed to the use of sub-2 μm particles [63,64]. The influence of various particle sizes on the optimal flow rate (F_{opt}) and the efficiency are shown in Figure 1.2 [64]. As particle sizes decrease, the factor that contributes to band broadening become less affected by employing a higher flow rate. The van Deemter curve becomes flatter as particle-size becomes smaller, with the efficiency less influenced by increasing the flow rate, which allows for higher sample throughput with high resolution and sensitivity. The column length can also be reduced when using smaller particle size packings without sacrificing resolution with increases in flow rate. This leads to further gains in the separation efficiency associated with reductions in diffusion related broadening with shorter separation times. The most significant change in the hardware associated with UHPLC systems is their tolerance for the high backpressures needed for these small particles, up to 15000 psi compared with 6000 psi in HPLC [63,65]. The differences between HPLC and UHPLC gives the latter advantages in speed and efficiency of separation, combined with smaller columns, reduced volumetric flow rates and lower

consumption of expensive high-purity solvents. These advantages are the driving force for the choice of UHPLC for the separation of the phenolic compounds presented in this thesis.

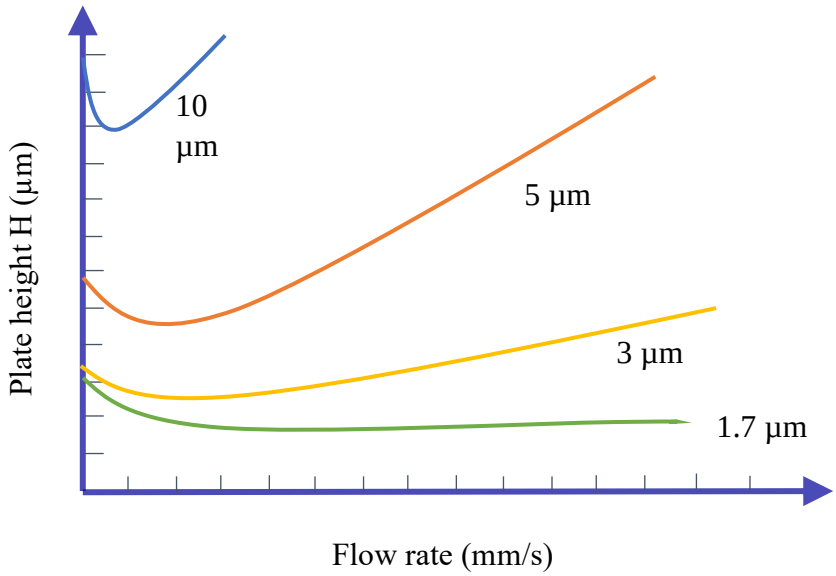

Figure 1.2. van Deemter Plot illustrating the effect of particle size (in µm) on plate height (H) van Demeter plot, illustrating the evolution of particle sizes over the last three decades [64,66].

1.6 Molecularly Imprinted Polymers

Although the concept of imprinted polymers emerged early in the 1970s (Wulff and co-workers), the specific use of the term 'imprinted polymer' only came into common use in 1984 [67–69]. The first paper that reported 'imprinted' polymers was written by Mosbach and B. Sellergren in 1984 [70]. MIPs are tailor-made materials with recognition sites that

rely on antibody-like interactions with target molecules [29]. MIPs potentially offer a degree of specificity and selectivity for a sorbent with the advantages of ease of preparation, mechanical and chemical stability, and ability to be used in harsh media (acidic, basic or with organic solvents). Moreover, unlike biological molecular recognition systems, they are inexpensive to make, do not need special storage conditions, and can be used over a wide temperature range [71,72].

The molecular imprinting technology is based on interactions between monomers and a template molecule, which, upon polymerization in the presence of an excess of a crosslinker, produces a stable three-dimensional polymeric network. The template is removed to produce MIPs that have cavities that are complementary in the functionality, shape, and size to the template. The geometry of binding sites of these cavities depends on the interactions created during the polymerization process (Figure 1.3) [73]. The polymerization process begins with dissolving the monomer, template, crosslinker agent and initiator in a porogenic solvent; then, the polymerization is started via thermal or photochemical initiation [74]. Non-imprinted polymers (NIPs) can be prepared using the same procedure as above, but in the absence of templates. The NIP is needed to investigate the imprinting factor in MIPs and non-selective interactions [73]. MIPs are used in many applications, such as separating and analyzing biological and environmental samples, drug delivery, catalysts, and selective sorbents in solid-phase extraction (MISPE) [73–75].

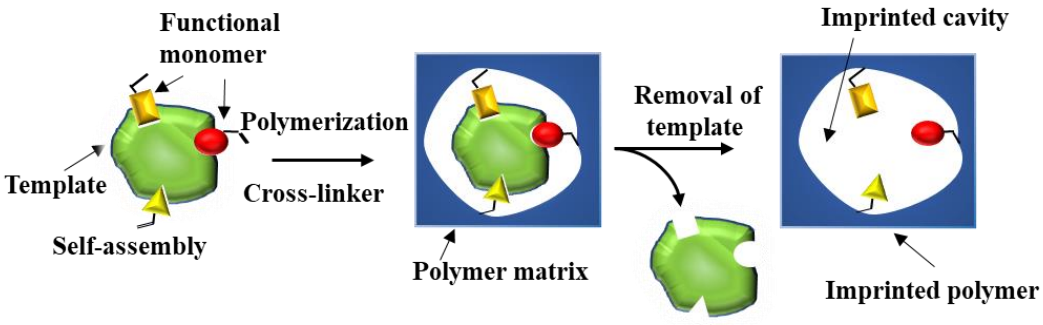

Figure 1.3. Preparation and recognition procedure for a molecularly imprinted polymer (MIP)

Depending on desired interactions between a template and a monomer in the pre-polymerization and rebinding steps, the MIP can be made using covalent, semi-covalent or noncovalent imprinting approaches. The covalent approach involves the formation of a covalent bond between the template and functional monomer prior to MIP synthesis and during the rebinding process. This approach provides more homogeneous and specific binding sites. However, it is least used due to the limited choice of templates and functional monomers, as well as the complexity of the rebinding process [76]. The semi-covalent imprinting may be thought of as a hybrid method based on both covalent and noncovalent interactions. Similar to the covalent approach, the semi-covalent imprinting needs more elaborate extraction processes, and it also has a limited range of suitable functional monomers, but the rebinding step involves noncovalent interactions [76]. In contrast, the noncovalent approach achieves imprinting and binding through noncovalent interactions such as hydrogen bonding, Van der Waals, and π-π interactions. The noncovalent approach was pioneered by the Mosbach group in 1984 [70]. The noncovalent methods afford

simplicity of synthesis and removal of templates from polymer matrices, as well as flexibility in the broader choice of functional monomers that can interact with different kinds of templates. However, the method suffers from the heterogeneity of the binding sites making it less selective and uptake behaviour non-linear over wide concentrations.

1.6.1 Composition of MIPs

As mentioned before, the synthesis of a MIP needs the following essential components: template, functional monomer, crosslinker, initiator, and solvent. The template could be the analyte it self or related structural analogue to the analyte [77]. The functional groups of monomers should have the ability to interact with the template to get selective binding sites. Figure 1.4A shows the most common functional monomers used in MIPs [78]. The crosslinkers (Figure 1.4B) play an important role in determining the morphology of the polymer matrix and in stabilizing the imprinted binding sites [77].

The selection of an initiator is determined by the required energy to initiate the radical polymerization process. The most common thermal initiator is 2,2′-azobis-(isobutyronitrile), which cleaves into radicals at about 60 °C [79]. The thermal initiator is usually used to induce the polymerization in a solution like precipitation and suspension polymerization. It generates isobutyronitrile radicals after homolytic cleavage under heat. In UV induced polymerization, 2,2-dimethoxy-2-phenylacetophenone (DMPA) is usually used as a photo-initiator, which forms radicals upon exposure to UV light under ambient conditions, even at lower temperatures. The MIPs in thin-film formats can be prepared quickly and easily by UV induced polymerization.

The porogen is responsible for dissolving all components present in a polymerization mixture and bringing all the components into one phase during polymerization. Solvents have an essential role in determining the porous structure and surface area of the imprinted polymers. The porosity originates during polymerization through the phase separation of the solvent and the growing polymer [80,81]. A polymer with a large pores size and low surface area is produced when the porogen has low solubility phase separation. On the contrary, a polymer with smaller pores and larger surface area is obtained using porogens that encourage phase separation relatively early in the growth of the polymer, i.e., a porogen is a solvent that is a relatively poor at keeping the growing polymer in solution [80,81]. The resulting porous structure in the polymers allows the substrates to access imprinted cavities.

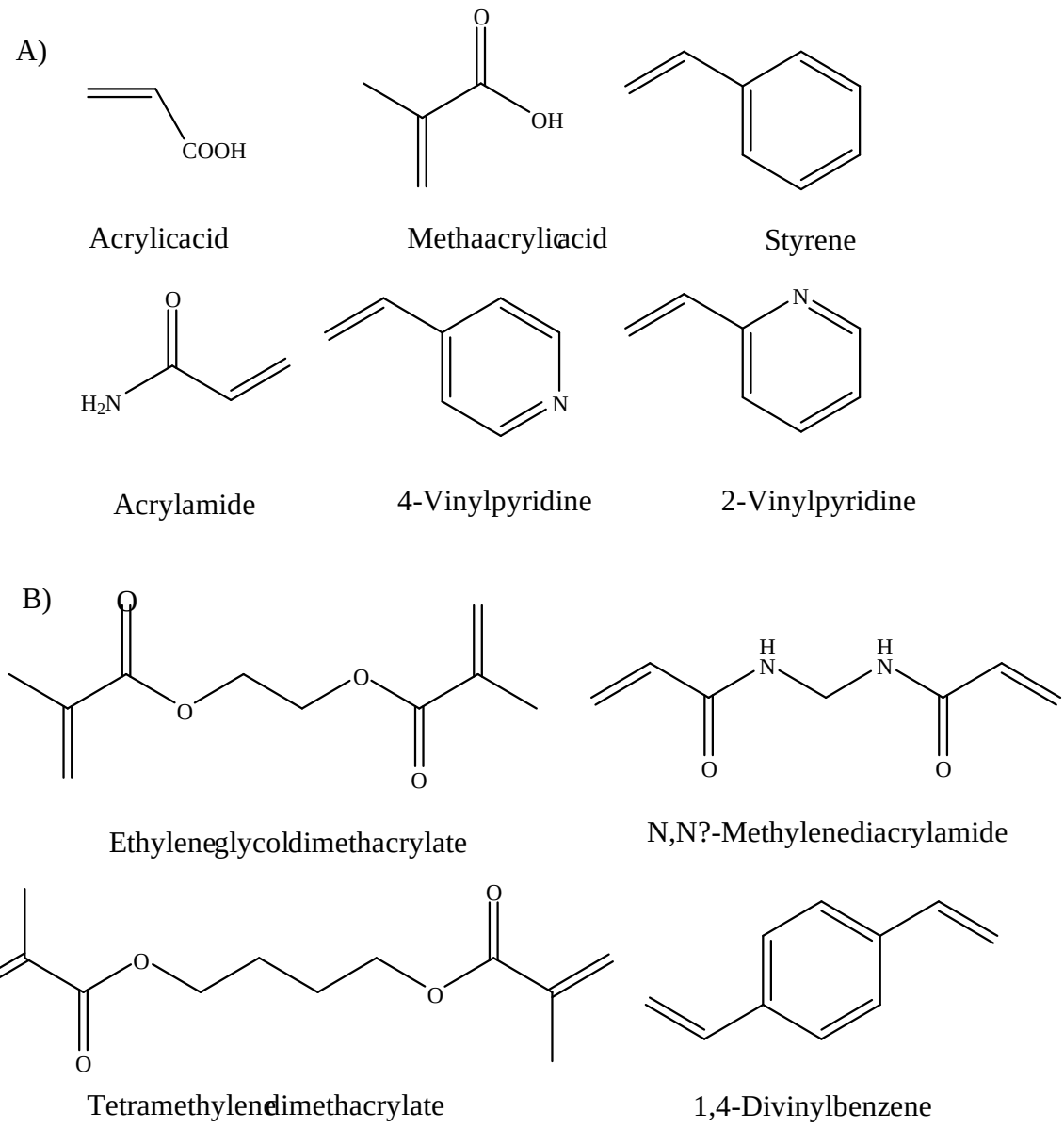

Figure 1.4. A) Common functional monomers used in noncovalent molecular imprinting

B) Common crosslinkers used in noncovalent molecular imprinting

1.6.2 Preparation methods for MIP

MIPs can be prepared in different physical formats; the choice of form depends on the final application. One of the most common is a bulk porous monolith, which can be prepared using bulk polymerization [72,78]. In this methodology, the polymer is converted to particle form by crushing and sieving the resulting polymer to yield the desired particle size. In fact, this method is quick and easy to execute, and it does not need operator skills. The obtained ground and sieved particles have irregular size and shape (which is unfavourable for chromatographic applications) [82]. Also, this method suffers from destruction of some binding sites during the grinding process, is time-consuming, and shows low loading capacity [72].

Suspension polymerization is a fast and straightforward way to obtain spherical porous beads. In this method, the polymerization mixture is suspended in a liquid (usually water) as a continuous phase and performed under vigorous stirring and by adding surfactant [72,83]. Using the surfactant in the mixture may create some problems because it could interfere in the template-monomer interactions. Furthermore, when water is used as a suspension phase, the non-covalent approach will be more challenging to occur.

The precipitation polymerization method is an alternative method to overcome the drawbacks that come from bulk polymerization. Precipitation polymerization method utilizes mostly more than 95% (w/v) of porogen; thus, it inhibits aggregation of the polymer particles [72]. So, the monomers should have sufficient strong interaction with the template under the precipitation polymerization conditions. This method provides MIP

microspherical shapes with a more uniform size with high binding capacity due to higher surface area than the corresponding bulk polymerization [77].

In situ-polymerization methods can be used in developing MIP monolith chromatographic columns and capillary electrochromatography by polymerization of a polymer mixture by UV or heating sources directly without grinding or sieving [84,85].

1.6.3 Optimization of MIP formulations

1.6.3.1 Choose the template and the functional monomer

MIPs fabricated using the non-covalent approach are the most attractive since they are relatively easy to make. In the non-covalent approach, the functional monomers should be chosen carefully, their selection ensuring their functional groups are complementary to that of the template. For example, the basic functional monomers are suitable for acidic template and vice versa [77]. The template plays an important role in creating imprinting cavities via interaction with the functional monomers. In most cases, the target molecule is selected as a template. However, a related structural analogue is used instead of the template to avoid template bleeding during trace analysis [77]. The selected template should be photostable, thermally stable, soluble in the pre-polymerization mixture, and should not contain polymerizable groups.

1.6.3.2 Optimization the ratio between the functional monomer and cross-linker

To obtain reliable imprinted cavities, the polymer should have the following properties: a) stiffness, allowing the cavities to conserve their shape after template removal; b) porosity, to give good accessibility to the imprinted cavities; and c) mechanical stability

[86]. These requirements must be balanced with the need for adsorption capacity and affinity and selectivity toward the target analytes [40]. Fixing the spatial arrangement of the monomer around the template by crosslinking is crucial to obtain rigid cavities and a good MIP. This is the usually achieved by formation of a copolymer of the monomer and a divinyl crosslinker. The morphology and stability of the polymer network are greatly influenced by the amount of crosslinker [77]. It has been found that the high crosslinker ratios are usually more favorable as these lead to high rigidity and stability for the imprinted cavities [87,88]. In fact, the physical characteristics of the polymer matrix are strongly dictated by the crosslinker properties. Sellergren was one of the first to investigate the optimum ratio for M:CL for the development of an enantioselective MIP for L-phenylalanine anilide as a template, methacrylic acid (MAA) as the functional monomer, and EGDMA as the crosslinker [89]. Sellergren varied the amount of functional monomer, kept the amount of crosslinker at the minimum required to produce a stiff polymer network that maintained binding site fidelity, and kept a fixed template:monomer ratio. It was found that the enantioselectivity for the MIPs towards L-phenylalanine anilide increased as MAA% was increased to 25%, but decrease above this ratio. Most reports emphasize that the best percentage of crosslinker in noncovalent imprinting polymer can be used in the range of 50% to 80% depending on the functional monomer nature [88,90]. This can only be achieved if the amount of monomer does not exceed 50%, which is consistent with the Sellergren study.

1.6.3.3 Optimization the ratio between the template and the functional monomer

After choosing a functional monomer that can form complementary interactions with the template and optimizing the M:CL ratio in the noncovalent imprinting approach, the spatial arrangement of monomers around the template should be optimized because the formation of high-affinity binding sites for the target analytes depends on the nature and the stability of the monomer-template complex [88,90–92]. The reason behind this is originated from the formation of the functional monomer-template complex, which is governed by Le Chatelier's principle [88]. In fact, the formation of an individual binding site in the MIP is attributed to the surrounding of the functional monomers around the template in the prepolymerization mixture, but based on Le Chatelier's principle, increasing either the amount of the monomer or the template could cause an increase in the monomer-template complex, consequently increasing the number of selective binding sites in the imprinted polymer. However, increasing the monomer concentration results in decreasing the M:CL ratio, which makes the percentage of the CL down of the limits required to maintain reliable the binding site. Thus, the monomer-template complex formation can be enhanced by increasing the template concentration while maintaining a fixed M:CL ratio. In theory, even if the template concentration increased to a high level, it will not change the composition of the imprinted polymer because the template is not covalently bonded to the monomer, and it is removed after the polymerization process. Kim *et al.* [91] studied the number of binding sites and the average association constant in the nicotine imprinted polymer over various template (nicotine) concentrations while keeping MAA:EGDMA (M:CL; 1:4) constant. They found that using more than 10% of

nicotine does not affect increasing the number of binding sites. This means that once all monomers have formed a complex with the template, any further addition of template will not find monomer to complex with, consequently, no more formation of binding sites. However, nicotine has two interactive amines groups; consequently, different interactions with MAA is expected. Thus, the average association constants were also studied over different template concentrations. They found that one-to-two stoichiometry of T:M has a greater affinity constant compared to the other T:M complexes. Therefore, the multiple functional monomer interactions in the final polymer seem to be responsible for the formation of binding sites with high affinity in the non-covalently imprinted polymers. Moreover, Andersson *et al.*[93] also investigated the effect of the nature of the monomer-template complex in the performance of nicotine imprinted polymer by using various concentrations of nicotine while maintaining the MAA:EGDMA (M:CL;1:4) ratio constant. They found that maximizing the template concentration did not improve the MIP performance. In contrast, the selectivity is much better when multiple functional monomers interact with the template in the polymer matrix. So, increasing binding interactions in the binding sites of the polymer may be responsible for obtaining binding sites with high fidelity and selectivity. This suggests that the optimum amount of functional monomers is determined after polymerization, not directly in the prepolymerization mixture. Also, the T:M stoichiometric ratios must be optimized by the study of a series of MIP formulations with different template concentrations at a constant M:CL ratio.

1.6.3.4 Choosing the porogen

The porogen plays an important role in the formation of the T:M pre-polymer complex before and after the polymerization process [77,82,88]. Before the polymerization, the noncovalent pre-polymer complex is influenced by the polarity of the porogen. The low polar porogens will enhance formation of polar noncovalent interactions in the pre-polymer complex, such as hydrogen bonding. In contrast, the more polar porogen, especially the protic, will disrupt the hydrogen bonding and enhance the hydrophobic effect, π-π interactions or Van der Waals forces. So, the selected porogen system should be able to dissolve all the MIPs components and give sufficient porous structure for the MIP.

1.6.4 Physical characterization of MIPs

MIPs are a solid material, thus cannot be characterized by the routinely used polymer characterization methods used for polymer solutions like gel permeation chromatography, solution NMR techniques, and direct UV measurements of the polymers. Moreover, MIPs are amorphous material, so the structure of the MIPs binding sites cannot be identified using crystallographic methods. Therefore, there are only limited methods for the physical characterization of MIPs, such as scanning electron microscopy (SEM), IR spectroscopy, surface area and porosity measurement. The spectroscopy methods can investigate the molecular-level properties for MIPs material, while surface area and porosity measurements describe the macroscopic characteristics of MIPs [88].

Microscopy has facilitated an understanding of the MIPs morphology [81]. In which, the surface morphology of MIPs can be investigated using SEM. As an example, Gonzalez G. *et al.* [94] used the morphological studies to connect the structural characteristics of

MIPs made with different formulation by changing the functional monomers types, porogens and the amounts of monomers, crosslinker and porogens with the results obtained from the binding experiments. Gryshchenko *et al.* [95] synthesized noncovalent MIPs for phenol using different monomers, crosslinkers and porogens. The surface morphologies for the different MIPs formulation were characterized using SEM. It was found the surface morphology gave an idea about the general structural characteristics but not in detail.

The surface area and porosity for MIPs are controlled by different factors, including the crosslinker percentage, the porogen and the applied temperature. Although the imprinting and selectivity for MIPs do not depend on the porosity, some applications like the drug delivery rely on the substrate transfer kinetics associated with porosity. The MIPs surface area can be measured using a nitrogen sorption porosimeter and analyzed using a BET (Brunauer, Emmett and Teller) [96] analysis routine. While pore size distributions in MIPs can be analyzed from the obtained nitrogen sorption data using BJH (Barret, Joyner and Halenda) methods [97].

FT-IR methods are useful for evaluating the degree of polymerization for the polymerizable groups in monomers and crosslinkers. As an example, quantifying the area under the peak corresponding to the C=C in the FT-IR spectrum at about 1640 cm^{-1} can help to evaluate the degree of polymerization [98,99].

1.6.5 Characterization of MIP performance

The performance of MIP can be described by the binding capacity and the selectivity. The binding capacity represents the maximum amount of substrate that can be bound by

MIP, and it can be determined by Langmuir, Freundlich or Langmuir-Freundlich adsorption isotherms, which will be described with details in Chapters 3 and 4 [77]. While the selectivity gives information about the ability of an MIP to distinguish the template among its analogues, the selectivity of an MIP can be determined by competitive rebinding experiments that involve incubation of the MIP and NIP in a solution containing a mixture of the different substrates. Then after equilibration, the supernatant solution is separated and analyzed [100]. There are two methods used to evaluate the MIPs for capacity and selectivity, including adsorption isotherms and chromatographic methods. Both are discussed in this section; however, only adsorption isotherms are applicable to thin-film MIPs.

1.6.5.1 Evaluation of binding sites in MIPs by adsorption isotherms from batch rebinding studies

The batch rebinding experiments are considered one of the best methods for evaluating the binding sites in the MIPs. Batch rebinding involves adding a specific amount of MIP to a solution of an analyte at specific concentration [88]. The amount of analyte bound to the MIP (B) is calculated from the difference between the total amount of the substrate added and the free substrate left in the solution (C_e). The amount of substrate is divided by the mass of the solid polymer, and an adsorption isotherm built by plotting B versus the free concentration of analyte remain in the solution (C_e) after the adsorption process, as shown in Figure 1.5 A. The curved part of the binding isotherm is suggestive of particular binding sites in the MIP, while a straight line indicates the existence of the availability of binding sites. It is necessary to optimize the rebinding batch experiment conditions and

adjust the amount of polymer to obtain a binding isotherm that is representative of the specific imprinted sites in the MIP.

The affinity towards the MIP emerges from the variation in the free energy of adsorption of one substrate against another. The binding of the substrate through the MIP is determined by the free energy (Eq. 2). Where *Q* represents the relative partition coefficient of the substrate between the MIP and solution (Eq. 3):

$$\Delta G^{\circ} = -RTlnQ \tag{2}$$

$$Q = \frac{B}{C_e} \tag{3}$$

The imprinting factor (*IF*) can be evaluated from the ratio of the partition coefficient of an analyte on the MIP (Q_{MIP}), and the partition coefficient using the same analyte on the NIP (Q_{NIP}) (Eq. 4) [101]. In this way, the binding produced as a result of non-specific interactions is removed, leaving behind the binding that can be attributed to the imprinting effect. The evaluation of the imprinting effect is complex when comparing different substrates. The differentiation in the binding behaviour between the different substrates towards the MIPs is generated by the differences in hydrophobicity, polarity, shape and conformation effects [88]. The selectivity factor (*SF*) can be estimated by taking the ratio of imprinting factors for two different analytes (Eq. 5).

$$IF = \frac{Q_{MIP}}{Q_{NIP}} \tag{4}$$

$$SF = \frac{IF_1}{IF_2} \tag{5}$$

The heterogeneous distribution of binding sites in MIP was reported early by Spivak [88], Shimizu *et al.*[79,102–105] and Kim and Spivak [91], in which they explained the formation of binding sites with different affinities in MIPs.

The distribution of the binding sites is, to some extent, hidden in the curvature in the binding isotherms (Figure 1.5 A); however, it is more clear when the isotherm is represented by the Scatchard plot (Figure 1.5 B), which is determined using Eq. 6.

$$\frac{B}{C_e} = KN - KB \tag{6}$$

Where *K* represents the association constant, and N is the total number of binding sites.

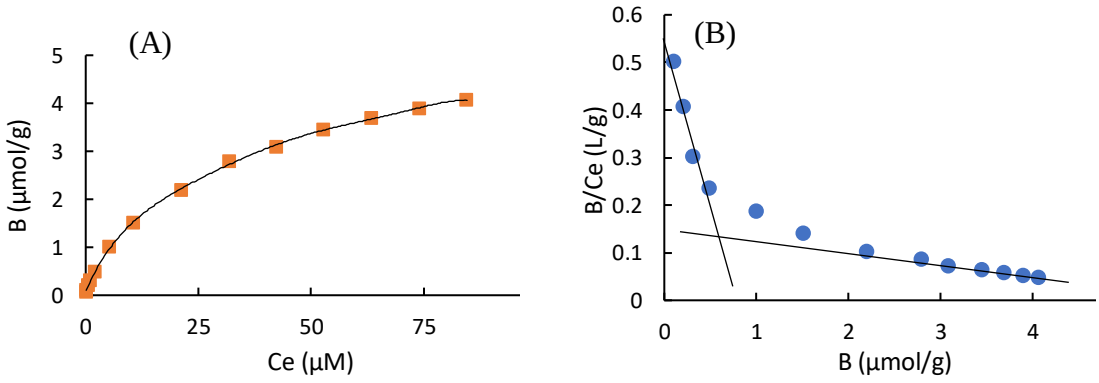

Figure 1.5. Graph of (A) binding isotherm [106] and (B) corresponding Scatchard plots (unpublished data from this work) for adsorption of phenol toward a catechol imprinted polymer.

For homogenous binding site system with a single binding site energy, the Scatchard plot gives a straight line, which means one group of the association constant and binding sites. However, most MIPs give curved Scatchard plots, which indicates the presence of a

distribution of binding sites (Figure 1.5 B). The two straight lines refer to two groups of binding parameters, which represent the high and low-affinity binding sites.

Shimizu *et al.*[79,102–105] and Guiochon *et al.*[107–109] have analyzed the adsorption isotherms for MIPs using the Freundlich equation (Eq. 7). Where *B* refers to amounts of analyte bound per gram of polymer, *a* represents Freundlich constant, and *m* is the Freundlich heterogeneity index, which supposes to be between 0 and 1.

$$B = aC^m \tag{7}$$

When the Freundlich equation is used successfully in making an acceptable fitting binding isotherm for the experimental data over the concentration range, the affinity distribution can be expressed in terms of the Freundlich parameters, *a* and *m,* (Eq. 8).

$$N(K_i) = a\frac{\sin(\pi m)}{\pi}K_i{}^{-m} \tag{8}$$

Eq. 8 can be written in the exponential form (Eq. 9) to represent the affinity distribution, as shown in Figure 1.6. The area under the curve gives an idea about the total binding sites within specific affinity limits. Thus, if Eq. 9 is integrated between the two affinities limit lnK_{min} and lnK_{max} (Eq. 10), a new function is obtained that estimates the area under the curve and, consequently, the total binding sites (Eq. 11).

$$N(K_i) = a\frac{\sin(\pi m)}{\pi}e^{-m\ln K_i} \tag{9}$$

$$N(K_i) = \int_{lnK_{min}}^{lnK_{max}} N(K_i)\, d(lnK_i) \tag{10}$$

$$N = a\frac{\sin(\pi m)}{m\pi}(K_{min}^{-m} - K_{max}^{-m}) \tag{11}$$

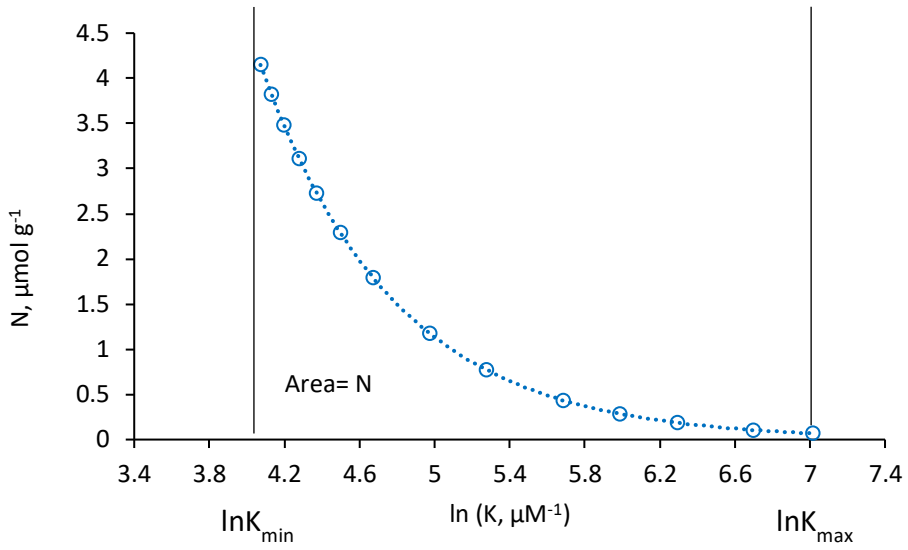

Figure 1.6. The affinity distribution for a catechol imprinted polymer toward phenol (data from our work in the simultaneous adsorption of phenols)

To evaluate the average binding affinity over the affinity range (K_{min}-K_{max}), the sum of all the product of binding sites, $N(K_i)$, and the corresponding affinity constant, K_i, is divided by the sum of $N(K_i)$ which is the total number of sites over the entire range, (Eq. 12). The summation expression in Eq. 12 can be replaced by the integration to obtain Eq. 13

$$\bar{K} = \frac{\sum N(K_i)\, K_i}{\sum N(K_i)} \tag{12}$$

$$\bar{K} = \frac{\int_{lnK_{min}}^{lnK_{max}} N(K_i) K_i \, d(lnK_i)}{\int_{lnK_{min}}^{lnK_{max}} N(K_i)\, d(lnK_i)} \tag{13}$$

Eq. 9 is substituted in the numerator and denominator, then the average affinity constant is obtained after the integration (Eq. 14).

$$\bar{K} = \left(\frac{m}{m-1}\right)\left(\frac{K_{min}^{1-m} - K_{max}^{1-m}}{K_{min}^{-m} - K_{max}^{-m}}\right) \quad (14)$$

Once the number of average affinities constant is calculated for each analyte, the separation factor ($\alpha = {\bar{K}_2}/{\bar{K}_1}$), which represents the relative average affinities between two substrates, indicates how many times better one substrate binds to the polymers than the other substrate. However, α values found are significantly dependent on the applied concentrations range. So, comparing α values alone may not be sufficient without considering how much the heterogeneity differences and the concentration range will affect the α values [88].

The analysis of the adsorption isotherm using the affinity distribution covers some crucial aspects of MIPs. As an example, the affinity distribution produced by the MIP made using the noncovalent approach has a wide exponential distribution over different binding strengths. While the MIPs made using the covalent approach is characterized by a narrow distribution around the modest affinity value [110]. This behaviour can be explained by better control of the template/monomer stoichiometry in the covalent approach compared to the noncovalent method.

1.6.5.2 Evaluation of MIPs using chromatographic methods

MIPs are a solid material, so they can be used as a stationary chromatographic phase by packing HPLC column with the MIP and NIP particles, which helps to evaluate the MIPs

in an easy and fast way. Sellergren [89] derived an equation to estimate the chromatographic binding related to the batch rebinding under equilibrium condition (Eq. 15).

$$\frac{B}{C_e} = \frac{k^{'}}{\emptyset} \tag{15}$$

Where $\emptyset$ represents the ratio between the stationary and mobile phase volumes, $k^{'}$ is the capacity factor which can be determined using Eq. 16:

$$k^{'} = \frac{t_R - t_0}{t_0} \tag{16}$$

Where t_R is the retention time of the substrate and t_0 is the retention time for the unretained sample.

The imprinting effect (*IF*) and the separation factor (α) for analogous analytes can be evaluated in the chromatograph using Eq. 17 and Eq. 18, respectively [111]. Where *IF* can be obtained from the ratio of the capacity factor of MIP relative to the corresponding NIP, α represents the relative ratio for the capacity factor between two analogous analytes.

$$IF = \frac{k^{'}_{MIP}}{k^{'}_{NIP}} \tag{17}$$

$$\alpha = \frac{k^{'}_2}{k^{'}_1} \tag{18}$$

The selectivity (*SF*) for the individual analyte can be assessed by taking ratio of imprinting factors for two different analytes (Eq. 19) [111].

$$SF = \frac{IF_1}{IF_2} \tag{19}$$

The chromatographic evaluation has some drawbacks because the binding characteristics and imprinting behaviour significantly depend on some factors such as particle size, the length and the diameter of the column, and the dynamic nature of the chromatographic separation [112]. The partitioning of adsorbates between the mobile phase that contains an organic modifier is significantly different from the adsorption in water samples. For example, MIP for 4-NP based on diethylaminoethyl methacrylate was evaluated using this chromatographic method. It was found that, as the percentage of water increases in the binary mobile phase system (Acetonitrile/water), the *IF* decreases [113]. Thus, the chromatographic evaluations are insufficient to characterize the binding of phenols in an aqueous solution, so the batch experiment was chosen to evaluate the MIPs in this project.

1.7 Parameters affecting adsorption efficiency

The adsorption of adsorbates (analytes) onto an adsorbent (MIP) is highly influenced by several factors such as the adsorbate concentration, adsorbent amount, adsorption time, salt and the pH of the solution. In this section, some of these parameters will be discussed below.

1.7.1 Salt effect

It has been known that organic compounds are mostly less soluble in aqueous salt solutions, like seawater compared to pure water; this phenomenon is called the "salting-out" effect. The solubility is inversely related to the activity coefficient, which affects the fate of organic compounds in the marine environment through different processes such as

adsorption and bioaccumulation [114]. In fact, adding strong electrolyte salt might either increase or decrease the solubility of the solute in water. The solubility of solutes depends on the polarity of both the solute and the salt. For example, strong salts like NaCl, increase the polarity of water; consequently, it decreases the solubility of the nonpolar solutes in water. Setschenow described the "salting-out" effect (Eq. 20) [114].

$$log\left(\frac{\gamma_o}{\gamma}\right) = log\left(\frac{S}{S_o}\right) = -K_{salt}C_{salt} \quad (20)$$

Where (γ_o, S_o) and (γ, S) are the activity coefficients and the solubilities of the organic solute in water and aqueous salt solution, respectively. C_{salt} (mol L^{-1}) is the molar concentration of the salt solution, and K_{salt} is the Setschenow constant or the salting-out constant and it relates to the type of the added salt.

El-sayed *et al.*[115] proposed a simple relationship for predicting the structural dependence of K_{salt} (for NaCl) with logP of the organic compound. They derived their assumption by referring to the log-linear relationship between the organic compound solubility and cosolvent concentration (Eq. 21), which is described by Alkowsky and coworkers [116]. They proved that the solubility of nonpolar solutes in an aqueous solution increase in the presence of organic cosolvents in water.

$$log\left(\frac{S}{S_o}\right) = \sigma C_{cosol} \quad (21)$$

Where S_o and S are the solubilities of the organic compound in water solution and cosolvent, respectively, C_{cosol} is the concentration of cosolvent and σ represents the solubilizing factor of the cosolvent for the organic compound solute, where the value of σ depends on both the polarity of the solute (logP) and the polarity of the solvent (Eq. 22).

$$\sigma = D \log P + T \tag{22}$$

Where *D* and *T* are constants related to the cosolvent. Merging Eq. 21 and 22 gives:

$$log\left(\frac{S}{S_o}\right) = (D \log P + T)C_{cosol} \tag{23}$$

Eq. 22 describes both the “solvating-in” and the “solvating-out” effects for polar solutes and nonpolar solutes.

The cosolvents and salts form homogenous solutions with water but with different effects. The cosolvents lower the polarity of the water and enhance the ability of the aqueous solution to “solvating in” the nonpolar solutes, consequently, increase of the solubility of nonpolar solutes. While the presence of salts increases the polarity of water, which causes a reduction in the solubility of nonpolar species "squeezing out". These facts are described in Eqs. 20 and 21, which indicate a log-linear relationship between the solubility of the solute and the concentration of salt or cosolvent, respectively. Thus, K_{salt} can also be correlated to logP producing:

$$K_{salt} = A \log P + B \tag{24}$$

Where *A* and *B* are constants related to the salt. Combining Eqs. 20 and 24 gives:

$$log\left(\frac{\gamma_o}{\gamma}\right) = log\left(\frac{S}{S_o}\right) = -(A \log P + B)C_{salt} \tag{25}$$

A linear relationship has been obtained by plotting the logP and Setschenow constant, K_{salt}, for 77 organic compounds, which emphasized the relationship between the added salt and the solubility of the organic compounds in water. As a result, the “salting-out” effect increases as the hydrophobicity of the solute increase.

1.7.2 pH of the solution effect

The pH has a significant effect on the adsorption of the organic compounds that contain protonated groups like phenols. Since the pH value of the solution is related to the dissociation constant (pKa) of the compound, which controls the amount of the ionized phenol molecules, thus, the rate of adsorption will be changed with the pH of an aqueous medium [117,118]. Phenols are weak organic acids. Therefore, when pH is less than pKa, the neutral forms are dominated for phenols; when the pH of the solution was increased above the pKa value, phenols molecules will be present as negative ions (phenolate ion). Moreover, the pH of the aqueous medium affects the surface charge of the adsorbent; consequently, it leads to a change in the adsorption behaviour of adsorbates. As an example, increasing the pH for the aqueous media will charge the surface with a negative charge for the adsorbent surface that has a hydrophobic nature like the activated carbon. Thus, the adsorption of phenols will be expected to decrease because of the repulsive force between the adsorbent surface and the phenolate species [118].

1.8 MIPs for phenols

Phenolic compounds are widespread and found in several environments based on their prevalence and potential for toxicity; it is necessary to study these compounds. This section will briefly summarize some MIPs for phenols.

An *et al.*[119] prepared a MIP for phenol-based on the grafting of polyethyleneimine (PEI) onto a surface of silica gel particles using 2,2′-(Ethylenebis(oxymethylene)) bisoxirane as a crosslinker. Phenol interacts with PEI through strong hydrogen bonding.

The adsorption and recognition toward phenol, resorcinol and *p*-nitrophenol were studied through static adsorption experiments for both the NIPs and MIPs Figure 1.7 shows the adsorption isotherms of NIP (A) and MIP (B) towards phenol, resorcinol and p-nitrophenol. Figure 1.7A indicates that the NIP has a similar binding affinity towards all substrates, but after imprinted with phenol, the MIP (Figure 1.7B) exhibited a strong affinity toward phenol only.

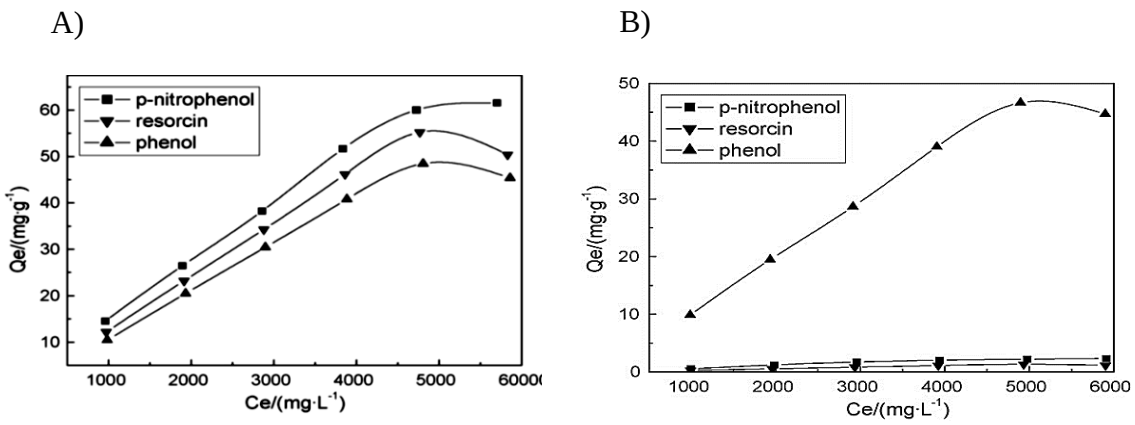

Figure 1.7. A) Adsorption isotherms of phenol, resorcinol and *p*-nitrophenol on CPPEI/SiO_2. Temperature: 20 ºC; time: 8 h; pH 7. B) Adsorption isotherms of phenol, resorcinol and *p*-nitrophenol on MIPPEI/SiO_2. Temperature: 20 ºC; time: 8 h; pH 7. [119]

Qi *et al.* [120] used the MISPE technique to pre-concentrate phenolic compounds from environmental water samples. The MIPs were synthesized through bulk polymerization, and 2,4-dimethylphenol (DMP) was used as a template. The imprinted polymer was optimized using three different porogens, including toluene, acetonitrile, and chloroform. The authors proved experimentally that the fabricated MIP using acetonitrile showed imprinting factor superiority compared with the other solvents. The imprinted and the non-imprinted SPE were used to pre-concentrate and determine the concentration of some

phenolic compounds in river water spiked with DMP, DCP, 4-chlorophenol (4-CP), 4-methylphenol (4-MP), Ph and 2,4,6-Trimethylphenol (2,4,6-TMP). The chromatograms of the samples were obtained by HPLC-PDA (Figure 1.8). The chromatograms illustrated that the MIP is more selective toward these phenolic compounds rather than the NIP.

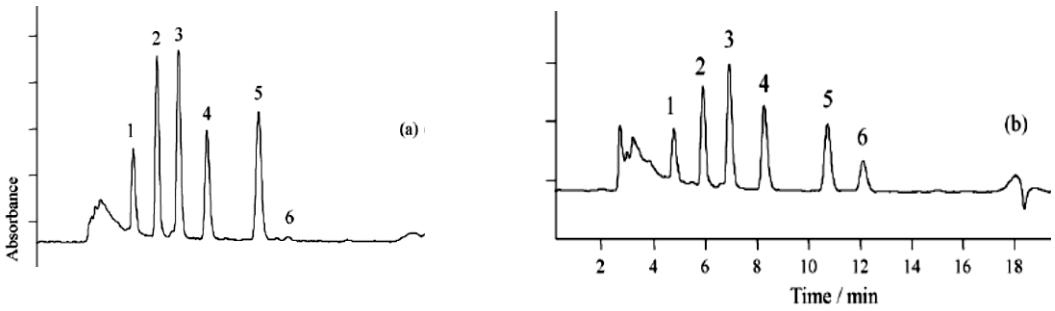

Figure 1.8 . Chromatograms obtained by MIP-SPE with the DMP imprinted polymer a) and non-imprinted polymer b) of 50 mL Yingkou river water spiked at 0.1μg/mL with each phenolic compound. Peak designation: (1) Ph, (2) 4-MP, (3) 4-CP, (4) DMP, (5) DCP and (6) 2,4,6-TMP. [120]

Qi *et al.*[76] synthesized MIPs for phenols via a semi-covalent imprinting approach. They used 4-chlorophenyl (4-vinyl) phenyl carbonate (4-CPC) as a covalently bound template monomer, ethylene glycol dimethylacrylate (EGDMA) as a crosslinker, and chloroform as porogen. The carbonyl group in 4-CPC acts as a spacer and can be easily hydrolyzed and lose CO_2 to produce specific homogenous binding sites (Figure 1.9).

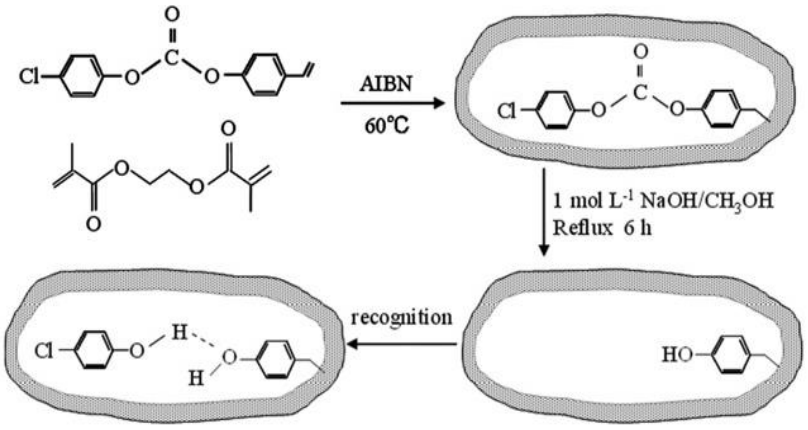

Figure 1.9. Schematic representation of the polymer preparation of 4-chlorophenol-imprinted polymers by semi-covalent approach. [76]

The ability of the MIPs to separate the phenolic compounds (Ph, 4-CP, DCP, TCP) was investigated by packing the MIPs in HPLC column. The results proved that the MIPs retain the analytes more strongly, and MIPs can separate the phenolic mixture better than the NIPs (Figure 1.10 a and b) [76].

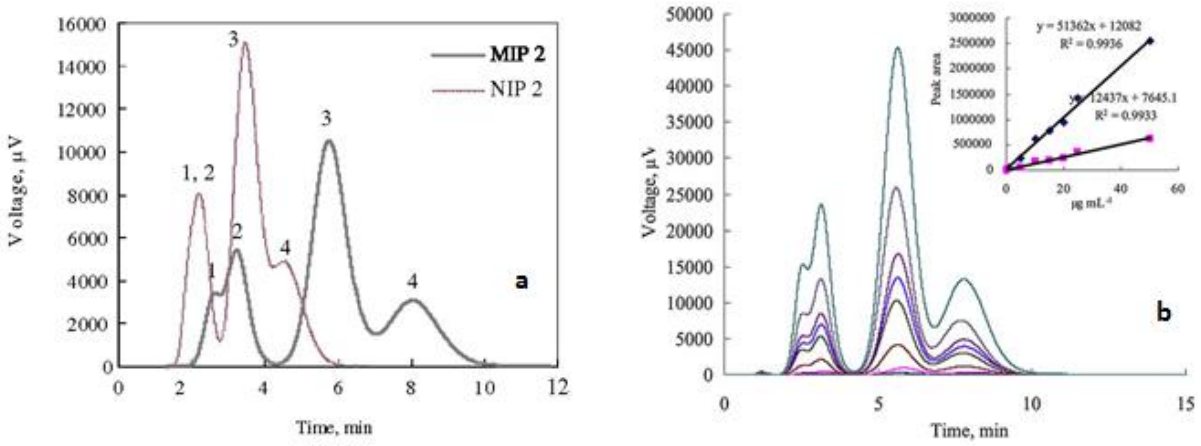

Figure 1.10. (a) Elution profiles of phenolic compounds on the HPLC columns packed with the semi-covalently imprinted polymer, (b) Elution profiles on MIP column of phenols with different concentrations, and corresponding calibration curves of phenol and 4-CP. Peak designation: (1) TCP, (2) DCP, (3) Ph, (4) 4-CP. [76]

Gryshchenko and Bottaro [95] fabricated thin films of MIPs on glass slides via the drop-casting technique. Various MIPs were prepared for phenol, in which itaconic acid, 4-VP, and styrene were used as monomers; EGDMA, triethylene glycol dimethacrylate (TGDMA), and pentacrythritol triacrylate (PETA) were used as crosslinkers. The porosity of the MIPs was achieved by using suitable porogens, such as methanol/water, chloroform, and DMF, along with some solvent modifiers (polyethyleneglycol and polyvinylacetate). The adsorption and the recognition of these MIPs toward phenol were evaluated using adsorption isotherms, where the rebinding process was in aqueous media. Among these MIPs, only styrene-PETA MIP showed modest imprinting effects. This result was expected because the recognition of phenol through hydrogen bonding is inhibited in aqueous media, and the π-π interactions in phenol are not as strong as hydrogen bonding interactions. Thus,

styrene enhances the π-π interactions and the hydrophobic effect, and the PETA crosslinker gave a strong network polymer matrix as well as a water-compatible surface, which helps in decreasing the non-specific binding sites.

1.9 Main Research goals

The overarching objective of this research project was to develop a simple, inexpensive, reproducible, scalable, and high throughput microextraction device based on adsorption by a novel MIP for phenolic compounds in environmental water samples. A catechol imprinted MIP was developed for simultaneous extraction of eleven phenols with a range of polarities; a new and fast method was developed for quantitation of the target phenolics using UHPLC-PDA.

In Chapter 2, a MIP thin-film coating for the microextraction device was optimized to improve the imprinting efficiency. The focus of this work was the selection of functional monomer, pseudo-template, and porogen, along with optimization of the ratios of each constituent in the MIP formulation evaluated in terms of adsorption capacity, reproducibility and selectivity. Multiple extraction parameters, such as salinity, pH, polymer mass, desorption solvent, and desorption time were investigated to optimize the extraction efficiency. The analytical performance of the MIP-UHPLC-PDA method was assessed based on the standard figure of merit (LOD, enrichment factor (EF), linearity, precision, and accuracy) and performance in complex matrices based on calibration in DI water. The MIP-UHPLC-PDA was validated to determine concentrations of the targeted phenolic compounds in spiked seawater and PW samples.

MIPs made through the non-covalent approach produce mostly heterogeneous binding site distributions with different affinities due to the formation of different template-functional monomer aggregates with a weak dynamic interaction, the non-selective interactions with the crosslinker, and excess functional monomers orientation before polymerization. Thus, in Chapter 3, the adsorption isotherm models have been used to characterize the interactions between analytes and MIP surfaces to enhance comprehension of the adsorption chemistry and give numerical descriptors of MIP binding characteristics to compare performance. The adsorption behaviour of five phenolic compounds loaded individually on catechol imprinted polymer was explained using four different isotherm models: Langmuir, Freundlich, Langmuir–Freundlich, and BET isotherms based on the fitting parameters of the adsorption isotherms like the total binding sites, the binding affinities for the target analytes towards the MIP and NIP.

In Chapter 4, the cross-reactivity of catechol imprinted polymer and analogous non-imprinted polymers (NIPs) for simultaneous adsorption of eleven phenolic compounds was studied using four different isotherm models: Langmuir, Freundlich, Langmuir–Freundlich, and BET isotherms. The binding affinity for binding sites was studied by fitting the experimental data at low and high concentration levels to find a new way to estimate the imprinting factor.

Chapter 5 includes a summary of my work and some future work ideas that could improve the performance of the catechol-MIPs device and help in proving the multilayer theory in the aqueous adsorption process.

1.10 Co-authorship Statement

Ghadeer F. Abu-Alsoud carried out all experiments, including developing the methodology, validation, formal analysis, and writing of the first draft and corrections as directed by Dr. Bottaro for all chapters. Each of the chapters reporting experimental results (Chapters 2-5) are slightly modified versions of the manuscripts published and indicated at the start of each chapter.

Kelly A. Hawboldt: Reviewed data and provided feedback on the manuscripts for Chapters 3 and 4.

Christina S. Bottaro: Participated in the project conceptualization, supervision, data analysis, editing and revision of papers reported in the chapters and the editing of all chapters in the thesis

Chapter 2 was published as a research paper: Ghadeer F. Abu-Alsoud and Christina S. Bottaro*; Talanta , 2021, 223, part 2, 121727; https://doi.org/10.1016/j.talanta.2020.121727.

Chapter 3 was published as a research paper: Ghadeer F. Abu-Alsoud, Kelly A. Hawboldt, and Christina S. Bottaro*; *ACS Appl. Mater. Interfaces* 2020, 12, 10, 11998–12009. https://doi.org/10.1021/acsami.9b21493.

Chapter 4 was published as a research paper: Ghadeer F. Abu-Alsoud, Kelly A. Hawboldt, and Christina S. Bottaro*; *Journal of Chromatography A,* 1629 (2020); https://doi.org/10.1016/j.chroma.2020.461463.

1.11 References

(1) Michałowicz, J.; Duda, W. Phenols – Sources and Toxicity. *Polish J. Environ. Stud.* **2007**, *16* (3), 347–362.

(2) Mahugo Santana, C.; Sosa Ferrera, Z.; Esther Torres Padrón, M.; Juan Santana Rodríguez, J. Methodologies for the Extraction of Phenolic Compounds from Environmental Samples: New Approaches. *Molecules* **2009**, *14* (1), 298–320. https://doi.org/10.3390/molecules14010298.

(3) Kadmi, Y.; Favier, L.; Yehya, T.; Soutrel, I.; Simion, A. I.; Vial, C.; Wolbert, D. Controlling Contamination for Determination of Ultra-Trace Levels of Priority Pollutants Chlorophenols in Environmental Water Matrices. *Arab. J. Chem.* **2015**. https://doi.org/10.1016/j.arabjc.2015.06.005.

(4) Shiu, W. Y.; Ma, K. C.; Varhanícková, D.; Mackay, D. Chlorophenols and Alkylphenols: A Review and Correlation of Environmentally Relevant Properties and Fate in an Evaluative Environment. *Chemosphere* **1994**, *29* (1), 1155–1224. https://doi.org/10.1016/0045-6535(94)90252-6.

(5) Environment Canada. *Priority Substances List Assessment Report (Phenol)*; 2013.

(6) Zheng, J.; Chen, B.; Thanyamanta, W.; Hawboldt, K.; Zhang, B.; Liu, B. Offshore Produced Water Management: A Review of Current Practice and Challenges in Harsh/Arctic Environments. *Mar. Pollut. Bull.* **2016**, *104* (1–2), 7–19. https://doi.org/10.1016/j.marpolbul.2016.01.004.

(7) Jerry M. Neff; Lee, K.; DeBlois, E. M. Produced Water: Produced Water: Overview of Composition, Fates and Effects; *produced Water. Springer, New York,* 2011. https://doi.org/10.1007/978-1-4614-0046-2.

(8) Stephenson, M. T. Components of Produced Water. A Compilation of Industry Studies. *JPT, J. Pet. Technol.* **1992**, *44* (5), 548–603. https://doi.org/10.2118/23313-pa.

(9) Dórea, H. S.; Bispo, J. R. L.; Aragão, K. A. S.; Cunha, B. B.; Navickiene, S.; Alves, J. P. H.; Romão, L. P. C.; Garcia, C. A. B. Analysis of BTEX, PAHs and Metals in the Oilfield Produced Water in the State of Sergipe, Brazil. *Microchem. J.* **2007**, *85* (2), 234–238. https://doi.org/10.1016/j.microc.2006.06.002.

(10) Ekins, P.; Vanner, R.; Firebrace, J. Zero Emissions of Oil in Water from Offshore Oil and Gas Installations: Economic and Environmental Implications. *J. Clean. Prod.* **2007**, *15* (13–14), 1302–1315. https://doi.org/10.1016/j.jclepro.2006.07.014.

(11) Fakhru'l-Razi, A.; Pendashteh, A.; Abdullah, L. C.; Biak, D. R. A.; Madaeni, S. S.; Abidin, Z. Z. Review of Technologies for Oil and Gas Produced Water Treatment. *J. Hazard. Mater.* **2009**, *170* (2–3), 530–551. https://doi.org/10.1016/j.jhazmat.2009.05.044.

(12) Bakke, T.; Klungsøyr, J.; Sanni, S. Environmental Impacts of Produced Water and Drilling Waste Discharges from the Norwegian Offshore Petroleum Industry. *Mar. Environ. Res.* **2013**, *92*, 154–169. https://doi.org/10.1016/j.marenvres.2013.09.012.

(13) Weber, M.; Weber, M.; kleine-Boymann, M. Phenol: *Ullman's encyclopedia of industrial chemistry*; 2012; Vol. 26, pp 503–519. https://doi.org/10.1002/14356007.a19.

(14) Babich, H.; Davis, D. L. Phenol: A Review of Environmental and Health Risks. *Regul. Toxicol. Pharmacol.* **1981**, *1* (1), 90–109. https://doi.org/10.1016/0273-2300(81)90071-4.

(15) US EPA. Hazard Summary Phenol, 2000. https://www.epa.gov/sites/production/files/2016-09/documents/phenol.pdf

(16) *Canadian Environmental Protection Act*, CEPA. *Chlorophenols*; 1987.

(17) Czaplicka, M. Sources and Transformations of Chlorophenols in the Natural Environment. *Sci. Total Environ.* **2004**, *322* (1–3), 21–39. https://doi.org/10.1016/j.scitotenv.2003.09.015.

(18) Gribble, G. W. The Diversity of Natural Organochlorines in Living Organisms. *Pure Appl. Chem.* **1996**, *68* (9), 1699–1712.

(19) Canadian Council of Ministers of the Environment. *Canadian Water Quality Guidelines*; 2008. https://www.ccme.ca/files/Resources/supporting_scientific_documents/cwqg_pn_1040.pdf

(20) Leatherland, T. M.; Warhurst, A. M. An Environmental Assessment of Alkylphenol Ethoxylates and Alkylphenols. *J. Appl. Ecol.* **1995**, *32* (January), 890.

https://doi.org/10.2307/2404838.

(21) Xie, X.; Ma, X.; Guo, L.; Fan, Y.; Zeng, G.; Zhang, M.; Li, J. Novel Magnetic Multi-Templates Molecularly Imprinted Polymer for Selective and Rapid Removal and Detection of Alkylphenols in Water. *Chem. Eng. J.* **2019**, *357*, 56–65. https://doi.org/10.1016/j.cej.2018.09.080.

(22) Williams, M.; Risher, J.; Fay, M.; Llados, F.; Paikoff, S.; Rhoades, J. Toxicological Profile for Cresols. *U.S Public Heal. Serv. Agency Toxic Subst. Dis. Regist.* **2008**, No. September. https://doi.org/10.3109/15569529909037564.

(23) Agency for Toxic Substances and Disease Registry U.S. Public Health Service. Toxicological profile for cresol*s*; 1992. https://doi.org/10.20595/jjbf.19.0_3.

(24) Relevance to public health; Background and environmental exposures to cresols in the united states. https://www.atsdr.cdc.gov/toxprofiles/tp34-c2.pdf

(25) Marine, N. Canadian Water Quality Guidelines for the Protection of Aquatic Life. *Fluoridealert.Org* **1999**, 1–5. http://st-ts.ccme.ca/

(26) U.S. National Library of Medicine National Center for Biotechnology Information https://pubchem.ncbi.nlm.nih.gov.

(27) United States Environmental Protection Agency. https://www.epa.gov/ground-water-and-drinking-water/national-primary-drinking-water-regulations.

(28) Directive 2013/39/EU of the European parliament and of the council of 12 August 2013. *Amending Directives 2000/60/EC and 2008/105/EC as Regards Priority*

Substances in the Field of Water Policy; 2013. https://doi.org/http://eur-lex.europa.eu/legal-content/EN/TXT/?uri=celex:32013L0039.

(29) El-Sheikh, A. H.; Al-Quse, R. W.; El-Barghouthi, M. I.; Al-Masri, F. S. Derivatization of 2-Chlorophenol with 4-Amino-Anti-Pyrine: A Novel Method for Improving the Selectivity of Molecularly Imprinted Solid Phase Extraction of 2-Chlorophenol from Water. *Talanta* **2010**, *83* (2), 667–673. https://doi.org/10.1016/j.talanta.2010.10.022.

(30) US EPA. *Method 604:* Phenols, Methods For Organic Chemical Analysis Of Municipal And Industrial Wastewater; 1984. https://www.epa.gov/sites/production/files/2015-08/documents/method_604_1984.pdf https://doi.org/10.2134/jeq1987.00472425001600010011x.

(31) EPA agency. Phenols by Gas Chromatography, *EPA Method (8041A)*; 2007. https://www.epa.gov/sites/production/files/2015-12/documents/8041a.pdf.

(32) USEPA. *Method 625 - Base/Neutrals and Acids*; 1984. https://19january2017snapshot.epa.gov/sites/production/files/2015-10/documents/method_625_1984.pdf

(33) Rodríguez, I.; Llompart, M. P.; Cela, R. Solid-Phase Extraction of Phenols. *J. Chromatogr. A* **2000**, *885* (1–2), 291–304. https://doi.org/10.1016/S0021-9673(00)00116-3.

(34) Santana, C. M.; Ferrera, Z. S.; Padrón, M. E. T.; Rodríguez, J. J. S. Methodologies for the Extraction of Phenolic Compounds from Environmental Samples: New Approaches. *Molecules* **2009**, *14* (1), 298–320. https://doi.org/10.3390/molecules14010298.

(35) González-Toledo, E.; Prat, M. D.; Alpendurada, M. F. Solid-Phase Microextraction Coupled to Liquid Chromatography for the Analysis of Phenolic Compounds in Water. *J. Chromatogr. A* **2001**, *923* (1–2), 45–52. https://doi.org/10.1016/S0021-9673(01)00975-X.

(36) Abu-Alsoud, G. F.; Hawboldt, K. A.; Bottaro, C. S. Comparison of Four Adsorption Isotherm Models for Characterizing Molecular Recognition of Individual Phenolic Compounds in Porous Tailor-Made Molecularly Imprinted Polymer Films. *ACS Appl. Mater. Interfaces* **2020**, *12* (10), 11998–12009. https://doi.org/10.1021/acsami.9b21493.

(37) Prieto, A.; Araujo, L.; Navalon, A.; Vilchez, J. Comparison of Solid-Phase Extraction and Solid-Phase Microextraction Using Octadecylsilane Phase for the Determination of Pesticides in Water Samples. *Curr. Anal. Chem.* **2010**, *5* (3), 219–224. https://doi.org/10.2174/157341109788680309.

(38) Arthur, C. L.; Pawliszyn, J. Solid Phase Microextraction with Thermal Desorption Using Fused Silica Optical Fibers. *Anal. Chem.* **1990**, *62* (19), 2145–2148. https://doi.org/10.1021/ac00218a019.

(39) Merkle, S.; Kleeberg, K.; Fritsche, J. Recent Developments and Applications of

Solid Phase Microextraction (SPME) in Food and Environmental Analysis—A Review. *Chromatography* **2015**, *2* (3), 293–381. https://doi.org/10.3390/chromatography2030293.

(40) Tamayo, F. G.; Turiel, E.; Martín-Esteban, A. Molecularly Imprinted Polymers for Solid-Phase Extraction and Solid-Phase Microextraction: Recent Developments and Future Trends. *J. Chromatogr. A* **2007**, *1152* (1–2), 32–40. https://doi.org/10.1016/j.chroma.2006.08.095.

(41) Sarafraz-Yazdi, A.; Amiri, A. Liquid-Phase Microextraction. *TrAC - Trends Anal. Chem.* **2010**, *29* (1), 1–14. https://doi.org/10.1016/j.trac.2009.10.003.

(42) Jeannot, M. A.; Cantwell, F. F. Solvent Microextraction into a Single Drop. *Anal. Chem.* **1996**, *68* (13), 2236–2240. https://doi.org/10.1021/ac960042z.

(43) Dolatto, R. G.; Messerschmidt, I.; Fraga Pereira, B.; Martinazzo, R.; Abate, G. Preconcentration of Polar Phenolic Compounds from Water Samples and Soil Extract by Liquid-Phase Microextraction and Determination via Liquid Chromatography with Ultraviolet Detection. *Talanta* **2016**, *148*, 292–300. https://doi.org/10.1016/j.talanta.2015.11.004.

(44) Environmental Protection Agency. Determination of Phenols in Drinking Water by Solid Phase Extraction and Capillary Column Gas Chromatography/Mass Spectrometry. *EPA method* 528, **2000.** file:///C:/Users/Ghadeer/Downloads/M_528.PDF

(45) Hu, X. Z.; Wu, J. H.; Feng, Y. Q. Molecular Complex-Based Dispersive Liquid-Liquid Microextraction: Analysis of Polar Compounds in Aqueous Solution. *J. Chromatogr. A* **2010**, *1217* (45), 7010–7016. https://doi.org/10.1016/j.chroma.2010.09.013.

(46) Çabuk, H.; Ata, Ş. Rotation Mixing-Assisted Liquid–Liquid Microextraction: A New Microextraction Approach for the Determination of Priority Phenols in Water Samples. *Anal. Methods* **2016**, *8* (15), 3123–3131. https://doi.org/10.1039/C6AY00062B.

(47) López-Darias, J.; Germán-Hernández, M.; Pino, V.; Afonso, A. M. Dispersive Liquid-Liquid Microextraction versus Single-Drop Microextraction for the Determination of Several Endocrine-Disrupting Phenols from Seawaters. *Talanta* **2010**, *80* (5), 1611–1618. https://doi.org/10.1016/j.talanta.2009.09.057.

(48) Zhang, P.-P.; Shi, Z.-G.; Feng, Y.-Q. Determination of Phenols in Environmental Water Samples by Two-Step Liquid-Phase Microextraction Coupled with High Performance Liquid Chromatography. *Talanta* **2011**, *85* (5), 2581–2586. https://doi.org/10.1016/j.talanta.2011.08.021.

(49) Bagheri, H.; Mohammadi, A.; Salemi, A. On-Line Trace Enrichment of Phenolic Compounds from Water Using a Pyrrole-Based Polymer as the Solid-Phase Extraction Sorbent Coupled with High-Performance Liquid Chromatography. *Anal. Chim. Acta* **2004**, *513*, 445–449. https://doi.org/10.1016/j.aca.2004.03.020.

(50) Turiel, E.; Martín-Esteban, A. Molecularly Imprinted Polymers-Based

Microextraction Techniques. *TrAC - Trends Anal. Chem.* **2019**, *118*, 574–586. https://doi.org/10.1016/j.trac.2019.06.016.

(51) Saraji, M.; Marzban, M. Determination of 11 Priority Pollutant Phenols in Wastewater Using Dispersive Liquid-Liquid Microextraction Followed by High-Performance Liquid Chromatography-Diode-Array Detection. *Anal. Bioanal. Chem.* **2010**, *396* (7), 2685–2693. https://doi.org/10.1007/s00216-010-3496-z.

(52) Çabuk, H.; Ata, Ş. Rotation Mixing-Assisted Liquid-Liquid Microextraction: A New Microextraction Approach for the Determination of Priority Phenols in Water Samples. *Anal. Methods* **2016**, *8* (15), 3123–3131. https://doi.org/10.1039/c6ay00062b.

(53) Lu, W.; Wang, X.; Wu, X.; Liu, D.; Li, J.; Chen, L.; Zhang, X. Multi-Template Imprinted Polymers for Simultaneous Selective Solid-Phase Extraction of Six Phenolic Compounds in Water Samples Followed by Determination Using Capillary Electrophoresis. *J. Chromatogr. A* **2017**, *1483*, 30–39. https://doi.org/10.1016/j.chroma.2016.12.069.

(54) Chen, M.; Zhu, P.; Xu, B.; Zhao, R.; Qiao, S.; Chen, X.; Tang, R.; Wu, D.; Song, L.; Wang, S.; Determination of Nine Environmental Phenols in Urine by Ultra-High-Performance Liquid Chromatography-Tandem Mass Spectrometry. *J. Anal. Toxicol.* **2012**, *36* (9), 608–615. https://doi.org/10.1093/jat/bks072.

(55) Zhong, C.; He, M.; Liao, H.; Chen, B.; Wang, C.; Hu, B. Polydimethylsiloxane/Covalent Triazine Frameworks Coated Stir Bar Sorptive

Extraction Coupled with High Performance Liquid Chromatography-Ultraviolet Detection for the Determination of Phenols in Environmental Water Samples. *J. Chromatogr. A* **2016**, *1441*, 8–15. https://doi.org/10.1016/j.chroma.2016.02.073.

(56) Puig, D.; Barcelo, D. Comparison of Three Different Liquid Chromatography-Mass Spectrometry Interfacing Techniques for the Determination of Priority Phenolic Compounds in Water. *J. Mass Spectrom.* **1996**, *31* (June), 1297–1307. https://doi.org/10.1002/(SICI)1096-9888(199611)31:11%3C1297::AID-JMS425%3E3.0.CO;2-L

(57) Neng, N. R.; Nogueira, J. M. F. Determination of Phenol Compounds in Surface Water Matrices by Bar Adsorptive Microextraction-High Performance Liquid Chromatography-Diode Array Detection. *Molecules* **2014**, *19* (7), 9369–9379. https://doi.org/10.3390/molecules19079369.

(58) Faraji, H.; Tehrani, M. S.; Husain, S. W. Pre-Concentration of Phenolic Compounds in Water Samples by Novel Liquid-Liquid Microextraction and Determination by Gas Chromatography-Mass Spectrometry. *J. Chromatogr. A* **2009**, *1216* (49), 8569–8574. https://doi.org/10.1016/j.chroma.2009.10.020.

(59) Regueiro, J.; Llompart, M.; Psillakis, E.; Garcia-Monteagudo, J. C.; Garcia-Jares, C. Ultrasound-Assisted Emulsification-Microextraction of Phenolic Preservatives in Water. *Talanta* **2009**, *79*, 1387–1397. https://doi.org/10.1016/j.talanta.2009.06.015.

(60) de Almeida, A. D.; Lacorte, S.; Vinhas, T.; Viana, P.; Barcelo, D. Monitoring of

Priority Pesticides and Other Organic Pollutants in River Water from Portugal by Gas Chromatography-Mass Spectrometry and Liquid Chromatography-Atmospheric Pressure Chemical Ionization Mass Spectrometry. *J Chromatogr.A* **2000**, *879* (1), 13–26. https://doi.org/10.1016/S0021-9673(00)00372-1.

(61) Fattahi, N.; Samadi, S.; Assadi, Y.; Hosseini, M. R. M. Solid-Phase Extraction Combined with Dispersive Liquid-Liquid Microextraction-Ultra Preconcentration of Chlorophenols in Aqueous Samples. *J. Chromatogr. A* **2007**, *1169* (1–2), 63–69. https://doi.org/10.1016/j.chroma.2007.09.002.

(62) van Deemter, J. J.; Zuiderweg, F. J.; Klinkenberg, A. Longitudinal Diffusion and Resistance to Mass Transfer as Causes of Nonideality in Chromatography. *Chem. Eng. Sci.* **1956**, *5* (6), 271–289. https://doi.org/10.1016/0009-2509(56)80003-1.

(63) Wren, S. A. C.; Tchelitcheff, P. Use of Ultra-Performance Liquid Chromatography in Pharmaceutical Development. *J. Chromatogr. A* **2006**, *1119* (1–2), 140–146. https://doi.org/10.1016/j.chroma.2006.02.052.

(64) Waters. The Promise of Small Particles. https://www.waters.com/waters/en_US/The-Promise-of-Small-Particles/nav.htm?cid=134804750&locale=en_US

(65) Fountain, K. J. UPLC versus UHPLC: Comparison of Loading and Peak Capacity for Small Molecule Drugs. https://www.waters.com/content/dam/waters/en/app-notes/2011/720003869/720003869-en.pdf

(66) Swetha Sri, R.; Bhavya Sri, K.; Mounika, C. A Review on Comparative Study of Hplc and Uplc. *Res. J. Pharm. Technol.* **2020**, *13* (3), 1570–1574. https://doi.org/10.5958/0974-360X.2020.00284.X.

(67) Wulff, G.; Sarhan, A.; Zabrocki, K. Enzyme-Analogue Built Polymers and Their Use for the Resolution of Racemates. *Tetrahedron Lett.* **1973**, *14* (44), 4329–4332. https://doi.org/10.1016/S0040-4039(01)87213-0.

(68) Wulff, G.; Grobe-Einsler, R.; Vesper, W.; Sarhan, A. Enzyme-Analogue Built Polymers, 5*). *Makromol. Chem.* **1977**, *178*, 2817–2825.

(69) Wulff, G.; Oberkobusch, D.; Minárik, M. Enzyme-Analogue Built Polymers, 18 Chiral Cavities in Polymer Layers Coated on Wide-Pore Silica. *React. Polym. Ion Exch. Sorbents* **1985**, *3* (4), 261–275. https://doi.org/10.1016/0167-6989(85)90017-0.

(70) Andersson, L.; Sellergren, B.; Mosbach, K. Imprinting of Amino Acid Derivatives in Macroporous Polymers. *Tetrahedron Lett.* **1984**, *25* (45), 5211–5214. https://doi.org/10.1016/S0040-4039(01)81566-5.

(71) Surikumaran, H.; Mohamad, S.; Muhamad Sarih, N.; Muggundha Raoov, R. β-Cyclodextrin Based Molecular Imprinted Solid Phase Extraction for Class Selective Extraction of Priority Phenols in Water Samples. *Sep. Sci. Technol.* **2015**, 50, 2342-2351. https://doi.org/10.1080/01496395.2015.1043016.

(72) Denderz, N.; Lehotay, J. Molecularly Imprinted Polymers. *Ceska Slov Farm.* **2012**,

61, 79–86. A Smithers Group Company Shawbury, United Kingdom.

(73) Vasapollo, G.; Sole, R. Del; Mergola, L.; Lazzoi, M. R.; Scardino, A.; Scorrano, S.; Mele, G. Molecularly Imprinted Polymers: Present and Future Prospective. *Int. J. Mol. Sci.* **2011**, *12* (12), 5908–5945. https://doi.org/10.3390/ijms12095908.

(74) Spivak, D.; Gilmore, M. a.; Shea, K. J. Evaluation of Binding and Origins of Specificity of 9-Ethyladenine Imprinted Polymers. *J. Am. Chem. Soc.* **1997**, *119* (19), 4388–4393. https://doi.org/10.1021/ja963510v.

(75) Haginaka, J. Monodispersed, Molecularly Imprinted Polymers as Affinity-Based Chromatography Media. *J. Chromatogr. B Anal. Technol. Biomed. Life Sci.* **2008**, *866*, 3–13. https://doi.org/10.1016/j.jchromb.2007.07.019.

(76) Qi, P.; Wang, J.; Wang, L.; Li, Y.; Jin, J.; Su, F.; Tian, Y.; Chen, J. Molecularly Imprinted Polymers Synthesized via Semi-Covalent Imprinting with Sacrificial Spacer for Imprinting Phenols. *Polymer (Guildf).* **2010**, *51* (23), 5417–5423. https://doi.org/10.1016/j.polymer.2010.09.037.

(77) Alvarez-lorenzo, C.; Angel, C. *Handbook of Molecularly Imprinted Polymers*; 2013.

(78) Yan, H.; Row, K. H. Characteristic and Synthetic Approach of Molecularly Imprinted Polymer. *Int. J. Mol. Sci.* **2006**, *7*, 155–178. https://doi.org/10.3390/i7050155

(79) Rampey, A. M.; Umpleby, R. J.; Rushton, G. T.; Iseman, J. C.; Shah, R. N.;

Shimizu, K. D. Characterization of the Imprint Effect and the Influence of Imprinting Conditions on Affinity, Capacity, and Heterogeneity in Molecularly Imprinted Polymers Using the Freundlich Isotherm-Affinity Distribution Analysis. *Anal. Chem.* **2004**, *76* (4), 1123–1133. https://doi.org/10.1021/ac0345345.

(80) Lloyd, L. L. Rigid Macroporous Copolymers as Stationary Phases in High-Performance Liquid Chromatography. *J. Chromatogr. A* **1991**, *544*, 201–217. https://doi.org/10.1016/S0021-9673(01)83986-8.

(81) Sellergren, B.; Shea, K. J. Influence of Polymer Morphology on the Ability of Imprinted Network Polymers to Resolve Enantiomers. *J. Chromatogr. A* **1993**, *635* (1), 31–49. https://doi.org/10.1016/0021-9673(93)83112-6.

(82) Włoch, M.; Datta, J. Chapter Two: Synthesis and Polymerisation Techniques of Molecularly Imprinted Polymers; *Comprehensive Analytical Chemistry*, **2019,** 86, 17-40, Editor(s): Mariusz Marć, Elsevier. https://doi.org/10.1016/bs.coac.2019.05.011.

(83) Bitas, D.; Samanidou, V. Molecularly Imprinted Polymers as Extracting Media for the Chromatographic Determination of Antibiotics in Milk. *Molecules* **2018**, *23* (2), 4–6. https://doi.org/10.3390/molecules23020316.

(84) Pichon, V.; Chapuis-Hugon, F. Role of Molecularly Imprinted Polymers for Selective Determination of Environmental Pollutants—A Review. *Anal. Chim. Acta* **2008**, *622* (1–2), 48–61. https://doi.org/10.1016/j.aca.2008.05.057.

(85) Rutkowska, M.; Płotka-Wasylka, J.; Morrison, C.; Wieczorek, P. P.; Namieśnik, J.; Marć, M. Application of Molecularly Imprinted Polymers in Analytical Chiral Separations and Analysis. *TrAC - Trends Anal. Chem.* **2018**, *102*, 91–102. https://doi.org/10.1016/j.trac.2018.01.011.

(86) Wulff, G. Molecular Imprinting in Cross-Linked Materials with the Aid of Molecular Templates— A Way towards Artificial Antibodies. *Angew. Chemie Int. Ed. English* **1995**, *34* (17), 1812–1832. https://doi.org/10.1002/anie.199518121.

(87) Sellergren, B.; Polymer And Template-Related Factors InfluePolymerncing the Efficiency in Molecularly Imprinted Solid-Phase Extractions. *TrAC Trends Anal. Chem.* **1999**, *18* (3), 164–174. https://doi.org/10.1016/S0165-9936(98)00117-4.

(88) Spivak, D. A. Optimization, Evaluation, and Characterization of Molecularly Imprinted Polymers. *Adv. Drug Deliv. Rev.* **2005**, *57* (12), 1779–1794. https://doi.org/10.1016/j.addr.2005.07.012.

(89) Sellergren, B. Molecular Imprinting by Noncovalent Interactions. Enantioselectivity and Binding Capacity of Polymers Prepared under Conditions Favoring the Formation of Template Complexes. *Macromol. Chem. Phys.* **1989**, *190* (11), 2703–2711. https://doi.org/10.1002/macp.1989.021901104.

(90) Fremielle Lim, K.; Holdsworth, C. I. Effect of Formulation on the Binding Efficiency and Selectivity of Precipitation Molecularly Imprinted Polymers. *Molecules* **2018**, *23* (11), 1–19. https://doi.org/10.3390/molecules23112996.

(91) Kim, H.; Spivak, D. A. New Insight into Modeling Non-Covalently Imprinted Polymers. *J. Am. Chem. Soc.* **2003**, *125* (37), 11269–11275. https://doi.org/10.1021/ja0361502.

(92) Mollnelli, A.; O'Mahony, J.; Nolan, K.; Smyth, M. R.; Jakusch, M.; Mizaikoff, B. Analyzing the Mechanisms of Selectivity in Biomimetic Self-Assemblies via IR and NMR Spectroscopy of Prepolymerization Solutions and Molecular Dynamics Simulations. *Anal. Chem.* **2005**, *77* (16), 5196–5204. https://doi.org/10.1021/ac050525f.

(93) Andersson, H. S.; Karlsson, J. G.; Piletsky, S. A.; Koch-Schmidt, A. C.; Mosbach, K.; Nicholls, I. A. Study of the Nature of Recognition in Molecularly Imprinted Polymers, II [1]: Influence of Monomer-Template Ratio and Sample Load on Retention and Selectivity. *J. Chromatogr. A* **1999**, *848* (1–2), 39–49. https://doi.org/10.1016/S0021-9673(99)00483-5.

(94) González, G. P.; Hernando, P. F.; Alegría, J. S. D. A Morphological Study of Molecularly Imprinted Polymers Using the Scanning Electron Microscope. *Anal. Chim. Acta* **2006**, *557* (1–2), 179–183. https://doi.org/10.1016/j.aca.2005.10.034.

(95) Gryshchenko, A. O.; Bottaro, C. S. Development of Molecularly Imprinted Polymer in Porous Film Format for Binding of Phenol and Alkylphenols from Water. *Int. J. Mol. Sci.* **2014**, *15* (1), 1338–1357. https://doi.org/10.3390/ijms15011338.

(96) Brunauer, S.; Emmett, P. H.; Teller, E. Adsorption of Gases in Multimolecular

Layers. *J. Am. Chem. Soc.* **1938**, *60* (2), 309–319. https://doi.org/10.1021/ja01269a023.

(97) Barrett E. P. ; Joyner L. G. ; Halend P. P. The Determination of Pore Volume and Area Distributions in Porous Substances. I. Computations from Nitrogen Isotherms. *J. Am. Chem. Soc.* **1951**, *73* (1), 373–380. https://doi.org/10.1021/ja01145a126.

(98) Shea, K. J.; Sasaki, D. Y. An Analysis of Small-Molecule Binding to Functionalized Synthetic Polymers by 13C/CP/MAS NMR and FT-IR Spectroscopy. *J. Am. Chem. Soc.* **1991**, *113* (11), 4109–4120. https://doi.org/10.1021/ja00011a009.

(99) Sibrian-Vazquez, M. Thesis: Design, Synthesis, and Applications of Bio-Derived Crosslinking Monomers for Molecular Imprinting. **2003**, No. December. http://etd.lsu.edu/docs/available/etd-1104103-130651.

(100) Mirsky V.M. and Yatsimirsky A. K. Artificial Receptors for Chemical Sensors; 2011. https://doi.org/10.1017/CBO9781107415324.004.

(101) Spivak, D. A. Molecularly Imprinted Materials: Science and Technology *:* Selectivity in Molecularly Imprinted Matrices; **2004,** 395-417. https://doi.org/10.1201/9781420030303.

(102) Umpleby, R. J.; Baxter, S. C.; Chen, Y.; Shah, R. N.; Shimizu, K. D. Characterization of Molecularly Imprinted Polymers with the Langmuir -

Freundlich Isotherm. *Anal. Chem.* **2001**, *73* (19), 4584–4591. https://doi.org/10.1021/ac0105686.

(103) Umpleby, R. J.; Baxter, S. C.; Bode, M.; Berch, J. K.; Shah, R. N.; Shimizu, K. D. Application of the Freundlich Adsorption Isotherm in the Characterization of Molecularly Imprinted Polymers. *Anal. Chim. Acta* **2001**, *435* (1), 35–42. https://doi.org/10.1016/S0003-2670(00)01211-3.

(104) Shimizu, K. D. Characterization of MIPs Using Heterogeneous Binding Models. *Mat. Res. Soc. Symp. Proc.* **2002**, *723*, 17–22.

(105) Umpleby, R. J.; Baxter, S. C.; Rampey, A. M.; Rushton, G. T.; Chen, Y.; Shimizu, K. D. Characterization of the Heterogeneous Binding Site Affinity Distributions in Molecularly Imprinted Polymers. *J. Chromatogr. B Anal. Technol. Biomed. Life Sci.* **2004**, *804* (1), 141–149. https://doi.org/10.1016/j.jchromb.2004.01.064.

(106) Abu-Alsoud, G. F.; Hawboldt, K. A.; Bottaro, C. S. Assessment of Cross-Reactivity in a Tailor-Made Molecularly Imprinted Polymer for Phenolic Compounds Using Four Adsorption Isotherm Models. *J. Chromatogr. A* **2020**, *1629* (461463). https://doi.org/10.1016/j.chroma.2020.461463.

(107) Sajonz, P.; Kele, M.; Zhong, G.; Sellergren, B.; Guiochon, G. Study of the Thermodynamics and Mass Transfer Kinetics of Two Enantiomers on a Polymeric Imprinted Stationary Phase. *J. Chromatogr. A* **1998**, *810* (1–2), 1–17. https://doi.org/10.1016/S0021-9673(98)00247-7.

(108) Szabelski, P.; Kaczmarski, K.; Cavazzini, A.; Chen, Y. B.; Sellergren, B.; Guiochon, G. Energetic Heterogeneity of the Surface of a Molecularly Imprinted Polymer Studied by High-Performance Liquid Chromatography. *J. Chromatogr. A* **2002**, *964* (1–2), 99–111. https://doi.org/10.1016/S0021-9673(02)00587-3.

(109) Stanley, B. J.; Szabelski, P.; Chen, Y. B.; Sellergren, B.; Guiochon, G. Affinity Distributions of a Molecularly Imprinted Polymer Calculated Numerically by the Expectation-Maximization Method. *Langmuir* **2003**, *19* (3), 772–778. https://doi.org/10.1021/la020747y.

(110) Umpleby, R. J.; Bode, M.; Shimizu, K. D. Measurement of the Continuous Distribution of Binding Sites in Molecularly Imprinted Polymers. *Analyst* **2000**, *125* (7), 1261–1265. https://doi.org/10.1039/b002354j.

(111) Cheong, S. H.; Mcniven, S.; Rachkov, A.; Levi, R.; Yano, K.; Karube, I. Testosterone Receptor Binding Mimic Constructed Using Molecular Imprinting. *Macromolecules* **1997**, *30* (5), 1317–1322. https://doi.org/10.1021/ma961014l

(112) Tóth, B.; Pap, T.; Horvath, V.; Horvai, G. Which Molecularly Imprinted Polymer Is Better? *Anal. Chim. Acta* **2007**, *591* (1 SPEC. ISS.), 17–21. https://doi.org/10.1016/j.aca.2007.01.016.

(113) Guerreiro, A.; Soares, A.; Piletska, E.; Mattiasson, B.; Piletsky, S. *Preliminary Evaluation of New Polymer Matrix for Solid-Phase Extraction of Nonylphenol from Water Samples*; *Anal. Chim. Acta* **2008**; 612, 99-104. https://doi.org/10.1016/j.aca.2008.02.010.

(114) Xie, W. H.; Shiu, W. Y.; Mackay, D. A Review of the Effect of Salts on the Solubility of Organic Compounds in Seawater. *Mar. Environ. Res.* **1997**, *44* (4), 429–444. https://doi.org/10.1016/S0141-1136(97)00017-2.

(115) Ni, N.; El-Sayed, M. M.; Sanghvi, T.; Yalkowsky, S. H. Estimation of the Effect of NaCl on the Solubility of Organic Compounds in Aqueous Solutions. *J. Pharm. Sci.* **2000**, *89* (12), 1620–1625. https://doi.org/10.1002/1520-6017(200012)89:12<1620::AID-JPS13>3.0.CO;2-N.

(116) Rubino, J. T.; Yalkowsky, S. H. Cosolvency and Cosolvent Polarity. *Pharm. Res*. **1987**, 4, 220–230. https://doi.org/10.1023/A:1016456127893.

(117) Peng, P.; Lang, Y. H.; Wang, X. M. Adsorption Behavior and Mechanism of Pentachlorophenol on Reed Biochars: PH Effect, Pyrolysis Temperature, Hydrochloric Acid Treatment and Isotherms. *Ecol. Eng.* **2016**, *90*, 225–233. https://doi.org/10.1016/j.ecoleng.2016.01.039.

(118) Abdelwahab, O.; Amin, N. K. Adsorption of Phenol from Aqueous Solutions by Luffa Cylindrica Fibers: Kinetics, Isotherm and Thermodynamic Studies. *Egypt. J. Aquat. Res.* **2013**, *39* (4), 215–223. https://doi.org/10.1016/j.ejar.2013.12.011.

(119) An, F.; Gao, B.; Feng, X. Adsorption and Recognizing Ability of Molecular Imprinted Polymer MIP-PEI/SiO(2) towards Phenol. *J. Hazard. Mater.* **2008**, *157* (2–3), 286–292. https://doi.org/10.1016/j.jhazmat.2007.12.095.

(120) Qi, P.; Wang, J.; Jin, J.; Su, F.; Chen, J. 2,4-Dimethylphenol Imprinted Polymers

as a Solid-Phase Extraction Sorbent for Class-Selective Extraction of Phenolic Compounds from Environmental Water. *Talanta* **2010**, *81* (4–5), 1630–1635. https://doi.org/10.1016/j.talanta.2010.03.015.

Chapter 2

2 Porous thin-film molecularly imprinted polymer device for simultaneous determination of phenol, alkylphenol and chlorophenol compounds in water

This chapter was published as a research paper: Ghadeer Abu-Alsoud.; Bottaro, C. Talanta 223 (2021) 121727. https://doi.org/10.1016/j.talanta.2020.121727

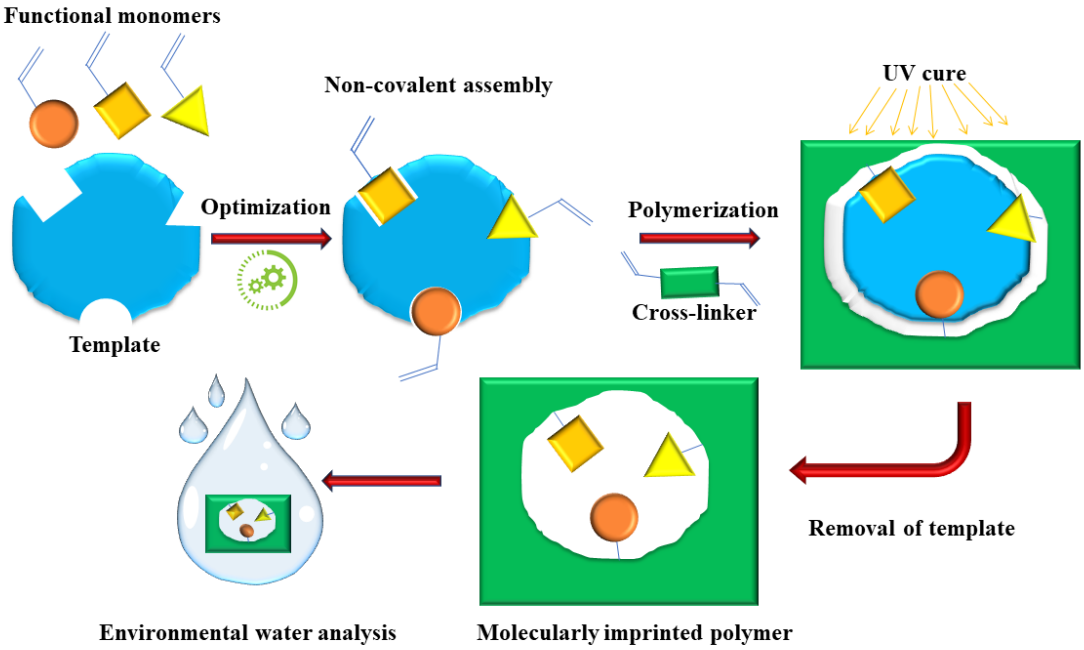

Keywords: Thin-film molecularly imprinted polymer; MIP formulation; Environmental water samples; UHPLC-PDA; Phenols

2.1 Abstract

A porous water-compatible molecularly imprinted polymer (MIP) coating using catechol as a pseudo-template and a water-soluble functional monomer (4-vinyl benzoic acid) with ethylene glycol dimethacrylate as the crosslinker was developed for extraction of phenols from environmental water samples. The MIP devices were combined with ultra high performance liquid chromatography with photodiode array detector (UHPLC-PDA) suitable for the simultaneous determination of trace levels of phenolic compounds with a wide range of polarities —phenol, alkylphenols and chlorophenols— in seawater and produced water. Parameters that influence extraction efficiency (salinity, pH, polymer mass, desorption solvent, and desorption time) were optimized to give method detection limits (LOD) ranging from 0.1 to 2 μg L^{-1} and linearity (R^2>0.99) over at least three orders of magnitude for the hydrophobic phenols (e.g., 0.5-1000 μg L^{-1} for 2,4,6-trichlorophenol) and ~2 orders of magnitude for the light phenols (e.g., 10-120 μg L^{-1} for phenol, 5-120 μg L^{-1} for methylphenols and 2-chlorophenol, 0.5-120 μg L^{-1} 3-methyl-4-chlorophenol and 2,4-dichlorophenol). The recoveries from authentic spiked samples ranged from 85-100% with %RSDs of 0.2-14% for seawater and 81-107% with %RSD of 0.1-11% for produced water. The resulting MIP-based extraction requires no pre-conditioning of the sorbent and because the required sample size is small and sample manipulation is limited, the method is easy to multiplex for high throughput sample processing.

2.2 Introduction

Phenols are common natural and anthropogenic compounds with a complex range of properties. Although phenol and related phenolic compounds can be released naturally through the degradation of plants and animal waste, the majority of the environmental burden of the more problematic phenolics is due to inputs from anthropogenic sources, e.g., from the processing of pulp and paper, metal, and petroleum products [1–3]. Estimates from Canada alone show that discharges of phenol/total phenolics into the air, water, and municipal treatment facilities exceed 400 tonnes per year [3]. Due to the volume of release and the potential of some phenolics for causing damage to human health and the environment, several phenols are found on priority pollutant lists worldwide [3–5].

Important phenols with respect to water pollution are chlorophenols [6,7] and alkylphenols [8,9]. Chlorophenols are persistent toxic substances that cause histopathological changes and mutations in aquatic life, and some are probable human carcinogens, e.g., pentachlorophenol (PCP) [10,11]. Alkylphenols have been found to be endocrine disrupters with wide-reaching impacts on the health and function of a range of aquatic organisms, as well as humans [12]. Health and Welfare Canada has set the maximum acceptable concentration (MAC) at 2 μg L^{-1} for phenols in drinking water, and chlorophenols in freshwater at 7, 0.2, 18, and 0.5 μg L^{-1} for monochlorophenols, dichlorophenols, trichlorophenols, and pentachlorophenol (PCP), respectively [13]. The United States Environmental Protection Agency (US EPA) classifies chlorophenols and alkylphenols as priority pollutants; however, they have focused regulation on PCP due to its potential effects on human health, setting the maximum contamination level (MCL) in

drinking water at 1 µg L^{-1} [11]. On the other hand, the European Union (EU) considers 4-tert-octylphenol (4-OP), and 4-nonylphenol (4-NP) priority pollutants along with PCP, with MACs at 1 µg L^{-1} for PCP and 2 µg L^{-1} for 4-NP in surface water [14]. Given these low regulatory limits, analytical methods usually require the incorporation of a pre-concentration step.

Regulatory requirements for monitoring, along with the diversity of physical-chemical properties among phenols has necessitated the development of numerous methods for isolation of phenols from aqueous sample matrices. One of the simplest methods for isolation of phenols from water samples is LLE (liquid-liquid extraction). This method is still in use, for example, US EPA Method 625, but it is labour intensive and consumes large sample and solvent volumes [15]. Solid-phase extraction (SPE) [16,17] is now more widely used due to the range of sorbents available and reduced solvent consumption. SPE methods have drawbacks, including use of toxic solvents, expensive cartridges for single-use applications, and numerous steps that can be time-consuming, e.g., sample filtration required to prevent clogging, cartridge conditioning, sample loading, analyte elution, and solvent reduction [18]. Additionally, the lack of selectivity can lead to co-extraction of undesired compounds, which can affect analyte behaviour during analysis [19].

In recent years, molecularly imprinted polymer (MIP) adsorbents have been introduced to overcome a lack of selectivity in solid adsorbent phases. Synthetic molecular recognition is achieved in MIPs by use of a template (T) molecule as a scaffold for functional monomers (M), which are then converted into a co-polymer matrix with the addition of a crosslinker (CL). Template removal leaves empty binding sites that complement the target

analytes with respect to the orientation of functional groups and size [20]. MIP particles have been used for analysis of phenols in SPE format [6,21–24]. However, given the limitations of traditional SPE already indicated, MIPs for phenolic compounds have been fabricated in different formats to ease sample manipulation and reduce solvent consumption. Feng *et al.* developed molecularly imprinted micro-SPE (MIMSPE) for analysis of phenol and chlorophenols in tap water, river water and sewage using 15 mg of MIP particles packaged in polypropylene envelopes [25]. Magnetic MIPs (MMIPs) have been used for extraction of alkylphenols from environmental water samples [9] and for 4-nitrophenol from seawater [26]. MIPs have been coated on a variety of substrates of different shapes and sizes for use in solid phase micro-extraction (SPME). For example, MIPs were prepared as a coating on a homemade glass stir bar in MI-stir-bar sorptive extraction (MISBSE) for analysis of chlorophenols from seawater samples [27], and various MIP films coated on glass slides were developed in our group for extraction of Ph from aqueous solutions [28]. The MIPs for Ph were based on co-polymers of itaconic acid, 4-vinylpyridine (4-VP) or styrene (Sty) monomers with ethylene glycol dimethacrylate (EGDMA), triethylene glycol dimethacrylate, or pentacrythritol triacrylate (PETA) crosslinkers and Ph as the template [28]. Among these MIPs, only the Sty-PETA MIP showed modest imprinting effects (IF~1.16). Although covalent or semi-covalent imprinted MIPs can give greater selectivity, they are difficult to develop because of the need to form a reversible covalently-bound template-functional monomer combination suitable for aqueous analytes [29,30]. Yet in a non-covalent system, the weaker dynamic template-monomer interactions result in adsorption sites with a broad range of binding

affinities. New MIPs require careful selection of the functional monomer(s) to ensure good interactions with the template, crosslinker for structural stability and water compatibility, and porogenic solvent to dissolve the pre-polymerization components and support appropriate phase separation for high surface area and satisfactory selectivity [31].

Here, a thin-film MIP adsorbent is combined with a fast UHPLC-PDA method for simultaneous analysis of regulated phenols with a wide range of polarities suitable for use in complex aqueous matrices. A simple drop-casting method is used to make uniform and reproducible MIPs which feature the use of a pseudo-template (1,2-dihydroxybenzene, catechol), which was selected for its similarity in structure to Ph. As reported by others [32–34], a pseudo-template is needed to eliminate concerns associated with false positives due to residual template bleed, although the choice of an appropriate pseudo-template adds an extra level of complexity to MIP development. Adsorption capacity and imprinting were assessed for five monomers: 4-vinyl benzoic acid (4-VBA), 4-vinylanilline (4-VA), N-allylaniline (NAA), 4-VP and Sty. The monomers were selected based on the potential for hydrogen bonding and π-π interactions with the template. A common crosslinker, EGDMA, was used based on previous success in aqueous samples and literature that indicates that shorter crosslinkers are better for producing a rigid porous material desired for the stability of the imprinted binding sites [35,36]. Two different ternary porogen systems were evaluated: octanol, methanol and water (54:36:10) and methanol/water (5:1) with linear polymer polyethylene glycol (PEG) as a solvent modifier. Using the optimal MIP formulation, extraction parameters (i.e., salinity, the pH, polymer mass, desorption solvent and time) were investigated to optimize the extraction efficiency. The optimized

method was validated using spiked seawater (SW) and produced water (PW) from oil and gas operations.

2.3 Experimental

2.3.1 Reagents and material

Standards and reagents (99% purity or better except where noted) of the following phenols (Figure 2.1) were purchased from Sigma-Aldrich (Oakville, Canada): Ph, 2-methylphenol (2-MP), 3-methylphenol (3-MP), 2-chlorophenol (2-CP), 2,4-dimethylphenol (2,4-DMP), 2,4-dichlorophenol (2,4-DCP), 2,4,6-trichlorophenol (2,4,6-TCP), 4-chloro-3-methylphenol (CMP), PCP (97%); 4-tert-octylphenol or (4-(2,4,4-trimethylpentan-2-yl)phenol) (4-OP) (97%), 4-nonylphenol (4-NP), catechol (1,2-dihydroxybenzene), 3-(trimethoxysilyl)propyl methacrylate (98%), EGDMA (98%), polyethylene glycol average MW 20,000 (PEG), 4-VBA (97%), NAA (95%), 4-VA(97%), Sty, 4-VP (≥95%), 1,4-dihydroxybenzene (hydroquinone, HQ), 4-hydroxybenzoic acid (4-HBA), 2,2-dimethoxy-2-phenylacetophenone (DMPA), potassium phosphate monobasic, potassium phosphate dibasic and ortho-phosphoric acid (85%) were also purchased from Sigma-Aldrich (Oakville, Canada). Sodium chloride was purchased from ACP chemicals (St. Leonard, Canada). Optima LC/MS grade acetonitrile, water and formic acid used in the gradient elution were obtained from Fisher Scientific (Ontario, Canada). Solvents used for derivatizing glass, washings, and template removal were ACS reagent grade: toluene from Caledon Laboratory Chemicals (Ontario, Canada); acetonitrile from ACP Chemicals (Montreal, Canada); and absolute ethanol from Commercial Alcohols (Ontario, Canada).

Plain glass microscope slides 75 × 25 mm^2 were sourced from Fisher Scientific (Ontario, Canada); 13 mm PTFE 0.2-µm syringe filters from Canadian Life Science (Peterborough, Ontario); the micro cover glass 18 x 18 mm^2 from VWR (Mississauga, Ontario); Rainin Mettler Toledo Pos-D positive displacement pipette (Mississauga, Canada).

A mixed standard solution containing 0.4 g L^{-1} of each phenolic compound was prepared in Optima acetonitrile and stored in an amber vial at -22 °C. All the rebinding solutions used in the batch experiments were prepared with deionized (DI) water, purified by a Barnstead Nanopure water purification system (Lake Balboa, USA).

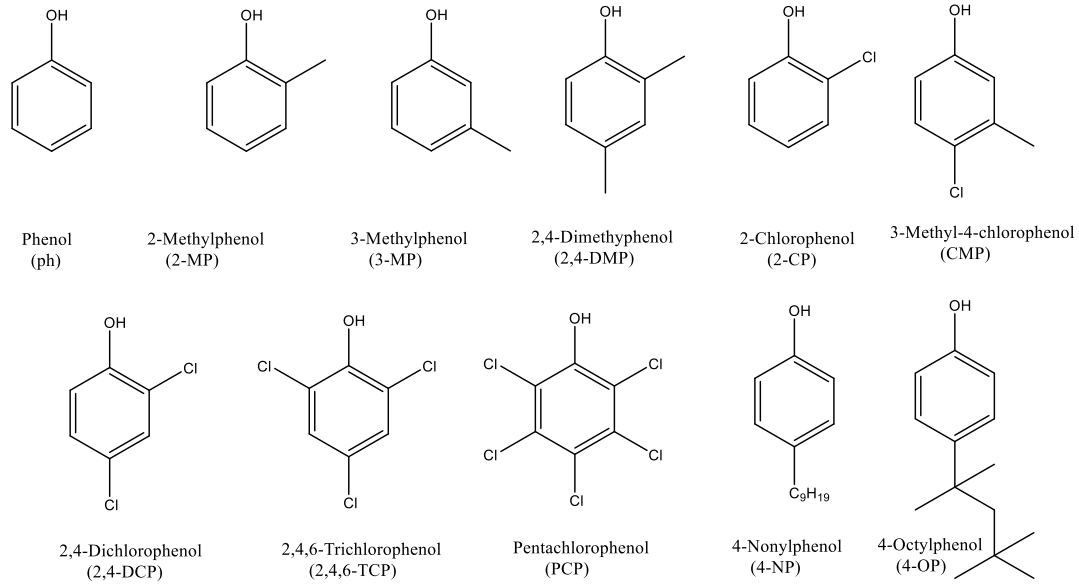

Figure 2.1. The chemical structures of phenols analytes under study.

2.3.2 Instrumentation

A Waters Acquity UHPLC system equipped with an autosampler, a photodiode array detector (PDA) and a HALO RP-amide column (2.7 µm, 2.1x 100 mm, Phenomenex,

California, USA) was used for separation and determination phenols. The sample and column were held at 25 ºC. Following injection of 10 µL samples, separations were completed at a flow rate of 0.45 mL/min using gradient elution with 0.1% (v/v) formic acid in water (solvent A) and 0.1% formic acid in acetonitrile (solvent B) in the following program: 35% B 0.00–2.00 min; increased to 40% B from 2.01–2.30 min then kept constant for 1.20 min; increased to 100% B 3.50 – 8.00 min, then returned to 35% B from 8.00 – 8.30 min then kept for 2.70 min to equilibrate the column for the next run. Signals for quantification were collected at two wavelengths near the λ_{max} of the analytes as noted: 275 nm for Ph, 2-MP, 3-MP, 2-CP, 2,4-DMP, 4-OP; and 285 nm for 2,4-DCP, 2,4,6-TCP, CMP, and PCP; 370 nm was used as a reference for baseline correction.

Polymerization was UV initiated with a Luzchem EXPO-1 UV photoreactor (Ontario, Canada). Adsorption and desorption procedures were multiplexed for high throughput using a VWR Scientific DVX-2500 digital multi-position vortex mixer (Hampton**,** USA).

2.3.3 Preparation of thin-film MIPs

The thin-films MIPs were fabricated by drop-casting the pre-polymerization mixture between a derivatized glass slide (20 x 25 mm) and a quartz cover glass slide (18 x 18 mm) with UV photopolymerization. Glass was derivatized overnight with 2% (v/v) 3-(trimethoxysilyl) propyl methacrylate in toluene, then washed with toluene, followed by ethanol, then air-dried and stored in a dark place [37]. To prepare the pre-polymerization mixture, template, functional monomer, photoinitiator (DMPA), crosslinker (EGDMA), and 200 µL porogen (with solvent modifier, if applicable) were combined in glass vials in varying amounts to achieve ratios presented in the Results and Discussion. The non-

imprinted polymer (NIP) was prepared in the same way but without the template. The components were vortex mixed until dissolved, then degassed to remove oxygen that might inhibit the polymerization process. A volume (10-40 µL) of the pre-polymerization solution was delivered onto the derivatized slide using a positive displacement pipette (Pos-D, Mettler Toledo Canada, ON, Canada) to accommodate the viscosity of the pre-polymerization mixture, then covered gently with the micro cover glass and exposed to UV light for 1 h at room temperature. Upon completion of the polymerization process, the micro cover glass was removed, leaving a thin polymer film bound to the glass substrate. Template and unreacted or soluble components were removed by immersion in acetonitrile/water (1:1) with stirring for 2 h. Polymer mass was determined by the difference after air-drying to constant mass. The fabrication scheme is illustrated in Figure 2.2.

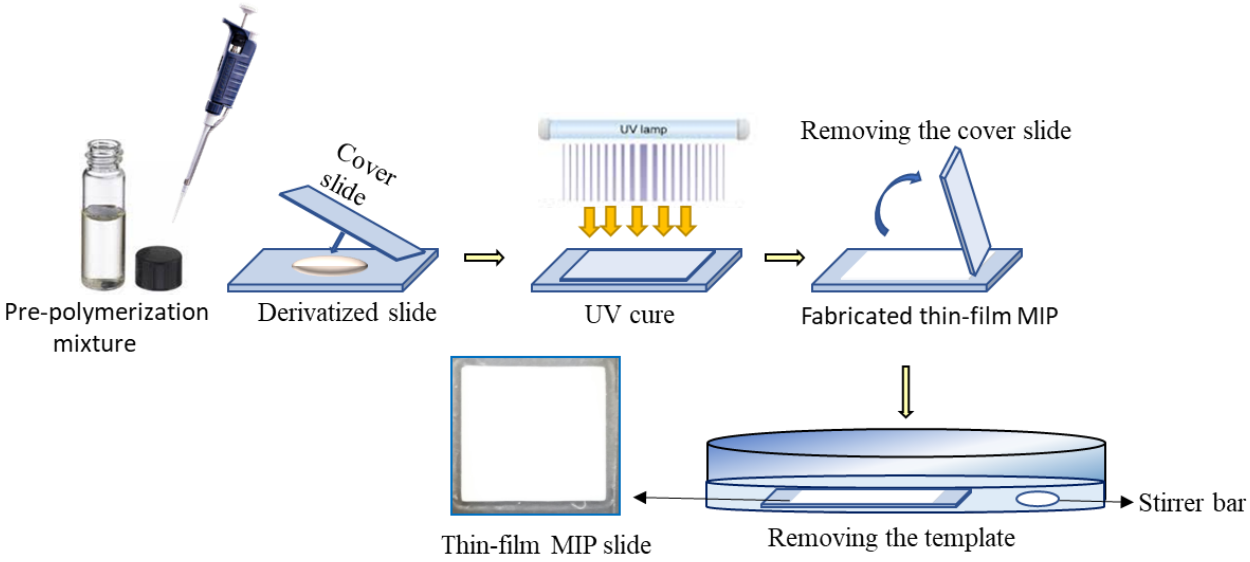

Figure 2.2. Fabrication of the MIP thin-film using drop-casting technique

2.3.4 Optimization of the extraction process

The thin-film MIPs (or NIPs) were placed in 50-mL centrifuge tubes containing 30 mL of DI water spiked with 1.0 mg L^{-1} of the phenol standard mixture. The sealed tubes were agitated using a multi-tube vortex mixer. After extraction, the thin-film MIPs were rinsed in-tube three times with DI water to remove the residual sample solution along with any unbound or weakly bound sample components. The desorption solvent was added to each tube in sufficient volume (8.0 mL) to cover the MIP-coated slide and vortex mixed for 15-90 min. The solution containing the desorbed analytes was filtered using a 0.2 µL PTFE syringe filter, and the volume was reduced under nitrogen gas to near dryness. Usually, the final volume was adjusted to 1 mL with 35% acetonitrile in water, which is the solvent composition at the start of the gradient elution program. However, for method validation over the low concentration range (0.0001 mg L^{-1}- 0.05 mg L^{-1}), sensitivity is a concern; thus, the final volume was adjusted to 100 µL. Several parameters were optimized: mass of sorbent (2.0, 3.5, 5.0 and 6.0 mg); percent salt added to the sample (NaCl; 5%, 10%, 15%, 20% and 25% w/v); adjusted sample pH (2, 4, 6, 8 and 10); and extraction times: 0.25, 0.50, 0.75, 1.00, 2.00, 3.00, 4.00, 6.00, 8.00, 12.00 and 24.00 h; desorption solvent (methanol, methanol/0.1% acetic acid (HAc) and ACN) and desorption time (15, 30, 60 and 90 min). Each experiment was carried out in triplicate.

2.4 Results and Discussion

Many factors, such as the nature and amounts of monomer, crosslinker, template and porogen, affect the performance of MIPs with respect to affinity, selectivity, and adsorption

capacity [38]. Thus, different polymer formulations were studied to optimize the molecular recognition of phenolic compounds.

2.4.1 Choosing the functional monomer and pseudo-template

The first and most important stage in the preparation MIPs is choosing a suitable functional monomer with high potential to form a complex through non-covalent interactions with the target analyte. Although this self-assembly can be measured in the prepolymerization solution, Xuewen *et al.* [39] found that selectivity of MIPs depends on the fidelity of the self-assembled complex in a three-dimensional polymer matrix. This can only be assessed following polymerization; thus, we did not screen for complex formation in solution but proceeded directly to adsorption studies to test the efficiency of the MIPs. Five functional monomers (

Figure 2.3) were carefully selected based on their potential to complement the chemistry of the pseudo-template (catechol). Since we are limited to hydrogen bonding and π-π interactions, all monomers have an aromatic ring and a hydrogen bond accepting functionality to interact with the hydroxyl group on the phenols. Specifically, hydrogen bonding can occur through a lone pair on nitrogenous functionalities, through the carboxylate of 4-VBA ionized at neutral pH, and through an aromatic ring.

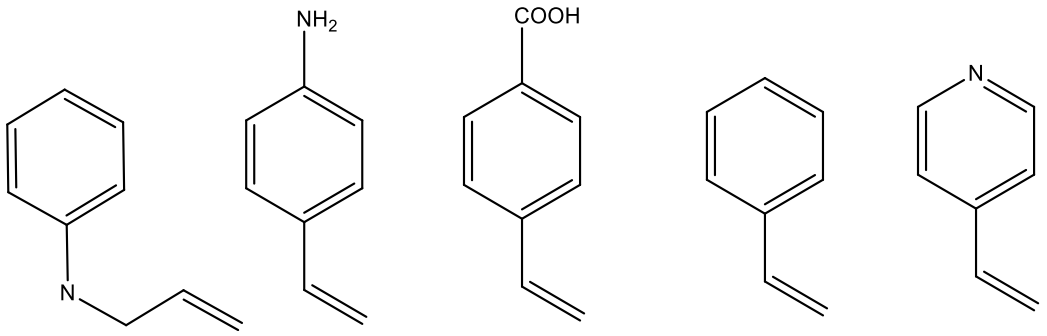

	N-allylaniline (NAA)	4-vinylanilline (4-VA)	4-vinylbenzoic acid (4-VBA)	Styrene (Sty)	4-vinypyridine (4-VP)
pk_b:	9.5	9.3	9.8		8.8

Figure 2.3. The chemical structures for the functional monomers under study

Five different MIP and NIP formulations were prepared, as illustrated in Table 2.1. The molar ratio of T:M:CL used in this work was 1:4:20, which is usually used in the literature [35]. The amount of free photoinitiator used was 2% (mol/mol) of the total amount of M and CL. These functional monomers were evaluated in terms of reproducibility and selectivity, which is a comparison of the adsorption capacity of the MIP relative to that of the NIP (Q_{MIP}/Q_{NIP}) for the suite of phenolic compounds (Figure 2.4A). The relative selectivity imparted by 4-VBA is the highest (1.25-1.47), with the next best system based on 4-VP (1.06 -1.39). In addition to the favourable selectivity, 4-VBA also gave the best reproducibility (0.002-0.043 propagated error for the standard deviation for Q_{MIP} and Q_{NIP}) with the next best being Sty (0.072-0.176 propagated error). The performance of 4-VBA is attributed to the ionized carboxylate moiety, which is a good proton acceptor for

hydrogen bonding through the phenolic hydrogen. Therefore, 4-VBA was chosen for subsequent studies.

Table 2.1. The Composition of the pre-polymerization mixtures

Polymer	Template	Monomer	Crosslinker	Photoinitiator	Solvent
MIP1	o-Catechol 0.024 mmol	4-VP 0.096 mmol	EGDMA 0.48 mmol	DMPA 0.012 mmol	200 µL octanol/MeOH /water (v/v/v) (54:36:10)
MIP2		4-VA 0.096 mmol			
MIP3		NAA 0.096 mmol			
MIP4		Sty 0.096 mmol			
MIP5		4-VBA 0.096 mmol			

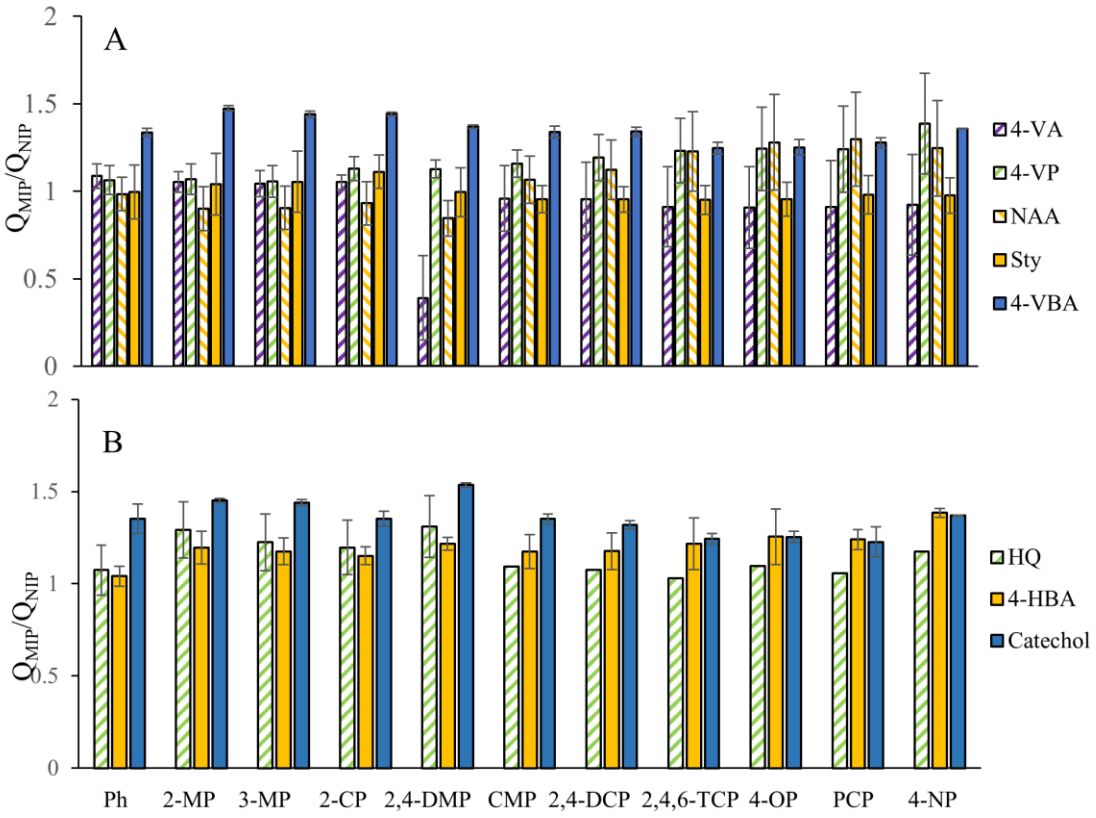

Figure 2.4. Optimization of MIP formulation using T:M:CL ratio of 1:4:20; cross-linker EGDMA; Porogen: octanol:MeOH:H_2O (54:36:10); 2 h extraction; analyte desorption with 8 mL 0.1% HAc in MeOH 30 min. Error bars (n=3) based on standard error propagation.

A. Monomer selection with catechol pseudo-template (T)

B. Pseudo-template study with 4-VBA (M)

Due to the required sensitivity and multiple phenolic target analytes, a pseudo template is preferred. Preliminary studies suggested that catechol was a good choice, and the functional monomer was selected and optimized accordingly [40]. It is well known that template-monomer interactions play an important role in creating imprinted cavities, and Javier *et al.* [41] proved that these interactions also contribute to macroscopic polymer properties, including surface area and pore size. Therefore, the performance of two other templates structurally similar to catechol, HQ and 4-HBA, were evaluated. The best pseudo-template is chosen on the basis of Q_{MIP}/Q_{NIP} ratio and the reproducibility of the results in the recognition behaviour. As shown in Figure 2.4B, catechol exhibited a higher Q_{MIP}/Q_{NIP} ratio compared to the other templates for most of the phenols, as well as it showed low standard deviation bars (n = 3). The most obvious explanation is the presence of the two adjacent (ortho) hydroxyl groups, which can both participate in hydrogen bonding through the delocalized electrons on the ionized carboxylate of the 4-VBA. Thus, the prepolymerization complex between catechol and 4-VBA is be enhanced by a OH-O bonding at two points and weak OH–π and π-π stacking between the aromatic ring structures. The performance is contrasted with the results using HQ as the template, which gives the poorest results of the three templates. Since HQ and catechol are constitution isomers that differ only in the placement of the hydroxyl group, the idea that the proximal groups are important for forming a more stable template-monomer complex is supported.

2.4.2 The solvent effect

The right porogenic solvent system is important in preparing porous MIP films since the solvent has a central role in dictating the porosity and surface chemistry of the polymer coating. Spivak *et al.* [42] found that the solvent affects the microenvironment of binding sites in the polymer, and polymers immersed in the same solvent type used in the polymerization process show better performance with respect to adsorption capacity and selectivity. This means that the ideal rebinding environment for the target analytes should be similar to that used to make the polymer; for example, if the analyte is adsorbed from water, then the porogen should be water. However, for several practical reasons, including the solubility of the polymer components, it is not usually possible to conform to this requirement. Therefore, the porogen should be similar to the sample in terms of polarity. In this study, two different ternary porogens: a medium polarity porogen of octanol, methanol and water (54:36:10) and a polar mixture of (5:1) methanol/water with 0.22 g mL^{-1} of linear polymer PEG as a solvent modifier. The results (Figure 2.5) show that polymers made with the more polar porogen of methanol/water/PEG yielded higher adsorption capacity compared to the octanol/methanol/water porogen mixture. There are several reasons for the improved results with the more polar porogen. The first is related to the rebinding environment in the sample and its similarity to the porogen polarity. During the polymerization process, the binding site microenvironment is influenced by porogen solvation effects, which can partially explain why rebinding is usually best from a sample matrix with similar polarity to the porogen. The other important factor is the role of the porogen in the phase separation process, which is aided, in this case, by the addition of

PEG to form interpenetrating polymer networks that maintain the pore structures as the polymer grows and phase separation begins [43–45]. PEG is a green solvent modifier, non-toxic, inexpensive, environmentally-friendly, and soluble in water and many organic solvents [43]. In 2016, Bartosz Z. *et al.*[46] used PEG as a porogen to improve the porosity of poly(N-isopropylacrylamide) gels with acrylic acid copolymerized into the structure. They found that PEG (MW 20000 g/mol) produced homogenous pores with a more porous morphology compared to the corresponding polymer without PEG. PEG was also used to increase the porosity of a poly(vinyl alcohol) hydrogel; it was found that porosity increased with increasing PEG content [47]. We found that polymer films formed without PEG were non-porous and irregular. As a result, methanol/water with PEG was chosen for the subsequent studies.

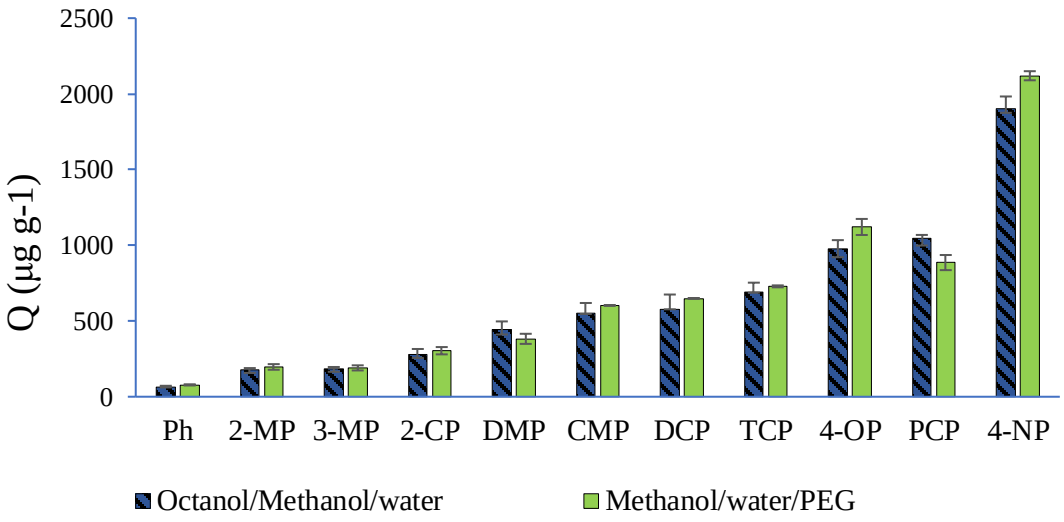

Figure 2.5. The effect of porogen in the adsorption efficiency. The T:M:CL ratio is 1:4:20, where 4-VBA and EGDMA were used as monomer and crosslinker respectively; the template was removed using ACN:H_2O (1:1); extraction for 2 h with 1 mg L^{-1} of each phenol in DI water; phenols were desorbed using 8 mL 0.1% glacial HAc in MeOH for 30 min. The error bars presented were determined using standard error for the calculated adsorption capacities (Q), n=3.

2.4.3 The influence of monomer and template concentration

The ratios of the constituent polymer components have a significant influence on molecular recognition, surface area, pore structure (influences mass transport) and mechanical stability of the MIP [38]. Typically the crosslinker is in excess of the monomer at 50-80 mol% of the final polymer (50-20 mol% monomer) [31]. Since the crosslinkers are usually larger molecules than the monomer, the crosslinker forms the bulk of the polymer mass. The optimum ratio of monomer-to-crosslinker (M:CL) was determined by

preparing MIPs with a fixed amount of crosslinker and varied amounts of monomer. Loadings of monomer in mol% (($n_M/(n_M+n_{CL})$)*100) were as follows: 17%, 20%, 25%, 33%, and 50% with a constant template-to-monomer ratio, 1:4. The data (Figure 2.6) shows that the best MIPs were made with monomer at 20 mol% (M:CL, 1:4), which is consistent with previous reports highlighting that highly porous stable films rely on a high degree of crosslinking [48]. Since we fixed the amount of crosslinker, non-selective adsorption associated with the crosslinker should not increase with increases in loadings of the monomer and template. Improvements in adsorption capacity with increased M:CL are attributed to an increase in the number of high-affinity binding sites. The decreases in performance for M mol%>20% is associated with reduced access to selective sites, as well as a reduction in the rigidity of the sites due to a decreased degree of crosslinking.

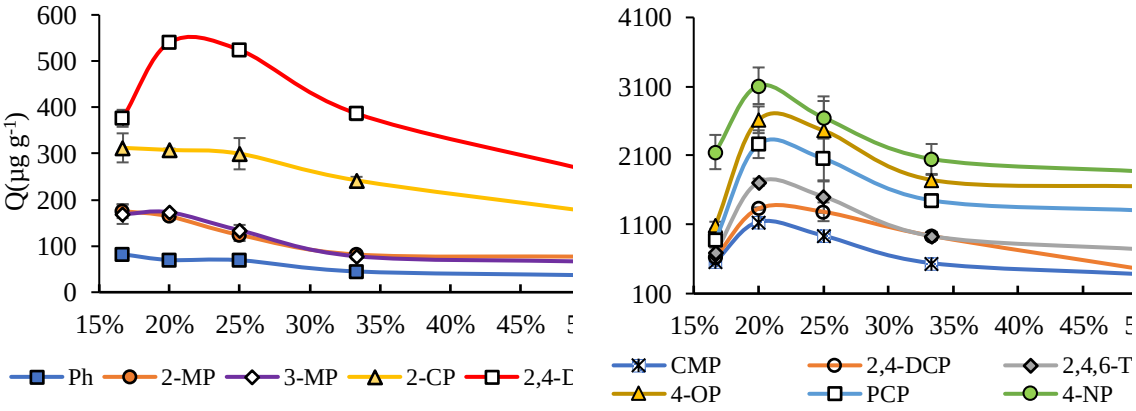

Figure 2.6. Study of monomer-crosslinker ratio (M:CL) for eleven phenolic compounds expressed as %mol fraction. Five different M:CL ratios were utilized while maintaining the T:M ratio at 1:4; CL: EGDMA; M: 4-VBA; T: catechol; porogen: MeOH/H_2O/PEG; 2 h extraction; phenols desorption with 8 mL 0.1% HAc in MeOH 30 min . The error bars represent the standard deviation for the calculated adsorption capacities, Q (n=3).

The theory for non-covalent molecular imprinting relies on formation of stable T-M_n complexes, where n depends on the number of non-covalent interactions possible between the T and M. In practice, an excess of monomer (greater than the stoichiometric amount) is used to ensure a maximum number of template molecules form the T-M_n complex according to Le Chatelier's Principle [31]. Using the optimized M:CL, the amount of template was varied to give T:M:CL ratios at four different levels, 1:4:16, 1.33:4:16, 2:4:16, 4:4:16 (corresponding to T:M of 1:4, 1:3, 1:2, 1:1, respectively), keeping the amounts of monomer and crosslinker constant. This allows us to study the loading of the template while keeping the polymer constituents at amounts established for good film formation. The influence of the template proportion on the adsorption capacities and imprinting factors is shown in Figure 2.7; increasing of the amount of the template from 1:4 to 1:3 gave modest improvements in adsorption capacity but more reproducible results. Further increases to 1:2 and 1:1 did not improve the performance of the MIP and provided materials with a lower affinity toward target analytes. These higher template loadings should give a higher theoretical maximum number of binding sites; however, it is likely that there is insufficient monomer to complex all the template molecules available; thus, fewer high-affinity sites are formed.

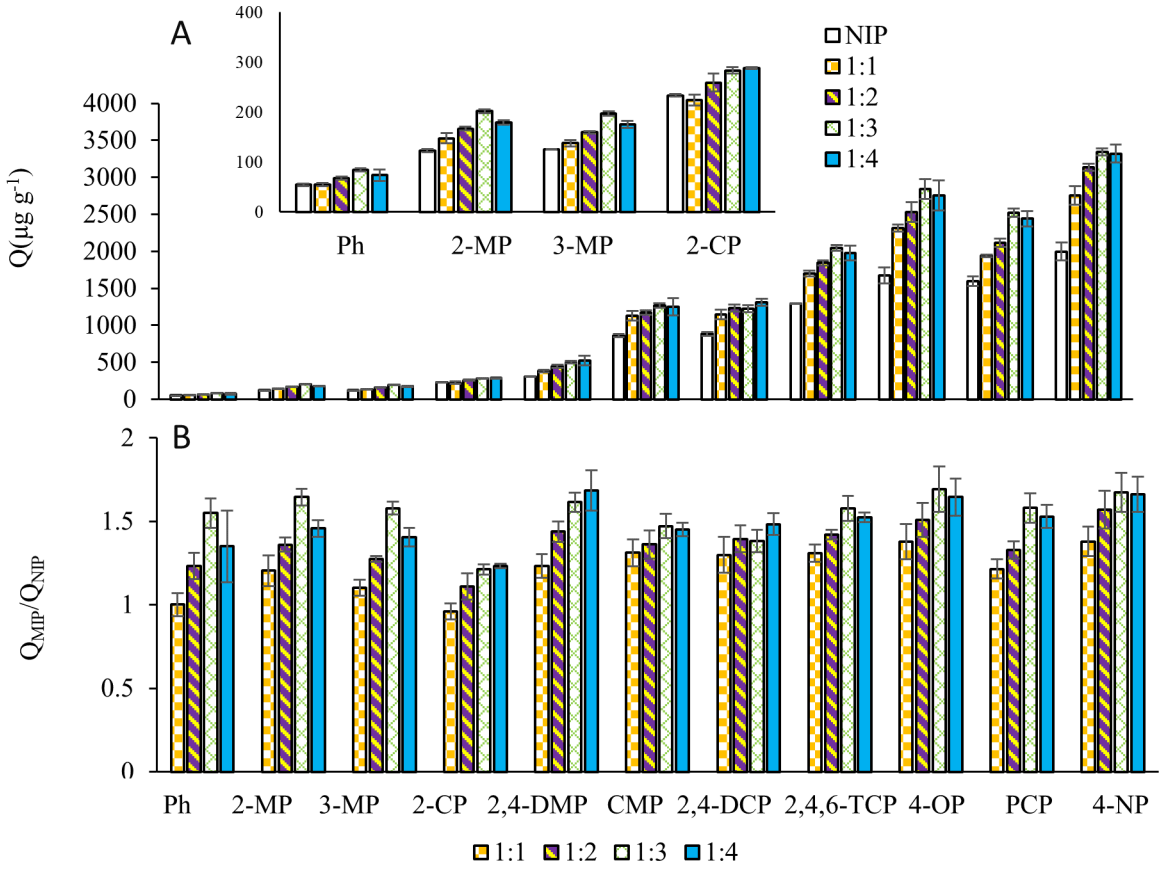

Figure 2.7. Study of the effect of template (catechol) to monomer ratio on: A. adsorption capacity (error bars ±1sd, n=3); and B. imprinting factors (error bars based on propagation of error for ±1sd of Q_{MIP} and Q_{NIP} data, n=3). Monomer (4-VBA) to cross-linker (EGDMA) ratio is constant (1:4); porogen is MeOH/H_2O/PEG; 2 h simultaneous extraction of eleven phenolic compounds from water; desorption with 8 mL 0.1% HAc in MeOH for 30 min.

2.4.4 MIP Mass and Adsorption

To study the effect of the polymer mass on the recovery of the phenolic compounds, four different volumes of the pre-polymerization mixture (10, 20, 30 and 40 μL) were used to obtain four different masses of the polymer (~2.0, 3.5, 5.0 and 6.0 mg) covering the same

area of the device (i.e., a higher mass of MIP yields a thicker coating). The morphology and thickness were studied using a scanning electron microscope and can be found in our previously published paper [37,49]. Figure 2.8 (A and B) shows the recoveries and the adsorption capacities for each of the phenols. The recoveries of Ph, 2-MP, 3-MP, 2-CP, 2,4-DMP, CMP, and 2,4-DCP increase with increasing mass of the polymer, while there is only a small improvement for 2,4,6-TCP, 4-OP, PCP and 4-NP. Recoveries are expected to increase with the mass of adsorbent [50,51]. However, the gains are more notable for the lighter phenols, which can be attributed to their smaller size and higher diffusion rates, allowing them to access sites throughout the thicker MIP coating. The differences in the adsorption behavior among the various phenols can be better evaluated in terms of the effect of increased mass on adsorption capacity (Q, in Figure 2.8 C and D) and these plots provide important insight into the structure of the porous coating. Q increases for Ph, 2-MP, 3-MP, 2-CP, and to a lesser extent 2,4-DMP, demonstrating that the thicker MIP films (3.5 – 6.0 mg) have a higher adsorption capacity. And yet, Q for the larger, more hydrophobic compounds (Figure 2.8 D) decreases substantially. Since the increased mass of polymer should only result in formation of a thicker coating (i.e. no morphological or chemical changes), Q should be constant for each analyte at equilibrium if the binding sites (energy) are consistent and equally available (can be reached by diffusion). Since this system is not at equilibrium (2 h loading studies), kinetic factors may be significant. The adsorption process occurs in a series of steps, including diffusion from the bulk solution to the boundary layer, then diffusion through the boundary layer to the film surface and into the pores, followed by partitioning to the adsorption sites [52]. Since all other factors are

constant, diffusion within the pores of the polymer is the key consideration; this is primarily influenced by the adsorbent pore size and diffusion rates, which are slower for molecules with a larger hydrodynamic radius [53]. Such large hydrophobic analytes are expected to strongly adsorb to sites near the surface of the coating, and diffusion deeper into the coating is limited by lower diffusion rates and poor water solubility [37,49]. Perhaps more useful is the Q data for the light phenols showing that the porous structure is accessible to small molecules throughout the coating. Higher sorbent masses on the devices showed better adsorption capacity ($\mu g\ g^{-1}$), which suggests that the fabrication process is more effective when used to fabricate slightly thicker films. Since only modest improvement in Q is measured beyond 3.5 mg films and thicker films require more time for analyte desorption, all further studies used 3.5 mg of thin-film adsorbent.

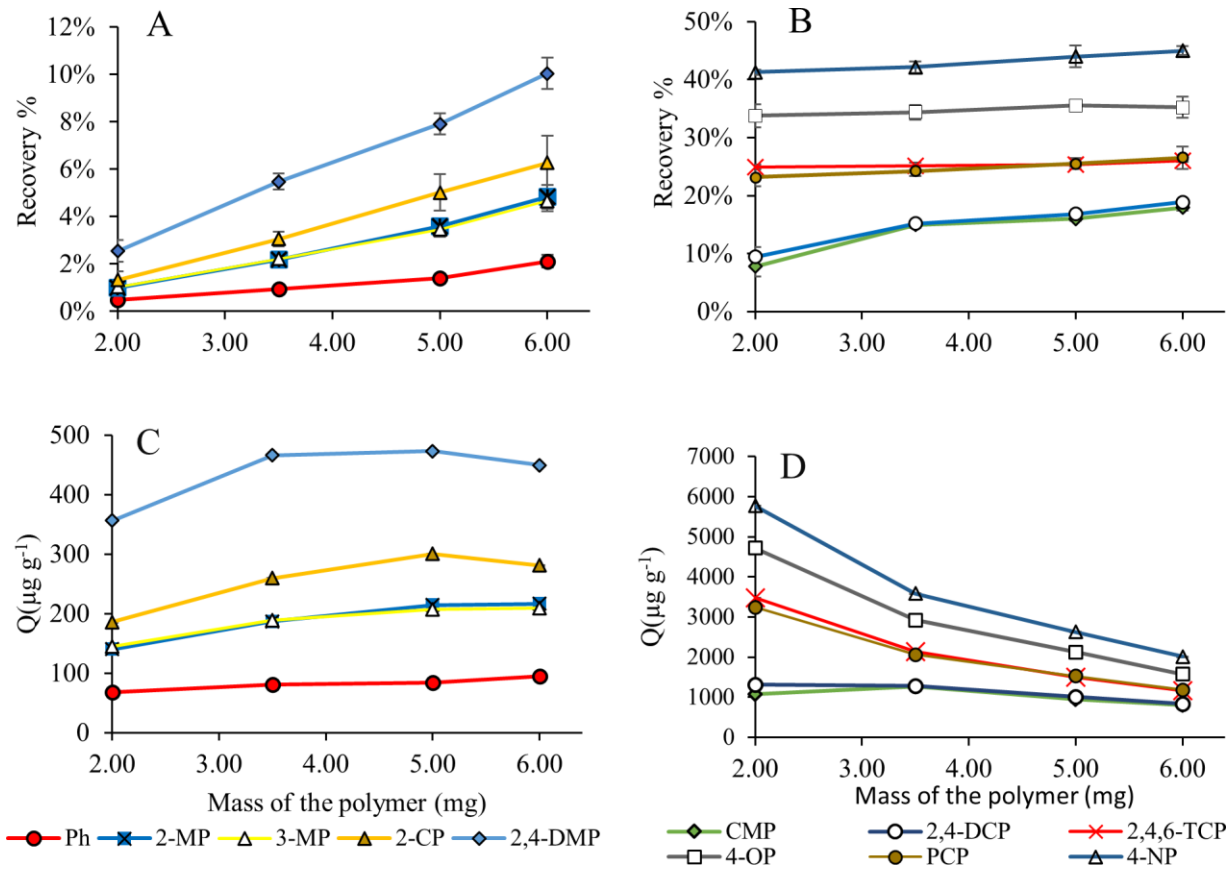

Figure 2.8**.** Effect of polymer mass on: A) recovery of small phenols; B). recovery of larger phenols; C) adsorption capacities for small phenols; D) adsorption capacities for larger phenols, based on extraction from a solution containing 1 mg L^{-1} of each phenol in DI water for 2 h (n=3).

2.4.5 Salt Effect

The addition of salt to aqueous solutions increases ionic strength, which for neutral hydrophobic analytes (log P values are presented in Table 2.2) leads to a decrease in the solubility and increases in the affinity for the adsorbent. Different amounts of NaCl (0, 5, 10, 15, 20, and 25% (w/v)) were added to solutions of standards in DI water to determine the effect on adsorption efficiency (Figure 2.9). The MIP adsorption capacities for the polar

water-soluble phenols, specifically Ph, 2-MP, 3-MP, and 2-CP, increased significantly with salt concentration. Increasing the salt concentration in aqueous solutions causes the salting-out phenomenon, which results in a higher partition coefficient which improved the adsorption of the analytes by the adsorbent [54]. This effect is thought to be in part related to hydration of the ionic salt by water molecules, which is favored over the solvation of the phenols and thereby reduces the available water to participate in hydrogen bonding [55]. The adsorption capacities for the moderately polar compounds (2,4-DMP, 2,4-DCP and CMP) increased with salt loadings only to 20%, while the more hydrophobic phenols (2,4,6-TCP, 4-OP, PCP, and 4-NP) show improved adsorption only up to 5-10% salt with decreased adsorption with higher amounts of salt. We attribute reductions in adsorption efficiency to at least two factors: increased adsorption of the light phenols reduces the availability of adsorption sites at the surface, and increased sample viscosity slows the diffusion process and has a significant effect on the analytes with the lowest diffusivity [6,56]. In light of these results and our interest in the analysis of SW (salinity 3.5%), 5% salt was applied for the subsequent experiments [1].

Table 2.2. Physical-chemical Properties of Phenols [57]

Analyte	Molecular weight (g mol^{-1})	Solubility in water (g L^{-1} (C°))	pKa	LogP
Ph	94.11	84 (20)	9.99	1.46
2-MP	108.14	25.9 (25)	10.29	1.95
3-MP	108.14	24.0 (25)	10.1	1.96
CP	128.55	28.5 (20)	8.5	2.15
DMP	122.16	7.87 (25)	10.60	2.30
CMP	142.58	3.8 (20)	9.55	3.10
DCP	163.00	4.5 (20)	7.89	3.20
TCP	197.45	0.8 (20)	6.23	3.69
PCP	266.34	0.014 (20)	4.70	5.12
4-OP	206.32	0.007 (25)	10.33	5.25
4-NP	220.35	0.007 (25)	10.31	5.76

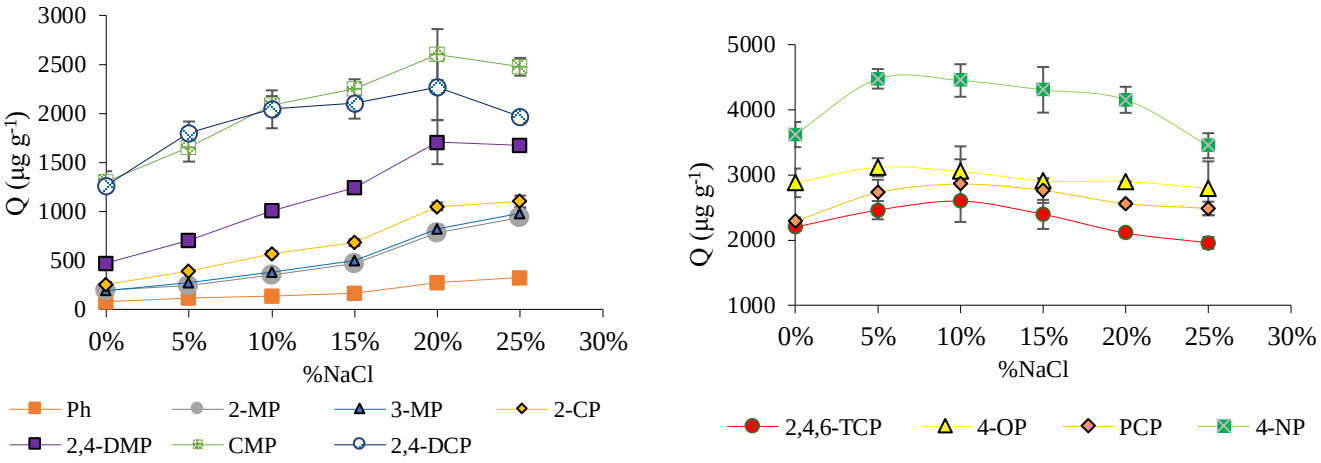

Figure 2.9. The salt effect on the extraction of the phenols from water sample using catechol imprinted MIP-thin-film based on simultaneous extraction for 2 h of 11 phenols each at 1 mg L^{-1} in DI water with a range of NaCl loadings (n=3), based on reuse of a single batch of 30 devices.

2.4.6 The effect of pH

Since phenols have an acidic ionizable hydroxyl proton, pH can influence their adsorption [58–60]. Phenols show a higher affinity for the adsorbent in the neutral form, which is established by keeping the sample pH well below the pKa (pKa can be found in Table 2.2) of the analytes. The phenols can be classified into two categories: phenol and alkylphenols, and chlorophenols, which corresponds to the effect of aromatic ring substitution on the acidity. Electron-withdrawing groups like chlorine increase acidity, and electron-donating (weakly) alkyl groups reduce the acidity of phenols. The pH of standard aqueous solutions was varied from 2–10 using phosphate buffers (~1 mmol L^{-1}), and the

adsorption capacities determined (Figure 2.10). Changes in pH had virtually no effect on adsorption capacity for phenols with pK_a values ≥9.5. Whereas the phenols with lower pKa values 2-CP (8.5), 2,4-DCP (7.89), 2,4,6-TCP (6.23), PCP (4.70) behaved as anticipated with adsorption capacities decreasing as ionization increases [57]. Ionization of the carboxylic acid functionality associated with the functional monomer used for these films (4-VBA) can also reduce adsorption capacity due to repulsive forces between the ionic form of the target analytes, phenolate anions, and the deprotonated sorbent surface. All but the most acidic phenol in this study (PCP) showed good behavior at pH ≤ 4; all samples were adjusted to pH 4 for the remaining studies.

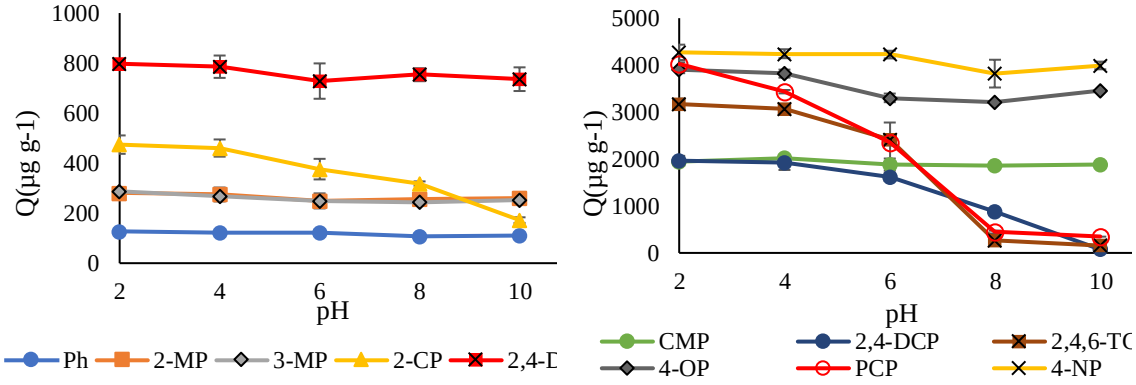

Figure 2.10. Effect of pH on extraction of phenols from water using catechol imprinted MIP-thin- film based on simultaneous extraction for 2 h of 11 phenols each at 1 mg L^{-1} in DI water and 5% of NaCl over a pH range of 2-10 (n=3), based on reuse of a single batch of 30 devices.

2.4.7 Selection of the desorption solvent and desorption time

Following optimization of the MIP formulation and adsorption conditions, the desorption efficiencies were assessed for three solvents: MeOH, ACN, and 0.1% HAc in MeOH. The desorption efficiencies (Figure 2.11 A) are similar, but ACN was slightly more efficient, more notably for the more hydrophobic targets, and is preferred for use with this UHPLC method as it is part of the mobile phase. Using ACN, the desorption time was varied from 15 to 90 min (Figure 2.11 B) with no significant improvement with increased desorption time. This confirms that mass transfer is relatively fast for these films. Note that a relatively large volume of solvent is necessitated by the tube and device geometry designed for use with the multi-position vortex mixer that allows for high throughput sample processing. The devices can be tailored to any shape and size, which would reduce solvent consumption. However, that would require re-engineering the devices and is beyond the scope of the current project.

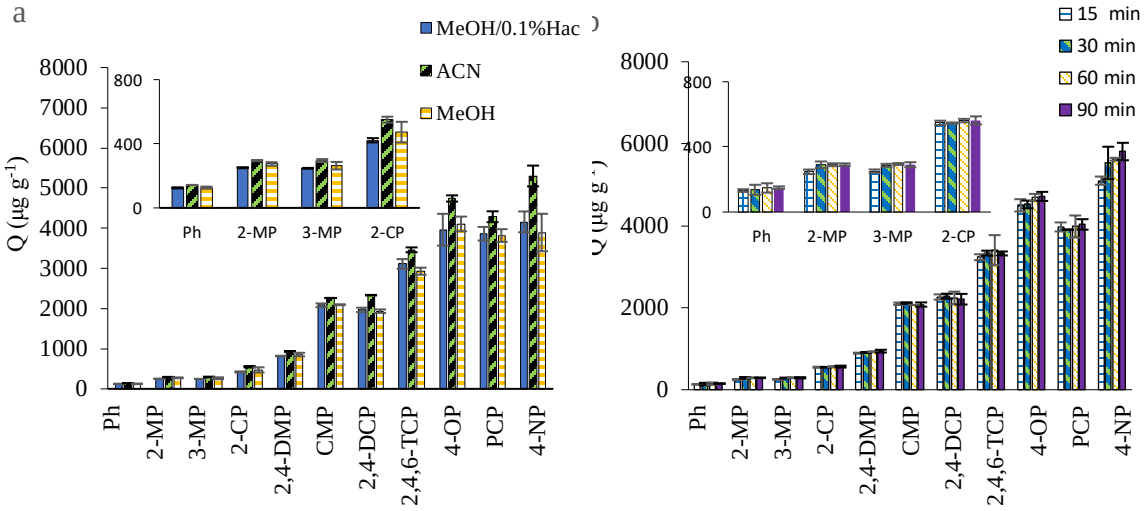

Figure 2.11**.** a) Effect of desorption solvent (desorption time: 30 min) b) the desorption time study using ACN as a desorption solvent. Extraction for 2 h with 1 mg L^{-1} of each phenol in salted (5%NaCl) and buffered (pH=4; mmol L^{-1} of phosphate buffer) DI water (n=3).

2.4.8 Optimal adsorption time

The extraction-time profiles over 24 h were assessed for simultaneous uptake for the 11 phenolic compounds (Figure 2.12). The behaviour of the analytes can be categorized in terms of their size, with small phenols reaching maximum adsorption most quickly, e.g., phenol and the cresols reached their maximum adsorption within 15 min. However, with time the larger phenols, with higher affinity for the MIPs but lower diffusion rates and slower mass transfer, displace the light compounds, leading to sharp decreases in their adsorption until equilibrium at ~2 h. The rate of adsorption for these larger phenols (CMP, 2,4-DCP, 2,4,6-TCP, 4-OP, PCP and 4-NP) is high for the first two hours with CMP, 2,4-

DCP, 2,4,6-TCP and PCP reaching equilibrium at about 3 h, while 4-OP and 4-NP attain equilibrium after 12 h. Although it is desirable to continue extraction until equilibrium is achieved completely, in routine analysis, some sacrifices in sensitivity are acceptable to improve throughput. In this work, 3 h gives extraction efficiencies >90% of the maximum for most of the phenols and no less than 60% for the worst case (4-OP), which is also the analyte that extracted most efficiently.

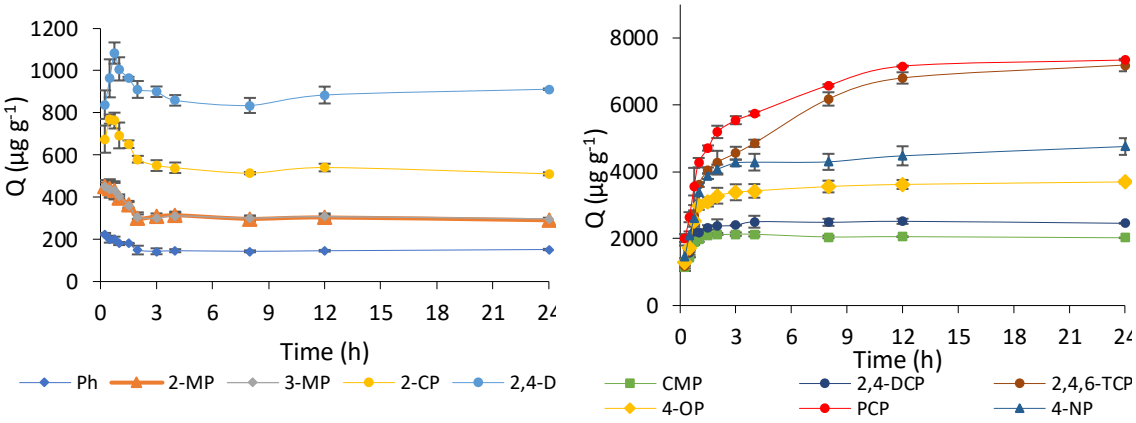

Figure 2.12**.** Extraction-time profile for phenols from a water sample using catechol MIP thin-film. Extraction of phenols from a multi-standard containing 1 mg L^{-1} of each phenol 5% aqueous NaCl buffered at pH=4 with 1 mmol L^{-1} of phosphate buffer, n=3.

2.4.9 Analytical performance of MIP-UHPLC-UV/vis analysis of eleven phenolic compounds

The analytical performance of the MIP-UHPLC-PDA method was evaluated for common figures of merit and performance in complex matrices based on calibration in DI water (Figure 2.13). The limit of detection (LOD) was determined based on the signal to

noise ratio of *S/N = 3*; the noise was estimated by running a blank of the method ten times. As shown in Table 2.3, the method gives good linearity for all analytes over 2 – 3 orders of magnitude with R^2 >0.99, which compares well with competing for analytical methods (Table 2.4), including the methods relying on LLE and SPE. The values of LOD for all the target analytes ranged from 0.1 µg L^{-1} (CMP, 2,4-DCP) to 2 µg L^{-1} (Ph), which are similar to other MIP methods, such as MIPSB-HPLC-PDA for chlorophenols in water (LOD: 2-CP 0.17 µg L^{-1}, 2,4-DCP 0.33 µg L^{-1}, 2,4,6-TCP 0.38 µg L^{-1}) [27]. Though these LODs are considered sensitive, they are somewhat higher than the LOD reported for a multi-template-MIP (mt-MIPs) SPE method with capillary electrophoresis UV/vis for Ph (0.17 µg L^{-1}) and chlorinated phenols (2,4-DCP 0.28 µg L^{-1}; 2,4,6-TCP 0.22 µg L^{-1}) in water [6]. Despite the better detection limits, our thin-film method has some advantages over MIP-SPE because these devices, which are suitable for single-use or multi-use, are easy and inexpensive to fabricate and require no conditioning before use. Moreover, the immersible format is easily amenable to automated high throughput sample processing. The precision (%RSD) was determined at different concentration levels (0.5 to 3000 µg L^{-1}), typically giving values well below 10%, with a few outliers of higher values for some low concentration measurements (e.g., CMP at 0.5 µg L^{-1} giving 15% RSD).

Phenol and alkylphenols are present in a range of wastewater streams, such as produced water (PW), seawater (SW) and municipal wastewater [1,2,61]. The catechol imprinted polymer was applied to the analysis of PW and SW samples, which were collected from a marine-based drilling and production facility and St. John's Harbour (Canada), respectively. SW and PW are complex matrices and good models for the study of typical

matrix effects. PW, in particular, shows high loadings of organic compounds like aliphatic and aromatic hydrocarbons, organic acids and phenols, as well as inorganic anions and metals [1]. Due to high concentrations of phenols and the high carbon loading in the sample, PW was analyzed at 50x dilution with 5% aqueous NaCl buffered at pH 4 with 1 mmol L^{-1} phosphate buffer, whereas SW was used as is with only pH adjustment. Typical chromatograms of spiked and unspiked PW can be found in Figure 2.14. The presence of Ph, 2-MP and 3-MP, as expected, can be clearly identified (Figure 2.14 B). As indicated in Table 2.5, the recoveries were obtained in the range of 85-100% with RSDs of 0.2-13.9% for SW and 81-107% with RSDs of 0.1-10.7 for PW. It is indicative from the results that the MIP-UHPLC-PDA method can be used to quantify eleven phenolic compounds simultaneously in SW and PW samples with minimal matrix effect with high accuracy and precision. Using this method, phenols were quantified in PW: Ph 4.28 mg L^{-1}; 2-MP 1.69 mg L^{-1}; 3-MP 1.73 mg L^{-1}; and 2,4-DMP 0.86 mg L^{-1}; none of the targeted phenols were detected in the SW sample. These results are consistent with the results in the literature, where phenol and some alkylphenols (C_1-C_5) have been reported in PW [1,2]. Although phenols are not found in natural waters unless there are clear sources of contamination—various studies report that phenols were not detected in seawater, tap water, stream, river, and well water samples [1,2,6,8,60,62]—they are common in many wastewater streams. For example, Hu *et al.* found Ph in hospital wastewater (980 µg L^{-1}) and in contaminated urban lake water (360 µg L^{-1}), which can be easily detected using the methodology reported here [61].

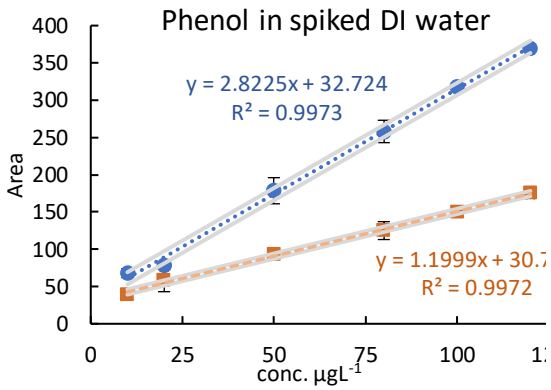
Phenol in spiked DI water
y = 2.8225x + 32.724
R² = 0.9973
y = 1.1999x + 30.7
R² = 0.9972
Area
conc. µgL-1

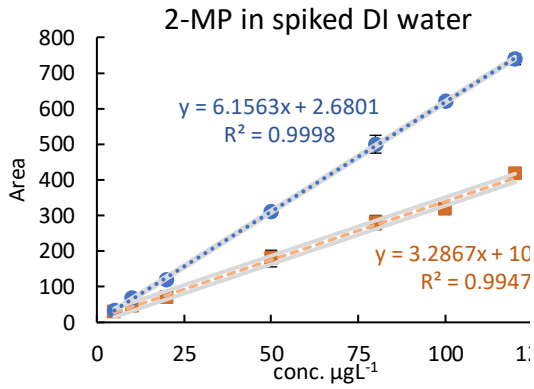
2-MP in spiked DI water
y = 6.1563x + 2.6801
R² = 0.9998
y = 3.2867x + 10
R² = 0.9947
Area
conc. µgL-1

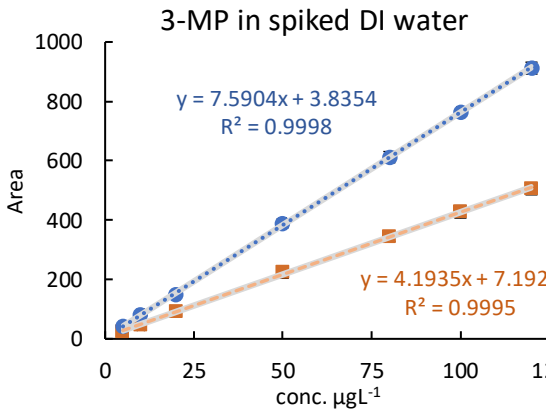
3-MP in spiked DI water
y = 7.5904x + 3.8354
R² = 0.9998
y = 4.1935x + 7.192
R² = 0.9995
Area
conc. µgL-1

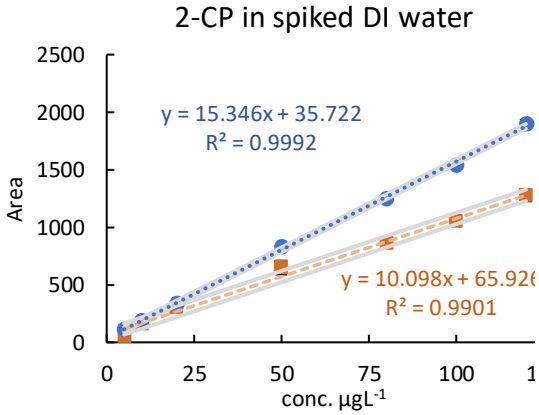
2-CP in spiked DI water
y = 15.346x + 35.722
R² = 0.9992
y = 10.098x + 65.926
R² = 0.9901
Area
conc. µgL-1

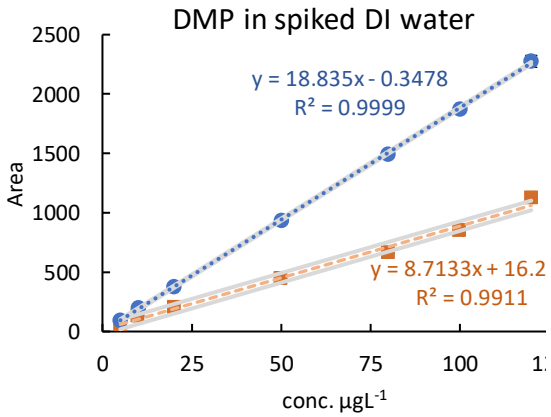
DMP in spiked DI water
y = 18.835x - 0.3478
R² = 0.9999
y = 8.7133x + 16.2
R² = 0.9911
Area
conc. µgL-1

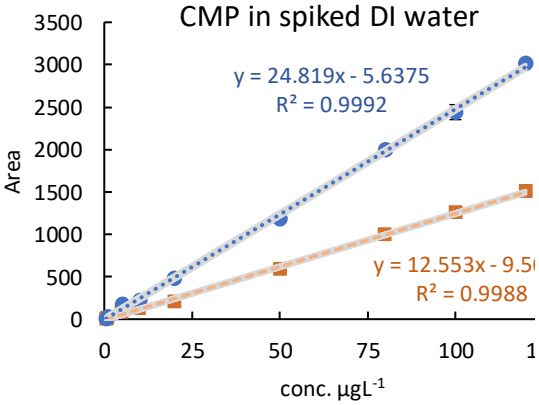
CMP in spiked DI water
y = 24.819x - 5.6375
R² = 0.9992
y = 12.553x - 9.5
R² = 0.9988
Area
conc. µgL-1

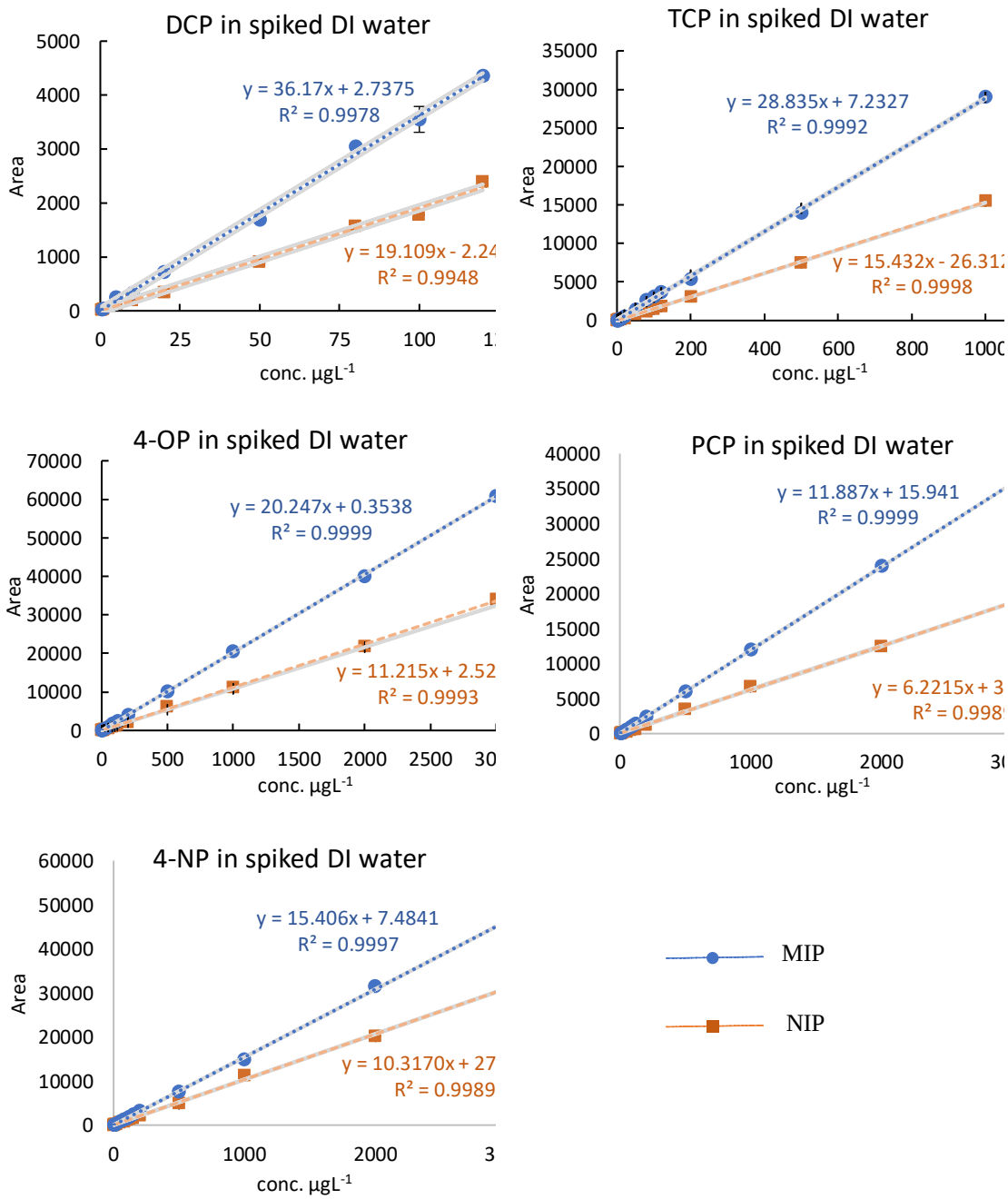

Figure 2.13. The calibration curves of the analysis of eleven phenolic compounds simultaneously in DI water sample (salted with 5%NaCl and buffered with pH = 4 (1mmol L^{-1} phosphate buffer)) using the MIP-UHPLC-PDA method (error bars represent standard deviation (n = 3)); the blue points for the MIP, and the red for the NIP.

Table 2.3**.** Figures of merit for the MIP-UHPLC-PDA method for analysis of eleven phenolic compounds in saline buffered DI water

Analyte	Calibration equation	Linear range (µg L^{-1})	R^2	LOD (µg L^{-1})	EF[a]	S_{res} (MIP)[b]	%RSD[c] Analyte Concentration (µg L^{-1})											
							0.5	1	5	10	20	50	100	200	500	1000	2000	3000
Ph	y=2.82x+32.7	10-120	0.9973	2.0	12.8	7.2	–	–	–	7.1	3.8	5.9	5.4	–	–	–	–	–
2-MP	y=6.16x+2.68	5-120	0.9998	2.0	25.9	4.1	–	–	6.1	4.1	0.9	2.3	1.1	–	–	–	–	–
3-MP	y=7.59x+3.84	5-120	0.9998	1.5	25.5	4.7	–	–	3.2	6	1.6	1.2	0.8	–	–	–	–	–
2-CP	y=15.4x+35.7	5-120	0.9992	1.0	47.8	21	–	–	13	1.5	2.2	1.2	1.7	–	–	–	–	–
2,4-DMP	y=18.8x-0.35	5-120	0.9999	1.0	65.5	11	–	–	2.1	3.9	1.0	1.4	1.1	–	–	–	–	–
CMP	y=24.8x-5.64	0.5-120	0.9992	0.1	123	35	15	5.1	0.2	3.5	3.4	1.2	3.6	–	–	–	–	–
2,4-DCP	y=36.2x+2.74	0.5-120	0.9978	0.1	124	84	11	5.3	0.4	2.0	5.7	3.9	6.7	–	–	–	–	–
2,4,6-TCP	y=28.8x+7.23	0.5-1000	0.9992	0.3	126	249	4.7	6.9	0.2	4.7	1.2	3.6	0.5	3.7	7.0	9.0	–	–
PCP	y= 11.9x+15.9	5–3000	0.9999	1.0	129	89		12	11	1.4	3.8	4.8	3.6	2.8	2.4	3.6	1.7	2.4
4-OP	y=20.3x-2.99	1–3000	0.9999	0.3	134	154	–	6.2	0.6	2.2	5.3	1.6	3.2	2.6	8.3	3.2	4.4	4.8
4-NP	y=15.4x + 7.48	3–3000	0.9997	0.9	111	251	–	–	4.6	7	8.2	4.1	5.8	4.1	9.2	8.4	2.9	3.9

[a] Enrichment factor

[b] The residual standard deviation for the calibration curve under the concentration range ($S_{res} = \sqrt{\frac{\sum(Residual)^2}{n-1}}$)

[c] Three replicate runs at different concentration levels for all the analytes to evaluate the precision

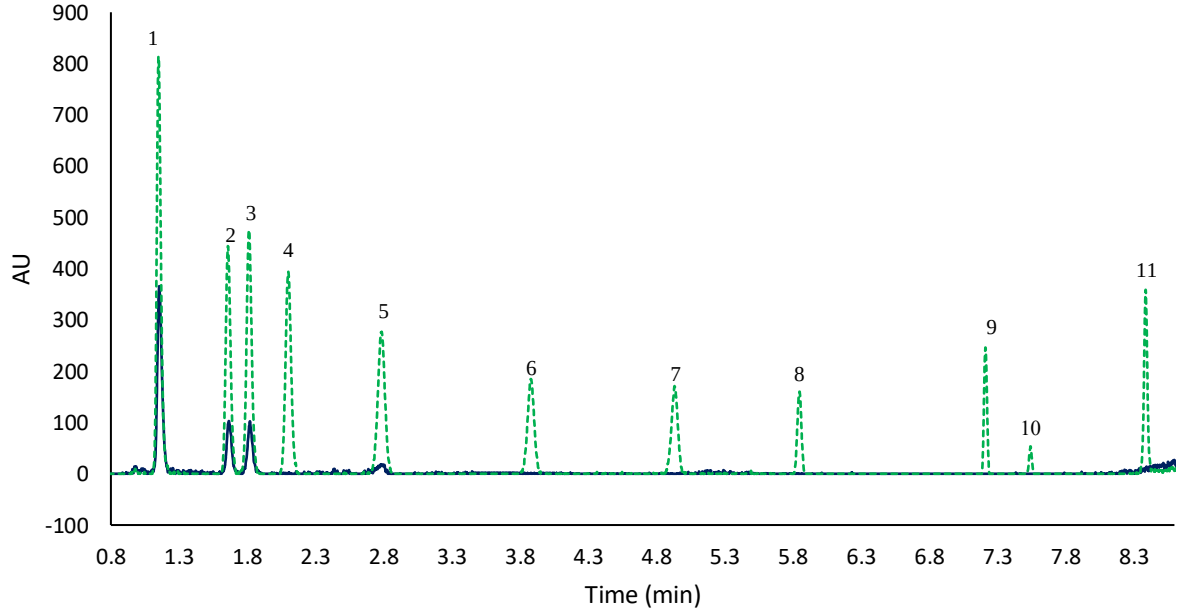

Figure 2.14. Chromatograms of phenolic compounds in PW (diluted 50x with 5% aqueous NaCl adjusted to pH 4.0 with 1 mmol L^{-1} phosphate buffer); solid line: phenols extracted from diluted PW; dashed line: phenols extracted from diluted PW spiked with 100 μg L^{-1} of each phenol.

Peak identification: 1) Ph, 2) 3-MP, 3) 2-MP, 4) 2-CP, 5) 2,4-DMP, 6) CMP, 7) DCP, 8) 2,4,6-TCP, 9) 4-OP, 10) PCP, and 11) 4-NP

Table 2.4. Comparison of the proposed MIP-UHPLC-PDA with other relevant methods for the determination of phenols

Analytes	Method	Sample Volume (mL)	LOD ($\mu g L^{-1}$)	RSD %	Linear Range ($\mu g\ L^{-1}$)	Enrichment Factor	Sample Type	Ref.
Ph, 2-MP, 3-MP, 4-MP, 2,4-DMP	LPME-HPLC-UV/vis	50	0.3 -3.5	0.3 - 11.5%.	2.50-50 (Ph) 12.5-250 (others)	15-70	Tap water, river water, SW, and groundwater	[8]
Ph, 2-CP, 2-MP, 2,4-DMP, DCP, 2,4,6-TCP, CMP, PCP, 2,4-DNP, 4-NP, 2-NP, 2-M-2,4-DNP (Nitrophenols)	SPE-GC-MS (EPA method 528)	1000	20,000-580,000	--	1.0×10^5-1.5×10^7	No Data	Ground water and chlorinated surface water	[63]
Ph, 2-CP, 2,4-DMP, DCP, 2,4,6-TCP, CMP, PCP, 2,4-DNP, 4-NP, 2-NP, 2-M-2,4-DNP (Nitrophenols)	LLE-GC-FID (EPA method 604)	1000	0.14-16	--	12-450	No Data	Surface water, and industrial wastewater	[64]
CMP, 2-CP, DCP, 2,4-DMP, PCP, Ph, 2,4,6-TCP, 2,4-DNP, 2-M-4,6-DNP, 2-NP, 4-NP (nitrophenols)	LLE-GC-MS (EPA method 625	1000	1.5-42	--	5-1300	No Data	Drinking water, surface water, and industrial wastewaters	[65]
Ph	DLLME-HPLC-UV/vis	3.7	29	2.1-13.1%	0.1-100	No Data	Tap water, lake water and wastewater	[61]
Ph, 4-CP, 2,4,6-TCP, DCP, 2-CP	MISPE-CE-DAD	15	0.17–0.31	1.68–6.96%	1-200	55-118	Reservoir water, river water, wastewater and tap water	[6]
4,6-DN-2-MP, 2-CP, 2,4-DMP, 4-C-3-MP, DCP, 2,4,6-TCP	RM-LLME-HPLC-UV/vis	8	0.29–0.63	1.0-8.1 %	5-500	61-138	Tap, stream and river waters	[60]

4-cumylphenol, 4-CP, 4-tertbutylphenol (t-BP), 4-OP, 4- NP	DLLME-HPLC-UV/vis	5	0.2-1.6	2.7-14%	2-20	123-275	SW	[66]
Ph, 4-CP, DCP, 2,4,6-TCP, PCP	MISPE-HPLC-UV/vis	10	0.57-1.08	0.9–4.9%	0.05-20	No Data	Tap water, river water and sewage waste	[24]
Ph, 4-CP, DCP, 2,4,6-TCP, PCP	MIMSPE-HPLC-UV/vis	60	0.56-4.5	0.8-7.8% 3.0-10% 3.2-8.8%	5–500 (Ph), 10–2000 (4-CP), 5–500 (DCP) 5–2000 (2,4,6-TCP), 10–2000 (PCP)	No Data	Tap water river water and raw sewage	[25]
4-Nitrophenol	MMIP-HPLC-UV/vis	10	7.24	less than 5.2%	25–1000	No Data	SW	[26]
2-CP, DCP and 2,4,6-TCP	MIPSB-HPLC-UV/vis	10	0.17–0.38	1.9–4%	1–100	97	SW	[27]
Ph, 2-MP, 3-MP,2-CP, 2,4-DMP, CMP, 2,4-DCP, 2,4,6-TCP, 4-OP, PCP, 4-NP	MIP-UHPLC-PDA	30	0.1-2.0	0.2-14% (SW) 0.1-11 (PW)	10-120 (Ph); 5-120 (MPs, 2-CP, 2,4-DMP); 0.5-120 (2,4-DCP, CMP), 0.5-1000 (2,4,6-TCP), 5-3000 (PCP); 1-3000 (4-OP), 3-3000 (4-NP)	12.8-134	SW and PW	this work

Table 2.5. Recovery percent and the relative standard deviation (RSD) of the phenolic compounds in spiked water samples using MIP-UHPLC-PDA method

	%Accuracy (%RSD)								
	SW[a]								
Analyte	Spiking Concentration (µg L^{-1})								
	10	20	50	100	200	500	1000	2000	3000
Ph	90 (8.1)	94 (6.8)	94 (2.1)	88 (2.3)	-	-	-	-	-
2-MP	87 (5.8)	95 (6.8)	93 (9.9)	91 (2.3)	-	-	-	-	-
3-MP	89 (9.0)	100 (9.3)	91 (7.5)	85 (3.1)	-	-	-	-	-
2-CP	93 (6.8)	100 (2.9)	87 (8.7)	85 (7.7)	-	-	-	-	-
2,4-DMP	93 (7.7)	89 (4.5)	90 (11)	86 (8.3)	-	-	-	-	-
CMP	91 (3.0)	100 (9.2)	91 (7.7)	90 (5.2)	-	-	-	-	-
2,4-DCP	90 (12)	91 (7.4)	91 (14)	87 (7.0)	-	-	-	-	-
2,4,6-TCP	91 (0.2)	99 (3.1)	100 (5.4)	97 (8.7)	96 (4.1)	91 (1.5)	93 (1.4)	-	-
4-OP	96 (6.3)	99 (12)	95 (12)	99 (5.2)	98 (11)	96 (8.3)	97 (6.3)	99 (3.7)	98 (2.0)
PCP	98 (5.6)	93 (3.8)	96 (5.5)	93 (8.3)	96 (11)	92 (6.3)	96 (6.0)	96 (7.9)	98 (2.8)
4-NP	96 (11)	99 (3.1)	91 (8.8)	96 (3.2)	90 (6.2)	97 (10)	88 (4.3)	90 (8.7)	98 (4.1)
	PW[b]								
Analyte	Spiking Concentration (µg L^{-1})								
	10	20	50	100	200	500	1000	2000	3000
Ph	87 (5.4)	88 (9.9)	92 (5.2)	94 (8.6)	-	-	-	-	-
2-MP	92 (9.4)	92 (7.8)	91 (4.1)	93 (2.4)	-	-	-	-	-
3-MP	82 (7.1)	88 (6.1)	83 (2.6)	85 (4.3)	-	-	-	-	-
2-CP	85 (11)	86 (8.8)	91 (3.9)	94 (5.2)	-	-	-	-	-
2,4-DMP	88 (8.3)	81 (7.5)	84 (6.8)	83 (2.0)	-	-	-	-	-
CMP	84 (8.7)	94 (6.9)	84 (7.4)	86 (6.6)	-	-	-	-	-

2,4-DCP	81 (7.0)	85 (9.2)	81 (7.1)	82 (2.3)	-	-	-	-	-
2,4,6-TCP	85 (7.0)	90 (4.8)	84 (2.1)	90 (4.5)	87 (8.8)	88 (5.3)	82 (0.1)	-	-
4-OP	87 (5.7)	90 (10)	88 (4.1)	89 (5.5)	84 (5.9)	88 (1.4)	86 (3.3)	87 (5.6)	85 (4.3)
PCP	89 (5.1)	83 (7.6)	88 (10.1)	88 (6.7)	87 (2.3)	88 (0.8)	83 (2.8)	85 (7.6)	89 (5.6)
4-NP	105 (6.5)	100 (7.3)	105 (9.4)	98 (3.2)	101 (7.9)	107 (2.5)	106 (6.8)	98 (5.0)	97 (5.9)

Experimental conditions: 30.0 mL of spiked water sample for 3 h extraction time.

[a]SW sample is only buffered.

[b]PW sample is filtered and diluted 50 times with 5% aqueous NaCl buffered at pH 4 with 1 mmol L^{-1} phosphate buffer

2.5 Conclusion

A microextraction method using catechol imprinted MIP extraction devices with UHPLC-PDA was found to be suitable for the simultaneous measurement of eleven phenols in complex aqueous samples. The analysis using UHPLC is robust, and the separation can be done quickly with low organic solvent consumption (about 2.5 mL ACN) per run. For effective imprinting, the formulation of the MIP was optimized through systematic optimization of critical factors influencing MIP performance, such as the nature and the amounts of functional monomer, crosslinker, template, and porogen. Phenolic compounds with a wide range of polarities can be extracted from real water samples using just a few milligrams of sorbent in 30 mL of the sample without a preconditioning step, which reduces the organic solvent consumption. Post-extraction clean-up (a short rinse in DI water) and desorption (15 min in ACN) are fast and uncomplicated. The method can be applied successfully to sample volumes as small as 10 mL and can be scaled to larger volumes to improve sensitivity as needed. Our method is characterized by its high tolerance to matrix effects using matched matrix external calibration. We also note that although the inter-device variability is low enough for single-use, we also used multiple batches of devices repeatedly with similar performance regardless of batch origin or number of uses (see Figure 2.9 and Figure 2.10). The method is easily made high throughput with simultaneous sample extraction using a simple multi-position vortex mixer. The important merits of this MIP method are its simplicity, low cost, reproducibility, and scalability.

2.6 References

(1) Zheng, J.; Chen, B.; Thanyamanta, W.; Hawboldt, K.; Zhang, B.; Liu, B. Offshore Produced Water Management: A Review of Current Practice and Challenges in Harsh/Arctic Environments. *Mar. Pollut. Bull.* **2016**, *104* (1–2), 7–19. https://doi.org/10.1016/j.marpolbul.2016.01.004.

(2) Bakke, T.; Klungsøyr, J.; Sanni, S. Environmental Impacts of Produced Water and Drilling Waste Discharges from the Norwegian Offshore Petroleum Industry. *Mar. Environ. Res.* **2013**, *92*, 154–169. https://doi.org/10.1016/j.marenvres.2013.09.012.

(3) Environment Canada. *Priority Substances List Assessment Report (Phenol)*; 2013.

(4) European Union. *European Union Risk Assessment Report: TDCPP*; 2008.

(5) ATSDR. Public Health Statement Arsenic. *U.S Public Heal. Serv. Agency Toxic Subst. Dis. Regist.* **2007**, No. September, 1–10. https://doi.org/10.1038/npg.els.0000869.

(6) Lu, W.; Wang, X.; Wu, X.; Liu, D.; Li, J.; Chen, L.; Zhang, X. Multi-Template Imprinted Polymers for Simultaneous Selective Solid-Phase Extraction of Six Phenolic Compounds in Water Samples Followed by Determination Using Capillary Electrophoresis. *J. Chromatogr. A* **2017**, *1483*, 30–39. https://doi.org/10.1016/j.chroma.2016.12.069.

(7) Fattahi, N.; Samadi, S.; Assadi, Y.; Hosseini, M. R. M. Solid-Phase Extraction Combined with Dispersive Liquid-Liquid Microextraction-Ultra Preconcentration of Chlorophenols in Aqueous Samples. *J. Chromatogr. A* **2007**, *1169* (1–2), 63–69. https://doi.org/10.1016/j.chroma.2007.09.002.

(8) Dolatto, R. G.; Messerschmidt, I.; Fraga Pereira, B.; Martinazzo, R.; Abate, G. Preconcentration of Polar Phenolic Compounds from Water Samples and Soil Extract by Liquid-Phase Microextraction and Determination via Liquid Chromatography with Ultraviolet Detection. *Talanta* **2016**, *148*, 292–300. https://doi.org/10.1016/j.talanta.2015.11.004.

(9) Xie, X.; Ma, X.; Guo, L.; Fan, Y.; Zeng, G.; Zhang, M.; Li, J. Novel Magnetic Multi-Templates Molecularly Imprinted Polymer for Selective and Rapid Removal and Detection of Alkylphenols in Water. *Chem. Eng. J.* **2019**, *357*, 56–65. https://doi.org/10.1016/j.cej.2018.09.080.

(10) Igbinosa, E. O.; Odjadjare, E. E.; Chigor, V. N.; Igbinosa, I. H.; Emoghene, A. O.; Ekhaise, F. O.; Igiehon, N. O.; Idemudia, O. G. Toxicological Profile of Chlorophenols and Their Derivatives in the Environment: The Public Health Perspective. *Sci. World J.* **2013**, *2013*, 1–11. https://doi.org/10.1155/2013/460215.

(11) United States Environmental Protection Agency. https://www.epa.gov/ground-water-and-drinking-water/national-primary-drinking-water-regulations.

(12) Thomas, K. V.; Balaam, J.; Hurst, M. R.; Thain, J. E. Identification of in Vitro Estrogen and Androgen Receptor Agonists in North Sea Offshore Produced Water Discharges. *Environ. Toxicol. Chem.* **2004**, *23* (5), 1156. https://doi.org/10.1897/03-239.

(13) Canadian Council of Ministers of the Environment. *Canadian Water Quality Guidelines*; 2008.

(14) Directive 2013/39/EU of the European parliament and of the council of 12 August

2013. *Amending Directives 2000/60/EC and 2008/105/EC as Regards Priority Substances in the Field of Water Policy*; 2013. https://doi.org/http://eur-lex.europa.eu/legal-content/EN/TXT/?uri=celex:32013L0039.

(15) Mahugo Santana, C.; Sosa Ferrera, Z.; Esther Torres Padrón, M.; Juan Santana Rodríguez, J. Methodologies for the Extraction of Phenolic Compounds from Environmental Samples: New Approaches. *Molecules* **2009**, *14* (1), 298–320. https://doi.org/10.3390/molecules14010298.

(16) Rodríguez, I.; Llompart, M. P.; Cela, R. Solid-Phase Extraction of Phenols. *J. Chromatogr. A* **2000**, *885* (1–2), 291–304. https://doi.org/10.1016/S0021-9673(00)00116-3.

(17) Bagheri, H.; Mohammadi, A.; Salemi, A. On-Line Trace Enrichment of Phenolic Compounds from Water Using a Pyrrole-Based Polymer as the Solid-Phase Extraction Sorbent Coupled with High-Performance Liquid Chromatography. *Anal. Chim. Acta* **2004**, *513*, 445–449. https://doi.org/10.1016/j.aca.2004.03.020.

(18) Prieto, A.; Araujo, L.; Navalon, A.; Vilchez, J. Comparison of Solid-Phase Extraction and Solid-Phase Microextraction Using Octadecylsilane Phase for the Determination of Pesticides in Water Samples. *Curr. Anal. Chem.* **2010**, *5* (3), 219–224. https://doi.org/10.2174/157341109788680309.

(19) Turiel, E.; Martín-Esteban, A. Molecularly Imprinted Polymers-Based Microextraction Techniques. *TrAC - Trends Anal. Chem.* **2019**, *118*, 574–586. https://doi.org/10.1016/j.trac.2019.06.016.

(20) Andersson, L.; Sellergren, B.; Mosbach, K. Imprinting of Amino Acid Derivatives

in Macroporous Polymers. *Tetrahedron Lett.* **1984**, *25* (45), 5211–5214. https://doi.org/10.1016/S0040-4039(01)81566-5.

(21) Surikumaran, H.; Mohamad, S.; Muhamad Sarih, N.; Muggundha Raoov, R. β-Cyclodextrin Based Molecular Imprinted Solid Phase Extraction for Class Selective Extraction of Priority Phenols in Water Samples. *Sep. Sci. Technol.* **2015**, *6395* (February 2016), 150615133334007. https://doi.org/10.1080/01496395.2015.1043016.

(22) El-Sheikh, A. H.; Al-Quse, R. W.; El-Barghouthi, M. I.; Al-Masri, F. S. Derivatization of 2-Chlorophenol with 4-Amino-Anti-Pyrine: A Novel Method for Improving the Selectivity of Molecularly Imprinted Solid Phase Extraction of 2-Chlorophenol from Water. *Talanta* **2010**, *83* (2), 667–673. https://doi.org/10.1016/j.talanta.2010.10.022.

(23) Caro, E.; Marcé, R. M.; Cormack, P. a G.; Sherrington, D. C.; Borrull, F. On-Line Solid-Phase Extraction with Molecularly Imprinted Polymers to Selectively Extract Substituted 4-Chlorophenols and 4-Nitrophenol from Water. *J. Chromatogr. A* **2003**, *995* (1–2), 233–238. https://doi.org/10.1016/S0021-9673(03)00543-0.

(24) Feng, Q.-Z.; Zhao, L.-X.; Yan, W.; Lin, J.-M.; Zheng, Z.-X. Molecularly Imprinted Solid-Phase Extraction Combined with High Performance Liquid Chromatography for Analysis of Phenolic Compounds from Environmental Water Samples. *J. Hazard. Mater.* **2009**, *167* (1–3), 282–288. https://doi.org/10.1016/j.jhazmat.2008.12.115.

(25) Feng, Q.; Zhao, L.; Lin, J.-M. Molecularly Imprinted Polymer as Micro-Solid Phase Extraction Combined with High Performance Liquid Chromatography to Determine Phenolic Compounds in Environmental Water Samples. *Anal. Chim. Acta* **2009**, *650* (1), 70–76. https://doi.org/10.1016/j.aca.2009.04.016.

(26) Mehdinia, A.; Baradaran Kayyal, T.; Jabbari, A.; Aziz-Zanjani, M. O.; Ziaei, E. Magnetic Molecularly Imprinted Nanoparticles Based on Grafting Polymerization for Selective Detection of 4-Nitrophenol in Aqueous Samples. *J. Chromatogr. A* **2013**, *1283*, 82–88. https://doi.org/10.1016/j.chroma.2013.01.093.

(27) Hashemi, S. H.; Najari, F. Response Surface Methodology of Pre-Concentration of Chorophenols from Seawater Samples by Molecularly Imprinted Stir Bar Sorptive Extraction Combined with HPLC: Box-Behnken Design. *J. Chromatogr. Sci.* **2019**, *57* (3), 279–289. https://doi.org/10.1093/chromsci/bmy107.

(28) Gryshchenko, A. O.; Bottaro, C. S. Development of Molecularly Imprinted Polymer in Porous Film Format for Binding of Phenol and Alkylphenols from Water. *Int. J. Mol. Sci.* **2014**, *15* (1), 1338–1357. https://doi.org/10.3390/ijms15011338.

(29) Qi, P.; Wang, J.; Wang, L.; Li, Y.; Jin, J.; Su, F.; Tian, Y.; Chen, J. Molecularly Imprinted Polymers Synthesized via Semi-Covalent Imprinting with Sacrificial Spacer for Imprinting Phenols. *Polymer (Guildf).* **2010**, *51* (23), 5417–5423. https://doi.org/10.1016/j.polymer.2010.09.037.

(30) Alvarez-lorenzo, C.; Angel, C. *Handbook of Molecularly Imprinted Polymers*; 2013.

(31) Spivak, D. A. Optimization, Evaluation, and Characterization of Molecularly Imprinted Polymers. *Adv. Drug Deliv. Rev.* **2005**, *57* (12), 1779–1794. https://doi.org/10.1016/j.addr.2005.07.012.

(32) Huang, Y.; Xu, Y.; He, Q.; Du, B.; Cao, Y. Preparation and Characteristics of a Dummy Molecularly Imprinted Polymer for Phenol. *J. Appl. Polym. Sci.* **2013**, *128* (5), 3256–3262. https://doi.org/10.1002/app.38391.

(33) Urraca, J. L.; Marazuela, M. D.; Merino, E. R.; Orellana, G.; Moreno-Bondi, M. C. Molecularly Imprinted Polymers with a Streamlined Mimic for Zearalenone Analysis. *J. Chromatogr. A* **2006**, *1116* (1–2), 127–134. https://doi.org/10.1016/j.chroma.2006.03.032.

(34) Matsui, J.; Fujiwara, K.; Takeuchi, T. Atrazine-Selective Polymers Prepared by Molecular Imprinting of Trialkylmelamines as Dummy Template Species of Atrazine. *Anal. Chem.* **2000**, *72* (8), 1810–1813. https://doi.org/10.1021/ac9911950.

(35) Barros, L. A.; Custodio, R.; Rath, S. Design of a New Molecularly Imprinted Polymer Selective for Hydrochlorothiazide Based on Theoretical Predictions Using Gibbs Free Energy. *J. Braz. Chem. Soc.* **2016**, *27* (12), 2300–2311. https://doi.org/10.5935/0103-5053.20160126.

(36) Moghadam, M. N.; Pioletti, D. P. Improving Hydrogels' Toughness by Increasing the Dissipative Properties of Their Network. *J. Mech. Behav. Biomed. Mater.* **2015**, *41*, 161–167. https://doi.org/10.1016/j.jmbbm.2014.10.010.

(37) Abu-Alsoud, G. F.; Hawboldt, K. A.; Bottaro, C. S. Comparison of Four

Adsorption Isotherm Models for Characterizing Molecular Recognition of Individual Phenolic Compounds in Porous Tailor-Made Molecularly Imprinted Polymer Films. *ACS Appl. Mater. Interfaces* **2020**, *12* (10), 11998–12009. https://doi.org/10.1021/acsami.9b21493.

(38) Ding, X.; Yang, J.; Dong, Y. Advancements in the Preparation of High-Performance Liquid Chromatographic Organic Polymer Monoliths for the Separation of Small-Molecule Drugs. *J. Pharm. Anal.* **2018**, *8* (2), 75–85. https://doi.org/10.1016/j.jpha.2018.02.001.

(39) Fu, X.; Yang, Q.; Zhou, Q.; Lin, Q.; Wang, C. Template-Monomer Interaction in Molecular Imprinting : Is the Strongest the Best ? *Open J. Org. Polym. Mater.* **2015**, *5* (April), 58–68.

(40) Dubey, L. Selective Recognition of Bifunctional Molecules by Synthetic Polymers Prepared by Covalent Molecular Imprinting. *Open Anal. Chem. J.* **2012**, *6* (1), 15–21. https://doi.org/10.2174/1874065001206010015.

(41) Urraca, J. L.; Carbajo, M. C.; Torralvo, M. J.; González-Vázquez, J.; Orellana, G.; Moreno-Bondi, M. C. Effect of the Template and Functional Monomer on the Textural Properties of Molecularly Imprinted Polymers. *Biosens. Bioelectron.* **2008**, *24* (1), 155–161. https://doi.org/10.1016/j.bios.2008.04.004.

(42) Spivak, D.; Gilmore, M. a.; Shea, K. J. Evaluation of Binding and Origins of Specificity of 9-Ethyladenine Imprinted Polymers. *J. Am. Chem. Soc.* **1997**, *119* (19), 4388–4393. https://doi.org/10.1021/ja963510v.

(43) Jia, M.; Sun, G.; Zhao, X.; Liu, Z. Effect of Polyethylene Glycol as a Molecular

Crowding Agent on Reducing Template Consumption for Preparation of Molecularly. *Anal. Methods* **2016**, *8*, 4554–4562. https://doi.org/10.1039/c6ay00383d.

(44) Chen, M.; Lu, Y.; Ma, Q.; Guo, L.; Feng, Y. Q. Boronate Affinity Monolith for Highly Selective Enrichment of Glycopeptides and Glycoproteins. *Analyst* **2009**, *134* (10), 2158–2164. https://doi.org/10.1039/b909581k.

(45) Irgum, K.; Courtois, J.; Bystro, E. Novel Monolithic Materials Using Poly (Ethylene Glycol) as Porogen for Protein Separation. *Polymer (Guildf).* **2006**, *47*, 2603–2611. https://doi.org/10.1016/j.polymer.2006.01.096.

(46) Bartosz Ziołkowski; Larisa, F.; Theobald, J.; Benito-Lopez, F.; Diamond, D. Porous Self-Protonating Spiropyran-Based NIPAAm Gels with Improved Reswelling Kinetics. *J Mater Sci* **2016**, *51*, 1392–1399. https://doi.org/10.1007/s10853-015-9458-2.

(47) Zhang, Y.; Ye, L. Improvement of Permeability of Poly (Vinyl Alcohol) Hydrogel by Using Poly (Ethylene Glycol) as Porogen Improvement of Permeability of Poly (Vinyl Alcohol) Hydrogel by Using Poly (Ethylene Glycol) as Porogen. *Polym. Plast. Technol. Eng.* **2011**, *50*, 776–782. https://doi.org/10.1080/03602559.2010.551443.

(48) Mirmohseni, A.; Shojaei, M.; Pourata, R. Experimental Design and Multi-Objective Optimization of Molecularly Imprinted Polymers for Monosaccharides. *RSC Adv.* **2014**, *4* (39), 20177–20184. https://doi.org/10.1039/c4ra00802b.

(49) Abu-Alsoud, G. F.; Hawboldt, K. A.; Bottaro, C. S. Assessment of Cross-

Reactivity in a Tailor-Made Molecularly Imprinted Polymer for Phenolic Compounds Using Four Adsorption Isotherm Models. *J. Chromatogr. A* **2020**, *1629* (461463). https://doi.org/10.1016/j.chroma.2020.461463.

(50) Zalloum, H. M.; Al-Qodah, Z.; Mubarak, M. S. Copper Adsorption on Chitosan-Derived Schiff Bases. *J. Macromol. Sci. Part A Pure Appl. Chem.* **2009**, *46* (1), 46–57. https://doi.org/10.1080/10601320802515225.

(51) Aravind, A.; Mathew, B. Tailoring of Nanostructured Material as an Electrochemical Sensor and Sorbent for Toxic Cd(II) Ions from Various Real Samples. *J. Anal. Sci. Technol.* **2018**, *9* (1), 1–17. https://doi.org/10.1186/s40543-018-0153-1.

(52) Liu, H.; Cai, X.; Wang, Y.; Chen, J. Adsorption Mechanism-Based Screening of Cyclodextrin Polymers for Adsorption and Separation of Pesticides from Water. *Water Res.* **2011**, *45* (11), 3499–3511. https://doi.org/10.1016/j.watres.2011.04.004.

(53) Annamma, K. M.; Beena, M. Design of 2,4-Dichlorophenoxyacetic Acid Imprinted Polymer with High Specificity and Selectivity. *Mater. Sci. Appl.* **2011**, *02* (03), 131–140. https://doi.org/10.4236/msa.2011.23017.

(54) Ni, N.; El-Sayed, M. M.; Sanghvi, T.; Yalkowsky, S. H. Estimation of the Effect of NaCl on the Solubility of Organic Compounds in Aqueous Solutions. *J. Pharm. Sci.* **2000**, *89* (12), 1620–1625. https://doi.org/10.1002/1520-6017(200012)89:12<1620::AID-JPS13>3.0.CO;2-N.

(55) Santana, C. M.; Ferrera, Z. S.; Padrón, M. E. T.; Rodríguez, J. J. S. Methodologies

for the Extraction of Phenolic Compounds from Environmental Samples: New Approaches. *Molecules* **2009**, *14* (1), 298–320. https://doi.org/10.3390/molecules14010298.

(56) Zhong, C.; He, M.; Liao, H.; Chen, B.; Wang, C.; Hu, B. Polydimethylsiloxane/Covalent Triazine Frameworks Coated Stir Bar Sorptive Extraction Coupled with High Performance Liquid Chromatography-Ultraviolet Detection for the Determination of Phenols in Environmental Water Samples. *J. Chromatogr. A* **2016**, *1441*, 8–15. https://doi.org/10.1016/j.chroma.2016.02.073.

(57) U.S. National Library of Medicine National Center for Biotechnology Information https://pubchem.ncbi.nlm.nih.gov.

(58) Hunter, C. A.; Sanders, J. K. M. The Nature of .Pi.-.Pi. Interactions. *J. Am. Chem. Soc.* **2005**, *112* (14), 5525–5534. https://doi.org/10.1021/ja00170a016.

(59) Zhu, D.; Hyun, S.; Pignatello, J. J.; Lee, L. S. Evidence for π-π Electron Donor-Acceptor Interactions between π-Donor Aromatic Compounds and π-Acceptor Sites in Soil Organic Matter through pH Effects on Sorption. *Environ. Sci. Technol.* **2004**, *38* (16), 4361–4368. https://doi.org/10.1021/es035379e.

(60) Çabuk, H.; Ata, Ş. Rotation Mixing-Assisted Liquid–Liquid Microextraction: A New Microextraction Approach for the Determination of Priority Phenols in Water Samples. *Anal. Methods* **2016**, *8* (15), 3123–3131. https://doi.org/10.1039/C6AY00062B.

(61) Hu, X. Z.; Wu, J. H.; Feng, Y. Q. Molecular Complex-Based Dispersive Liquid-Liquid Microextraction: Analysis of Polar Compounds in Aqueous Solution. *J.*

Chromatogr. A **2010**, *1217* (45), 7010–7016. https://doi.org/10.1016/j.chroma.2010.09.013.

(62) Zhang, P.-P.; Shi, Z.-G.; Feng, Y.-Q. Determination of Phenols in Environmental Water Samples by Two-Step Liquid-Phase Microextraction Coupled with High Performance Liquid Chromatography. *Talanta* **2011**, *85* (5), 2581–2586. https://doi.org/10.1016/j.talanta.2011.08.021.

(63) Environmental Protection Agency. Determination of Phenols in Drinking Water by Solid Phase Extraction and Capillary Column Gas Chromatography/Mass Spectrometry. *EPA method* **2000**, No. April, 1–46.

(64) US EPA. *Method 604: Phenols, methods for organic chemical analysis of municipal and industrial wastewater*; 1987. https://doi.org/10.2134/jeq1987.00472425001600010011x.

(65) USEPA. *Method 625 - Base/Neutrals and Acids*; 1984.

(66) López-Darias, J.; Germán-Hernández, M.; Pino, V.; Afonso, A. M. Dispersive Liquid-Liquid Microextraction versus Single-Drop Microextraction for the Determination of Several Endocrine-Disrupting Phenols from Seawaters. *Talanta* **2010**, *80* (5), 1611–1618. https://doi.org/10.1016/j.talanta.2009.09.057.

Chapter 3

3 Comparison of Four Adsorption Isotherm Models for Characterizing Molecular Recognition of Individual Phenolic Compounds in Porous Tailor-Made Molecularly Imprinted Polymer Films

This chapter was published as a research paper: Ghadeer F. Abu-Alsoud, Kelly A. Hawboldt, and Christina S. Bottaro*; *ACS Appl. Mater. Interfaces* 2020, 12, 10, 11998–12009. https://doi.org/10.1021/acsami.9b21493

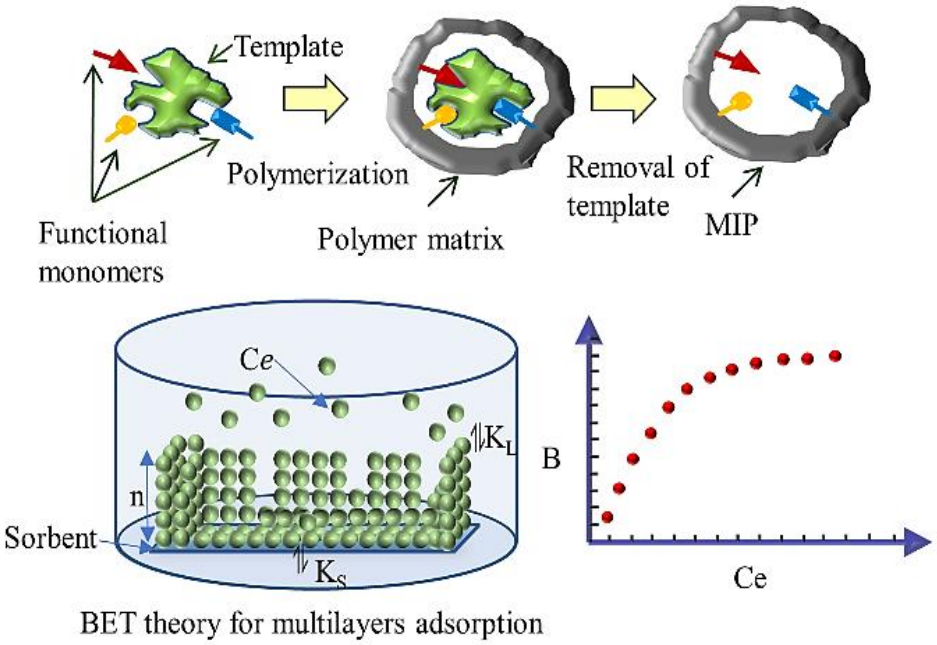

Keywords: Adsorption isotherm, Langmuir isotherm, Freundlich isotherm, Langmuir–Freundlich isotherm, Brunauer, Emmett, and Teller (*BET*) isotherm model, molecularly imprinted polymer (MIP), thin film, phenols, multilayer adsorption, binding site energy, affinity distribution

3.1 Abstract

A molecularly imprinted polymer (MIP) film using catechol as the template was designed for adsorption of a range of phenols from water. Four different isotherm models (Langmuir (LI), Freundlich (FI), Langmuir–Freundlich (L-FI), and Brunauer, Emmett, and Teller (BET)) were used to study the MIP adsorption of five phenolic compounds: phenol (Ph), 2-methylphenol (2-MP), 3-methylphenol (3-MP), 2-chlorophenol (2-CP), 4-teroctylphenol (4-OP). Each model was evaluated for its fit with the experimental data, and key parameters, including number of binding sites and binding site energies, were compared. Though the LI, L-FI and BET models showed good agreement for estimation of number of binding sites and affinity for most adsorbates, no single model was suitable for all. The LI and L-FI models gave the best fitting statistics for the Ph, 2-MP, 3-MP and 2-CP. The recognition of 4-OP, which has much higher binding affinities than the smaller phenolic compounds and not attributable to hydrophobicity alone, was explained only by the BET model which indicates by the formation of multilayers. The BET model failed only with phenol. MIPs also showed higher adsorption capacities and improved homogeneity over the analogous non-imprinted polymers (NIPs).

3.2 Introduction

Molecularly imprinted polymers (MIPs) are synthetic polymeric materials with specific recognition sites complementary in shape, size, and functional groups to a template molecule [1–9]. Their stability, low cost, and ease of preparation make MIPs attractive for many applications such as sensors, chromatography, solid phase extraction, and for a clean-

up and pre-concentration of analytes in biological and environmental samples [10,11]. Ideally, MIPs are designed to provide specific affinity and selectivity for a single compound or a class of compounds. MIPs are much like other porous adsorbents in which physisorption occurs through interaction with surface functional groups, though MIPs feature more sites favourably oriented to bind with target moieties. Since isotherm models have been developed to account for adsorbate binding with materials both heterogeneous and homogeneous binding sites, these models can be applied to MIPs.

Adsorption isotherm models have already been used to characterize interactions between analytes and MIP surfaces to enhance understanding of the adsorption chemistry and to provide numerical descriptors of MIP binding properties for comparison of performance.[3,12–29] Models that have been applied to MIPs include Langmuir (LI),[30] Freundlich (FI),[31] and Langmuir–Freundlich (L-FI) isotherms.[32] Although the Brunauer, Emmett, and Teller (BET) has not been previously used to characterize MIPs, its ability to model multilayer formation warrants investigation of its suitability.[33] Umpleby *et al.*[34–37] were among the earliest to apply the isotherm models to MIPs as a means to compare the performance of different formulations; they relied primarily on the FI and L-FI models. Martin-Esteban and co-workers extended the use adsorption isotherms, specifically the L-FI model, to evaluate cross-reactivity in MIPs.[38,39] However, no quantitative or qualitative comparison of the four models has been undertaken for MIPs.

A key element of the isotherm models is the idea that polymer surfaces can be classified based on two types of recognition, homogeneous and heterogeneous, which influence the

choice of isotherm model.[37] In a homogeneous polymer, the binding sites have the same energy, which suggests consistent distribution and orientation of functionalities for the accessible sites on the polymer surface. In such a system, the affinity of the analyte for the surface is independent of concentration. In a heterogeneous polymer, the binding sites available can have a range of energies leading to significant differences in binding affinities depending on the concentration of the analyte. In theory, MIPs can produce homogeneous binding site distributions, but heterogeneous distributions are more common, particularly with non-covalent imprinting. In non-covalent imprinting, the functional monomer is added in excess of the template according to Le Chatelier's principle to shift the equilibrium toward the formation of the template-monomer complex prior to polymerization. Small differences in the arrangement of the functional monomers in the template-monomer complex broadens the distribution of binding constants. However, most heterogeneity arises from randomly oriented free functional monomer giving binding sites with different association constants and increased non-selective interactions.[37,40] The radical-initiated copolymerization process, which is influenced by many factors (e.g., the type of solvent, number of initiation sites, and ratio of monomer to cross-linker) also influences homogeneity.[41] Since, the binding site homogeneity is dependent on both the nature of the adsorbate and the features of the MIP, it is possible that more than one model will be needed to characterize a single novel formulation.

3.2.1 Adsorption models

The adsorption models are classified into two groups: (i) models of discrete distribution for the homogeneous surface and (ii) models of continuous distribution that take into

consideration the surface heterogeneity. [37] The LI and bi-LI are most common discrete models, where LI describes only one type of binding site and bi-LI two. The BET isotherm model is an extension of the LI model, incorporating the possibility of the formation of multilayers of adsorbate on the sorbent surface. The FI and L-FI are the most common continuous distribution models. The key elements of the theory for the adsorption models are introduced below.

3.2.2 Discrete distribution models

In 1916, Irving Langmuir introduced a new adsorption isotherm model to describe the adsorption behavior of gaseous molecules onto a solid surface at a constant temperature; the eponymous Langmuir isotherm is the most widely used model for adsorption studies.[30,42] LI assumes that all surface binding sites are the same, adsorption cannot occur beyond monolayer coverage, and each binding site can be occupied by only one molecule.[43–47] The LI model has been used to characterize MIP adsorption based on these assumptions.[12,22] The Langmuir equation (Eq. 1) illustrates the assumed relationship between the amount of bound (B) analyte and the free analyte in the system (C_e) at equilibrium:

$$B = \frac{NKC_e}{1 + KC_e} \tag{1}$$

where N is the binding site density, and K is the adsorption constant (a measure of the adsorbate affinity). This equation can be rearranged into a linear form (Eq. 2) to calculate N and K by linear regression analysis:

$$\frac{1}{B} = \frac{1}{NKC_e} + \frac{1}{N} \tag{2}$$

Scatchard analysis can also be used to determine the LI parameters. In this instance, B/C_e is plotted versus B (Eq. 3). A straight line indicates homogeneous binding site energies (a single partition coefficient K applies at all solute concentrations), and a curved line is evidence of the heterogeneous distribution of binding site energies.[37,48] In some systems, curves in the data can be fitted with two straight lines (assumes there are discrete high and low affinity binding sites) and thus two groups of binding parameters (K_1, N_1 *and* K_2, N_2) are generated; this is termed a bi-LI.

$$\frac{B}{C_e} = KN - KB \tag{3}$$

In 1938, Brunauer, Emmett, and Teller[33] proposed a multilayer adsorption model, giving their names to the common abbreviation BET. In this model, gas-solid adsorption begins with formation of an incomplete monolayer (n = 1) to which additional molecules are adsorbed through intermolecular interactions to form layers (n = 2→∞). BET assumes the following: 1) there is no interaction between the solute molecules; 2) the adsorbent surface is homogenous; 3) adsorption can occur in multilayers as the adsorbed molecules provide adsorption sites, which is a key feature of the model. The general form of BET isotherm is shown in Eq. 4.

$$\frac{q}{q_m} = \frac{cx(1-(n+1)x^n + nx^{n+1})}{(1-x)(1+(c-1)x - cx^{n+1})} \tag{4}$$

For the gas-solid adsorption: x is the ratio of the partial pressure of the adsorbate to saturation vapour pressure of the system ($x = P/P^{sat}$); $c = K_S/K_L$ where K_S is the equilibrium adsorption constant for the first layer and K_L is the equilibrium adsorption constant for all upper layers (related to intermolecular interactions between adsorbed solute molecules); n is the number of adsorbed layers;[49] q is the amount (moles or mass) of analyte adsorbed relative to mass of sorbent; and q_m the amount adsorbed corresponding to formation of a complete monolayer. The LI is a special case of the general form of the BET isotherm model; when $n = 1$, Eq. 4 reduces to the LI Eq. 1.

The general form of the BET isotherm model (Eq. 4) can be simplified to the more familiar *BET* equation (5), which assumes $x < 1$ and $n \rightarrow \infty$. This can be rearranged to the linear form (Eq. 6); estimates of the adsorption capacity for the monolayer (q_m) and the relative adsorption equilibrium constants (as c) can be calculated from the slope and the intercept using the linear regression of data for q and x.

$$\frac{q}{q_m} = \frac{cx}{(1-x)(1-x+cx)} \tag{5}$$

$$\frac{x}{q(1-x)} = \frac{1}{q_m c} + \left(\frac{c-1}{q_m c}\right)x \tag{6}$$

Ebadi *et al.*[49] adapted the BET theory for gas adsorption (Eq. 4) to liquid phase systems by replacing ($1/P^{sat}$) with the equilibrium constant K_L, and P with C_e (the equilibrium concentration in the liquid phase) to yield Eq. 7. Using experimental data for q and C_e, the values of q_m, K_L, K_S, and n (the same fitting parameters as described in Eq. 4) can be determined by nonlinear regression.

$$q = \frac{q_m K_S C_e[1-(n+1)(K_L C_e)^n + n(K_L C_e)^{n+1}]}{(1-K_L C_e)\left[1+\left(\frac{K_S}{K_L}-1\right)K_L C_e - \left(\frac{K_S}{K_L}\right)(K_L C_e)^{n+1}\right]} \quad (7)$$

3.2.3 Continuous distribution models

In 1906, Freundlich presented a model of the relationship between the amount of gas adsorbed per unit mass of adsorbent and pressure at a constant temperature.[31] The FI is the most familiar continuous distribution isotherm model providing a descriptor of the surface binding site energy heterogeneity, which can be more useful than the LI model as most solid surfaces, including MIPs, tend to be heterogeneous.[34,37,50,51] The FI assumes a power function relationship between *B* and C_e (Eq. 8), where *B* and C_e are the concentrations of bound and the free analyte, respectively.

$$B = aC_e^m \quad (8)$$

The pre-exponential constant *a* is the product of the total number of binding sites (N_t) and average binding affinity (K_o); *m* is the heterogeneity index and is constrained to values between 0 and 1. Systems with *m* closer to 1 are more homogeneous.[37,50] Eq. 8 can be linearized to give Eq. 9

$$log\, B = m\, log\, C_e + log\, a \quad (9)$$

Rampey and co-workers[37,50] developed the affinity distribution (*AD*) expression for the FI that integrates the Freundlich fitting parameters, *a* and *m* in Eq. 10, where *N(K)* represents the number of binding sites as a function of binding affinity *(K)*.

$$N(K) = 2.303am(1-m^2)e^{-2.303mlogK} \quad (10)$$

They further modified Eq. 10 to derived two further binding parameters in Eqs. 11 and 12.[37,50]

$$N_{K1-K2} = a(1-m^2)(K_1^{-m} - K_2^{-m}) \quad (11)$$

$$\overline{K}_{K1-K2} = \left(\frac{m}{m-1}\right)\left(\frac{K_1^{1-m} - K_2^{1-m}}{K_1^{-m} - K_2^{-m}}\right) \quad (12)$$

N_{K1-K2} is the apparent number of sites, and $\overline{K}_{K1-K2}$, the weighted average affinity. K_1–K_2 refers to the range of concentrations over which the experimental binding affinities have been modeled. Any range of concentrations can be chosen if they are below the saturation limit, and are implemented as $K_1 = 1/C_1$ and $K_2 = 1/C_2$, where $C_1 < C_2$, and $K_1 > K_2$. It has been noted that the FI is appropriate for only part of the entire binding isotherm range because of the deviation from the linearity at high concentrations.[37] In a heterogeneous material, high affinity binding sites are populated first and predominate for low adsorbate concentrations. As concentrations increase, the average affinity of the available binding sites decreases, which leads to a deviation in the isotherm plots.

In 1948, Sips described the hybrid L-FI model, which gives the Langmuir binding parameters along with the heterogeneity index, *m,* as found in the FI [32,37] The L-FI model reduces to the classical FI equation at low analyte concentration, and to the LI equation as the adsorption site energies become homogeneous (*m* approaching unity). This means that the L-FI isotherm can be applied to homogeneous and heterogeneous MIPs at low and high concentrations, including saturation concentrations.[38] In the L-FI model, a relationship between the concentration of a bound analyte (*B*) and the free analyte concentration in the solution (C_e) is described by Eq. 13; where N_t represents the total

number of binding sites; a is related to the affinity constant, $K_o = a^{1/m}$; and m is the heterogeneity index.

$$B = \frac{N_t a C_e^m}{1 + a C_e^m} \tag{13}$$

To determine if the more complex L-FI is required, a simple test can be applied by plotting the isotherm as log B versus $log\ C_e$. If the plot is linear over the concentration range, then the FI is sufficient to characterize the adsorption behavior. If the isotherm is linear at low concentrations and curved at high concentrations then L-FI must be used.[37]

This chapter aims to evaluate the differences between MIP and analogous non-imprinted polymers (NIPs) binding sites of catechol imprinted polymer toward five phenolic compounds using four different isotherm models: LI, FI, L-FI and BET models. The binding behavior of MIPs and NIPs were assessed using batch rebinding experiments, and the experimental data were processed with Eqs. 2,7,9, and 13 for LI, BET, FI, and L-FI, respectively. The experimental FI parameters were analyzed with the AD method using Eq. 10; FI's binding parameters N_{K1-K2} and $\overline{K}_{K1-K2}$ were calculated using Eqs.11 and 12. The performance of the adsorption isotherms is compared on the basis of correlation coefficients (R^2) and errors (relative errors) in the fitting parameters. The results from all four models are presented and their suitability for evaluating the materials are evaluated.

3.3 Experimental

3.3.1 Reagents and material

The following reagents were purchased from Sigma-Aldrich (Oakville, Canada) at 99% purity or better, except where noted. Phenol (Ph); 2-methylphenol (2-MP); 3-methylphenol

(3-MP); 2-chlorophenol (2-CP); catechol (Cat); 4-tert-octylphenol (4-(2,4,4-trimethylpentan-2-yl)phenol), (97%) (4-OP); ethylene glycol dimethacrylate (98%) (EGDMA); 4-vinyl benzoic acid (97%) (VBA), polyethylene glycol (PEG) (average MW 20,000), 3-(trimethoxysilyl)propyl methacrylate (98%), 2,2- dimethoxy-2-phenylacetophenone (DMPA) (99%); pH 4.0 buffer using potassium phosphate monobasic and phosphoric acid, and formic acid for LC-MS (98% -100%). Optima LC/MS grade acetonitrile and water were sourced from Fisher Scientific (Ontario, Canada); the solvents for cleaning the polymers and other lab use were ACS reagent grade: absolute ethanol from Commercial Alcohols (Ontario, Canada), toluene from Caledon Laboratory Chemicals (Ontario, Canada), and acetonitrile from ACP Chemicals (Montreal, Canada). Plain glass microscope slides 75 × 25 mm^2 were obtained from Fisher Scientific; the micro cover glass 18 x 18mm^2 from VWR (Mississauga, ON); a 13 mm PTFE 0.2 µm syringe filters from Canadian Life Science (Peterborough, ON).

Each standard stock solution 5 g L^{-1} was prepared in optima acetonitrile and stored in an amber headspace vial at -22 ◦C. All the rebinding solutions were freshly prepared with deionized (DI) water (18 MΩ cm) purified by a Barnstead Nanopure water purification system, (Lake Balboa, USA).

3.3.2 Instrumentation

Waters Acquity UHPLC-PDA is equipped with an autosampler and a photodiode array detector (PDA) for the detection of phenols. An RP-amide column (2.7 µm, 2.1x 100 mm, HALO column) was connected to a C18 guard column. The gradient elution was carried

out with 0.1% (v/v) formic acid in water (solvent A) and 0.1% formic acid in acetonitrile (solvent B). The gradient elution program was set up as follows: 0.00–2.00 min, 65% of solvent A; 2.01–2.30 min 60% of solvent A and kept constant for 1.20 min; then the ratio of solvent B increased to 100% in 4.50 min. Subsequently, we returned to the initial conditions 65% of solvent A in 0.30 min and kept for 2.70 min to equilibrate the column for the next run. The flow rate, the injection volume, the column and sample vial temperatures were set at 0.45 mL/min, 10 µL and 25 ºC, respectively. PDA was set at two wavelengths: 275 nm for Ph, 2-MP, 3-MP, 2-CP, 4-OP and 370 nm for baseline correction.

An analytical balance (Sartorius Secura 225D-1S, Germany), a pH-meter (Crison GLP 22, Barcelona, Spain), a vortex mixer (Corning LSE, USA), and an Elma T 660/H ultrasonic bath (Singen, Germany) were used in the pre-polymerization mixture and sample preparation steps. A Phoenix, RSM-01H magnetic stirrer (Garbsen, Germany) and a Luzchem EXPO-1 UV lamp 254 nm (Ontario, Canada) were used in the fabrication of the thin-film MIPs, and a VWR Scientific DVX-2500 digital multi-position vortex mixer (Hampton, USA) was used in the rebinding batch experiments.

3.3.3 Derivatization of glass microscope slides

Glass slides were cut in 20 × 25 mm^2 pieces, washed with water, then derivatized using 2% (v/v) 3-(trimethoxysilyl) propyl methacrylate in toluene overnight. The derivatized glass slides were rinsed with toluene, then ethanol, air-dried and stored in a dark place until use. The salinization process is essential to achieve uniform polymer adhesion to the glass surface.

3.3.4 Fabrication of thin-film MIPs

The prepolymerization mixture was prepared by weighing 4.40 mg (0.04 mmol) of pseudo-template (Cat), 17.77 mg (0.12 mmol) of functional monomer 4-VBA, 2.60 mg (0.01 mmol) of the photoinitiator (DMPA), and 0.044 g of PEG) as a solvent modifier into a vial. Then 90.6 µL (0.48 mmol) EGDMA and 200 µL of methanol/water (5:1) are added into the same vial. The non-imprinted polymer (NIP) prepolymerization mixture was prepared in the same way but without the pseudo-template. The components were mixed by vortex until all components dissolved, then the mixture was degassed to remove any oxygen that might inhibit the radical polymerization process. The prepolymerization solution was used within one day.

Individually-coated slides were made using the drop-casting technique (Figure 3.1) by depositing 20 µL of the prepolymerization onto the derivatized glass slide using positive displacement pipette Pos-D to accommodate the viscous prepolymerization mixture, then the solution was covered gently and quickly with 18 x 18 mm^2 micro cover glass. The dispensed prepolymerization mixture was irradiated with UV 1 h. Upon completion of the polymerization process, the micro cover glass was removed, leaving a uniform thin film polymeric coating on the glass slide substrate. To remove the template and unreacted components, the film was washed with acetonitrile/water (1:1) under stirring for 2 h, then washed with water, then acetonitrile, and finally air-dried. The mass of the thin-film MIP, ~3.5 mg, was measured by difference.

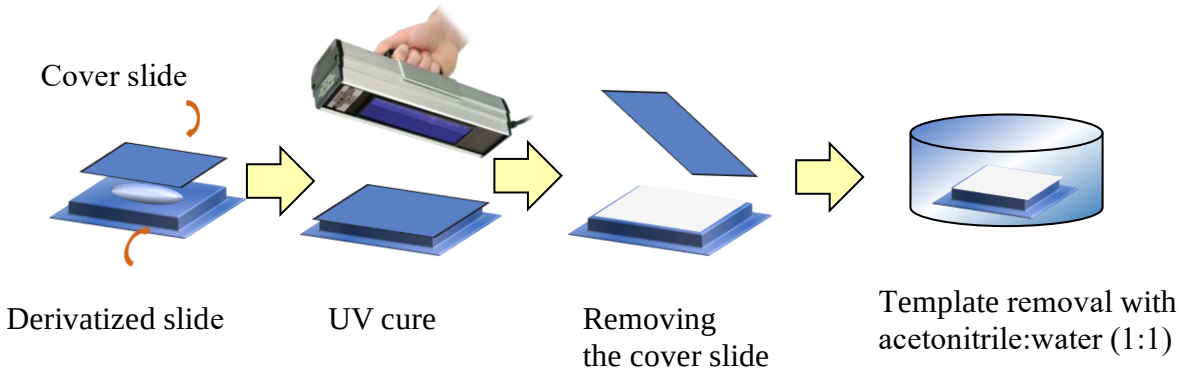

Figure 3.1. Fabrication of the MIP thin-film using a drop-casting technique

3.3.5 Physical Characteristics of the Films

The morphology and the thickness of MIPs and NIPs films were studied using the FEI MLA 650 F scanning electron microscope (SEM) and the resulting images are shown in Figure 3.2. Prior to the SEM measurements, the thin-film MIP and NIP devices were affixed to a metal surface using carbon tape and then coated with a thin layer of gold under vacuum. The coated films were scanned with a beam at an acceleration voltage of 10 kV at various magnifications, which in our case were x40000 and x5000 for the morphology and the thickness measurements, respectively. A typical coating is shown in Figure 3.2 (a) and the thickness measurements showed a uniform average thickness of about ~20 µm, Figure 3.2 (b). Exemplar SEM images of the NIPs and MIPs are shown in Figure 3.2 (c) and (d); the MIPs consistently exhibited more porous surfaces with deeper cavities and a mix of larger and small pores that, in part, explains the better performance of the MIP sorbents.

(a)

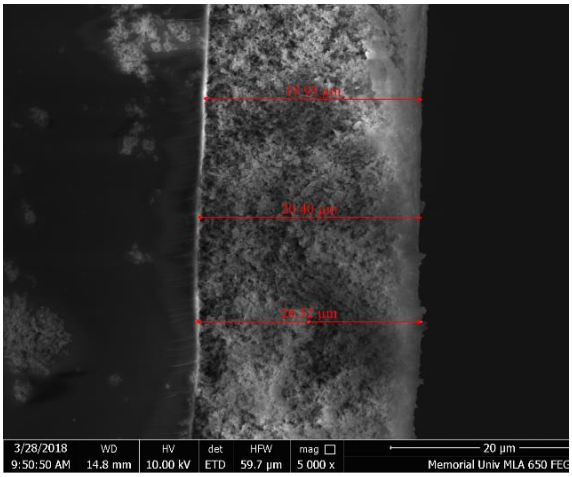

(b)

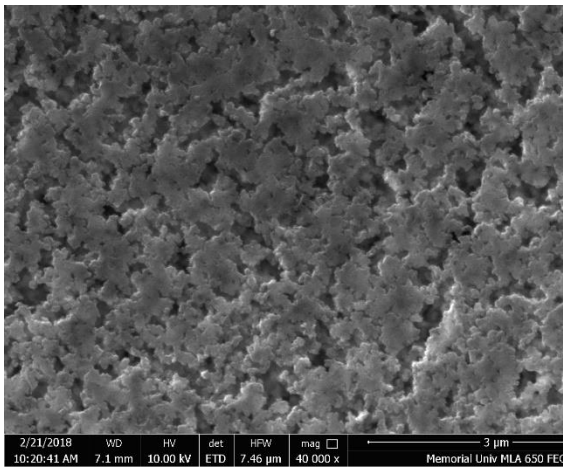

(c)

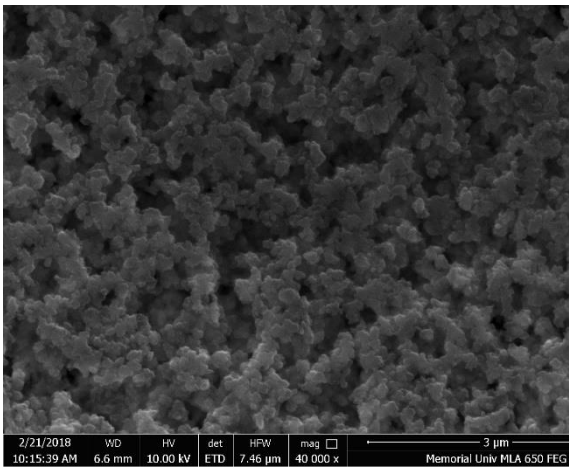

(d)

Figure 3.2. a) MIP thin-film slide; b) SEM image of cross-section and thickness of MIP film; c) SEM image of the NIP film surface; d) SEM image of the MIP film surface.

3.3.6 Batch rebinding experiments

All extraction experiments were carried out in the following way except where noted. The MIPs were placed into 50-mL centrifuge tubes containing 30 mL of an aqueous solution of 5% NaCl; 1 mM of phosphate buffer, pH 4, and spiked with various

concentrations of phenols (structures of the monomer, template and phenols can be found in Figure 3.3). For individual experiments Ph, 2-MP, 3-MP, or 2-CP were spiked from 1 mg L^{-1} to 20 mg L^{-1} and 4-OP was spiked at 0.2 mg L^{-1} to 7 mg L^{-1}, the upper solubility limit. The centrifuge tube was capped, and vortex mixed using a multi-tube mixer at 1500 rpm at room temperature for 3 h to 24 h. After extraction, the thin-film MIP was rinsed with DI water to remove any unbound components, including salts, then placed in a centrifuge tube containing 8 mL acetonitrile and vortex mixed at 1000 rpm for 15 min to desorb the bound analytes. The solution containing the desorbed phenolic compound was filtered using a 13 mm 0.2-µm PTFE syringe filter and then reduced to near dryness under N_2 and made to 1-mL with 35% acetonitrile in water. The final volumes were adjusted to 1 mL (1 mL volumetric flask).

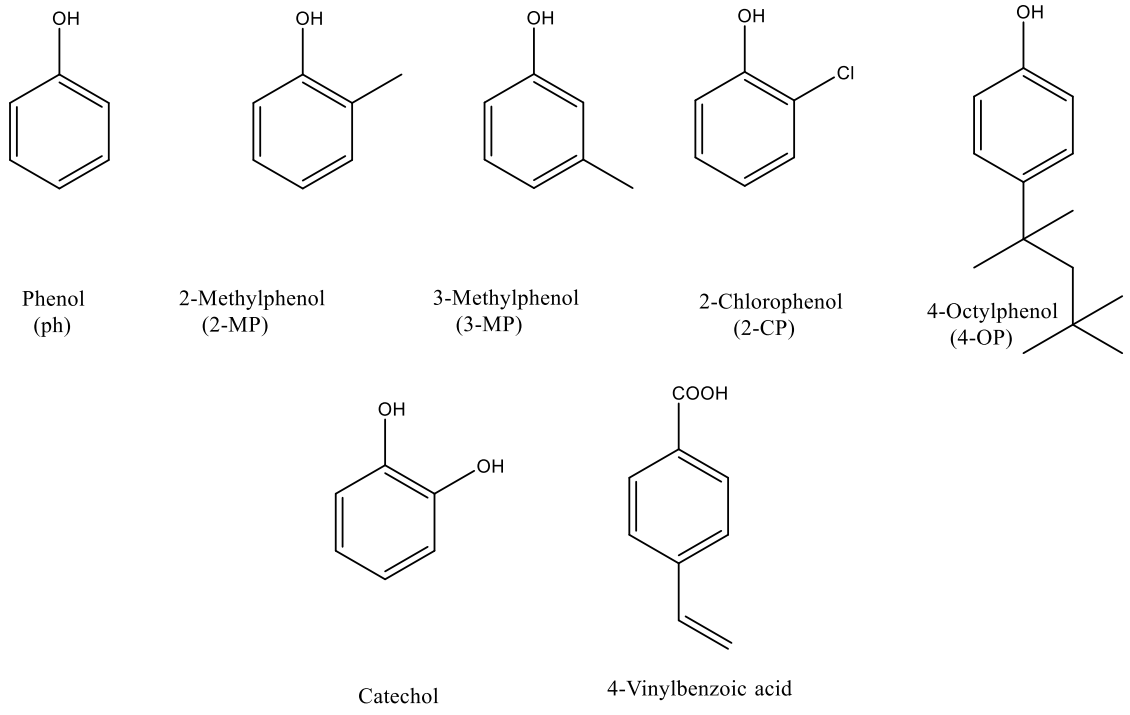

Figure 3.3. The chemical structures of phenols analytes under study.

3.3.7 Evaluation of isotherm models

Batch rebinding studies were used to obtain binding isotherms for these MIPs and corresponding NIPs. Analytes, over a range of concentrations, were allowed to adsorb to the polymer films of a known mass until equilibrium was achieved. The concentration of the bound analyte, *B,* is measured by UHPLC-PDA after desorption, while Ce, the concentration of the adsorbate remaining free in solution, is calculated by the difference between the spiked analyte concentration and the amount of analyte bound to MIP. The experimental data were fitted to the four isotherm models based on Eqs. (2,7,9, and 13) for LI, FI, L-FI, and BET, respectively.

For each adsorption isotherm model the following figures of merit are determined: relative error of each fitting coefficient, the correlation coefficients (R^2) and the sum of squares of the residual (*RSS*) between the data and fitted line. It is crucial to make sure that the isotherm fitting parameters have consistent and comparable units of measurement. In our studies, the units of B and C_e are μmol g^{-1} and μmol L^{-1}, respectively. In the case of FI and L-FI, the unit of the coefficient a depends on the value of the heterogeneity index m. LI and FI models were fitted by linear regression, and L-FI and BET isotherms were fitted via non-linear regression using Origin 2018 64-bit (Northampton, Massachusetts, USA) statistical software. The errors in the LI and FI parameters were estimated using the propagation of error equations. On the other hand, the errors in the fitting parameter for L-FI and BET can be estimated using Origin 2018 directly. All the isotherms coefficients, R^2, and *RSS* were illustrated in Tables below.

3.4 Results and discussion

3.4.1 Determination of Optimal Adsorption Time

The extraction-time profiles over 24 h were constructed for individual uptake of the phenols. Figure 3.4 illustrates the adsorption capacities of the phenolic compound as a function of time. The extraction time profile and time to establish equilibrium depends on the analyte characteristics. As shown in Figure 3.4, the light phenols including Ph, 2-MP, 3MP, and 2-CP have different behavior in which phenol reaches equilibrium instantly; 2-MP and 3-MP reach equilibrium within only one hour while 2-CP needs 2 h to reach equilibrium. On the other hand, the equilibrium time for 4-OP was reached after 12 h. However, adsorption was near equilibrium at 3 h; so, in the interest of efficiency, 3 h was chosen for all the binding studies for the isotherm evaluation.

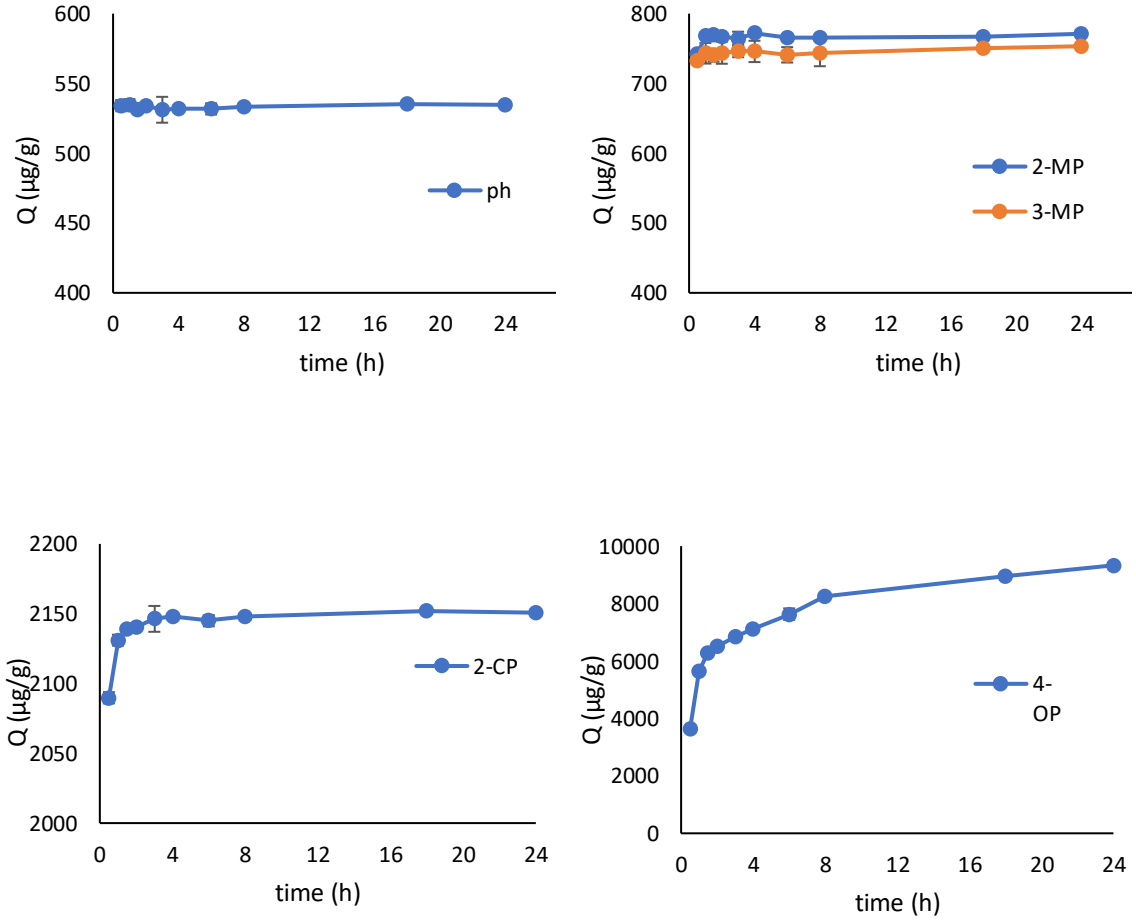

Figure 3.4. Individual extraction-time profile for some phenols from a water sample using a catechol imprinted MIP. 30 mL water spiked with 1 ppm individual analyte; salted with 5% of NaCl; buffered with pH 4 (1mM, phosphate buffer); the analyte was desorbed using 8 ACN for 15 min at 1000 rpm vortex speed. Error bars represent standard deviation (n = 3)

3.4.2 Assessment of Adsorption Isotherm Models for Characterizing MIP-Films Performance with Phenolic Analytes

We have used four different adsorption models to assess the behavior of our tailor-made MIP sorbent. This study aims to evaluate each isotherm for its suitability to model the uptake of phenols by MIPs. We have found that different binding isotherms may apply for the same system depending on the solute concentration, thus concentration ranges studied include both saturation and sub-saturation regions for a more thorough examination of the binding adsorption models. The experimental data were fitted to the isotherm models. To characterize and to evaluate the MIP binding sites, binding experiments were carried out on solutions of Ph, 2-MP, 3-MP, 2-CP and 4-OP individually as described in the experimental section. The experimental data were fitted to FI, LI, L-FI and BET adsorption isotherm models.

3.4.3 Freundlich Isotherm Model

The FI model is ideal for materials with heterogeneous binding site energies and typically with analytes that have a low tendency to form multilayers. The fitting parameters *a* and *m* are calculated from the plots shown in Figure 3.5 and presented in Table 3.1. The fitting parameters were then used to calculate N_{K1-K2} according to Eq. 11 and $\overline{K}_{K_{1-K_2}}$ using Eq. 12, also presented in Table 3.1. Excluding 4-OP from the discussion, for now, we attribute the adsorption trends to three main factors: surface area of the sorbent, hydrophobicity of the adsorbates, and degree of imprinting. Looking closely at the data for 2-CP, the plots in Figure 3.5 show that there is only a small difference in adsorption behavior between the MIPs and NIPs, which give comparable results for the fitting parameters. This suggests

that there is little to no selectivity toward the 2-CP in the MIP (i.e., low *IF* as shown in Table 3.2) and that adsorption is driven by the hydrophobicity of the adsorbate and the surface area of the sorbent. The hydrophobicity is estimated from the octanol/water partition coefficient (logP): logP values for Ph, 2-MP, 3-MP, 2-CP and 4-OP are 1.46, 1.95, 1.96, 2.15 and 5.25, respectively [52]. The values for $\overline{K}_{K_{1-K_2}}$ shown in Table 3.1 are consistent with logP values, with higher values for more hydrophobic compounds. When compared to Ph and 2-MP or 3-MP, 2-CP has a higher logP and consequently both the MIPs and NIPs show the higher binding capacities for 2-CP. Though the MIPs adsorb 2-CP slightly better than the NIPs, we attribute this to a small difference in surface area. This feature appears in the calculation of N_{K1-K2} and $\overline{K}_{K_{1-K_2}}$ (Table 3.1), where the MIP has more sites than the NIP, but they share very similar average binding site energies. We conclude that since the difference in surface area for the MIPs and NIPs are small, significant differences in the results for Ph, 2-MP and 3-MP are related to molecular imprinting. The results for Ph, 2-MP, and 3-MP indicate that the MIPs possess a higher number of binding sites and that these sites have a higher affinity for the adsorbates than the NIPs. Since the only difference in the preparation is the presence of the catechol template, the data supports the conclusion that the template facilitates the formation of higher affinity sites. It is also clear that the N_{K1-K2} and $\overline{K}_{K_{1-K_2}}$ values of the 2-MP and 3-MP are very close, proving that these two analytes have been adsorbed by the same mechanism. The differences in results for the 2-MP and 3-MP are also consistent with the role of the template in the formation of selective adsorption sites, with ortho-substituted 2-MP making a better fit with cavities formed using the ortho-substituted catechol.

The data for 4-OP are the most difficult rationalize by the FI model. Again, the MIPs outperform the NIPs in terms of bind capacities over the full range of concentrations studied (Figure 3.5 E). And the fitting parameters seem to bear that out, with higher values for a and $\overline{K}_{K1-K2}$ for the MIPs. However, the estimation of m seems to be where the model falls down. We expect the MIP to be more heterogeneous than the NIP, as with the other adsorbates, but this trend does not hold true for the 4-OP.

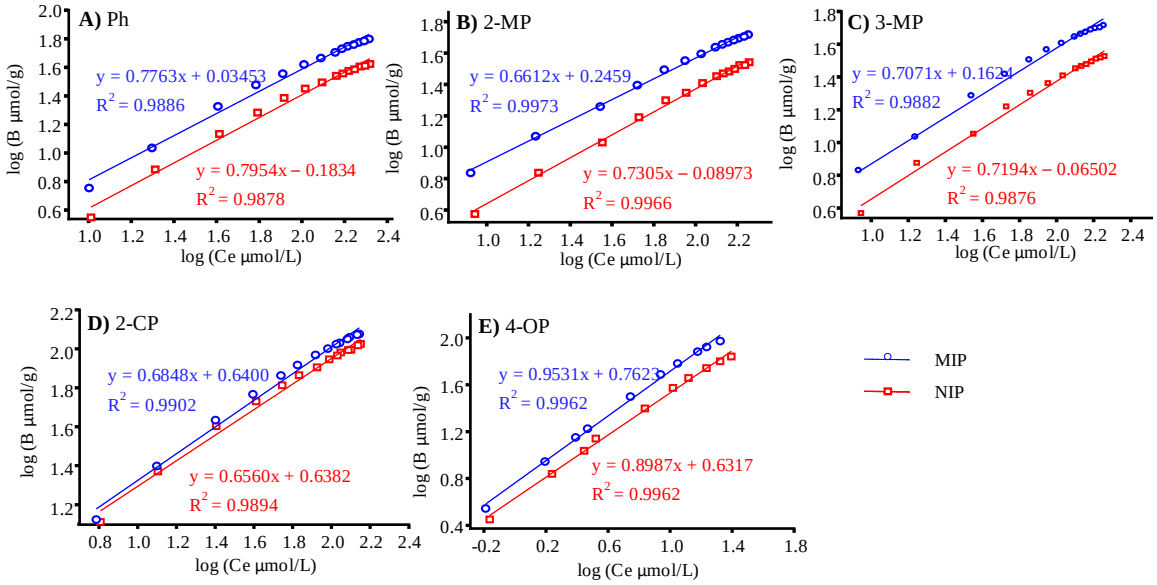

Figure 3.5. The experimental data for individual study (circle points for MIP, squares points for NIP) were fit to FI (solid lines) for MIP and NIP over the entire concentration range (A) Ph, B) 2-MP, C) 3-MP, D) 2-CP, E) 4-OP).

Table 3.1 FI fitting parameters over the full concentration range

MIP							
Analyte	*a* (µmol g^{-1}) (µM^{-1})^{m} *(RSD%)*	*m (RSD%)*	*K limits* (µM^{-1})[a]	N_{K1-K2} (µmol/g)	$\overline{K}_{K1-K2}$ (µM^{-1})	R^2	*RSS*
Ph	1.08 (10.6%)	0.776 (3.0%)	0.0048-0.0994	24.4	0.0179	0.9886	0.0134
2-MP	1.76 (4.2%)	0.661 (1.4%)	0.0056-0.119	26.5	0.0229	0.9973	0.0023
3-MP	1.45 (9.5%)	0.707 (3.0%)	0.0056-0.118	25.1	0.0220	0.9883	0.0117
2-CP	4.37 (7.9%)	0.685 (2.8%)	0.0072-0.164	60.1	0.0296	0.9902	0.0097
4-OP	5.78 (3.9%)	0.953 (2.0%)	0.0474-1.54	2.36	0.445	0.9962	0.0070
NIP							
Analyte	*a* (µmol g^{-1}) (µM^{-1})^{m} *(RSD%)*	*m (RSD%)*	*K limits* (µM^{-1})[a]	N_{K1-K2} (µmol g^{-1})	$\overline{K}_{K1-K2}$ (µM^{-1})	R^2	*RSS*
Ph	0.655 (11%)	0.795 (3.1%)	0.0048-0.0974	15.3	0.0174	0.9878	0.0149
2-MP	0.813 (5.3%)	0.730 (1.6%)	0.0055-0.114	15.0	0.0212	0.9966	0.0036
3-MP	0.861 (10%)	0.719 (3.1%)	0.0055-0.114	15.5	0.0213	0.9876	0.0126
2-CP	4.35 (7.9%)	0.656 (2.9%)	0.0071-0.156	55.4	0.0294	0.9894	0.0094
4-OP	4.28 (4.0%)	0.899 (2.0%)	0.0402-1.46	4.08	0.388	0.9962	0.0065

[a] Calculated from the minimum and maximum of the concentration of the free analyte in the rebinding solution ($K_{max} = 1/C_{min}$ and $K_{min} = 1/C_{max}$)

The data can be visualized in FI AD plots (Figure 3.6), where the number of binding sites (*N*) is plotted against the log binding affinities (*logK*), which are proportional to the binding energy, ΔG. *N* is calculated (Eq. 10) using the *FI* fitting parameters *a* and *m* obtained from fitting the data over the entire concentration range. The graphs show that the MIPs have more binding sites with slightly higher energy on average, particularly for Ph, 2-MP and 3-MP, and there are few of the highest energy sites. Although the trend is weaker for 2-CP, the MIPs still show slightly higher binding capacities than the NIPs, mainly manifested as more available sites. Although the adsorption data confirms that the MIPs outperform the NIPs, the plot in Figure 3.6E for 4-OP indicates that there are more binding sites of higher energy for the NIP which is inconsistent with the experimental data (Figure 3.5E). As will be seen later in this paper, other models can be used to more effectively explain the observed behavior.

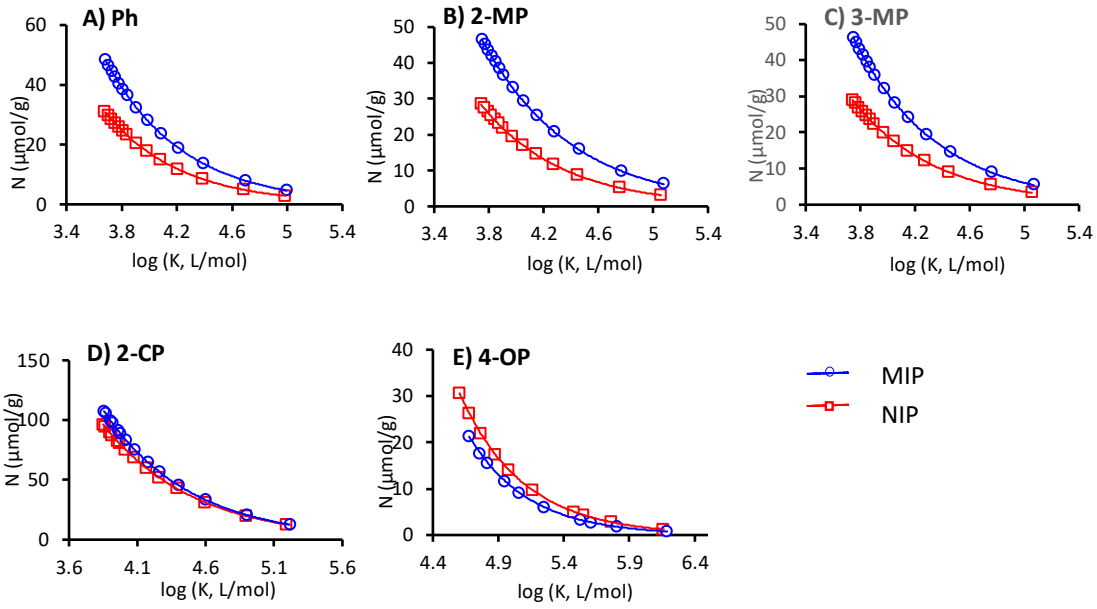

Figure 3.6**.** The AD with Freundlich fit for the MIP and NIP over the entire concentration range for the phenols that were loaded individually (A) Ph, B) 2-MP, C) 3-MP, D) 2-CP, E) 4-OP).

Overall the fit of the model to the data (Table 3.1) shows very good R^2, *RSS* values, and low relative errors in the FI coefficients for all five analytes. Closer inspection of Figure 3.5 shows that the FI model fails at high concentrations. Umpleby *et al.*[37] have attributed this to the low average binding affinity of the sites available at high analyte concentrations. There are a limited number of high energy binding sites and once these are occupied the analyte must adsorb to the remaining lower energy sites, which tend to be more abundant. Based on the poor fit at high concentrations, the binding parameters $N_{K1\text{-}K2}$ and $\bar{K}_{K1\text{-}K2}$ were recalculated with only the lower concentration data (Table 3.2 and Figure 3.7). Although

the fit between the model and the data is better (R^2 >0.99 for the MIPs and *RSS* <0.0012) and it is recommended that high concentration data be excluded from calculations, the broader conclusions have not changed.

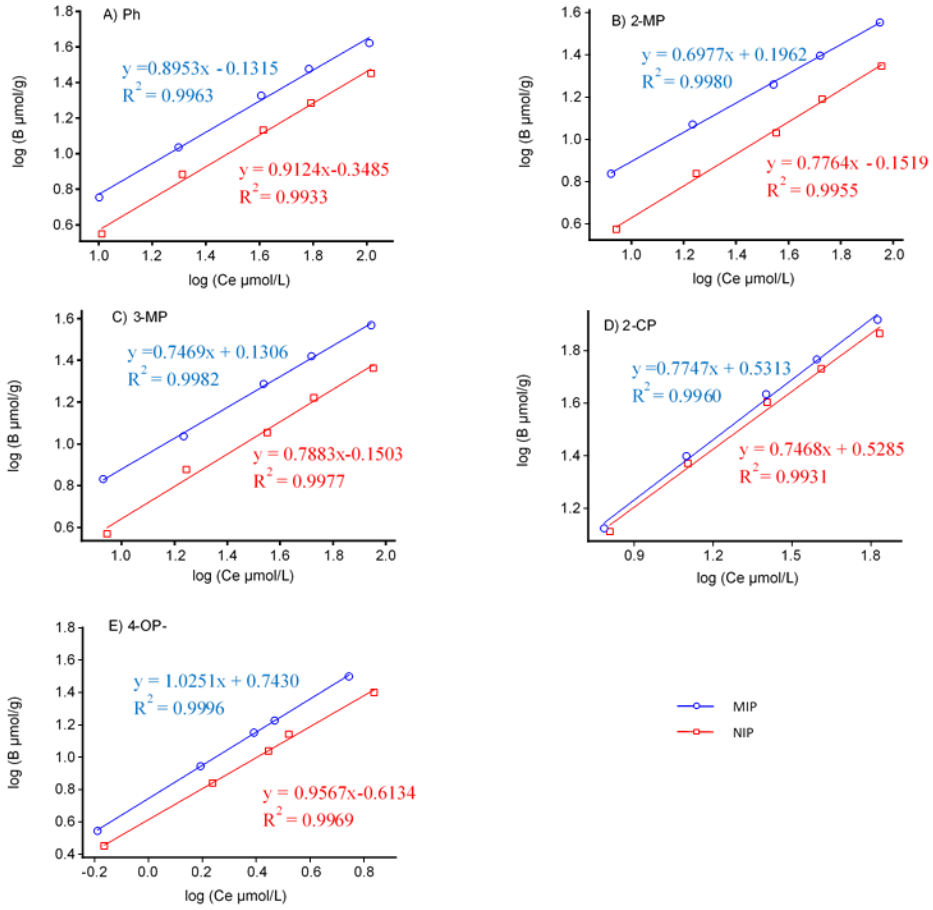

Figure 3.7**.** The experimental data for individual study at low concentration levels (blue circle points for MIP, red squares points for NIP) were fit to a FI isotherm (solid lines) for MIP and NIP (a. Ph, b. 2-MP, c. 3-MP, d. 2-CP, e. 4-OP).

Table 3.2. FI Fitting Parameters over low concentration levels

MIP								
Analyte	*a* (µmol g^{-1}) (μM^{-1})^m *(RSD%)*	*m (RSD%)*	*K limits* (μM^{-1})^a	N_{K1-K2} (µmol/g)	$\bar{K}_{K1-K2}$ (μM^{-1})	R^2	*RSS*	*IF*^{b}
Ph	0.739 (9.8%)	0.895 (3.1%)	0.0123-0.0994	6.37	0.0303	0.9963	0.0012	1.78
2-MP	1.57 (5.4%)	0.698 (2.2%)	0.014-0.119	12.2	0.0381	0.9980	0.0004	1.96
3-MP	1.35 (5.5%)	0.747 (2.1%)	0.014-0.118	11.4	0.0372	0.9982	0.0004	1.81
2-CP	3.40 (7.8%)	0.775 (3.2%)	0.018-0.164	24.7	0.0491	0.9960	0.0010	1.02
4-OP	5.53 (1.0%)	1.03 (1.0%)	0.180-1.54	-1.45	0.434	0.9996	0.0001	NA
NIP								
Analyte	*a* (µmol g^{-1}) (μM^{-1})^m *(RSD%)*	*m (RSD%)*	*K limits* (μM^{-1})^a	N_{K1-K2} (µmol/g)	$\bar{K}_{K1-K2}$ (μM^{-1})	R^2	*RSS*	
Ph	0.448 (14%)	0.912 (4.1%)	0.0121-0.0974	3.58	0.0297	0.9933	0.0022	
2-MP	0.705 (9.0%)	0.776 (3.3%)	0.014-0.114	6.24	0.0360	0.9955	0.0011	
3-MP	0.708 (15%)	0.788 (5.6%)	0.014-0.114	6.31	0.0358	0.9977	0.0031	
2-CP	3.38 (9.9%)	0.747 (4.2%)	0.018-0.156	24.1	0.0481	0.9931	0.0016	
4-OP	4.11 (3.1%)	0.957 (2.8%)	0.145-1.46	1.96	0.379	0.9969	0.0012	

[a] Calculated from the minimum and maximum of the concentration of the free analyte in the rebinding solution ($K_{max} = 1/C_{min}$ and $K_{min} = 1/C_{max}$)

[b] The imprinting factor is the ratio of the MIP N_{K1-K2} values to the NIP N_{K1-K2} values.

3.4.4 Langmuir-Freundlich and Langmuir Models

While closely related to LI, the obvious advantage of the L-FI is that it can be used without making assumptions about heterogeneity. The experimental and fitted LI and L-FI adsorption isotherms are presented in Figure 3.8 and Figure 3.9 with the calculated fitting parameters given in Table 3.3 and Table 3.4. Both models fit the experimental data well for Ph, 2-MP, 3-MP and 2-CP well, with very good R^2 and *RSS* values, and low relative errors for the fitting parameters. Furthermore, the applicability of the L-FI model for the concentration range studied was confirmed by a fit test, where the K_o from the fitting analysis is within the binding affinity limits K_{max} $(1/C_{min})$ and K_{min} $(1/C_{max})$ shown as ranges of values in Table 3.4.

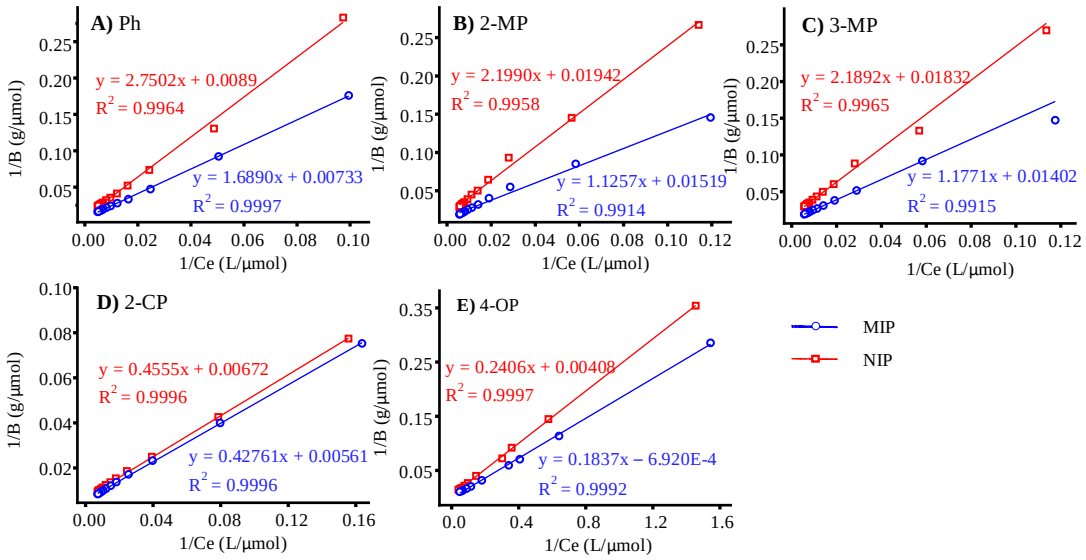

Figure 3.8. The experimental data for individual study (circle points for MIP, squares points for NIP) were fit to a LI (solid lines) for MIP and NIP (A) Ph, B) 2-MP, C) 3-MP, D) 2-CP, E) 4-OP).

Table 3.3. LI Fitting Parameters

MIP				
Analyte	*N* (µmol/g) *(RSD%)*	*K* (μM^{-1}) *(RSD%)*	R^2	*RSS*
Ph	136. (3.9%)	0.0043 (4.7%)	0.9997	9.00E-06
2-MP	65.8 (7.2%)	0.0135 (7.4%)	0.9914	0.0001
3-MP	71.3 (8.0%)	0.0119 (8.4%)	0.9915	1.37E-04
2-CP	178. (2.1%)	0.0131 (2.3%)	0.9996	1.50E-06
4-OP	1445 (142%)	0.0038 (142%)	0.9992	4.70E-05
NIP				
Analyte	*N* (µmol/g) *(RSD%)*	*K* (μM^{-1}) *(RSD%)*	R^2	*RSS*
Ph	112 (16%)	0.0032 (16%)	0.9964	0.0002
2-MP	51.5 (7.4%)	0.0088 (8.0%)	0.9958	0.0002
3-MP	54.6 (7.0%)	0.0084 (7.1%)	0.9965	1.81E-04
2-CP	149 (1.9%)	0.0148 (2.0%)	0.9996	1.90E-06
4-OP	245 (18%)	0.0170 (18%)	0.9997	2.60E-05

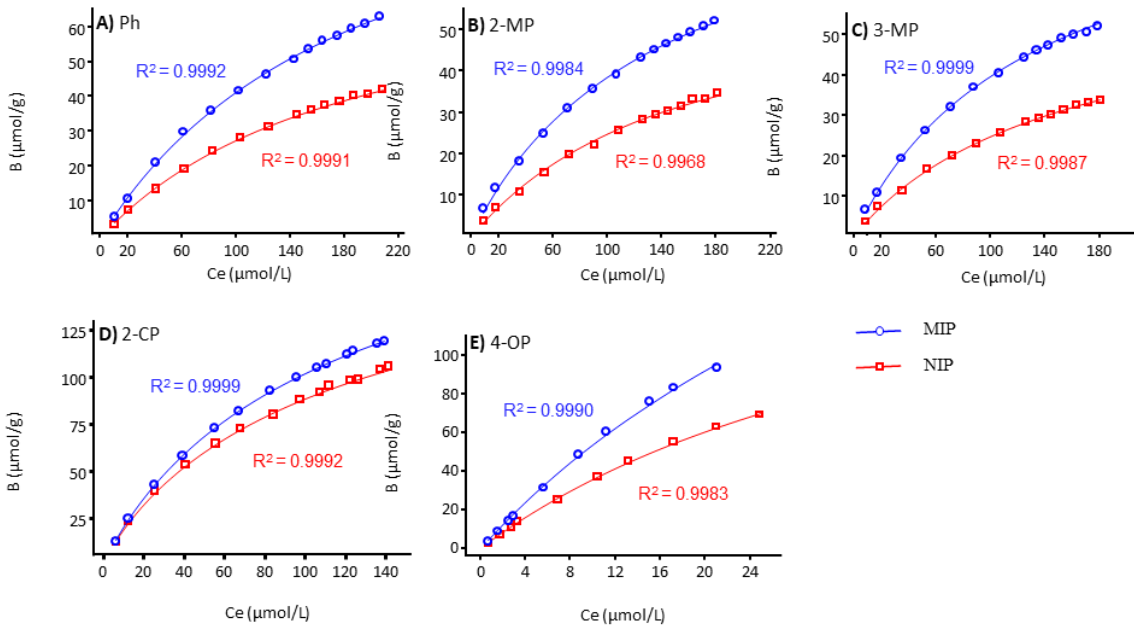

Figure 3.9. The experimental data for individual study (circle points for MIP, squares points for NIP) were fit to a L-FI isotherm (solid lines) for MIP and NIP (A) Ph, B) 2-MP, C) 3-MP, D) 2-CP, E) 4-OP).

Table 3.4. L-FI Fitting Parameters.

MIP							
Analyte	N_t (µmol/g) *(RSD%)*	*a* (µmol g^{-1}) $(\mu M^{-1})^m$ *(RSD%)*	m *(RSD%)*	K_o (μM^{-1})	*K limits* (μM^{-1})	R^2	*RSS*
Ph	124 (7.2%)	0.0053 (7.5%)	0.988 (3.7%)	0.0050	*0.0048-0.099*	0.9992	3.0235
2-MP	98.9 (9.4%)	0.0084 (8.4%)	0.941 (5.2%)	0.0061	0.0056-0.119	0.9984	4.0046
3-MP	93.0 (2.0%)	0.0084 (2.4%)	0.974 (1.3%)	0.0073	0.0056-0.118	0.9999	0.2588
2-CP	225 (2.6%)	0.0120 (1.7%)	0.921 (1.5%)	0.0082	0.0072-0.164	0.9999	1.8002
4-OP	313 (30%)	0.0209 (23%)	1 (6.6%)	0.0209	0.0124-0.282	0.9990	13.2008
NIP							
Analyte	N_t (µmol/g) *(RSD%)*	*a* (µmol g^{-1} $(\mu M^{-1})^m$ *(RSD%)*	m *(RSD%)*	K_o (μM^{-1})	*K limits* (μM^{-1})	R^2	*RSS*
Ph	80.1 (7.7%)	0.0053 (9.4%)	0.997 (4.3%)	*0.0052*	*0.0048-0.0974*	0.9991	1.8051
2-MP	64.9 (14%)	0.0061 (15%)	1 (7.6%)	0.0061	*0.0055-0.114*	0.9968	3.7892
3-MP	65.2 (8.7%)	0.0075 (8.0%)	0.957 (4.7%)	0.0059	0.0055-0.114	0.9987	1.421
2-CP	204 (7.1%)	0.0139 (5.1%)	0.875 (3.8%)	0.0074	0.0071-0.156	0.9992	8.6523
4-OP	197 (18%)	0.0223 (13%)	1 (4.9%)	0.0223	0.00033-0.167	0.9983	4.096

[a] Calculated from ($K_o = a^{1/m}$)

[b] Calculated from the minimum and maximum of the concentration of the free analyte in the rebinding solution ($K_{max} = 1/C_{min}$ and $K_{min} = 1/C_{max}$)

Compared to the data from the FI model, the L-FI heterogeneity indices are closer to unity (more homogeneous) for both the MIPs and NIPs, though a comparison of MIP and NIP heterogeneity is inconclusive. The obtained N_t, m and K_o coefficients for 2-MP and 3-MP are almost the same, which indicates consistency in the recognition mechanism. Although Ph has lower K than 2-MP and 3-MP, its N value is higher. This tells us that more binding sites are accessible for Ph, likely due to its small size and ability to diffuse into sites not available to other larger molecules. The results also illustrate the imprinting effects, with the MIPs giving superior adsorption capacity to the NIPs for Ph, 2-MP, and 3-MP. Although 2-CP has a higher molar mass than the cresols or phenol, it has a similar molar volume to the cresols, and is both more acidic and more hydrophobic (Table 3.5). Consequently, the 2-CP is small enough to diffuse into the same sites as the cresols, and as well has stronger interactions with the polymer surface leading to greater numbers of non-specific interactions and higher N values for both MIPs and NIPs. We also note that the degree of imprinting is lowest for 2-CP because of the predominance of non-specific interactions. These results are consistent with the FI modeling, from which we credited some of the higher MIP adsorption capacity to differences in the MIP and NIP surface areas.

Table 3.5**.** Physical properties of the phenols under study[52]

	Molecular weight (g/mol)	Solubility in water (g/L)	Density (g/ml)	pKa	LogP	Molar volume (mL/mol)*
Ph	94.11	84	1.07	9.99	1.46	88.9
2-MP	108.14	25.9	1.05	10.3	1.95	103
3-MP	108.14	24.0	1.03	10.1	1.96	105
2-CP	128.55	28.5	1.26	8.5	2.15	102
4-OP	206.32	0.007	0.961	10.3	5.25	214
Catechol	110.1	461	1.34	9.45	0.88	82.1

*The molar volume obtained from the relative ratio between the molecular weight and density

The average binding site energies for the MIPs and NIPs (K_o) are nearly the same, however, the numbers of binding sites are much higher for the MIPs. Ignoring the small degree of heterogeneity displayed in the L-FI data, the LI model was applied resulting in good fitting statistics with similar trends in the number of binding sites, but with consistently higher binding site energies for MIPs. This supports the conclusion that the number of binding sites and the average binding site energies are higher for MIPs. As shown in Figure 3.8, the LI gave acceptable results with respect to the fit to the experimental data for both MIPs and NIPs in all cases except for the 4-OP. Close inspection of Figure 3.8 (a, b and c) shows that the LI model does not fit the low concentration data especially for NIPs. We returned to the raw experimental data to address this discrepancy and found that the NIPs give less reproducible results overall (Table 3.6 and Table 3.7). We attribute this to the positive effect of the template on the consistency of the phase separation process, giving a more homogenous sorbent in the case of MIPs. A further explanation for the increased error with the NIPs is that in the absence of the high affinity binding sites associated with the MIPs, the adsorption of the analytes at low concentrations

is weaker and loadings are much lower giving lower concentrations in the extracts analyzed by LC-UV-vis. Although the fits are good, the models also fail with 4-OP, manifested in high relative errors in the binding site density (*N*). This arises from the way *N* is calculated for the LI model using the inverse of the intercept (Figure 3.8e). When the adsorption capacity is very high at high concentrations, as measured for 4-OP, the intercept approaches zero and even relatively a small relative error translates into high value for the error in *N*. Although not as dramatic, the error in N_t from the L-FI model is also unacceptably high. The high adsorption capacities at high concentrations may be a consequence of the formation of multilayers, which is predictable for 4-OP given its amphiphilic nature (polar head and large non-polar functional group). Further elaboration on this behavior will be provided in the next section in which the BET model is applied.

Although the results show that the simpler LI model can be applied fairly effectively when *m* in L-FI is close to 1, L-FI is still useful because it can model subtle differences resulting in a better fit with experimental data. In addition, the three parameters (N_t, *a* and *m)*, rather than 2, give us more tools to understand differences in adsorption behavior.

Table 3.6**.** The relative standard errors (%RSD) for the experimental data

Conc.(µg L^{-1})	Phenol		2-MP		3-MP		2-CP	
	NIP	MIP	NIP	MIP	NIP	MIP	NIP	MIP
1000	19.9	8.7	10.9	3.6	19.8	3.5	1.5	2.0
2000	14.9	5.2	8.9	6.3	20.0	11.0	18.0	2.9
4000	9.2	4.0	15.9	4.2	25.2	13.3	9.3	16.2
6000	13.9	10.7	10.0	15.0	21.7	7.8	16.2	17.6
8000	9.2	1.0	15.0	10.2	21.1	9.0	19.4	14.0
10000	14.7	7.0	20.1	5.1	8.8	0.4	20.1	4.8
12000	11.7	7.0	2.2	2.9	17.0	2.5	7.9	3.9
14000	7.5	0.1	16.9	18.9	1.4	9.0	17.0	12.0
15000	10.8	9.2	5.7	12.0	17.1	7.5	19.1	4.6
16000	5.2	0.8	0.8	14.1	1.2	7.1	12.0	14.6
17000	13.2	6.8	7.5	8.6	2.9	6.0	18.0	9.8
18000	8.2	6.0	16.7	8.6	7.0	6.3	14.4	10.8
19000	11.0	8.9	10.1	9.8	13.7	11.0	18.0	8.3
20000	16.1	11.1	9.7	6.9	14.5	9.8	11.9	9.3

Table 3.7**.** The relative standard errors (%RSD) for 4-OP the experimental data

Conc.(µg L-1)	NIP	MIP
200	3.6	2.7
500	6.0	9.0
800	7.4	5.0
1000	7.7	1.6
2000	3.5	2.0
3000	6.1	4.5
4000	1.8	1.8
5000	8.0	5.5
6000	4.4	3.0
7000	2.1	3.9

3.4.5 BET Isotherm Model

Finally, BET adsorption isotherms are applied to attempt to ascertain the contribution of multilayer formation to the adsorption mechanism. The experimental and fitted data for MIPs and NIPs with each phenolic compound are presented in Figure 3.10 and Table 3.8.

The results suggest that the BET model is effective in describing the recognition of all the phenols with visibly good fitting and favourable R^2 and *RSS* values. However, the weakness of the model for the small phenols can be detected in the relative errors in the fitting parameters, particularly for Ph with the MIPs (~18-47% *RSD*). While the parameters can be combined to fit the adsorption data very well, the uncertainty in each parameter indicates that the model is not effective for describing the chemical behavior. We conclude the model underestimates the phenol adsorption to the surface and overestimates the formation of multi-layers. Thus, in this instance, it is unlikely that phenol will form extensive multi-layers.

The relative errors for 4-OP range from 5-13%; this combined with the goodness of fit supports the conclusion that the BET model is the best for providing an insight into the adsorption of 4-OP by the MIP. The moderate number of surface binding sites (q_m), the high K_S and the tendency to form multi-layers (n = 3.75) are consistent with the data and reflect what we expect from the chemistry of 4-OP, including its hydrophobicity. The q_m value is not the highest of those calculated, which suggests that 4-OP is recognized by fewer number of sites, likely because 4-OP is bulkier it can access fewer sites on the polymer surface. On the other hand, the K_S and K_L values trend with *logP*. An important observation for the model is the large K_L (with relatively small error) for 4-OP, which highlights the importance of the layers formed beyond the first layer adsorbed to the surface. The adsorption of the 4-OP is not only associated with π-π interactions and hydrogen bonding of the phenol moiety with the polymer surface but also by London

dispersion forces and entropic effects, typical of interactions with larger alkyl groups like that in 4-OP.

While the relative errors are significant, the q_m and K_S values for the MIPs are higher than for the NIPs for all the phenols, which is as expected based on the adsorption data.

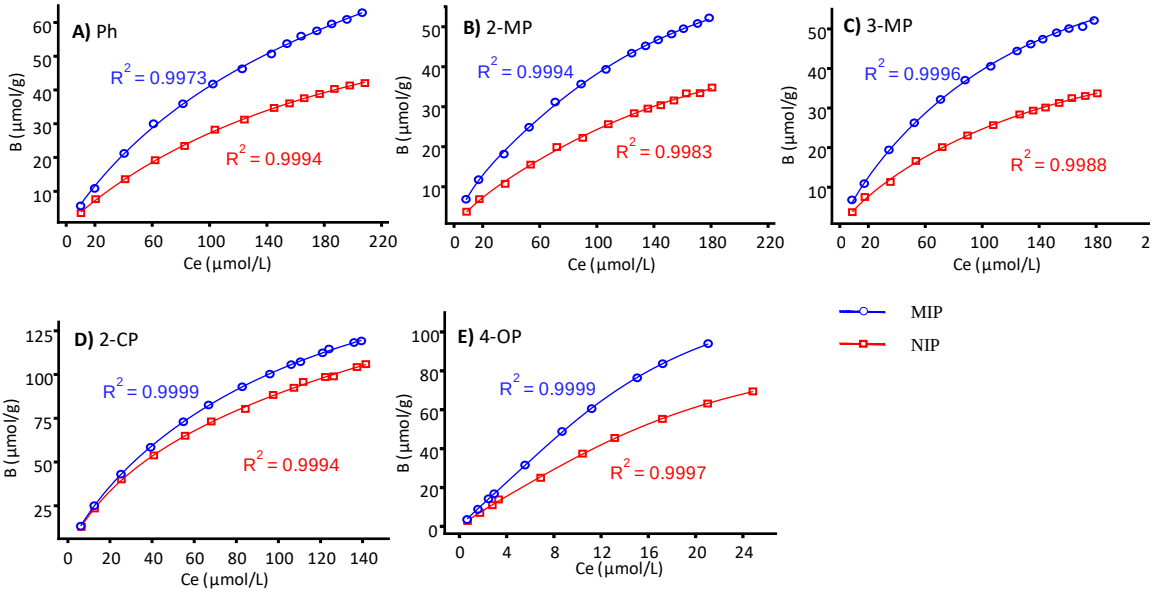

Figure 3.10**.** The experimental data for individual study (circle points for MIP, squares points for NIP) were fit to a BET isotherm (solid lines) for MIP and NIP (A) Ph, B) 2-MP, C) 3-MP, D) 2-CP, E) 4-OP).

Table 3.8. BET Fitting Parameters.

MIP						
Analyte	q_m (µmol/g) *(RSD%)*	K_S (µM^{-1}) *(RSD%)*	K_L (µM^{-1}) *(RSD%)*	*n* *(RSD%)*	R^2	*RSS*
Ph	24.4 (28%)	0.0326 (47%)	0.0065 (23%)	3.65 (18%)	0.9973	2.4379
2-MP	19.9 (9.4%)	0.0517 (16%)	0.0076 9.2%)	3.68 (5.5%)	0.9994	1.3021
3-MP	22.3 (12%)	0.0394 (19%)	0.0082 (11%)	3.21 (8.5%)	0.9996	1.0041
2-CP	66.6 (11%)	0.0374 (14%)	0.0074 (15%)	2.79 (6.5%)	0.9999	1.5277
4-OP	36.5 (10%)	0.166 (13%)	0.0639 5.2%)	3.75 (6.9%)	0.9999	0.5423
NIP						
Analyte	q_m (µmol/g) *(RSD%)*	K_S (µM^{-1}) *(RSD%)*	K_L (µM^{-1}) *(RSD%)*	*n* *(RSD%)*	R^2	*RSS*
Ph	16.4 (15%)	0.0303 (24%)	0.0065 (11%)	3.65 (9.5%)	0.9994	0.7184
2-MP	14.9 (25%)	0.0324 (37%)	0.0064 (24%)	3.55 (14%)	0.9983	1.8381
3-MP	15.8 (25%)	0.0325 (35%)	0.0066 (26%)	3.19 (15%)	0.9988	1.2418
2-CP	85.2 (31%)	0.0273 (36%)	0.0031 (84%)	2.68 (9.2%)	0.9994	5.8155
4-OP	27.7 (19%)	0.161 (25%)	0.0515 (12%)	3.72 (12%)	0.9997	1.1670

3.4.6 Concluding Statements on the Models

Each model has its strengths depending on the chemistry of the adsorbates and the binding site heterogeneity. However, regardless of how the models describe the binding mechanism, the total bound adsorbate is determined experimentally and thus the models must converge in the estimation of the number of binding sites available to the adsorbate. Consequently, the maximum adsorption capacity (N) in the LI model, the total binding sites (N_t) in the L-FI model and monolayer capacity q_m in the BET model (if only a single layer is formed) should be comparable. Since the BET model shows the formation of multi-layers, then we use the product of q_m and n (the finite number of layers formed) to calculate the number of binding sites available. Looking at the data (Table 3.8), one can see that the three models give similar results (%*RSD* of the mean of model binding sites 13-22%), except for 4-OP. The lack of agreement between the results for 4-OP is related to an over-estimation of the number of binding sites by the LI and L-FI models. These show much higher numbers of binding sites available for the 4-OP than the smaller phenols, which should not be the case for the bulkier molecule if adsorption was solely dependent on interactions with the surface of the MIP. This supports the idea that 4-OP forms multilayers.

Finally, we compared the magnitude of the affinity constants. To compare the affinity constants for the LI and L-FI models (both assume a single layer of adsorbate) with the data from the BET model with n layers, we combine the K_S (equilibrium constant for the first layer adsorption, n=1) and K_L (equilibrium constant for upper layers, n-1) according to Eq. 14. Although it is common to combine individual equilibrium constants for a multi-

step process by simply taking the product of the constants, this would yield an expression that is n^{th} in the order adsorbate concentration and, consequently, gives an affinity constant that is too low. By taking the n-root of the product we arrive at composite affinity *(K_{ca})*, which can be compared directly with the affinity constants from the other models.

$$K_{ca} = (K_S K_L^{n-1})^{1/(n)} \quad (14)$$

Both BET and LI assume homogeneous binding site energies and we find that *K* values for these models are in excellent agreement for 2-MP, 3-MP and 2-CP (the discrepancy is less than 11%). In the cases of Ph and 4-OP, we see divergence, which is consistent with our earlier discussion; the LI model is poor at describing the behaviour of 4-OP, and the BET model fails for Ph. Looking at the range of *K* values from L-FI *(K* limits), we find good agreement with the data from the BET model for all adsorbates, whereas LI data underestimates *K* relative to the L-FI affinity data for Ph and 4-OP.

Table 3.9**.** Comparison between the binding sites and affinity constants in LI, L-FI and BET models

		Ph	2-MP	3-MP	2-CP	4-OP
LI	*N (µmol/g)*	136	65.8	71.3	178	1445
	K (μM^{-1})	0.0043	0.0135	0.0119	0.0131	0.0038
L-FI	N_t *(µmol/g)*	124	98.9	93.0	225	313
	K limits (μM^{-1})	0.0048-0.099	0.0056-0.119	0.0056-0.118	0.0072-0.164	0.0124-0.282
BET	q_m *n (µmol/g)*[1]	89.3	73.3	71.6	186	137
	K_{ca} (Composite affinity) [2]	0.0101	0.0128	0.0134	0.0132	0.0824
Statistics	Average of modeled binding sites (µmol/g)	117	79.3	78.6	196	632
	RSD% for binding sites	21	22	16	13	112
	Discrepancy% (between the LI and BET affinities	57	5.5	11	1.0	95

[1]Total relative amount of adsorbate bound to MIP
[2] Composite affinities estimated using Eq.14

3.5 Conclusions

In this paper, four isotherm models proved valuable in characterizing binding behavior in MIPs. Of the four models, the L-FI is the most useful, since it is a can be used for any system, whether demonstrating homogeneous (LI) or heterogeneous (FI) binding site energy distributions. The heterogeneity is a relative phenomenon for a given material and can differ with the chemistry of the adsorbate. These MIPs tended to be nearly

homogeneous, indicating that the MIPs feature defined binding sites arising from the imprinting process. Nevertheless, this does not mean that this MIP has one only type of binding site, but that similar binding sites in terms of shape and active functionality are engaged when interacting with a given adsorbate. In general, the LI, L-FI and BET isotherms showed better fit to the data compared to FI over the entire concentration range, as they can model both the linear subsaturation and the curved saturation regions of the isotherms. And yet, the BET isotherm was the only model effective in describing the interaction of 4-OP with the MIP because it allowed for the formation of multilayers.

Finally, the use of the adsorption models can provide invaluable tools to describe molecular recognition by MIPs, which is important in developing and validating new MIPs. Such models may also be critical in better understanding MIP behavior in complex systems, where more than one adsorbate may be interacting with the surface simultaneously.

3.6 References

(1) Azizi, A.; Shahhoseini, F.; Bottaro, C. S. Magnetic Molecularly Imprinted Polymers Prepared by Reversible Addition Fragmentation Chain Transfer Polymerization for Dispersive Solid Phase Extraction of Polycyclic Aromatic Hydrocarbons in Water. *J. Chromatogr. A* **2019**, *1610*, 460534. https://doi.org/10.1016/j.chroma.2019.460534.

(2) Van Biesen, G.; Wiseman, J. M.; Li, J.; Bottaro, C. S. Desorption Electrospray Ionization-Mass Spectrometry for the Detection of Analytes Extracted by Thin-Film Molecularly Imprinted Polymers. *Analyst* **2010**, *135* (9), 2237–2240. https://doi.org/10.1039/c0an00331j.

(3) Gryshchenko, A. O.; Bottaro, C. S. Development of Molecularly Imprinted Polymer in Porous Film Format for Binding of Phenol and Alkylphenols from Water. *Int. J. Mol. Sci.* **2014**, *15* (1), 1338–1357. https://doi.org/10.3390/ijms15011338.

(4) Egli, S. N.; Butler, E. D.; Bottaro, C. S. Selective Extraction of Light Polycyclic Aromatic Hydrocarbons in Environmental Water Samples with Pseudo-Template Thin-Film Molecularly Imprinted Polymers. *Anal. Methods* **2015**, *7*, 2028–2035. https://doi.org/10.1039/C4AY02849J.

(5) Hijazi, H. Y.; Bottaro, C. S. Selective Determination of Semi-Volatile Thiophene Compounds in Water by Molecularly Imprinted Polymer Thin Films with Direct Headspace Gas Chromatography Sulfur Chemiluminescence Detection. *Analyst* **2018**, *143*, 1117–1123. https://doi.org/10.1039/C7AN01686G.

(6) Shahhoseini, F.; Azizi, A.; Egli, S. N.; Bottaro, C. S. Single-Use Porous Thin Film Extraction with Gas Chromatography Atmospheric Pressure Chemical Ionization Tandem Mass Spectrometry for High-Throughput Analysis of 16 PAHs. *Talanta* **2020**, *207* (15 January), 120320. https://doi.org/10.1016/j.talanta.2019.120320.

(7) Hijazi, H. Y.; Bottaro, C. S. Analysis of Thiophenes in Seawater: Molecularly Imprinted Polymer Thin-Film Extraction with Desorption Electrospray Ionization Mass Spectrometry. *Int. J. Mass Spectrom.* **2019**, *443*, 9–15. https://doi.org/10.1016/j.ijms.2019.05.003.

(8) Azizi, A.; Shahhoseini, F.; Modir-Rousta, A.; Bottaro, C. S. High Throughput Direct Analysis of Water Using Solvothermal Headspace Desorption with Porous Thin Films. *Anal. Chim. Acta* **2019**, *1087*, 51–61. https://doi.org/10.1016/j.aca.2019.08.022.

(9) Azizi, A.; Bottaro, C. S. A Critical Review of Molecularly Imprinted Polymers for the Analysis of Organic Pollutants in Environmental Water Samples. *J. Chromatogr. A* **2019**, 460603. https://doi.org/10.1016/j.chroma.2019.460603.

(10) Malik, M. I.; Shaikh, H.; Mustafa, G.; Bhanger, M. I. Recent Applications of Molecularly Imprinted Polymers in Analytical Chemistry. *Sep. Purif. Rev.* **2018**, 1–41. https://doi.org/10.1080/15422119.2018.1457541.

(11) Speltini, A.; Scalabrini, A.; Maraschi, F.; Sturini, M.; Profumo, A. Newest Applications of Molecularly Imprinted Polymers for Extraction of Contaminants from Environmental and Food Matrices: A Review. *Anal. Chim. Acta* **2017**, *974*, 1–26. https://doi.org/10.1016/j.aca.2017.04.042.

(12) Manera, C.; Tonello, A. P.; Perondi, D.; Godinho, M. Adsorption of Leather Dyes on Activated Carbon from Leather Shaving Wastes: Kinetics, Equilibrium and Thermodynamics Studies. *Environ. Technol.* **2019**, *40* (21), 2756–2768. https://doi.org/10.1080/09593330.2018.1452984.

(13) Zhang, W.; Li, Q.; Cong, J.; Wei, B.; Wang, S. Mechanism Analysis of Selective Adsorption and Specific Recognition by Molecularly Imprinted Polymers of Ginsenoside Re. *Polymers (Basel).* **2018**, *10* (2), 216. https://doi.org/10.3390/polym10020216.

(14) Wang, L. C.; Ni, X. jiong; Cao, Y. H.; Cao, G. qun. Adsorption Behavior of Bisphenol A on CTAB-Modified Graphite. *Appl. Surf. Sci.* **2018**, *428*, 165–170. https://doi.org/10.1016/j.apsusc.2017.07.093.

(15) Zheng, P.; Zhang, B.; Luo, Z.; Du, W.; Guo, P.; Zhou, Y.; Chang, R.; Chang, C.; Fu, Q. Facile Preparation of Polydopamine-Coated Imprinted Polymers on the Surface of SiO2 for Estrone Capture in Milk Samples. *J. Sep. Sci.* **2018**, *41* (12), 2585–2594. https://doi.org/10.1002/jssc.201600611.

(16) Zhou, X.; Lai, C.; Huang, D.; Zeng, G.; Chen, L.; Qin, L.; Xu, P.; Cheng, M.; Huang, C.; Zhang, C.; Preparation of Water-Compatible Molecularly Imprinted Thiol-Functionalized Activated Titanium Dioxide: Selective Adsorption and Efficient Photodegradation of 2, 4-Dinitrophenol in Aqueous Solution. *J. Hazard. Mater.* **2018**, *346*, 113–123. https://doi.org/10.1016/j.jhazmat.2017.12.032.

(17) Rahmanian, O.; Dinari, M.; Abdolmaleki, M. K. Carbon Quantum Dots/Layered Double Hydroxide Hybrid for Fast and Efficient Decontamination of Cd(II): The

Adsorption Kinetics and Isotherms. *Appl. Surf. Sci.* **2018**, *428*, 272–279. https://doi.org/10.1016/j.apsusc.2017.09.152.

(18) Ostovan, A.; Ghaedi, M.; Arabi, M. Fabrication of Water-Compatible Superparamagnetic Molecularly Imprinted Biopolymer for Clean Separation of Baclofen from Bio-Fluid Samples: A Mild and Green Approach. *Talanta* **2018**, *179*, 760–768. https://doi.org/10.1016/j.talanta.2017.12.017.

(19) Zhi, K.; Wang, L.; Zhang, Y.; Zhang, X.; Zhang, L.; Liu, L.; Yao, J.; Xiang, W. Preparation and Evaluation of Molecularly Imprinted Polymer for Selective Recognition and Adsorption of Gossypol. *J. Mol. Recognit.* **2017**, *31* (3), 1–9. https://doi.org/10.1002/jmr.2627.

(20) Murray, A.; Örmeci, B. Competitive Effects of Humic Acid and Wastewater on Adsorption of Methylene Blue Dye by Activated Carbon and Non-Imprinted Polymers. *J. Environ. Sci. (China)* **2018**, *66*, 310–317. https://doi.org/10.1016/j.jes.2017.04.029.

(21) Ostovan, A.; Ghaedi, M.; Arabi, M.; Yang, Q.; Li, J.; Chen, L. Hydrophilic Multitemplate Molecularly Imprinted Biopolymers Based on a Green Synthesis Strategy for Determination of B-Family Vitamins. *ACS Appl. Mater. Interfaces* **2018**, *10* (4), 4140–4150. https://doi.org/10.1021/acsami.7b17500.

(22) Shi, S.; Fan, D.; Xiang, H.; Li, H. Effective Synthesis of Magnetic Porous Molecularly Imprinted Polymers for Efficient and Selective Extraction of Cinnamic Acid from Apple Juices. *Food Chem.* **2017**, *237*, 198–204. https://doi.org/10.1016/j.foodchem.2017.05.086.

(23) Feng, Y.; Liu, Q.; Ye, L.; Wu, Q.; He, J. Ordered Macroporous Quercetin Molecularly Imprinted Polymers: Preparation, Characterization, and Separation Performance. *J. Sep. Sci.* **2017**, *40* (4), 971–978. https://doi.org/10.1002/jssc.201601011.

(24) Dorkó, Z.; Tamás, B.; Horvai, G. Isotherm Charts for Material Selection and Method Development with Molecularly Imprinted Polymers and Other Sorbents. *Talanta* **2017**, *162* (October 2016), 167–173. https://doi.org/10.1016/j.talanta.2016.10.027.

(25) Machyňáková, A.; Hroboňová, K. Synthesis and Evaluation of Molecularly Imprinted Polymers as Sorbents for Selective Extraction of Coumarins. *Chromatographia* **2017**, *80* (7), 1015–1024. https://doi.org/10.1007/s10337-017-3325-z.

(26) Wang, R. Z.; Huang, D. L.; Liu, Y. G.; Peng, Z. W.; Zeng, G. M.; Lai, C.; Xu, P.; Huang, C.; Zhang, C.; Gong, X. M. Selective Removal of BPA from Aqueous Solution Using Molecularly Imprinted Polymers Based on Magnetic Graphene Oxide. *RSC Adv.* **2016**, *6* (108), 106201–106210. https://doi.org/10.1039/c6ra21148h.

(27) Bayramoglu, G.; Arica, M. Y.; Liman, G.; Celikbicak, O.; Salih, B. Removal of Bisphenol A from Aqueous Medium Using Molecularly Surface Imprinted Microbeads. *Chemosphere* **2016**, *150*, 275–284. https://doi.org/10.1016/j.chemosphere.2016.02.040.

(28) Song, D.; Zhang, Y.; Geer, M. F.; Shimizu, K. D. Characterization of Molecularly

Imprinted Polymers Using a New Polar Solvent Titration Method. *J. Mol. Recognit.* **2014**, *27* (7), 448–457. https://doi.org/10.1002/jmr.2365.

(29) Jeppu, G. P.; Clement, T. P. A Modified Langmuir-Freundlich Isotherm Model for Simulating PH-Dependent Adsorption Effects. *J. Contam. Hydrol.* **2012**, *129–130*, 46–53. https://doi.org/10.1016/j.jconhyd.2011.12.001.

(30) Langmuir, I. The Constitution and Fundamental Properties of Solids and Liquids. *J. Am. Chem. Soc.* **1916**, *38* (3), 2221–2295. https://doi.org/10.1007/s00145-005-0319-z.

(31) Freundlich HMF. Over the Adsorption in Solution. *J. Phys. Chem.* **1906**, *57*, 385–471.

(32) Sips, R. On the Structure of a Catalyst Surface. *J. Chem. Phys.* **1948**, *16* (5), 490–495. https://doi.org/10.1063/1.1746922.

(33) Brunauer, S.; Emmett, P. H.; Teller, E. Adsorption of Gases in Multimolecular Layers. *J. Am. Chem. Soc.* **1938**, *60* (2), 309–319. https://doi.org/10.1021/ja01269a023.

(34) Umpleby, R. J.; Baxter, S. C.; Bode, M.; Berch, J. K.; Shah, R. N.; Shimizu, K. D. Application of the Freundlich Adsorption Isotherm in the Characterization of Molecularly Imprinted Polymers. *Anal. Chim. Acta* **2001**, *435* (1), 35–42. https://doi.org/10.1016/S0003-2670(00)01211-3.

(35) Umpleby, R. J.; Baxter, S. C.; Chen, Y.; Shah, R. N.; Shimizu, K. D. Characterization of Molecularly Imprinted Polymers with the Langmuir - Freundlich Isotherm. *Anal. Chem.* **2001**, *73* (19), 4584–4591.

https://doi.org/10.1021/ac0105686.

(36) Umpleby, R. J.; Bode, M.; Shimizu, K. D. Measurement of the Continuous Distribution of Binding Sites in Molecularly Imprinted Polymers. *Analyst* **2000**, *125* (7), 1261–1265. https://doi.org/10.1039/b002354j.

(37) Umpleby, R. J.; Baxter, S. C.; Rampey, A. M.; Rushton, G. T.; Chen, Y.; Shimizu, K. D. Characterization of the Heterogeneous Binding Site Affinity Distributions in Molecularly Imprinted Polymers. *J. Chromatogr. B Anal. Technol. Biomed. Life Sci.* **2004**, *804* (1), 141–149. https://doi.org/10.1016/j.jchromb.2004.01.064.

(38) Tamayo, F. G.; Casillas, J. L.; Martin-Esteban, A. Evaluation of New Selective Molecularly Imprinted Polymers Prepared by Precipitation Polymerisation for the Extraction of Phenylurea Herbicides. *J. Chromatogr. A* **2005**, *1069* (2), 173–181. https://doi.org/10.1016/j.chroma.2005.02.029.

(39) Turiel, E.; Perez-Conde, C.; Martin-Esteban, A. Assessment of the Cross-Reactivity and Binding Sites Characterisation of a Propazine-Imprinted Polymer Using the Langmuir-Freundlich Isotherm. *Analyst* **2003**, *128* (2), 137–141. https://doi.org/10.1039/b210712k.

(40) García-Calzón, J. A.; Díaz-García, M. E. Characterization of Binding Sites in Molecularly Imprinted Polymers. *Sensors Actuators, B Chem.* **2007**, *123* (2), 1180–1194. https://doi.org/10.1016/j.snb.2006.10.068.

(41) Lanza, F.; Ruther, M.; Hall, A. J.; Dauwe, C.; Sellergren, B. Studies on the Process of Formation, Nature and Stability of Binding Sites in Molecularly Imprinted Polymers. *Mater. Res. Soc. Symp. Proc.* **2002**, *723*, 93–103.

(42) Latour, R. A. The Langmuir Isotherm: A Commonly Applied but Misleading Approach for the Analysis of Protein Adsorption Behavior. *J. Biomed. Mater. Res. - Part A* **2015**, *103* (3), 949–958. https://doi.org/10.1002/jbm.a.35235.

(43) Tsai, H. A.; Syu, M. J. Synthesis and Characterization of Creatinine Imprinted Poly(4- Vinylpyridine-Co-Divinylbenzene) as a Specific Recognition Receptor. *Anal. Chim. Acta* **2005**, *539* (1–2), 107–116. https://doi.org/10.1016/j.aca.2005.03.016.

(44) Baggiani, C.; Giraudi, G.; Giovannoli, C.; Tozzi, C.; Anfossi, L. Adsorption Isotherms of a Molecular Imprinted Polymer Prepared in the Presence of a Polymerisable Template: Indirect Evidence of the Formation of Template Clusters in the Binding Site. *Anal. Chim. Acta* **2004**, *504* (1), 43–52. https://doi.org/10.1016/S0003-2670(03)00671-8.

(45) Cunliffe, D.; Kirby, A.; Alexander, C. Molecularly Imprinted Drug Delivery Systems. *Adv. Drug Deliv. Rev.* **2005**, *57* (12), 1836–1853. https://doi.org/10.1016/j.addr.2005.07.015.

(46) Kim, H.; Kaczmarski, K.; Guiochon, G. Intraparticle Mass Transfer Kinetics on Molecularly Imprinted Polymers of Structural Analogues of a Template. *Chem. Eng. Sci.* **2006**, *61* (4), 1122–1137. https://doi.org/10.1016/j.ces.2005.08.012.

(47) Chen, Y.; Kele, M.; Sajonz, P.; Sellergren, B.; Guiochon, G. Influence of Thermal Annealing on the Thermodynamic and Mass-Transfer Kinetic Properties of d- and l-Phenylalanine Anilide on Imprinted Polymeric Stationary Phases. *Anal. Chem.* **1999**, *71* (5), 928–938. https://doi.org/10.1021/ac981154o.

(48) Allender, C. J.; Brain, K. R.; Heard, C. M. Binding Cross-Reactivity of Boc-Phenylalanine Enantiomers on Molecularly Imprinted Polymers. *Chirality* **1997**, *9* (3), 233–237. https://doi.org/10.1002/(SICI)1520-636X(1997)9:3<233::AID-CHIR5>3.0.CO;2-G.

(49) Ebadi, A.; Soltan Mohammadzadeh, J. S.; Khudiev, A. What Is the Correct Form of BET Isotherm for Modeling Liquid Phase Adsorption? *Adsorption* **2009**, *15* (1), 65–73. https://doi.org/10.1007/s10450-009-9151-3.

(50) Rampey, A. M.; Umpleby, R. J.; Rushton, G. T.; Iseman, J. C.; Shah, R. N.; Shimizu, K. D. Characterization of the Imprint Effect and the Influence of Imprinting Conditions on Affinity, Capacity, and Heterogeneity in Molecularly Imprinted Polymers Using the Freundlich Isotherm-Affinity Distribution Analysis. *Anal. Chem.* **2004**, *76* (4), 1123–1133. https://doi.org/10.1021/ac0345345.

(51) Rushton, G. T.; Karns, C. L.; Shimizu, K. D. A Critical Examination of the Use of the Freundlich Isotherm in Characterizing Molecularly Imprinted Polymers (MIPs). *Anal. Chim. Acta* **2005**, *528* (1), 107–113. https://doi.org/10.1016/j.aca.2004.07.048.

(52) U.S. National Library of Medicine National Center for Biotechnology Information https://pubchem.ncbi.nlm.nih.gov.

Chapter 4

4 Assessment of Cross-reactivity in a Tailor-Made Molecularly Imprinted Polymer for Phenolic Compounds Using Four Adsorption Isotherm Models

This chapter was published as a research paper: Ghadeer F. Abu-Alsoud, Kelly A. Hawboldt, and Christina S. Bottaro*; *Journal of Chromatography A,* 1629 (2020). https://doi.org/10.1016/j.chroma.2020.461463.

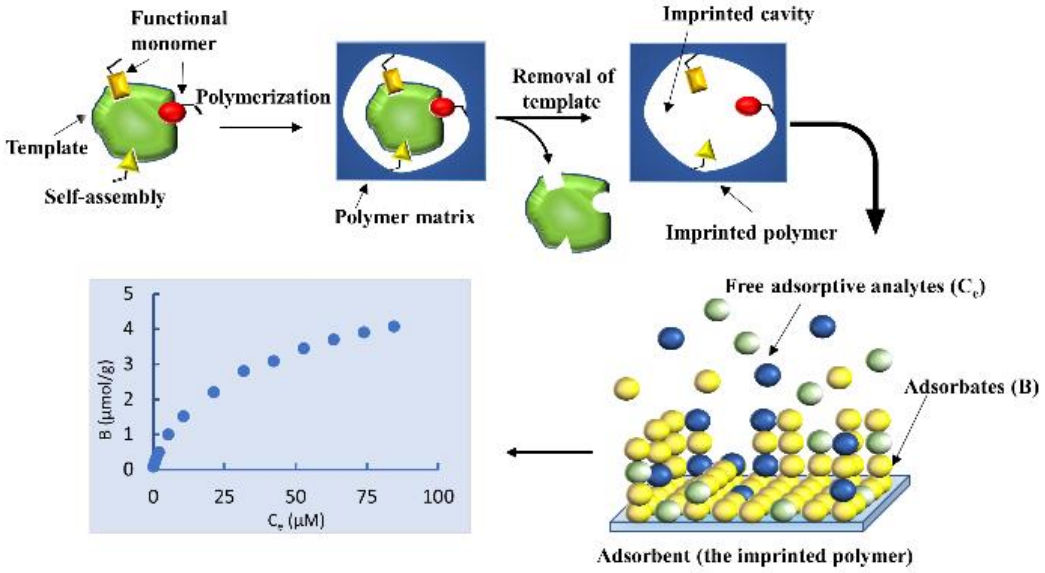

Keywords: Langmuir isotherm; Freundlich isotherm; Langmuir-Freundlich isotherm; Brunauer, Emmett, and Teller (BET) isotherm; Phenols; Molecularly imprinted polymer cross-reactivity

4.1 Abstract

Cross-reactivity is an important feature of molecularly imprinted polymers (MIPs), and is central to successful use of a pseudo-template in molecular imprinting. The adsorption and cross-reactivity of a molecularly imprinted polymer (MIP) designed for recognition of phenols from water was assessed using four different isotherm models (Langmuir (LI), Freundlich (FI), Langmuir–Freundlich (L-FI), and Brunauer, Emmett, and Teller (BET)). The L-FI model succeeded in explaining the cross-reactivity behavior through the total number of binding sites, the affinity constants and heterogeneity indices of the small phenols (phenol (ph), 2-methylphenol (2-MP), 3-methylphenol (3-MP), 2-chlorophenol (2-CP), 2,4-dimethylphenol (DMP), 2,4-dichlorophenol (DCP), 4-chloro-3-methylphenol (CMP)) with evidence that the phenols compete for binding sites based on their hydrophobicity as well as π-π, π-σ and *dipole-dipole* intermolecular forces. The recognition of the large phenols (2,4,6-trichlorophenol (TCP), pentachlorophenol (PCP), 4-teroctylphenol (4-OP), 4-nonylphenol (4-NP)), which have much higher binding affinities than the smaller phenolic compounds, was explained with the BET isotherm model that predicts that multiple layers adsorb to the adsorbed monolayer. The adsorption behavior with MIPs is also shown to be superior to corresponding non-imprinted polymers, and the applicability of MIPs for trace analysis is highlighted.

4.2 Introduction

Wulff *et al.* made the first imprinted polymer using a template covalently-linked to a functional monomer to form stereoselective cavities more than 40 years ago [1]. Non-

covalent molecular imprinting was developed by the Mosbach group in the 1980s, and the basic features of molecularly imprinted polymers (MIPs) were established [2]. The process is conceptually simple, where a highly cross-linked macroporous polymer is prepared by radical polymerization of a functional monomer-template complex and a cross-linker in a suitable porogenic solvent. Once the template is removed, three-dimensional cavities (recognition sites) complementary to the template in shape, size, and functionality remain [3]. MIPs have been used for numerous applications because of their desirable properties, such as high selectivity and affinity, ease of preparation, and mechanical and chemical stability under harsh conditions. MIPs have been used as sorbents in solid phase extraction (SPE), solid phase microextraction (SPME) [4], chromatography [5], membranes [6–9], sensors [10–12], and drug delivery [13]. MIPs have been used in the analysis of a range of complex matrices, including biological [14], environmental [15–23], and food samples [24], with varying tolerance of matrix effects. As new MIPs are developed, it is important to understand binding site chemistry, including the efficiency of the imprinting, selectivity and sorption capacity in light of the anticipated operational demands of the analysis. Factors such as concentration ranges, salinity, matrix components, and sampling conditions are usually significant. One valuable method of characterizing MIP performance relies on adsorption isotherm models to explain the interactions of analytes with MIP adsorbents. Such models describe the nature of the MIPs surface with respect to the number and affinity of the binding sites for a specific adsorbate (analyte) [25–31,31–33]. The most common models applied to MIPs are the Langmuir (LI) [34], Freundlich (FI) [35], and Langmuir–Freundlich (L-FI), (also call the Sips or hybrid model) [36], while the Brunauer, Emmett,

and Teller (BET) isotherm model has been used on rare occasions to describe the multilayer adsorption process in liquid phases [37–39].

Adsorption and molecular recognition by MIPs can be divided into homogeneous and heterogeneous, based on the chemistry and shape of the binding sites formed on the polymer surface. Homogeneous recognition requires that all the binding sites have the same affinity or binding site energy for a single adsorbate. On the other hand, a heterogeneous system has a distribution of site energies with different affinities for adsorbates [32,40]. Binding site formation in MIPs is largely dependent on the strength of the interaction between the functional monomer and the template prior to the polymerization process [32]. The template may interact through covalent or non-covalent interactions with the functional monomers giving rise to the covalent, non-covalent, and semi-covalent imprinting approaches, with the fully covalent methods giving the most homogeneous imprinting with the strongest and most selective binding. But covalent imprinting is also the least adaptable and rarely applied to uptake from aqueous media. Though the non-covalent approaches have been used more widely, it is recognized that formation of the pre-polymerization complex is a dynamic process based on relatively weak intermolecular interactions, with hydrogen bonding or electrostatic interactions being the strongest, resulting in a heterogeneous distribution of binding site energies [41,42]. Specifically, different binding sites form based on the stoichiometry and geometry of the template-monomer complex and non-selective interactions with the cross-linker and excess monomer. Based on Le Chatelier's principle, a molar excess of the functional monomer is typically used to ensure all the template is consumed in the formation of the template-

monomer complex. The optimum stoichiometry is driven by the chemistry of the template, monomers and porogens used, and is predicted from theory but determined experimentally [40]. Thus, adsorption isotherm parameters such as adsorption capacity (number of binding sites), binding affinity, and the heterogeneity that are characteristic of the MIP adsorbent can be estimated using an appropriate adsorption isotherm model, which should be evaluated based on its fit with the experimental adsorption data.

4.2.1 Adsorption isotherms

Adsorption isotherms have been used to evaluate how adsorbates interact with a solid sorbent phase over various concentration levels under constant conditions, e.g., temperature and pH. For new adsorbents, isotherm data gives insight into the performance of the material. To be truly useful, the data from the models should provide both qualitative and quantitative information that is comparable for different systems. As the application of the common isotherm models can vary (i.e., fitting of linearized or non-linear data), some details of the four models, as applied in this study, are given below.

The LI model, initially developed for gas adsorption to activated carbon, assumes monolayer adsorption to homogeneous binding sites [34]. LI plots have two characteristic regions, a linear region and a plateau, which occurs at saturation [43,44]. The non-linearized mathematical expression for LI is given in Eq. 1, where B is the amount of bound analyte, C_e is the concentration of the analyte left in the solution at equilibrium, N is the number of bindings per unit mass of adsorbent required for a complete the monolayer, and K the affinity constant for the system [37].

$$B = \frac{NKC_e}{1 + KC_e} \quad (1)$$

The equation is rearranged to a suitable form (Eq. 2) for estimation of the binding parameters, *N* and *K,* by linear regression of a plot of 1/*B* against 1/*Ce*.

$$\frac{1}{B} = \frac{1}{NKC_e} + \frac{1}{N} \quad (2)$$

The FI model (Eq. 3) is used to evaluate adsorbate interactions with solids bearing heterogeneous binding sites and is the model used most often for characterization MIPs [20,22,25]. Eq. 3 describes a power function relating the concentrations of bound adsorbate, *B,* to the concentration of a free analyte, C_e with two binding parameters, *a* and *m*. The heterogeneity index, *m*, describes the degree of site heterogeneity and can range from 0 to 1 with 1 being completely homogenous [45]. The pre-exponential constant, *a*, represents the product of the total number of binding sites (N_t) and the average binding site affinity (*K°).* The linear form (Eq. 4) is applied in this study.

$$B = aC_e^m \quad (3)$$

$$\log B = m \log C_e + \log a \quad (4)$$

However, the individual values for N_t and *K°* cannot be determined directly with FI. Umpleby et al [31] derived the affinity distribution for FI (Eq.5) *N(K)* determined by substituting the experimentally derived FI binding parameters (*a* and *m*) into Eq. 5 and plotting *N(K)* versus *logK.* where $K = 1/C_e$. The limits of *K* are of K_{min} ($1/C_{max}$) and K_{max} ($1/C_{min}$), where C_{min} and C_{max} represent the range of free analyte concentrations used in the

binding experiments. However, it is important to note that N_t and K can be determined for any subset of concentrations ($K1$-$K2$ from C_{e2}-C_{e1}) [46]. Affinity distributions (N versus K) for MIPs were reported for the first time in 2000 [47], revealing that the highest energy binding sites (high K) are formed in the fewest number (low N).

$$N(K) = 2.303am(1-m^2)e^{-2.303mlogK} \tag{5}$$

The number of binding sites measured over a discrete range of concentrations, N_{K1-K2}, (Eq. 6) and the weighted average affinity of those sites, $\overline{K}_{K1-K2}$, (Eq. 7) can be derived from Eq. 5 [31,32].

$$N_{K1-K2} = a(1-m^2)(K_1^{-m} - K_2^{-m}) \tag{6}$$

$$\overline{K}_{K1-K2} = \left(\frac{m}{m-1}\right)\left(\frac{K_1^{1-m} - K_2^{1-m}}{K_1^{-m} - K_2^{-m}}\right) \tag{7}$$

However, FI has an important limitation in that the FI relationship deviates from linearity at high concentrations where the adsorption process becomes independent of the free adsorbate concentration because of the low affinity for available binding sites [32].

Sips proposed the hybrid L-FI in 1948 [36]. It can be applied to any adsorbent, whether it possesses homogeneous or heterogeneous binding site energies, and it can also model adsorption behaviour for subsaturation or saturation conditions. The general form for the L-FI model has three fitting parameters (N_t, a and m) that should be solved using non-linear regression and is shown in Eq. 8:

$$B = \frac{N_t a C_e^m}{1 + aC_e^m} \tag{8}$$

B is the amount of analyte adsorbed per gram of sorbent and C_e is the corresponding free analyte concentration at equilibrium; N_t is the adsorption capacity (total binding sites per gram sorbent material); the affinity binding constant, $K°$, is determined from a and m ($K° = a^{1/m}$) where m is the heterogeneity index as used in the FI model. When $m = 1$, the L-FI expression is reduced to the LI form (Eq. 1). If $m<1$ and the adsorbate is at low concentrations, Eq. 8 can be simplified Eq. 3, the FI form [26,28,29,48,49].

LI, FI and L-FI models assume that the adsorbates form a monolayer. However, for hydrophobic molecules at high concentration levels, the assumption can be unreliable since it is energetically more favourable for the molecules to interact with hydrophobic molecules bound to the substrate than to stay in solution. This formation of layers of adsorbate can be modeled using the BET isotherm introduced by Brunauer–Emmett–Teller for gas-solid systems in 1938 [39]. In 2009, Ebadi *et al.* used first principles to adapt the BET model to adsorption in liquid phase, eschewing the classical linear approach used for gas phase adsorption for a more comprehensive non-linear model [38]. A summary of their derivation is provided in Appendix 1. The general form of BET isotherm is given in Eq. 9:

$$\frac{q}{q_m} = \frac{cx(1-(n+1)x^n+nx^{n+1})}{(1-x)(1+(c-1)x-cx^{n+1})} \tag{9}$$

where q_m is the monolayer adsorption capacity; n the number of the layers formed; $c = K_S/K_L$, where K_S is equilibrium constant for adsorption to the surface and K_L is the equilibrium constant for adsorption to a bound layer; x is the adsorbate partial pressure relative to its saturation pressure ($x = P/P^{sat}$) at constant temperature; q is the amount of analyte adsorbed relative to mass of sorbent. Ebadi *et al.*[38] adapted the general form of the BET isotherm model (Eq. 9) for a liquid-phase system. The most important changes

include replacing P by the equilibrium concentration (C_e) and $1/P_{sat}$ by K_L. Substitution and rearrangement yield Eq.10.

$$q = \frac{q_m K_S C_e [1 - (n+1)(K_L C_e)^n + n(K_L C_e)^{n+1}]}{(1 - K_L C_e)\left[1 + \left(\frac{K_S}{K_L} - 1\right) K_L C_e - \left(\frac{K_S}{K_L}\right)(K_L C_e)^{n+1}\right]} \quad (10)$$

This equation is solved using non-linear regression of the q and C_e data determined experimentally over a range of adsorbate loadings to obtain the four fitting parameters (q_m, K_L, K_S, and n).

Beyond simply applying models in a new way for characterization of the adsorption behaviour of MIPs, a further aim of our work is to understand the cross-reactivity of this catechol imprinted polymer. Though there is limited literature using adsorption isotherms to study MIPs in this way, Martin-Esteban and co-workers published two excellent papers [28,29] in which the cross-reactivity of propazine MIPs for other triazine herbicides was evaluated by comparing the fitting parameters N_t, $K°$, and m from the L-FI model. They found that the recognition of triazines is partly dependant on the molecular size of triazine substrates and they were able to rationalize the observed adsorption behavior using fitting parameter data. The same group published another paper in 2005, in which the L-FI was used to probe the effects of different templates and functional monomers on the performance of MIPs for extraction phenylurea herbicides [49]. In this study, we compare the binding performance of MIPs and analogous non-imprinted polymers (NIPs) for simultaneous adsorption of eleven phenolic compounds using the LI, FI, L-FI and BET models, applying Eqs. 2, 4, 8 and 10, respectively. The FI binding parameters N_{K1-K2} and $\overline{K}_{K1-K2}$ were calculated using Eqs. 6 and 7. Since performance differences may be subtle,

the best isotherm should fit the experimental data well, so that conclusions are meaningful. Prior to evaluation of the fitting parameters, the correlation coefficients (R^2), sum of the square of the residuals (*RSS*), and relative error from the fit of the isotherm models to experimental data are evaluated.

4.3 Experimental

4.3.1 Reagents and material

Phenol (Ph) (≥99.5%), 2-methylphenol (2-MP) (≥99%), 3-methylphenol (3-MP) (99%), 2-chlorophenol (2-CP) (≥99%), 2,4-dimethylphenol (DMP) (≥99), 2,4-dichlorophenol (DCP) (99%), 2,4,6-trichlorophenol (TCP) (99%), 4-chloro-3-methylphenol (CMP) (99%), pentachlorophenol (PCP) (97%); 4-tert-octylphenol or (4-(2,4,4-trimethylpentan-2-yl)phenol) (4-OP) (97%), 4-nonylphenol (4-NP) (analytical standard), catechol (≥99%), 3-(trimethoxysilyl)propyl methacrylate (98%), ethylene glycol dimethacrylate (EGDMA) (98%), polyethylene glycol (PEG) (average MW 20,000), 4-vinyl benzoic acid (VBA) (97%), 2,2- dimethoxy-2-phenylacetophenone (DMPA) (99%), potassium phosphate monobasic (99%) and ortho-phosphoric acid (85%) were purchased from Sigma-Aldrich (Oakville, Canada). Optima LC/MS grade acetonitrile, water and formic acid used in the gradient elution were obtained from Fisher Scientific (Ontario, Canada). The solvents used for derivatization the glass slides, washing the slides, and removing the template were ACS reagent grade, including toluene from Caledon Laboratory Chemicals (Ontario, Canada), acetonitrile from ACP Chemicals (Montreal, Canada) and absolute ethanol from Commercial Alcohols (Ontario, Canada). Plain glass microscope slides 75 × 25 mm were

sourced from Fisher Scientific (Ontario, Canada); 13 mm PTFE 0.2-µm syringe filters from Canadian Life Science (Peterborough, Ontario); the micro cover glass 18 x 18mm from VWR (Mississauga, Ontario); Rainin Mettler Toledo Pos-D positive displacement pipette from VWR (Mississauga, Canada).

A mixed standard solution containing 0.4 g L^{-1} of each phenolic compound was prepared in Optima acetonitrile in amber vials and kept at -22 °C until use. All the rebinding solutions used in the batch experiments were prepared with deionized (DI) water purified by a Barnstead Nanopure water purification system (Lake Balboa, USA) and adjusted to pH 4.0 (phosphate buffer at final concentration of ~1.0 mM) and 5% (w/w) sodium chloride (ACP chemicals, St. Leonard, Canada).

All the thin-film MIPs used in this study were fabricated on derivatized glass using drop casting with UV photopolymerization as in our previously published method [50]. A schematic of the fabrication methods along with representative scanning electron microscope (SEM) images can be found in a previously published paper [50].

4.3.2 Instrumentation

A Waters Acquity UHPLC-PDA equipped with an autosampler, a photodiode array detector (PDA) and an RP-amide column (2.7 µm, 2.1x 100 mm, HALO column) connected to C18 guard column was used for separation and determination of phenols. Gradient elution with 0.1% (v/v) formic acid in water (solvent A) and 0.1% formic acid in acetonitrile (solvent B) was applied in the following program: 35% B 0.00–2.00 min; increased to 40% B from 2.01–2.30 min then kept constant for 1.20 min; increased to 100% B 3.50 – 8.00 min, then returned to 35% B from 8.00 – 8.30 min then kept for 2.70 min to

equilibrate the column for the next run. The sample vials and column temperatures, the flow rate, the injection volume, were set at, 25 ºC, 0.45 mL/min and 10 µL, respectively. Signals for quantification were collected at two wavelengths near the λ_{max} of the analytes as noted: 275 nm for Ph, 2-MP, 3-MP, 2-CP, DMP, 4-OP; and 285 nm for DCP, TCP, CMP, and PCP; 370 nm was used as a reference for baseline correction.

Other key equipment included a Sartorius Secura 225D-1S analytical balance (Goettingen, Germany), a Crison GLP 22 pH-meter (Barcelona, Spain), and a VWR Scientific DVX-2500 digital multi-position vortex mixer (Hampton**,** USA), which was used for simultaneous batch rebinding experiments.

4.3.3 Batch rebinding experiments

MIP films were placed in the bottom of plastic centrifuge tubes contained in 30.0 mL of buffered, salted DI water either as a blank or spiked to contain a mixture of 11 phenols (Figure 2.1) at concentrations ranging from 0.01 mg L^{-1} to 8 mg L^{-1}, except for 4-OP and 4-NP, which were spiked from 0.01 mg L^{-1} to 7 mg L^{-1}, the upper limit of solubility. The capped tubes were vortex mixed at 1500 rpm for 3 h under ambient conditions, then the MIPs were removed from solution, and rinsed with DI water. The slides were then immediately placed in clean centrifuge tubes with 8 mL acetonitrile to desorb the bound analytes assisted by vortex mixing at 1000 rpm for 15 min. After extraction, the acetonitrile containing the desorbed analyte was filtered using a 13 mm PTFE 0.2-µm syringe filter and the volume reduced to no less than ~35 µL under N_2 then made to volume using 35% acetonitrile in water. The final volumes of samples were adjusted to 100 µL (using a

Hamilton syringe) for the low concentration range (0.01 mg L^{-1}- 0.05 mg L^{-1}) and to 1 mL (1-mL volumetric flask) for higher concentrations.

4.3.4 Optimum adsorption time

The extraction-time profiles were constructed for simultaneous uptake of the eleven phenols at 1 mg L^{-1} each as described in the batch experiments except the extent of adsorption was followed for 24 h (Figure 4.1). While the lighter phenolic compounds (Ph, 2-MP, 3-MP, DMP, and 2-CP) were at equilibrium within 2 h, the other compounds took longer to reach a plateau (as much as 12 h). However, by 3 h a local quasi-plateau was reached for most of the heavier phenolic compounds (except 4-OP and 2-NP), which allows us to carry out the experiments in a timely fashion and in a time-frame more aligned with the need for high throughput in analytical methods.

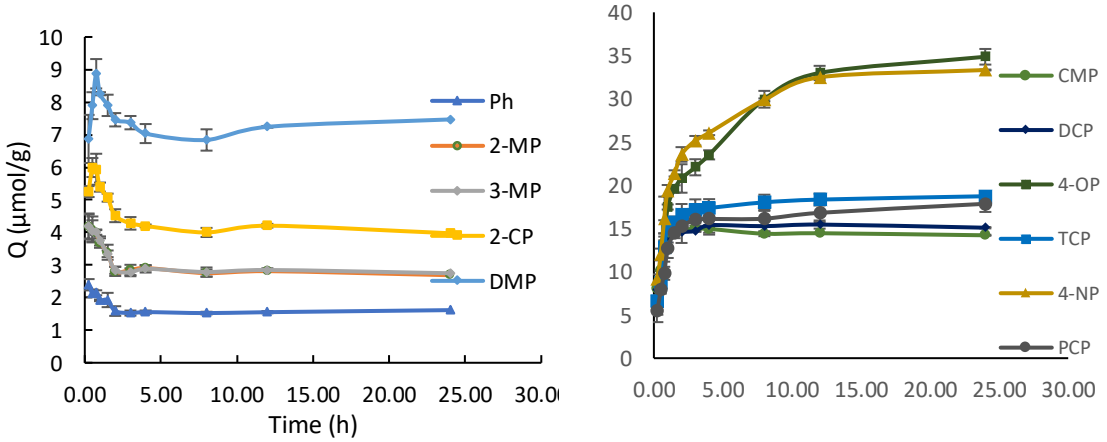

Figure 4.1. Extraction-time profile for phenols for MIP from 30 mL of water MIP film spiked with 1 ppm phenols; salted with 5% of NaCl; buffered with pH 4 (1mM, phosphate buffer); the phenols were desorbed using 8 ACN for 15 min at 1000 rpm vortex speed. Error bars represent standard deviation (n = 3).

4.3.5 Evaluation of isotherm models

A detailed description of the fitting methodology is provided in our prior paper demonstrating the effectiveness of different isotherms for modeling adsorption of four single adsorbates to these MIPs [50]. This approach is extended to a mixture of 11 phenolics with a range of functionalities. The experimental data were fitted to the four isotherm models using Eqs. 2,4,8, and 10 for LI, FI, L-FI, and BET, respectively. LI, FI, L-FI and BET isotherms were fitted using Origin 2018 (Northampton, Massachusetts, USA) statistical software by linear or non-linear regression as required by the model. All the isotherms' coefficients, R^2, and *RSS* are given with the fitting parameters shown in the tables below.

4.4 Results and discussion

4.4.1 Optimum adsorption time

The extraction-time profiles over 24 h were built for simultaneous uptake for the 11 phenolic compounds (Figure 4.1). For phenol and the cresols, the highest adsorption was detected in the first series of measurements taken at 15 min; 2-CP and DMP reached maximum adsorption at 45 min. However, the presence of phenols with higher affinity for the MIPs led to sharp decreases in adsorption for these five compounds until equilibrium was established at ~2 h. This behaviour occurs because the light phenols bound to lower affinity sites are displaced by the larger more hydrophobic phenols, which also have lower diffusion rates with slower mass transfer. The rate of adsorption for these larger phenols (CMP, DCP, TCP, 4-OP, PCP and 4-NP) is high for the first two hours. For CMP, DCP,

TCP and PCP, the adsorption continued to increase slowly after the first 2 h until it reached equilibrium at about 3 h, while the equilibrium time of 4-OP and 4-NP was obtained after about 12 h. The rate of adsorption can be attributed to the availability of the binding sites, which is high at the onset but decreases when the fraction of available binding sites decreases, and those that are available have lower affinity for the solutes. Although it is desirable to continue extraction until equilibrium is achieved completely, in routine analysis, there is usually insufficient time to do so. Thus, based on the curves from Figure 4.1, 3 h provides extraction at >90% of the maximum extracted at equilibrium for most of the phenols and no less than 63% for the worst case (4-OP). Data from fitting of the adsorption isotherms show that the relationship between the bound adsorbates and the bulk solution are well behaved at 3 h, with good reproducibility and good fit with the appropriate isotherm model (>0.99). From an analytical perspective, this means that calibration curves can be constructed with confidence using this timeframe.

4.4.2 Assessment of Adsorption Isotherm Models for Characterizing MIP-Films Performance with Phenolic Analytes

Each of the adsorption models is evaluated for its suitability to fit data for the simultaneous uptake of phenols by MIPs. As we have found that different binding isotherms may apply for the same system depending on the solute concentration, saturation and sub-saturation concentration ranges, these were included in this study for a more comprehensive examination of the binding adsorption models.

The N and K fitting parameters for the LI model (Table 4.1) all show high relative standard deviation, in spite of reasonable R^2 values (0.9178 – 0.9984). Although the lighter

alkyl phenols gave relative errors <50%, the *%RSD* for the larger phenols was very large, including DCP which gives nearly 2000% *RSD*. Looking at the data in Figure 4.2, a significant proportion of adsorption data points, mainly in the higher concentration range (low *1/Ce* values), do not fit well with the modeled line. In light of these results, we conclude that the sorption of a mixture of analytes relies on the intrinsic heterogeneity of the adsorbent binding sites; this is further complicated by competition for sites that are cross-reactive; thus the LI model cannot be applied to this system.

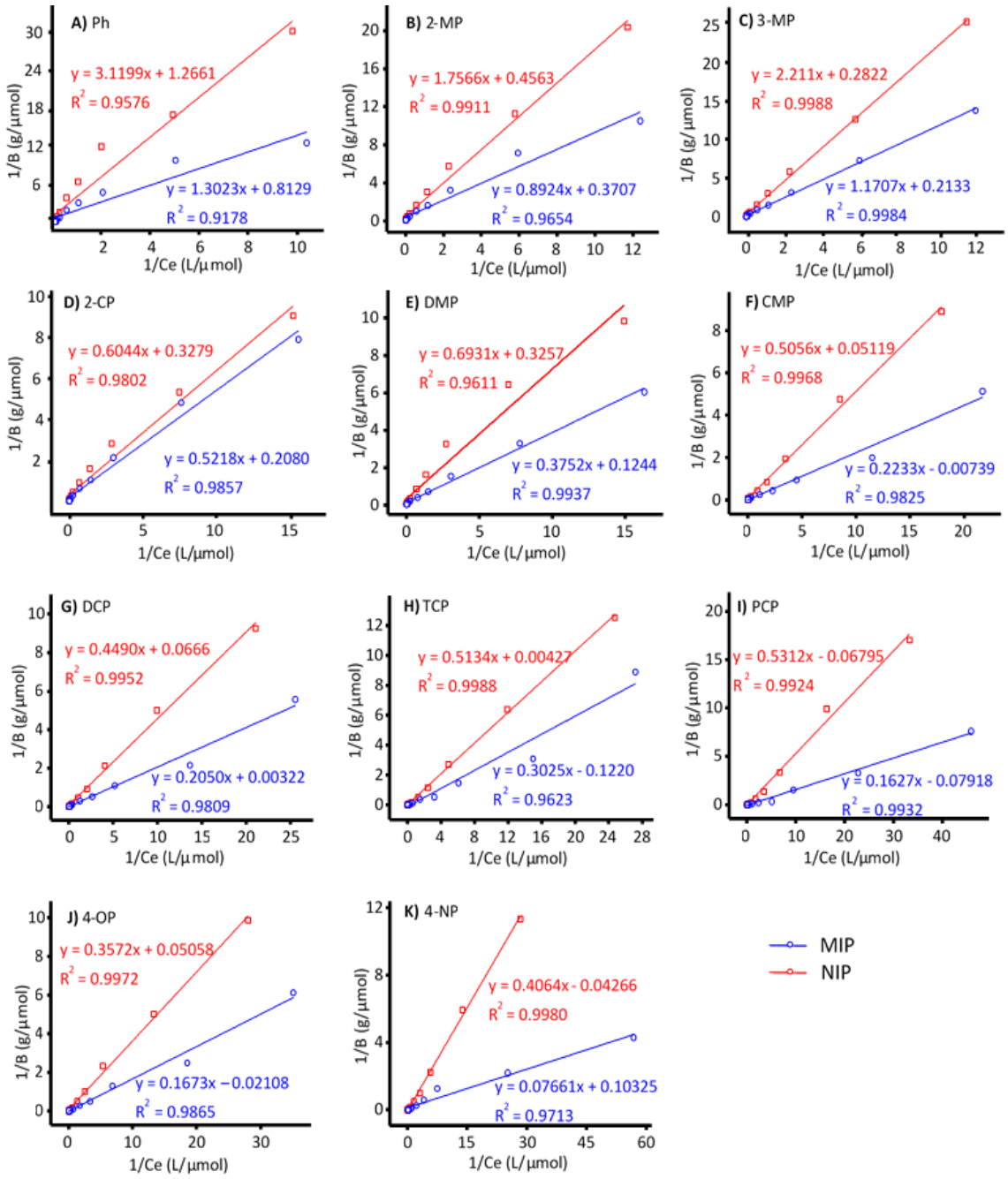

Figure 4.2. The experimental data for simultaneous study (circle points for MIP, squares points for NIP) were fit to a Langmuir (solid lines) for MIP and NIP), A) Ph, B) 2-MP, C) 3-MP, D) 2-CP, E) DMP, F) CMP, G) DCP, H) TCP, I) PCP, J) 4-OP, K) 4-NP).

Table 4.1. LI fitting parameters for the phenols that were loaded simultaneously

Analyte	N (μmol g^{-1}) *(RSD%)*	K (μmol^{-1}) *(RSD%)*	R^2	*RSS*
		MIP		
Ph	1.23 (42%)	0.624 (43%)	0.9178	15.494
2-MP	2.69 (47%)	0.415 (48%)	0.9654	4.1584
3-MP	4.68 (22%)	0.182 (22%)	0.9984	0.2936
2-CP	4.81 (40%)	0.398 (40%)	0.9857	0.9235
DMP	8.04 (33%)	0.331 (33%)	0.9937	0.224
CMP	135. (750%)	0.0331 (2.4x10^6%)*	0.9825	0.4137
DCP	310. (1944%)	0.0157 (1944%)	0.9809	0.5291
TCP	8.20 (115%)	0.403 (116%)	0.9623	2.6486
PCP	12.6 (66%)	0.486 (66%)	0.9932	0.3665
4-OP	47.4 (301%)	0.126 (301%)	0.9865	0.4539
4-NP	9.68 (64%)	1.35 (64%)	0.9713	0.5081
		NIP		
Ph	0.790 (43%)	0.406 (43%)	0.9576	39.7332
2-MP	2.19 (36%)	0.260 (36%)	0.9911	3.648
3-MP	3.54 (26%)	0.127 (26%)	0.9988	0.7414
2-CP	3.05 (34%)	0.543 (34%)	0.9802	1.6526
DMP	3.07 (53%)	0.469 (53%)	0.9611	4.0756
CMP	19.5 (84%)	0.101 (84%)	0.9968	0.2490
DCP	15.0 (82%)	0.148 (82%)	0.9952	0.4053
TCP	234. (856%)	0.0083(856%)	0.9988	0.1806
PCP	14.7 (192%)	0.128 (192%)	0.9924	2.2861
4-OP	19.8 (94%)	0.142 (94%)	0.9972	0.2568
4-NP	23.4 (110%)	0.105 (109%)	0.9980	0.2450

* High relative standard deviation

4.4.2.1 Freundlich Isotherm

In our study of adsorption of single compounds, we found that the FI model was poor at fitting adsorption data at high concentrations.[50] Umpleby *et al.*[32] described this phenomenon and related it to limits in the number of high energy imprinted binding sites

available at high concentrations. Thus, we included only low concentration data (0.01 – 1 mg L^{-1}) for the simultaneous adsorption study, which gave linear slopes in the determination of the fitting parameters (Figure 4.3 and Table 4.2). Data for the higher concentration range can be found in Figure 4.4 and Table 4.3.

The fitting parameters m, $\overline{K}_{K_{1-K_2}}$, and $N_{K1\text{-}K2}$ presented in Table 4.2 show very good R^2 and *RSS* values, and a low *RSD*s for both MIPs and NIPs, except for the larger analytes (i.e., TCP, PCP, 4-OP and 4-NP) where the model fails to describe the behaviour effectively (e.g. $m \geq 1$). Except for 2-CP, the MIPs show a higher degree of heterogeneity (m) for the small phenolic compounds (Ph, 2-MP, 3-MP, DMP, DCP, CMP). This makes chemical sense since the introduction of a template creates new ordered higher affinity sites, leaving the lower limits of the affinity constants (K_1) essentially unchanged and expanding the upper limits (K_2), which are calculated for adsorption at low concentrations. These imprinted sites have the highest affinity but are less numerous than the non-selective binding sites present in both MIPs and NIPs. The relationship between relative binding selectivity between MIPs and NIPs at different concentrations is well illustrated in Figure 4.3, which plots the bound adsorbate against the free adsorbate. The MIPs show a higher capacity than the NIPs, but typically the slopes are lower for the MIPs (except 2-CP); as concentrations increase, the amount of adsorbate bound to the MIPs and NIPs will approach convergence. Ultimately this means that imprinting factors should be higher at low concentrations. This is in contrast to the high imprinting factors sometimes reported for MIPs using data at the point of adsorbate saturation, which may be attributed to surface

area differences between MIPs and NIPs rather than the formation of a large number of high energy sites.[51–54]

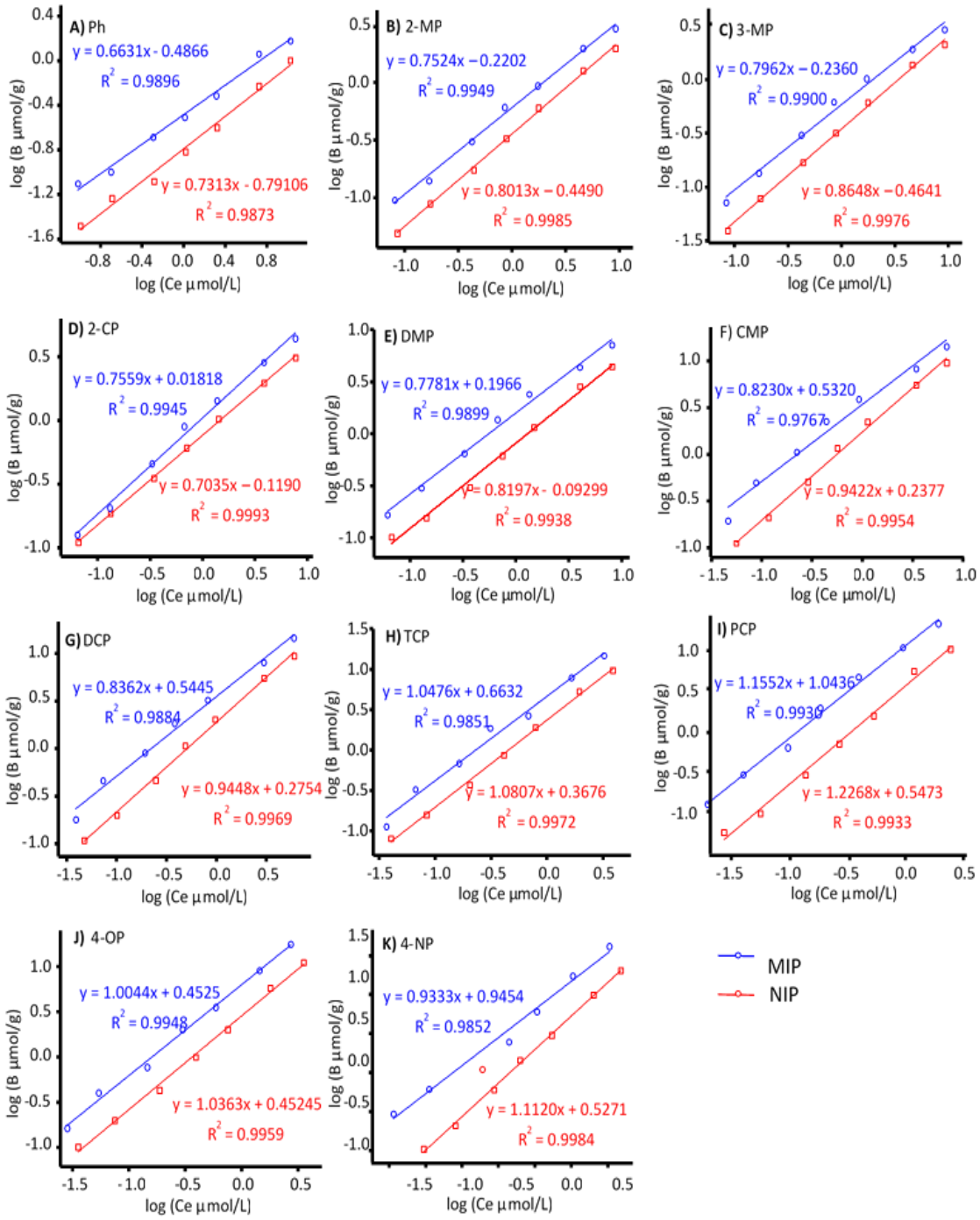

Figure 4.3**.** The experimental data for simultaneous study at low concentration levels (circle points for MIP, squares points for NIP) fit to FI isotherm (solid lines) for MIP and NIP (A) Ph, B) 2-MP, C) 3-MP, D) 2-CP, E) DMP, F) CMP, G) DCP, H) TCP, I) PCP, J) 4-OP, K) 4-NP).

Table 4.2. FI Fitting Parameters, $\overline{K}_{K_{1-K_2}}$, $N_{K1\text{-}K2}$ at low concentration levels for the phenols that were loaded for the phenols that were loaded simultaneously

Analyte	a (μmol g^{-1}) (μM^{-1})^m	m	*Klimits* (μM^{-1})[a]	N_{K1-K2} (μmol/g)	$\overline{K}_{K1-K2}$ (μM^{-1})	R^2	*RSS*	*IF* [b]
			MIP					
Ph	0.326 (4.4%)	0.663(4.2%)	0.094-10.4	0.836	0.752	0.9896	0.0127	2.04
2-MP	0.602(3.5%)	0.752(2.9%)	0.109-12.4	1.35	0.757	0.9949	0.0080	1.83
3-MP	0.581(5.2%)	0.796(4.1%)	0.109-11.9	1.22	0.698	0.9900	0.0176	2.10
2-CP	1.04(3.8%)	0.756(3.0%)	0.129-15.6	**2.04**	**0.915**	0.9945	0.0090	1.31
DMP	1.57(5.4%)	0.778(4.1%)	0.123-16.3	3.09	0.865	0.9899	0.0182	2.13
CMP	3.40(9.5%)	0.823(6.3%)	0.155-21.7	5.01	1.02	0.9767	0.0514	4.21
DCP	3.50(7.0%)	0.836(4.4%)	0.168-25.5	4.62	1.11	0.9884	0.0265	4.24
TCP	4.61(9.8%)	1.05(5.0%)	0.309-27.2	-1.52	1.32	0.9851	0.0421	0.90
PCP	11.1(8.6%)	1.16(3.4%)	0.503-45.9	-8.13	1.90	*0.9930*	0.0235	1.48
4-OP	6.26(5.9%)	1.00(3.0%)	0.367-35.1	-0.15	1.68	0.9948	0.0140	0.19
4-NP	8.82(11%)	0.933(5.5%)	0.411-56.8	2.58	2.26	0.9852	0.0356	-0.91
			NIP					
Ph	0.162(5.3%)	0.731(4.6%)	0.094-9.80	0.409	0.659	0.9873	0.0183	
2-MP	0.356(2.0%)	0.801(1.6%)	0.108-11.7	0.737	0.687	0.9985	0.0026	
3-MP	0.344(2.7%)	0.865(2.0%)	0.108-11.5	0.581	0.620	0.9976	0.0048	
2-CP	0.760(1.2%)	0.703(1.1%)	0.129-15.3	**1.56**	**0.990**	0.9993	0.0009	
DMP	0.807(4.3%)	0.820(3.2%)	0.123-14.9	1.45	0.784	0.9938	0.0118	
CMP	1.73(4.4%)	0.942(2.8%)	0.145-17.9	1.19	0.766	0.9954	0.0118	
DCP	1.89(3.8%)	0.945(2.3%)	0.166-21.1	1.09	0.880	0.9969	0.0081	
TCP	2.33(4.1%)	1.08(2.1%)	0.257-24.7	-1.69	1.07	0.9972	0.0083	
PCP	3.53(8.0%)	1.23(3.4%)	0.397-33.2	-5.51	1.37	0.9933	0.0244	
4-OP	2.83(5.0%)	1.04(2.6%)	0.282-28.0	-0.77	1.25	0.9959	0.0115	
4-NP	3.37(3.3%)	1.11(1.6%)	0.317-28.3	-2.84	1.25	0.9984	0.0049	

[a] Calculated from the minimum and maximum of the concentration of a free analyte in the rebinding solution
($K_{max}=1/C_{min}$ and $K_{min}=1/C_{max}$)

[b] The imprinting factor is the ratio of the MIP N_{K1-K2} values to the NIP N_{K1-K2} values.

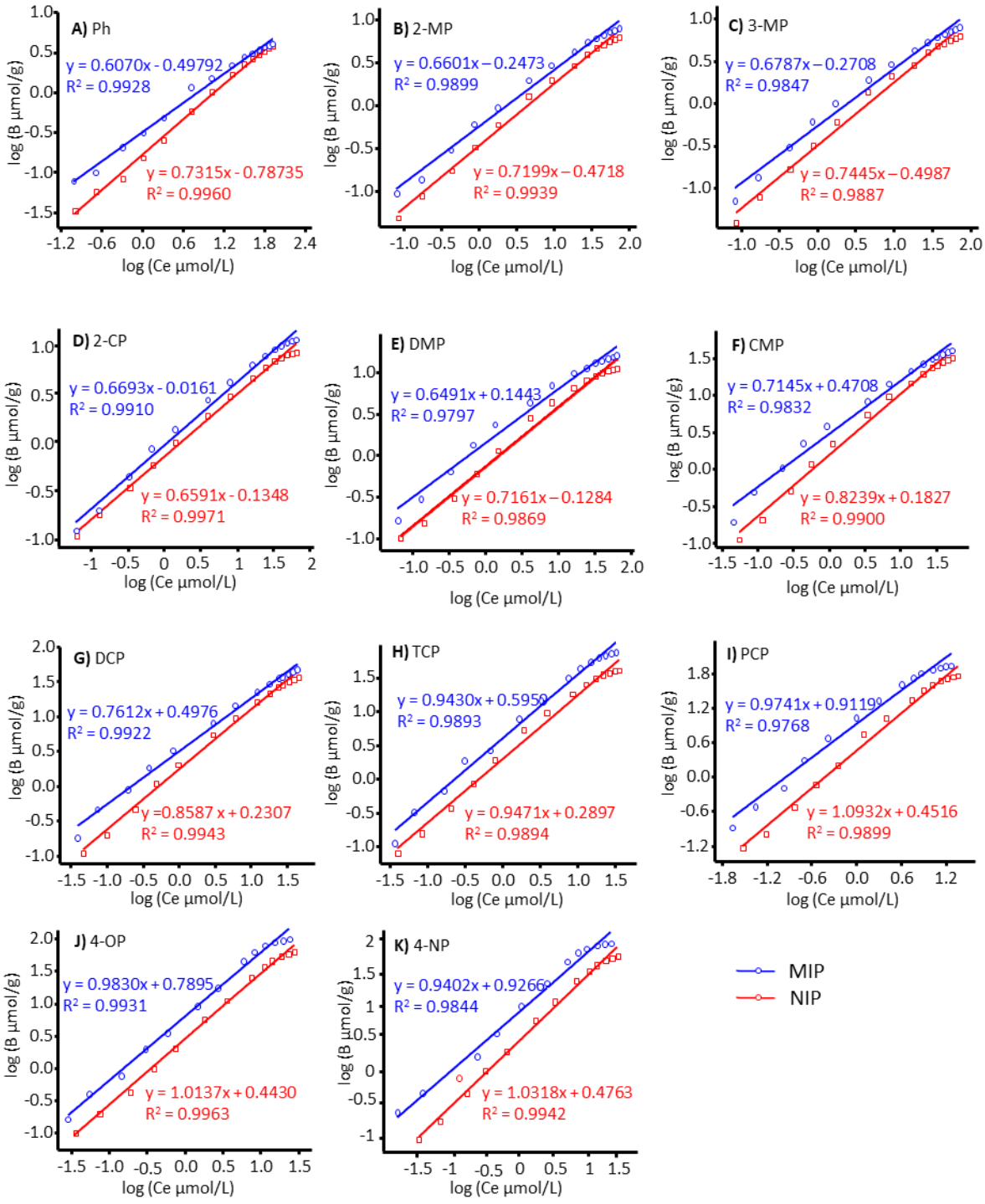

Figure 4.4. The experimental data for simultaneous study for the entire concentration levels (circle points for MIP, squares points for NIP) fit to FI isotherm (solid lines) for MIP and NIP (A) Ph, B) 2-MP, C) 3-MP, D) 2-CP, E) DMP, F) CMP, G) DCP, H) TCP, I) PCP, J) 4-OP, K) 4-NP).

Table 4.3. FI fitting parameters over entire concentration range

Analyte	a (μmol g^{-1}) (μM^{-1})^m (%RSD)	m (%RSD)	*K limits* (μM^{-1})[a]	N_{K1-K2} (μmol/g)	$\bar{K}_{K1-K2}$ (μM^{-1})	R^2	*RSS*
			MIP				
Ph	0.317 (4.3%)	0.607 (2.4%)	0.0118-10.4	2.918	0.248	0.9928	0.033
2-MP	0.566 (5.4%)	0.660 (2.8%)	0.0136-12.4	5.37	0.245	0.9899	0.0556
3-MP	0.536 (6.8%)	0.678 (3.4%)	0.0136-11.9	5.27	0.228	0.9847	0.0885
2-CP	0.964 (4.9%)	0.669 (2.6%)	0.0164-15.6	8.24	0.290	0.9910	0.0518
DMP	1.39 (7.3%)	0.649 (4.0%)	0.0156-16.3	11.8	0.306	0.9797	0.114
CMP	2.96 (7.1%)	0.715 (3.6%)	0.0191-21.7	24.3	0.311	0.9832	0.1214
DCP	3.14 (5.0%)	0.761 (2.5%)	0.0225-25.5	23.6	0.315	0.9922	0.0634
TCP	3.94 (6.6%)	0.943 (2.9%)	0.0311-27.2	11.5	0.243	0.9893	0.1215
PCP	8.16 (9.4%)	0.974 (4.3%)	0.0532-45.9	7.26	0.384	*0.9768*	0.2713
4-OP	6.16 (5.4%)	0.983 (2.4%)	0.0415-35.1	4.75	0.292	0.9931	0.0749
4-NP	8.44 (7.9%)	0.940 (3.6%)	0.0487-56.8	-13.3	0.317	0.9844	0.1641
			NIP				
Ph	0.163 (3.8%)	0.732 (1.7%)	0.0118-9.80	1.93	0.165	0.9960	0.0258
2-MP	0.337 (4.5%)	0.720 (2.2%)	0.0136-11.7	3.55	0.199	0.9939	0.0390
3-MP	0.317 (6.3%)	0.744 (3.0%)	0.0136-11.5	3.43	0.184	0.9887	0.0774
CP	0.733 (2.8%)	0.659 (1.5%)	0.0163-15.3	6.176	0.297	0.9971	0.0160
DMP	0.744 (6.4%)	0.716 (3.2%)	0.0155-14.9	7.09	0.237	0.9869	0.0858
CMP	1.52 (6.3%)	0.823 (2.8%)	0.0189-17.9	12.8	0.208	0.9900	0.0881
DCP	1.70 (4.8%)	0.859 (2.1%)	0.0220-21.1	11.8	0.219	0.9943	0.0545
TCP	1.95 (6.8%)	0.947(2.9%)	0.0279-24.7	5.94	0.216	0.9894	0.119
PCP	2.83 (7.0%)	1.09 (2.8%)*	0.0435-33.2	-16.9	0.236	0.9899	0.1427
4-OP	2.77 (4.1%)	1.01 (1.7%)*	0.0361-28.0	-2.21	0.234	0.9963	0.0411
4-NP	2.99 (5.2%)	1.03 (2.2%)*	0.0393-28.3	-5.44	0.241	0.9942	0.0669

[a] Calculated from the minimum and maximum of the concentration of free analyte in the rebinding solution ($K_{max} = 1/C_{min}$ and $K_{min} = 1/C_{max}$)

* the heterogeneity index should be less than 1, therefore the model fails for systems where m ≥ 1.

As shown in Table 4.2, the more hydrophobic phenolic compounds (logP values [55] are given in Table 4.4) bind more strongly, tending to displace the less hydrophobic adsorbates and giving higher values for apparent binding sites ($N_{K1\text{-}K2}$). Plotting the affinity constants (averages and at the limits) and $N_{K1\text{-}K2}$ against *logP* for both the MIPs and NIPs (Figure 4.5) confirms that uptake is correlated with hydrophobicity. The strongest trends are apparent for the high (upper limit) and average affinities ($\overline{K}_{K_{1-K_2}}$), with the MIPs showing a slightly better correlation. We also note that the values of the average affinity constants for MIPs and NIPs tend to be weighted toward the minimum values of the limits, indicating that most of the sites are of lower energy. The number the apparent binding sites shows a much stronger relationship with hydrophobicity for MIPs as compared to the NIPs. Two key conclusions can be made here. First, the MIP has a greater number of sites available for analyte binding, even though the range of estimated site energies is not dramatically different. Second, since this is a study of simultaneous uptake from a protic solvent, hydrophobic interactions dominate and are best exploited by hydrophobic molecules.

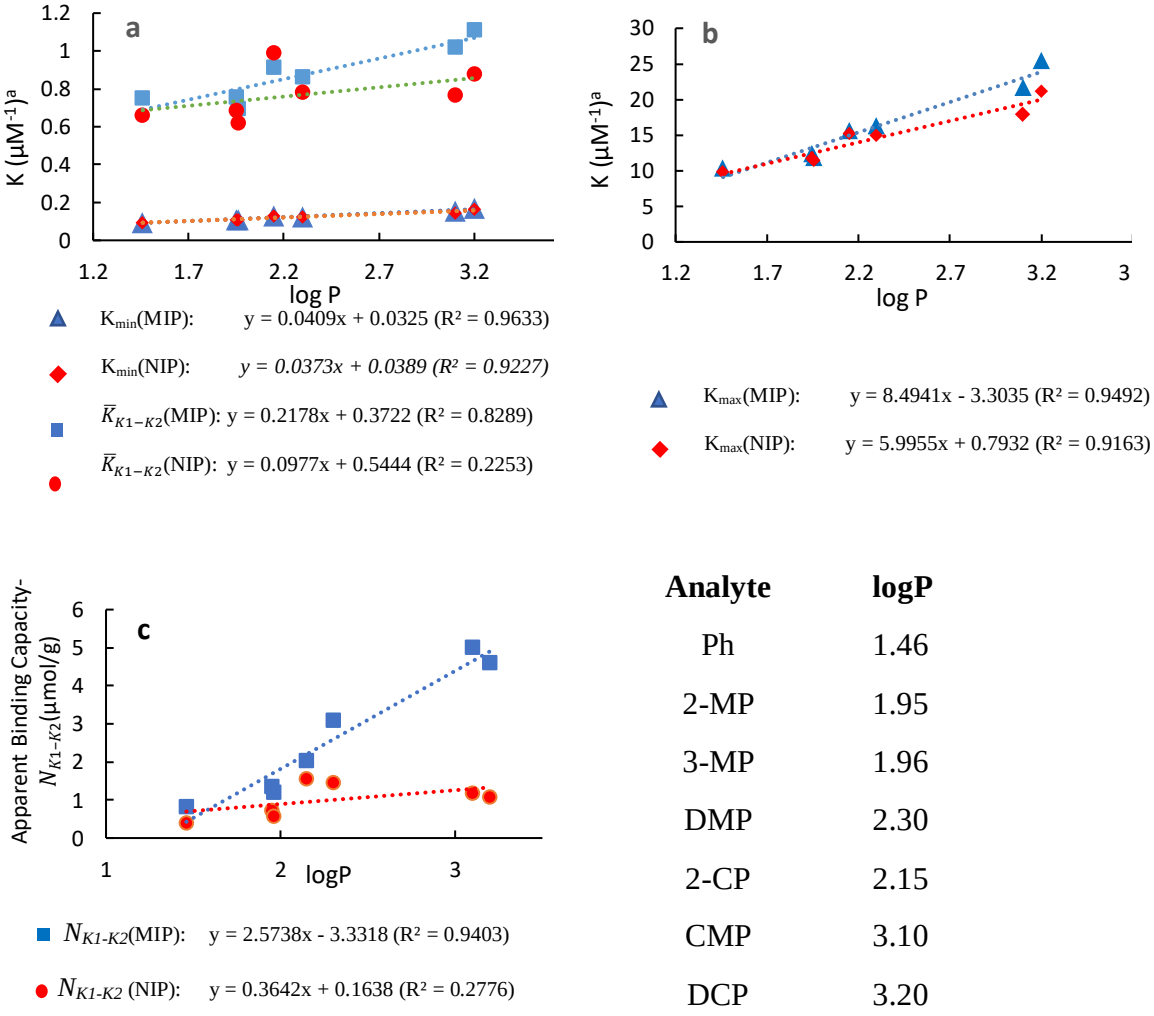

Analyte	logP
Ph	1.46
2-MP	1.95
3-MP	1.96
DMP	2.30
2-CP	2.15
CMP	3.10
DCP	3.20

Figure 4.5.Correlation of Freundlich data for MIPs and NIPs with log P for the seven phenolic compounds that fit the model (low concentration range): a) average affinity and minimum affinity (lower limit); b) maximum affinity; c) apparent binding capacity (N_{K1-K2}).

The imprinting factors (*IF*) were also estimated from the ratio of the number of apparent binding sites for MIPs relative to NIPs (Table 4.2). Looking closely at the unique case of

2-CP, the plots in Figure 4.3 show that there is a relatively small difference in sorption behaviour between the MIPs and NIPs, which also give comparable results for the fitting parameters. Though the MIP showed appreciably higher numbers of apparent binding sites, the affinity is lower for the MIP; thus, we attribute the limited improvement in selectivity toward the 2-CP (i.e., low *IF*) to surface area effects. The recognition behaviour of 2-CP in this study is very similar to its behaviour in a previous study of adsorption of individual adsorbates.[50] Since the only difference in the preparation is the presence of the catechol template, the data supports the conclusion that the template facilitates the formation of higher affinity sites for most adsorbates.

Table 4.4. Properties of phenols under study [56]

	Molecular weight (g/mol)	Solubility in water (g/L(C°))	Density (g/mL)	pKa	logP	Molar volume (mL/mol)*
Ph	94.11	84 (20)	1.07	9.99	1.46	88.9
2-MP	108.14	25.9 (25)	1.05	10.3	1.95	103
3-MP	108.14	24.0 (25)	1.03	10.1	1.96	105
CP	128.55	28.5 (20)	1.26	8.5	2.15	102
DMP	122.16	7.87 (25)	0.97	10.60	2.30	126
CMP	142.58	3.8 (20)	1.37	9.55	3.10	104
DCP	163.00	4.5 (20)	1.4	7.89	3.20	116
TCP	197.45	0.8 (20)	1.7	6.23	3.69	116
PCP	266.34	0.014 (20)	1.98	4.70	5.12	135
4-OP	206.32	0.007 (25)	0.961	10.33	5.25	215
4-NP	220.35	0.007 (25)	0.95	10.31	5.76	232
Catechol	110.1	461	1.34	9.45	0.88	82.1

*The molar volume obtained from the relative ratio between the molecular weight and the density

4.4.2.2 Langmuir-Freundlich Isotherm Model

The experimental and fitted L-FI adsorption isotherms for sub-saturation and saturation concentrations are presented in Figure 4.6 with the corresponding fitting parameters, and their relative errors are summarized in Table 4.5. According to the L-FI model, the concentration range selected for the study is appropriate as the $K°$ from the fitting analysis is within the binding affinity limits K_{max} $(1/C_{min})$ and K_{min} $(1/C_{max})$.

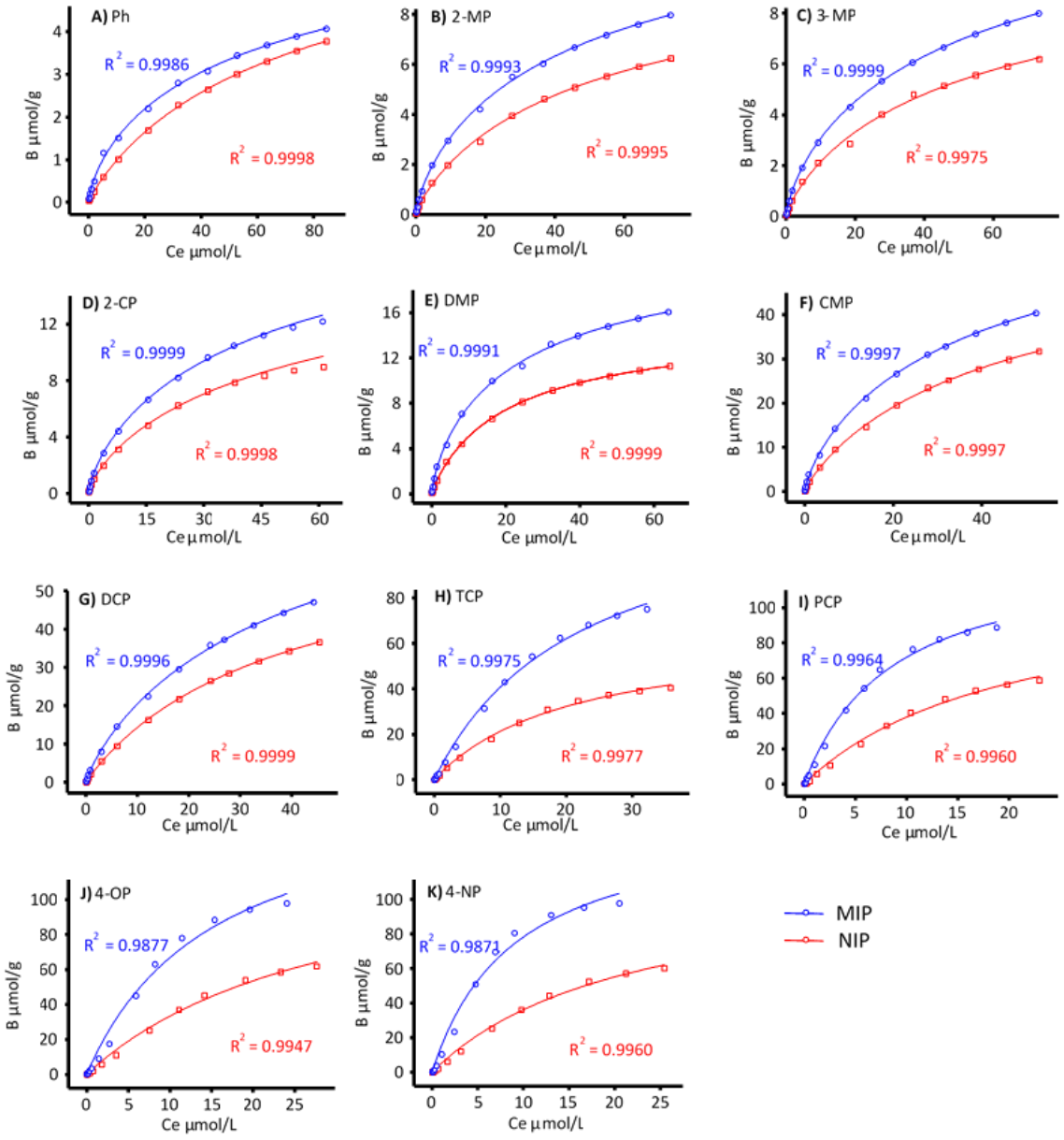

Figure 4.6**.** The experimental data for simultaneous study (circle points for MIP, squares points for NIP) were fit to L-FI (solid lines) for MIP and NIP A) Ph, B) 2-MP, C) 3-MP, D) 2-CP, E) DMP, F) CMP, G) DCP, H) TCP, I) PCP, J) 4-OP, K) 4-NP).

Table 4.5. L-FI Fitting Parameters for the phenols that were loaded simultaneously.

			MIP				
Analyte	N_t (μmol/g)	a (μmol g^{-1}) ($L\mu mol^{-1})^m$	m	$K°$ $(\mu M^{-})^a$	*K limits* $(\mu M^{-1})^b$	R^2	*RSS*
Ph	7.80(10.6%)	0.0453 (7.5%)	0.718 (5.2%)	0.0134	0.0118-10.4	0.9986	0.0349
2-MP	14.4 (6.4%)	0.0475 (4.4%)	0.759 (3.5%)	0.0180	0.0136-12.4	0.9993	0.0602
3-MP	15.2 (2.9%)	0.0455 (2.0%)	0.742 (1.5%)	0.0156	0.0136-11.9	0.9999	0.0103
CP	23.3 (3.7%)	0.0467 (2.3%)	0.752 (1.9%)	0.0170	0.0164-15.6	0.9999	0.0317
DMP	24.3 (5.4%)	0.0786 (4.7%)	0.772 (4.2%)	0.0379	0.0156-16.3	0.9991	0.3944
CMP	77.8 (5.6%)	0.0481 (3.7%)	0.785 (2.8%)	0.0210	0.0191-21.7	0.9997	0.8258
DCP	96.4 (7.3%)	0.0371 (4.6%)	0.858 (3.3%)	0.0215	0.0225-25.5	0.9996	1.4791
TCP	130. (12%)	0.0454 (9.0%)	1 (7.9%)	0.0454	0.0311-27.2	0.9975	25.4918
PCP	134 (10%)	0.114 (8.7%)	1 (8.7%)	0.114	0.0532-45.9	0.9964	51.1395
4-OP	170. (26%)	0.0647 (20%)	1 (17%)	0.0647	0.0415-35.1	0.9877	200.9286
4-NP	149 (19%)	0.110 (18%)	1 (17%)	0.110	0.0487-56.8	0.9871	217.4954
			NIP				
Ph	*7.25 (4.1%)*	*0.0190 (2.6%)*	*0.912 (2.1%)*	*0.0129*	0.0118-9.80	*0.9998*	*0.0040*
2-MP	*11.5 (8.1%)*	*0.0314 (5.4%)*	*0.846 (4.3%)*	0.0167	0.0136-11.7	*0.9995*	*0.0522*
3-MP	11.6 (14%)	0.0342 (9.4%)	0.818 (7.4%)	0.0162	0.0136-11.5	0.9975	0.1531
2-CP	18.7 (4.8%)	0.0381 (3.0%)	0.789(2.4%)	0.0167	0.0163-15.3	0.9998	0.0367
DMP	15.4 (1.6%)	0.0584 (2.1%)	0.851 (1.6%)	0.0355	0.0155-14.9	0.9999	0.0296
CMP	60.7 (8.1%)	0.0322 (5.0%)	0.883 (4.0%)	0.0204	0.0189-17.9	0.9997	1.0207
DCP	69.8 (3.3%)	0.0279 (2.2%)	0.963 (1.7%)	0.0243	0.0220-21.1	0.9999	0.2294
TCP	66.2 (10%)	0.0472 (8.7%)	1 (7.4%)	0.0472	0.0279-24.7	0.9977	7.0412
PCP	115 (20%)	0.0491 (13%)	1 (10%)	0.0491	0.0435-33.2	0.9960	24.3501
4-OP	135(29%)	0.0324 (19%)	1 (12%)	0.0325	0.0361-28.0	0.9947	32.6056
4-NP	116(26%)	0.0431 (17%)	1 (13%)	0.0430	0.0393-28.3	0.9960	33.5916

[a] Calculated from ($K^o = a^{1/m}$)

[b] Calculated from the minimum and maximum of the concentration of the free analyte in the rebinding solution ($K_{max} = 1/C_{min}$ and $K_{min} = 1/C_{max}$)

Some conclusions can be derived from the comparison of the binding parameters in Table 4.5. Like the FI model, the L-FI cannot describe the recognition mechanism for large phenols (TCP, 4-OP, PCP and 4-NP); the corresponding *RSS* values (25 – 217 compared to <2 for the small phenols) and the standard deviation errors in the binding capacities (12-26% compared to 2-10%) are high. Unlike the large phenols, the small phenols (Ph, 2-MP, 3-MP, 2-CP, DMP) show the highest degree of binding site heterogeneity *m*, which indicates that the small phenolics can occupy a larger range of site-types. The availability of the binding sites is related to accessibility (small phenols can diffuse into smaller pores), and site geometry (larger phenols are hindered by the number and size of the functional groups). This trend is more evident in the MIPs, where higher site heterogeneity and adsorption capacity is attributed to the formation of ordered binding sites.

The K_{max} for MIPs is higher than for the NIPs for all phenols, which is consistent with the FI data. However, since the model can effectively fit higher adsorbate concentrations, the $K°$ (affinity binding constant) is shifted toward the K_{min}, which is indicative of partitioning to more of the lower energy sites at high concentrations. Consequently, the selective interaction present in the MIPs is not evident at high concentrations, and the *K* values for the MIPs and NIPs converge. Thus, it is more appropriate to use K_{max} rather than $K°$ to evaluate selective imprinting in MIPs for analytical applications. These conclusions are evident in plots of the *K* values against logP (Figure 4.5). Although the differences between K_{max} for the MIPs and NIPs are somewhat subtle, the differences in the number of binding sites for each analyte are higher for all adsorbates, with dramatic differences for the most hydrophobic species.

As a hybrid of the LI and FI models, there are some advantages of the L-FI with respect to fitting. First, because the model uses non-linear regression, it can fit the entire range of concentrations we have studied, whereas the FI model fails at high concentrations. Second, L-FI can simultaneously model homogeneous and heterogeneous site energies. While this is obvious from the purpose of the model, there is value in comparing data from different models for confirmation. For example, in earlier work, the LI model was more effective than the FI model for fitting adsorption of individual compounds by MIPs/NIPs (i.e. no competition for binding sites) [50]. In that work, the L-FI model was in poor agreement with the FI model but matched well with the LI data. In this work, we found good agreement between the FI and L-FI models for the small phenols.

4.4.2.3 BET Isotherm Model

The BET adsorption isotherms were plotted for each phenolic compound for adsorption to MIPs and NIPs (Figure 4.7) and their corresponding BET binding parameters calculated (Table 4.6). The BET model provides a good fit *(R^2* and *RSS*) to the data for all compounds. The corresponding fitting parameters (q_m, K_S, K_L, n) showed a range of relative errors. If we limit our discussion to data exceeding 20% *RSD*, the BET failed to model Ph behaviour adequately, with the relative errors for all fitting parameters ranging from 22 to 50% with MIPs. In general, the small phenols (e.g. 2-CP and CMP) showed higher %*RSDs* for the K_L and K_S data. We attribute this to the weakness of the intermolecular interactions being modeled in K_L, where these molecules do not tend to form multi-layers. With large differences in K_S and K_L (Eq. 10 $c=K_s/K_L$), small changes in the weighting of these interactions to achieve a global fit can lead to larger errors in the individual parameters.

In terms of the relative performance of the MIPs versus NIPs, for all 11 phenols, the q_m and K_S values are higher with the MIPs. This supports the conclusion that there are more binding sites available, and the interactions are stronger at these sites. However, the K_L values give us important clues regarding the adsorption mechanisms. The K_L values for the lighter phenols (Ph to CMP) are similar for the MIPs and NIPs and are much lower than K_S. Two things can be concluded. First, adsorption to the surface is much more likely than the formation of the multilayers. Second, the adsorption to the surface does not seem to increase the probability of multilayer formation for small molecules. This conclusion is made based on the difference between the MIPs and NIPs, where increased adsorption has little effect on K_L. Conversely, for the larger phenols (PCP, 4-OP, and 4-NP), the model suggests that the interactions between the molecules in the formation of layers are enhanced with stronger adsorption to the surface. For example, 4-NP gives K_S = 0.316 and K_L = 0.0925 for the NIP increasing to K_S = 0.437 and K_L = 0.180 for the MIPs (both have n=4.9). The increase in K_L can be attributed to establishing the correct orientation as a foundation for the formation of multilayers. Since the chemistry of the functionality of these three molecules is quite different, (PCP, chlorine; 4-NP, linear alkyl chain; and 4-OP, highly branched alkyl group), various non-covalent interactions (e.g., π-π, π-σ, and dipole-dipole interactions) may be enhanced through induction effects.

As with the FI and L-FI, q_m tracks well with *logP* (Figure 4.8). We also note that K_L tends to correlate to hydrophobicity, though the trend is weak for K_S. This confirms our postulation that the adsorption process is not based exclusively on hydrophobic effects;

shape and orientation of key functional groups contributes to affinities for ordered templated binding sites.

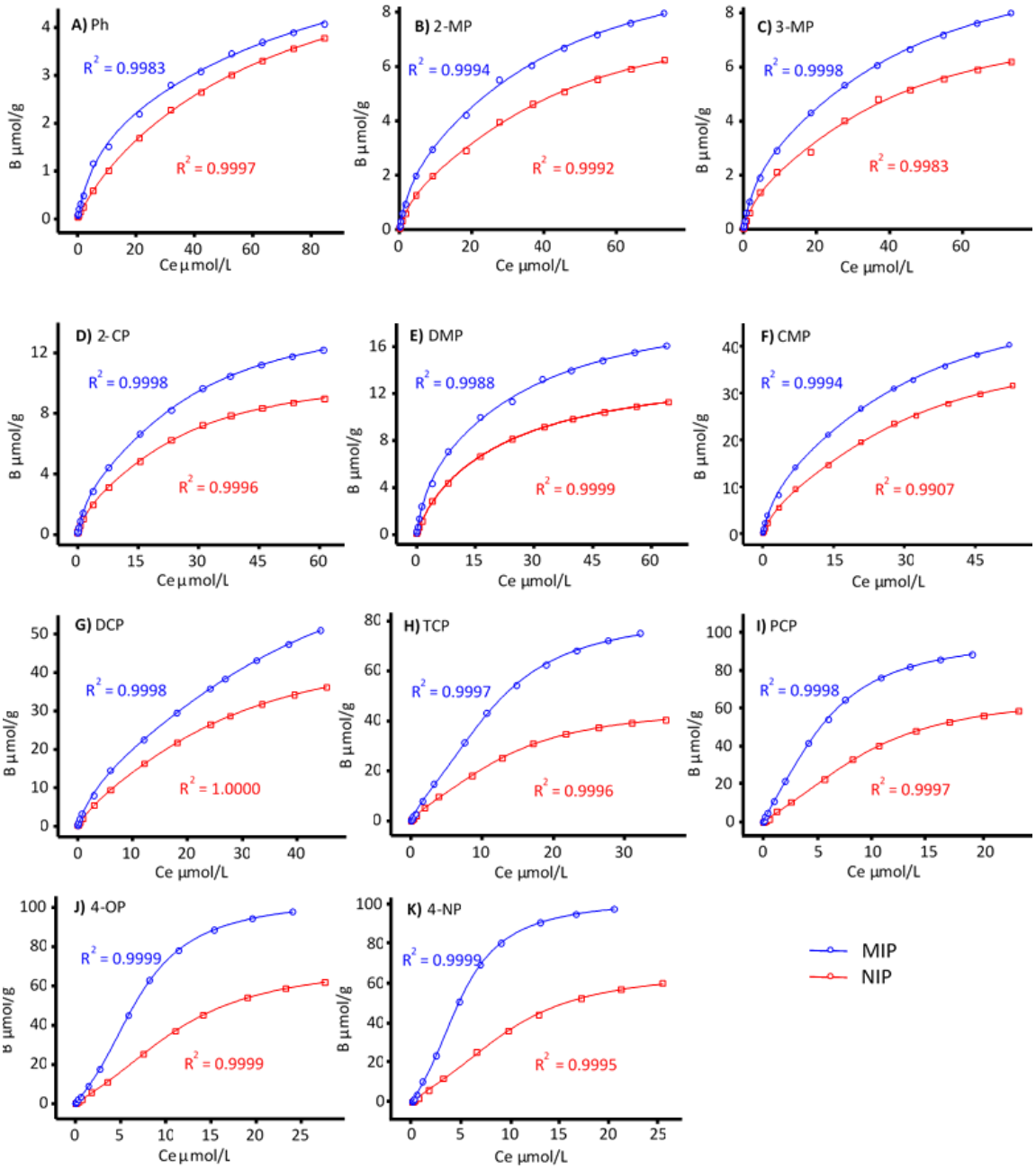

Figure 4.7. The experimental data for simultaneous study (circle points for MIP, squares points for NIP) were fit to BET isotherm model (solid lines) for MIP and NIP A) Ph, B) 2-MP, C) 3-MP, D) 2-CP, E) DMP, F) CMP, G) DCP, H) TCP, I) PCP, J) 4-OP, K) 4-NP).

Table 4.6. BET Fitting Parameters for the phenols that were loaded simultaneously.

Analyte	q_m (μmol/g) (%RSD)	K_S (μM^{-1}) (%RSD)	K_L (μM^{-1}) (%RSD)	n (%RSD)	R^2	*RSS*
			MIP			
Ph	2.26 (22%)	0.139 (32%)	0.0114 (50%)	2.78 (7.3%)	0.9983	0.0395
2-MP	3.28 (10%)	0.226 (18%)	0.0229 (14%)	3.15 (6.2%)	0.9994	0.0578
3-MP	3.27 (5.0%)	0.230 (8.9%)	0.0222 (6.8%)	3.20 (3.0%)	0.9998	0.0153
2-CP	4.26 (3.8%)	0.298 (25%)	0.0295 (23%)	3.51 (2.6%)	0.9998	0.029
DMP	7.23 (15%)	0.335 (7.6%)	0.0342 (3.8%)	2.79 (9.4%)	0.9988	0.4444
CMP	16.0 (11%)	0.270 (20%)	0.0307 (13%)	3.32 (6.9%)	0.9994	1.4686
DCP	21.2 (9.0%)	0.186 (15%)	0.0253 (11%)	3.69 (4.3%)	0.9998	0.8649
TCP	18.4 (7.2%)	0.324 (15%)	0.0780 (2.8%)	4.66 (5.8%)	0.9997	2.5612
PCP	26.7 (8.7%)	0.469 (15%)	0.156 (2.8%)	3.79 (7.4%)	0.9998	2.5612
4-OP	22.8 (4.3%)	0.258 (8.3%)	0.130 (0.8%)	4.75 (3.8%)	0.9999	0.7246
4-NP	21.6 (4.8%)	0.437 (11%)	0.180 (1.0%)	4.90 (4.3%)	0.9999	1.4158
			NIP			
Ph	2.03 (21%)	0.0641 (26%)	0.0127 (26%)	2.85 (12%)	0.9997	0.0054
2-MP	2.23 (8.9%)	0.194 (16%)	0.0231 (9.1%)	3.60 (5.6%)	0.9992	0.0277
3-MP	2.25 (17%)	0.199 (31%)	0.0244 (18%)	3.52 (11%)	0.9983	0.0952
2-CP	2.96 (5.5%)	0.159 (13%)	0.0276 (13%)	3.62 (4.1%)	0.9996	0.029
DMP	5.84 (10%)	0.296 (11%)	0.0383 (4.7%)	2.48 (7.2%)	0.9999	0.021
CMP	11.1 (7.9%)	0.216 (14%)	0.0312 (7.1%)	3.71 (5.1%)	0.9907	0.4149
DCP	13.6 (2.3%)	0.165 (3.6%)	0.0343 (1.8%)	3.58 (1.6%)	0.9999	0.0224
TCP	11.2 (8.5%)	0.294 (16%)	0.0685 (3.8%)	4.23 (6.8%)	0.9996	0.8916
PCP	17.4 (12%)	0.248 (19%)	0.0972 (3.5%)	4.06 (9.5%)	0.9997	1.5516
4-OP	17.8 (5.2%)	0.170 (8.5%)	0.0785 (1.3%)	4.19 (4.3%)	0.9999	0.2372
4-NP	14.3 (11%)	0.316 (21%)	0.0925 (3.5%)	4.86 (8.6%)	0.9995	2.4837

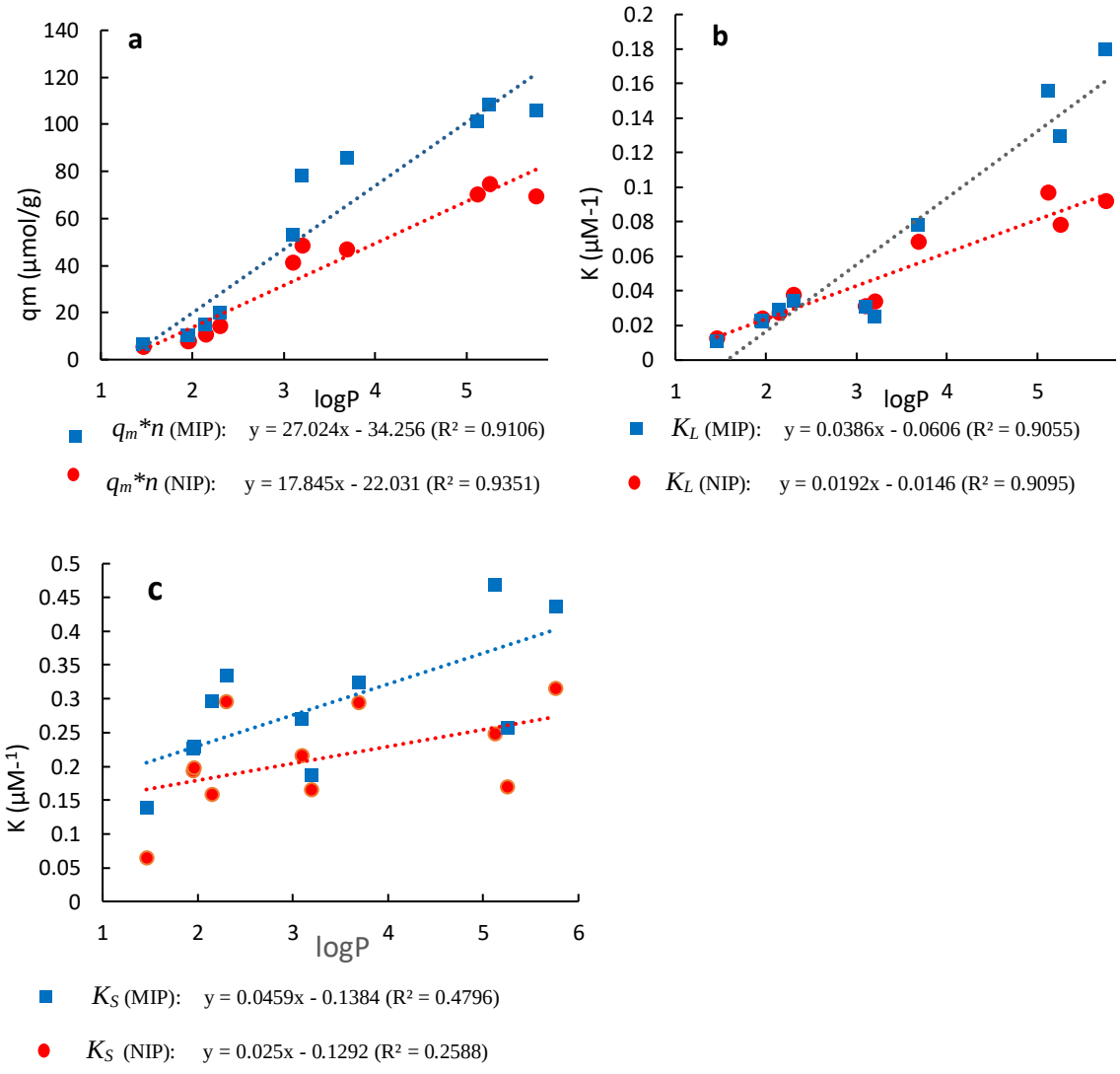

Figure 4.8. Correlation of BET data for MIPs and NIPs with log P for the eleven phenolic compounds: a) total amounts of analyte adsorbed in all layers q_m*n b) the equilibrium adsorption constant of the upper layers (K_L) c) the equilibrium adsorption constant for the first layer

4.4.3 Assessment of Model Performance

Each type of isotherm has its strengths in modeling the interaction of sorbates with an adsorbent surface; for this work, we have found the differences to be largely dependent on the characteristics of the adsorbate rather than the intrinsic nature of the adsorbent. Definitive conclusions about the relative performance of the models must be attenuated with the understanding that intermolecular interactions in a system with eleven adsorbates are complex. Nevertheless, important trends and correlations can be observed.

Overall, the L-F and BET isotherm approaches fit the data over the full concentration range studied. The FI and the hybrid L-FI measures of heterogeneity of the MIP binding sites gave similar results for the light phenols, indicating that their binding sites have a range of affinities (m = 0.66-0.84 for FI, m= 0.72-0.86 for L-FI). The heterogeneity indices for the large phenols were near unity, suggesting that the accessible binding sites on the polymers have relatively uniform binding sites energies. Although the larger phenols are much more hydrophobic, it appears that they cannot compete with smaller phenols for all available sites, which is partly a consequence of their lower diffusivity and steric bulk. With respect to the binding site affinities, the FI model gives higher weighted average affinities ($\overline{K}_{K1-K2}$) than the affinity constants (K^o) from the L-FI model because the FI is used only to fit the linear (sub-saturation) portion of the isotherm. This skews the fit with data from the higher energy sites, which are populated first. Since the BET model provides two affinity constants, one for the adsorption to the surface (K_S) and one for the interaction between the adsorbate molecules in the layers (K_L), we compared both to *logP* (Figure 4.8). We also reduced the K_S and K_L to a single composite affinity constant (K_{ca}= (K_S K_L^{n-1})$^{1/n}$)

for comparison with the affinities from the L-FI model. In all instances, the affinities calculated using BET are within the range of the *K limits* (Table 4.7) and were within an order of magnitude of K^o. The differences can be partially explained in how the models treat binding capacities and affinity constants.

This brings us to the other important data coming from the models–the adsorption capacities (i.e., numbers of binding sites) of the adsorbents, which tend to track with hydrophobicity (Figure 4.5c) and are higher for the MIPs than the NIPs for all adsorbates. The L-FI and BET models show agreement in terms of the total binding sites (N_t in the L-FI model) and the total amount of adsorbate on the solid surface in all layers calculated using the BET model, which can be estimated from the product of q_m and n (Table 4.7). The number of binding sites estimated by the models are very similar for all phenols. This work demonstrates that no one model is sufficient to assess the all the underlying processes in physisorption and molecular recognition by MIP sorbents, noting that homogeneity of the binding site energies is dependent on the chemistry and size of the adsorbates. Rigorous application of the models without simplifying assumptions yields more robust data compared to that from simple linearized models for wide concentration ranges. Thus, data from L-FI and BET models correlate well, though the FI model is satisfactory for low concentrations.

Table 4.7. Comparison between the binding sites in *L-FI* and *BET* models

Analyte	*L-FI*		*BET*		Statistics
	N_t (µmol/g)	*K limits* (μM^{-1})[b]	$q_m n$* (µmol/g)	K_{ca} (Composite affinity)** (μM^{-1})	*%Discrepancy in the binding sites between L-FI and BET*
Ph	*7.8*	0.0118-10.4	6.28	0.0280	20%
2-MP	14.4	0.0136-12.4	10.3	0.0474	28%
3-MP	15.2	0.0136-11.9	10.4	0.0461	31%
2-CP	23.3	0.0164-15.6	15.0	0.0656	36%
DMP	24.3	0.0156-16.3	20.2	0.0673	17%
CMP	77.9	0.0191-21.7	53.1	0.0591	32%
DCP	96.4	0.0225-25.5	78.3	0.0435	19%
TCP	130	0.0311-27.2	85.6	0.106	34%
PCP	135	0.0532-45.9	101	0.208	25%
4-OP	169	0.0415-35.1	108	0.150	36%
4-NP	149	0.0487-56.8	106	0.216	29%

*Total relative amount of adsorbate bound to MIP

**Composite affinities estimated using $K_{ca} = (K_S K_L^{n-1})^{1/n}$

4.5 Conclusions

The processes for simultaneous adsorption of different adsorbates are complex and rarely explained in the literature, particularly for MIPs. The adsorption equilibria are affected by various factors like the adsorbate structure and the energetic heterogeneity of the binding sites, from which MIP cross-reactivity toward non-template adsorbates arises. In using MIPs for trace analysis, we rely on this feature to engineer materials that can strongly adsorb target analytes without the concern of template bleed that hampers MIP use in analytical methods. In this study, the

results from different isotherms help to understand the limits of cross-reactivity and selectivity of the MIPs toward adsorbates with shared functionality (i.e. phenolic compounds) but other substituents that change the physiochemical properties. For the small phenols, the competition for the binding sites is related to their hydrophobicity and solubility in water. More hydrophobic phenols tend to displace the small phenols, which is obvious from the extraction time profile (Figure 4.1). And yet, MIP adsorption of the light phenols persists even with increases in concentrations of the more hydrophobic phenolics, likely resulting from binding sites that are right-sized for the smaller adsorbates. The BET isotherm suggests that hydrophobicity drives many adsorbates to form multilayers rather than remain in solution under unfavorable conditions. The approaches support our assertion that non-covalent molecular imprinting tends to be relatively inefficient but still sufficient for selective adsorption at low concentrations consistent with trace analysis. Finally, adsorption models that effectively estimate binding site energetics can be used to better understand molecular recognition mechanisms in MIPs, which can lead to improved materials with more predictable performance.

4.6 References

(1) Wulff, G.; Grobe-Einsler, R.; Vesper, W.; Sarhan, A. Enzyme-Analogue Built Polymers, 5*). *Makromol. Chem.* **1977**, *178*, 2817–2825.

(2) Andersson, L.; Sellergren, B.; Mosbach, K. Imprinting of Amino Acid Derivatives

in Macroporous Polymers. *Tetrahedron Lett.* **1984**, *25* (45), 5211–5214. https://doi.org/10.1016/S0040-4039(01)81566-5.

(3) Canfarotta, F.; Cecchini, A.; Piletsky, S. *CHAPTER 1: Nano-Sized Molecularly Imprinted Polymers as Artificial Antibodies*; The Royal Society of Chemistry, 2018; Vol. 2018-Janua. https://doi.org/10.1039/9781788010474-00001.

(4) Liu, Y.; Liu, Y.; Liu, Z.; Hu, X.; Xu, Z. β-Cyclodextrin Molecularly Imprinted Solid-Phase Microextraction Coatings for Selective Recognition of Polychlorophenols in Water Samples. *Anal. Bioanal. Chem.* **2018**, *410* (2), 509–519. https://doi.org/10.1007/s00216-017-0746-3.

(5) Yang, Y. J.; Liu, X. W.; Kong, X. J.; Qin, Z.; Jiao, Z. H.; Li, S. H.; Li, J. Y. Preparation and Evaluation of Oseltamivir Molecularly Imprinted Polymer Silica Gel as Liquid Chromatography Stationary Phase. *Molecules* **2018**, *23* (8), 1881. https://doi.org/10.3390/molecules23081881.

(6) Sojo, L. E.; Djauhari, J. Determination of Chlorophenolics in Waters by Membrane Solid-Phase Extraction: Comparison between C18and Activated Carbon Membranes and between Modes of Extraction and Elution. *J. Chromatogr. A* **1999**, *840* (1), 21–30. https://doi.org/10.1016/S0021-9673(99)00186-7.

(7) Yusof, N. A.; Zakaria, N. D.; Maamor, N. A. M.; Abdullah, A. H.; Haron, M. J. Synthesis and Characterization of Molecularly Imprinted Polymer Membrane for the Removal of 2,4-Dinitrophenol. *Int. J. Mol. Sci.* **2013**, *14* (2), 3993–4004. https://doi.org/10.3390/ijms14023993.

(8) Dong, J.; Li, L.; Jiang, Z.; Zhang, G.; Sun, T. Sampling of Phenol in Water by Diffusive Gradients Using Thin Film Technique. *Chem. Lett.* **2014**, *43* (7), 1164–1166. https://doi.org/10.1246/cl.140231.

(9) Sergeyeva, T. A.; Chelyadina, D. S.; Gorbach, L. A.; Brovko, O. O. Colorimetric Biomimetic Sensor Systems Based on Molecularly Imprinted Polymer Membranes for Highly-Selective Detection of Phenol in Environmental Samples. *Biopolym. Cell* **2014**, *30*, 209–215.

(10) Fu, Y.; Finklea, H. O. Quartz Crystal Microbalance Sensor for Organic Vapor Detection Based on Molecularly Imprinted Polymers. *Anal. Chem.* **2003**, *75* (20), 5387–5393. https://doi.org/10.1021/ac034523b.

(11) Blanco-López, M. C.; Lobo-Castañón, M. J.; Miranda-Ordieres, A. J.; Tuñón-Blanco, P. Electrochemical Sensors Based on Molecularly Imprinted Polymers. *TrAC Trends Anal. Chem.* **2004**, *23* (1), 36–48. https://doi.org/10.1016/S0165-9936(04)00102-5.

(12) Sontimuang, C.; Suedee, R.; Canyuk, B.; Phadoongsombut, N.; Dickert, F. L. Development of a Rubber Elongation Factor, Surface-Imprinted Polymer-Quartz Crystal Microbalance Sensor, for Quantitative Determination of Hev B1 Rubber Latex Allergens Present in Natural Rubber Latex Products. *Anal. Chim. Acta* **2011**, *687* (2), 184–192. https://doi.org/10.1016/j.aca.2010.12.021.

(13) Han, S.; Su, L.; Zhai, M.; Ma, L.; Liu, S.; Teng, Y. A Molecularly Imprinted Composite Based on Graphene Oxide for Targeted Drug Delivery to Tumor Cells.

J. Mater. Sci. **2019**, *54* (4), 3331–3341. https://doi.org/10.1007/s10853-018-3023-8.

(14) Javanbakht, M.; Shaabani, N.; Abdouss, M.; Ganjali, M. R.; Mohammadi, A.; Norouzi, P. Molecularly Imprinted Polymers for Selective Solid-Phase Extraction of Verapamil from Biological Fluids and Human Urine. *Curr. Pharm. Anal.* **2009**, *5* (3), 269–276. https://doi.org/10.2174/157341209788922011.

(15) Shahhoseini, F.; Azizi, A.; Egli, S. N.; Bottaro, C. S. Single-Use Porous Thin Film Extraction with Gas Chromatography Atmospheric Pressure Chemical Ionization Tandem Mass Spectrometry for High-Throughput Analysis of 16 PAHs. *Talanta* **2020**, *207* (15 January), 120320. https://doi.org/10.1016/j.talanta.2019.120320.

(16) Hijazi, H. Y.; Bottaro, C. S. *Molecularly Imprinted Polymer Thin-Film as a Micro-Extraction Adsorbent for Selective Determination of Trace Concentrations of Polycyclic Aromatic Sulfur Heterocycles in Seawater*; Elsevier B.V., 2019. https://doi.org/10.1016/j.chroma.2019.460824.

(17) Azizi, A.; Shahhoseini, F.; Bottaro, C. S. Magnetic Molecularly Imprinted Polymers Prepared by Reversible Addition Fragmentation Chain Transfer Polymerization for Dispersive Solid Phase Extraction of Polycyclic Aromatic Hydrocarbons in Water. *J. Chromatogr. A* **2019**, *1610*, 460534. https://doi.org/10.1016/j.chroma.2019.460534.

(18) Azizi, A.; Shahhoseini, F.; Modir-Rousta, A.; Bottaro, C. S. High Throughput Direct Analysis of Water Using Solvothermal Headspace Desorption with Porous

Thin Films. *Anal. Chim. Acta* **2019**, *1087*, 51–61. https://doi.org/10.1016/j.aca.2019.08.022.

(19) Hijazi, H. Y.; Bottaro, C. S. Analysis of Thiophenes in Seawater: Molecularly Imprinted Polymer Thin-Film Extraction with Desorption Electrospray Ionization Mass Spectrometry. *Int. J. Mass Spectrom.* **2019**, *443*, 9–15. https://doi.org/10.1016/j.ijms.2019.05.003.

(20) Hijazi, H. Y.; Bottaro, C. S. Selective Determination of Semi-Volatile Thiophene Compounds in Water by Molecularly Imprinted Polymer Thin Films with Direct Headspace Gas Chromatography Sulfur Chemiluminescence Detection. *Analyst* **2018**, *143*, 1117–1123. https://doi.org/10.1039/C7AN01686G.

(21) Egli, S. N.; Butler, E. D.; Bottaro, C. S. Selective Extraction of Light Polycyclic Aromatic Hydrocarbons in Environmental Water Samples with Pseudo-Template Thin-Film Molecularly Imprinted Polymers. *Anal. Methods* **2015**, *7*, 2028–2035. https://doi.org/10.1039/C4AY02849J.

(22) Gryshchenko, A. O.; Bottaro, C. S. Development of Molecularly Imprinted Polymer in Porous Film Format for Binding of Phenol and Alkylphenols from Water. *Int. J. Mol. Sci.* **2014**, *15* (1), 1338–1357. https://doi.org/10.3390/ijms15011338.

(23) Van Biesen, G.; Wiseman, J. M.; Li, J.; Bottaro, C. S. Desorption Electrospray Ionization-Mass Spectrometry for the Detection of Analytes Extracted by Thin-Film Molecularly Imprinted Polymers. *Analyst* **2010**, *135* (9), 2237–2240.

https://doi.org/10.1039/c0an00331j.

(24) Speltini, A.; Scalabrini, A.; Maraschi, F.; Sturini, M.; Profumo, A. Newest Applications of Molecularly Imprinted Polymers for Extraction of Contaminants from Environmental and Food Matrices: A Review. *Anal. Chim. Acta* **2017**, *974*, 1–26. https://doi.org/10.1016/j.aca.2017.04.042.

(25) Umpleby, R. J.; Baxter, S. C.; Bode, M.; Berch, J. K.; Shah, R. N.; Shimizu, K. D. Application of the Freundlich Adsorption Isotherm in the Characterization of Molecularly Imprinted Polymers. *Anal. Chim. Acta* **2001**, *435* (1), 35–42. https://doi.org/10.1016/S0003-2670(00)01211-3.

(26) Umpleby, R. J.; Baxter, S. C.; Chen, Y.; Shah, R. N.; Shimizu, K. D. Characterization of Molecularly Imprinted Polymers with the Langmuir - Freundlich Isotherm. *Anal. Chem.* **2001**, *73* (19), 4584–4591. https://doi.org/10.1021/ac0105686.

(27) Shimizu, K. D. Characterization of MIPs Using Heterogeneous Binding Models. *Mat. Res. Soc. Symp. Proc.* **2002**, *723*, 17–22.

(28) Turiel, E.; Perez-Conde, C.; Martin-Esteban, A. Assessment of the Cross-Reactivity and Binding Sites Characterisation of a Propazine-Imprinted Polymer Using the Langmuir-Freundlich Isotherm. *Analyst* **2003**, *128* (2), 137–141. https://doi.org/10.1039/b210712k.

(29) Cacho, C.; Turiel, E.; Martin-Esteban, A.; Pérez-Conde, C.; Cámara, C.

Characterisation and Quality Assessment of Binding Sites on a Propazine-Imprinted Polymer Prepared by Precipitation Polymerisation. *J. Chromatogr. B Anal. Technol. Biomed. Life Sci.* **2004**, *802* (2), 347–353. https://doi.org/10.1016/j.jchromb.2004.03.035.

(30) Baggiani, C.; Giraudi, G.; Giovannoli, C.; Tozzi, C.; Anfossi, L. Adsorption Isotherms of a Molecular Imprinted Polymer Prepared in the Presence of a Polymerisable Template: Indirect Evidence of the Formation of Template Clusters in the Binding Site. *Anal. Chim. Acta* **2004**, *504* (1), 43–52. https://doi.org/10.1016/S0003-2670(03)00671-8.

(31) Rampey, A. M.; Umpleby, R. J.; Rushton, G. T.; Iseman, J. C.; Shah, R. N.; Shimizu, K. D. Characterization of the Imprint Effect and the Influence of Imprinting Conditions on Affinity, Capacity, and Heterogeneity in Molecularly Imprinted Polymers Using the Freundlich Isotherm-Affinity Distribution Analysis. *Anal. Chem.* **2004**, *76* (4), 1123–1133. https://doi.org/10.1021/ac0345345.

(32) Umpleby, R. J.; Baxter, S. C.; Rampey, A. M.; Rushton, G. T.; Chen, Y.; Shimizu, K. D. Characterization of the Heterogeneous Binding Site Affinity Distributions in Molecularly Imprinted Polymers. *J. Chromatogr. B Anal. Technol. Biomed. Life Sci.* **2004**, *804* (1), 141–149. https://doi.org/10.1016/j.jchromb.2004.01.064.

(33) Rushton, G. T.; Karns, C. L.; Shimizu, K. D. A Critical Examination of the Use of the Freundlich Isotherm in Characterizing Molecularly Imprinted Polymers (MIPs). *Anal. Chim. Acta* **2005**, *528* (1), 107–113.

https://doi.org/10.1016/j.aca.2004.07.048.

(34) Langmuir, I. The Constitution and Fundamental Properties of Solids and Liquids. *J. Am. Chem. Soc.* **1916**, *38* (3), 2221–2295. https://doi.org/10.1007/s00145-005-0319-z.

(35) Freundlich HMF. Over the Adsorption in Solution. *J. Phys. Chem.* **1906**, *57*, 385–471.

(36) Sips, R. On the Structure of a Catalyst Surface. *J. Chem. Phys.* **1948**, *16* (5), 490–495. https://doi.org/10.1063/1.1746922.

(37) Saadi, R.; Saadi, Z.; Fazaeli, R.; Fard, N. E. Monolayer and Multilayer Adsorption Isotherm Models for Sorption from Aqueous Media. *Korean J. Chem. Eng.* **2015**, *32* (5), 787–799. https://doi.org/10.1007/s11814-015-0053-7.

(38) Ebadi, A.; Soltan Mohammadzadeh, J. S.; Khudiev, A. What Is the Correct Form of BET Isotherm for Modeling Liquid Phase Adsorption? *Adsorption* **2009**, *15* (1), 65–73. https://doi.org/10.1007/s10450-009-9151-3.

(39) Brunauer, S.; Emmett, P. H.; Teller, E. Adsorption of Gases in Multimolecular Layers. *J. Am. Chem. Soc.* **1938**, *60* (2), 309–319. https://doi.org/10.1021/ja01269a023.

(40) García-Calzón, J. A.; Díaz-García, M. E. Characterization of Binding Sites in Molecularly Imprinted Polymers. *Sensors Actuators, B Chem.* **2007**, *123* (2), 1180–1194. https://doi.org/10.1016/j.snb.2006.10.068.

(41) Stanley, B. J.; Szabelski, P.; Chen, Y. B.; Sellergren, B.; Guiochon, G. Affinity Distributions of a Molecularly Imprinted Polymer Calculated Numerically by the Expectation-Maximization Method. *Langmuir* **2003**, *19* (3), 772–778. https://doi.org/10.1021/la020747y.

(42) Lanza, F.; Ruther, M.; Hall, A. J.; Dauwe, C.; Sellergren, B. Studies on the Process of Formation, Nature and Stability of Binding Sites in Molecularly Imprinted Polymers. *Mater. Res. Soc. Symp. Proc.* **2002**, *723*, 93–103.

(43) Limousin, G.; Gaudet, J. P.; Charlet, L.; Szenknect, S.; Barthès, V.; Krimissa, M. Sorption Isotherms: A Review on Physical Bases, Modeling and Measurement. *Appl. Geochemistry* **2007**, *22* (2), 249–275. https://doi.org/10.1016/j.apgeochem.2006.09.010.

(44) Foo, K. Y.; Hameed, B. H. Insights into the Modeling of Adsorption Isotherm Systems. *Chem. Eng. J.* **2010**, *156* (1), 2–10. https://doi.org/10.1016/j.cej.2009.09.013.

(45) Feng, Q. Z.; Zhao, L. X.; Chu, B. L.; Yan, W.; Lin, J. M. Synthesis and Binding Site Characteristics of 2,4,6-Trichlorophenol- Imprinted Polymers. *Anal. Bioanal. Chem.* **2008**, *392* (7–8), 1419–1429. https://doi.org/10.1007/s00216-008-2390-4.

(46) Thakur, A. K.; Munson, P. J.; Hunston, D. L.; Rodbard, D. Characterization of Ligand-Binding Systems by Continuous Affinity Distributions of Arbitrary Shape. *Anal. Biochem.* **1980**, *103* (1), 240–254. https://doi.org/10.1016/0003-2697(80)90263-8.

(47) Umpleby, R. J.; Bode, M.; Shimizu, K. D. Measurement of the Continuous Distribution of Binding Sites in Molecularly Imprinted Polymers. *Analyst* **2000**, *125* (7), 1261–1265. https://doi.org/10.1039/b002354j.

(48) Jeppu, G. P.; Clement, T. P. A Modified Langmuir-Freundlich Isotherm Model for Simulating PH-Dependent Adsorption Effects. *J. Contam. Hydrol.* **2012**, *129–130*, 46–53. https://doi.org/10.1016/j.jconhyd.2011.12.001.

(49) Tamayo, F. G.; Casillas, J. L.; Martin-Esteban, A. Evaluation of New Selective Molecularly Imprinted Polymers Prepared by Precipitation Polymerisation for the Extraction of Phenylurea Herbicides. *J. Chromatogr. A* **2005**, *1069* (2), 173–181. https://doi.org/10.1016/j.chroma.2005.02.029.

(50) Abu-Alsoud, G. F.; Hawboldt, K. A.; Bottaro, C. S. Comparison of Four Adsorption Isotherm Models for Characterizing Molecular Recognition of Individual Phenolic Compounds in Porous Tailor-Made Molecularly Imprinted Polymer Films. *ACS Appl. Mater. Interfaces* **2020**, *12* (10), 11998–12009. https://doi.org/10.1021/acsami.9b21493.

(51) Wang, X.; Kang, Q.; Shen, D.; Zhang, Z.; Li, J.; Chen, L. Novel Monodisperse Molecularly Imprinted Shell for Estradiol Based on Surface Imprinted Hollow Vinyl-SiO2 Particles. *Talanta* **2014**, *124*, 7–13. https://doi.org/10.1016/j.talanta.2014.02.040.

(52) Li, X.; Zhang, B.; Li, W.; Lei, X.; Fan, X.; Tian, L.; Zhang, H.; Zhang, Q. Preparation and Characterization of Bovine Serum Albumin Surface-Imprinted

Thermosensitive Magnetic Polymer Microsphere and Its Application for Protein Recognition. *Biosens. Bioelectron.* **2014**, *51*, 261–267. https://doi.org/10.1016/j.bios.2013.07.008.

(53) Zheng, P.; Zhang, B.; Luo, Z.; Du, W.; Guo, P.; Zhou, Y.; Chang, R.; Chang, C.; Fu, Q. Facile Preparation of Polydopamine-Coated Imprinted Polymers on the Surface of SiO2 for Estrone Capture in Milk Samples. *J. Sep. Sci.* **2018**, *41* (12), 2585–2594. https://doi.org/10.1002/jssc.201600611.

(54) Lu, W.; Wang, X.; Wu, X.; Liu, D.; Li, J.; Chen, L.; Zhang, X. Multi-Template Imprinted Polymers for Simultaneous Selective Solid-Phase Extraction of Six Phenolic Compounds in Water Samples Followed by Determination Using Capillary Electrophoresis. *J. Chromatogr. A* **2017**, *1483*, 30–39. https://doi.org/10.1016/j.chroma.2016.12.069.

(55) U.S. National Library of Medicine National Center for Biotechnology Information (https://pubchemdocs.ncbi.nlm.nih.gov).

(56) U.S. National Library of Medicine National Center for Biotechnology Information https://pubchem.ncbi.nlm.nih.gov.

Chapter 5

5 Conclusion and future work

The work reported in this thesis is the sum of efforts to develop a new water-compatible molecularly imprinted polymer (MIP) adsorbent with selective binding sites for the extraction of phenols from seawater and produced water. MIPs were prepared successfully using a catechol pseudo-template with water-soluble carboxylic acid monomers. These MIPs were prepared in thin-film format on a glass substrate with a photo-induced radical polymerization process. For effective imprinting, the MIP formulation was optimized through systematic optimization of critical factors influencing MIP performance, like the nature and the amounts of functional monomer, crosslinker, template, and porogen. To obtain a fast and robust analytical method, various parameters were also optimized like salt effect, pH, desorption solvent type, desorption time, and adsorbent mass. The optimized method (MIP-UHPLC-PDA) was used to determine trace levels of eleven phenol compounds, including phenol, alkylphenols, and chlorophenols, in seawater and produced water samples. The analysis of the spiked DI water sample using the MIP-UHPLC-PDA method was evaluated by LOD, EF, LR and linearity. The accuracy and precision for the MIP-UHPLC-PDA method were validated by determining the recoveries of the phenols at different concentration levels in seawater and produced water samples. It was found that the MIP-UHPLC-PDA method is suitable for the simultaneous determination of trace levels of phenolic compounds from complex water samples using just a few milligrams of sorbent in a 30 mL water sample without a preconditioning step, which reduces the organic solvent consumption. Post-extraction clean-up (a short rinse in DI water) and desorption

(15 min in ACN) are fast and easy. A worthy note is that the method can also be applied successfully to volumes as small as 10 mL and can also be applied to larger volumes to improve sensitivity as needed. Also, our device could be reused at least five times, with no decrease in performance. The MIP-UHPLC-PDA method is characterized by high throughput and sensitivity to determine various phenolic compounds simultaneously in water samples, without suffering from a matrix effect even at low concentration, while demonstrating high accuracy and precision. These simple, robust, inexpensive devices can be used in automation and high throughput sample processing.

Binding isotherms were also used to carefully characterize the binding characteristics of MIPs. The binding isotherms provide a means to quantify the binding properties, such as the total number of binding sites and average affinity constant. Generally, the MIPs made via the covalent approach produce homogenous binding sites, which can be described using the Langmuir isotherm, the simplest binding isotherm model. On the other hand, the behaviour of non-covalently imprinted polymers is better assessed using the Freundlich model and affinity distribution. The affinity distributions allow comparison of the binding properties between different MIPs quantitatively and graphically. Thus, evaluating the properties of MIPs using binding isotherms has become important in the optimization and in the explanation of the recognition mechanism of different substrates during the adsorption process.

The binding behaviour for single adsorbates toward MIPs and NIPs was assessed for five phenolic compounds (Ph, 2-MP, 3-MP, 2-CP, and 4-OP) uploaded individually. It was proven that heterogeneity is a relative phenomenon depending on the chemistry of the

adsorbates. In this study, the results show that the MIP exhibited a high degree of homogeneity, so LI and L-FI (hybrid between LI and FI) models explained the adsorption behaviour for small phenolic compounds, while the BET adsorption model was the only model able to explain the recognition mechanism for 4-OP. This shows that a MIP can have different binding sites suited to adsorption of a range of analytes with different shapes and sizes. A justifiable conclusion then is that a single isotherm model is not enough to explain the behaviour of the analytes toward the adsorbent surface. Each model gives valuable quantitative data that help to explain the recognition mechanism for the adsorbates.

In fact, the simultaneous adsorption process for a range of adsorbates are complex and rarely explained. That is because the adsorption equilibria are affected by various factors like the shape and the energetic heterogeneity of the binding sites and the different physical and chemical properties of the adsorbates. Nevertheless, in another study, we examined the cross-reactivity of the MIPs toward eleven phenolic compounds loaded simultaneously using the adsorption isotherm models. It was observed that the competition of the phenols for the binding sites of the catechol imprinted polymer depends on their hydrophobicity and solubility in water. Thus, a more hydrophobic analyte will replace the small phenols. However, this does not mean that the small adsorbates will be replaced entirely, but some remain bound to higher energy binding sites better suited for selective adsorption of these analytes. In contrast to the individual study, the MIPs showed a degree of heterogeneity, which emphasizes that the heterogeneity depends on the chemistry of the competitive adsorbates. In this work, FI and L-FI explained the recognition mechanism for all small

phenols. Only the BET adsorption model fit the experimental data for the large phenols like TCP, 4-OP, PCP, and 4-NP, which suggests the formation of the multilayers driven by the hydrophobic nature of the adsorbates. It is worth noting that the formation of a multilayer of adsorbates in the aqueous adsorption process has not been mentioned before in the literature.

Finally, the data confirmed that the MIP surface exhibited greater selectivity toward adsorbates at low concentrations, which means that imprinting factors should be higher at low concentrations. This is in contrast to high imprinting factors sometimes reported for MIPs using data at the point of adsorbate saturation, which may be the result of surface area differences between MIPs and NIPs rather than the formation of a large number of high energy sites.

Future work

The MIP formulation can be optimized using a Design of Experiments. The evaluation of catechol imprinted polymer using the adsorption isotherm models can be expanded by studying all the target analytes individually to compare each analyte adsorption behaviour in individual and simultaneous studies. For a better understanding of the multilayer theory, it will be useful to expand the applied concentration to higher levels to know if the small phenols tend to form multilayers or not. Additionally, testing the recognition behaviour for another group of large hydrophobic analytes can be used to assess the validity of this theory.

The method developed using the MIP on glass requires 8 mL of solvent for desorption followed by solvent blowdown, which is time consuming, wastes solvent, and is a source of error. This volume is required because of the device geometry. However, new fabrication methods would allow for the MIP device geometry to be changed to a smaller size specifically to decrease organic solvent required for the desorption process [1]. Provided there is still sufficient coating to meet the sensitivity requirements, this will allow for substantial gains in time and resources required for analysis.

In order to reduce the analysis time and make our device more environmentally friendly, a new method using headspace (HS) GC-MS can be developed for the analysis of phenols from the water sample. The new method is characterized by its ability to make the analysis without using the desorption solvent and blowdown steps. HS-GC-MS allows for desorption of the phenols directly from the films into the headspace, which is then injected into the GC column with an automated program. Since optimizing for headspace sample introduction can be complex, with numerous factors to consider, including oven temperature, equilibration time and shaking, the design of the experiment principles would be studied. To avoid broadening and tailing and to reduce the time needed for derivatization of phenols, it would also be interesting to equip the GC with less common column chemistry, e.g., an electrophilic stationary phase (like trifluoropropyl phase) with a deactivated surface, which may be an improvement over traditional phases like DB-5 [2].

References

[1]) Shahhoseini, F.; Azizi, A.; Egli, S. N.; Bottaro, C. S. Single-Use Porous Thin Film Extraction with Gas Chromatography Atmospheric Pressure Chemical Ionization Tandem Mass Spectrometry for High-Throughput Analysis of 16 PAHs. *Talanta* **2020**, *207* (15 January), 120320. https://doi.org/10.1016/j.talanta.2019.120320.

(2) The National Center for Biotechnology Information. O-Xylene www.angilent.com/chem/myGCcolumns. https://doi.org/10.3200/CHNG.38.4.52-53.

Appendix 1

Derivation of the BET equation for liquid phase adsorption process

The general form of BET isotherm is given in Eq. 1:

$$\frac{q}{q_m} = \frac{cx(1-(n+1)x^n + nx^{n+1})}{(1-x)(1+(c-1)x - cx^{n+1})} \quad (1)$$

where q_m is the monolayer adsorption capacity; n the number of the layers formed; $c = K_S/K_L$, where K_s is equilibrium constant for adsorption to the surface and K_L is the equilibrium constant for adsorption to a bound layer; x is the adsorbate partial pressure relative to its saturation pressure ($x = P/P^{sat}$) at constant temperature; q is the amount of analyte adsorbed relative to mass of sorbent. To apply BET to adsorption to MIPs in solutions rather than the gas phase, Eq. 1 must be modified. The mathematical expressions for K_S and K_L are indicated in Eq. 3 and 4, respectively:

$$K_S = \frac{a_1}{b_1} e^{E_1/RT} \quad (2)$$

$$K_L = \frac{a_2}{b_2} e^{E_L/RT} \quad (3)$$

where (a_1 & b_1) and (a_2 and b_2) are the adsorption and desorption rate constants on the first layer and the upper layers, respectively. E_1 and E_2 are the heat of adsorption at the sorbent surface and the heat of condensation of the adsorbates, respectively. Brunauer *et al.*[1] assumed that heat of adsorption is equal for all upper layers and it is equivalent to the heat of condensation because the molecules in the second and subsequent layers act as

the molecules in the bulk system. On the other hand, they put another expression for x (Eq. 4) based on the Clausius-Clapeyron equation (ln $P^{sat} = -E_L/RT + constant$).

$$x = P\frac{a_2}{b_2}e^{E_L/RT} \tag{4}$$

By substituting Eq. 3 in Eq. 4 we will get Eq. 5:

$$x = P \cdot K_L \tag{5}$$

So, in this way they reduced the K_L fitting parameter. They also proposed three important assumptions.

1) q will be infinite when the partial pressure reaches the saturation pressure ($P = P^{sat}$), where the adsorbates will condense at the sorbent solid material. This assumption makes the value of $x = 1$.

2) Eq. 1 is reduced to the LI equation when $n = 1$, which emphasizes that the LI equation is a particular case from the general form of BET isotherm.

3) The general form of BET Eq. 1 is reduced to the classical form (Eq. 6) when $x < 1$ and $n \to \infty$. Where the classical form is developed for the gas phase adsorption process only. Eq. 7 represents the linear form of Eq.6, and the values of q_m and c can be estimated using the linear regression of Eq.7.

$$\frac{q}{q_m} = \frac{cx}{(1-x)(1-x+cx)} \tag{6}$$

$$\frac{x}{q(1-x)} = \frac{1}{q_m c} + \left(\frac{c-1}{q_m c}\right)x \tag{7}$$

The classical form for BET isotherm is developed for gas phase adsorption in which the concentration was represented as $x = P/P^{sat}$. P^{sat} was replaced by $1/K_L$ based on Clausius-Clapeyron equation and Eq. 3. However, this is not consistent with liquid-phase adsorption

in which the actual saturation concentration is not equal to $1/K_L$. Besides, Brunauer *et al.* also assumed infinite adsorption ($n \rightarrow \infty$) at saturation for gas phase adsorption, but this assumption is not valid in liquid phase adsorption, because there might be no affinity of adsorbate toward the adsorbent material, or when the system is already saturated with adsorbate, the adsorption will not increase with increasing the concentration since both solvent and adsorbate will be in the condensed form. So Ebadi *et al.*[2] adapted the general form for BET isotherm model (Eq. 1) for liquid-phase adsorption and replaced the partial pressure of adsorbate by the equilibrium concentration of the adsorbate in the liquid phase (C_e) and kept the equilibrium constant of adsorption of upper layers (K_L) in the equation as a fitting parameter to yield Eq. 8. This equation can be solved through fitting q against C_e using the non-linear regressing to obtain four fitting parameters (C_e, q_m, K_L, K_S, and n).

$$q = \frac{q_m K_S C_e [1 - (n+1)(K_L C_e)^n + n(K_L C_e)^{n+1}]}{(1 - K_L C_e)\left[1 + \left(\frac{K_S}{K_L} - 1\right) K_L C_e - \left(\frac{K_S}{K_L}\right)(K_L C_e)^{n+1}\right]} \quad (8)$$

References

[1] S. Brunauer, P.H. Emmett, E. Teller, Adsorption of Gases in Multimolecular Layers, J. Am. Chem. Soc. 60 (1938) 309–319. https://doi.org/10.1021/ja01269a023.

[2] A. Ebadi, J.S. Soltan Mohammadzadeh, A. Khudiev, What is the correct form of BET isotherm for modeling liquid phase adsorption?, *Adsorption.* 15 **(2009)** 65–73. https://doi.org/10.1007/s10450-009-9151-3.